# The UK wind regime - Observational trends and extreme event analysis and modelling

Nick Earl

This thesis is submitted in fulfilment of the requirements for the degree of Doctor of Philosophy at the University of East Anglia.

School of Environmental Sciences

June 2013

## Abstract

The UK has one of the most variable wind climates; NW Europe as a whole is a challenging region for forecast- and climate-modelling alike. In Europe, strong winds within extra-tropical cyclones (ETCs) remain on average the most economically significant weather peril when averaged over multiple years, so an understanding how ETCs cause extreme surface winds and how these extremes vary over time is crucial.

An assessment of the 1980-2010 UK wind regime is presented based on a unique 40-station network of 10m hourly mean windspeed and daily maximum gustspeed (DMGS) surface station measurements. The regime is assessed, in the context of longer- and larger-scale wind variability, in terms of temporal trends, seasonality, spatial variation, distribution and extremes. Annual mean windspeed ranged from 4.4 to 5.4 $ms^{-1}$ (a 22% difference) with 2010 recording the lowest annual network mean windspeed over the period, attracting the attention of the insurance and wind energy sectors, both highly exposed to windspeed variations.

A short subjective climatology (2008-2010) is developed of the ETCs and their sub-storm features which are associated with the strongest DMGSs. The little studied UK Quasi-linear convective systems (QLCSs) and pseudo-QLCSs are found to account for 22% of the top 1% of DMGSs, with the better known Sting Jet accounting for at most 5%.

This same climatology of 2008-10 ETCs then forms the basis of performance assessments of global forecast ensemble systems. At T+48, an ensemble consisting of just the ECMWF and Canadian EPS members (total-70) is found to capture the same set of extreme events as an ensemble consisting of nine global centres (157-239) highlighting the value of using model physics perturbations at this range. A prominent ETC, *Emma*, then forms the basis of a high-resolution model sensitivity analysis using the Weather Research and Forecasting model. Surface wind simulations display greater sensitivity to different cloud microphysics schemes and to horizontal resolution than to vertical resolution, the former highlighting the importance of diabatic processes within extreme European ETCs.

# Acknowledgements

This project was carried out under funding from the Worshipful Company of Insurers, at the University of East Anglia, under the supervision of Drs Stephen Dorling and Roland von Glasow.

For the provision of observational wind data thanks are due to the UK Met Office, British Atmospheric Data Centre and Richard Hewston. Richard Hewston also for helping me get going with it and continued support throughout my PhD. Thanks must go to Chris Collins and Julie Harold for useful and continuous IT support, instrumental in getting the WRF model running at UEA, along with their consistent and excellent support of the UEA cluster. Thanks to Rob Neal at the UK Met Office for kindly supplying me with synoptic surface pressure charts and informing me of any interesting extra-tropical cyclone examples of interest in the operational forecasting department. Thanks goes to Chris Steele for helping me out with an awkward figure on Christmas Eve, also consistently being available to discuss anything meteorological.

Andy Elvidge must be credited, always able to put a smile on my face and whose morale boosting ridiculous antics will live long in the memory. My housemates over the years deserve a mention, Tara, Amy, Webber and Julia, able to put up with me and my muddy shoes, along with Walker-Brown, Ninja and the witches for the tea breaks. I thank my running buddies Josh, Rich, Dazzer, Beaney, Glenbo and Siberia for getting me out of the office for lovely countryside runs on would be stressful days, and the rest of UEA Athletics club members for going on amazing trips with me all over the country. My fellow PhD students and office mates must be credited for their constant support, help and morale boosting games of golf and table tennis.

Special thanks goes to Steve, my primary supervisor, for his constant support throughout the project. I greatly appreciate his advice and his ability to understand when I needed time to get to grips with things. Thanks must also be given for numerous free lunches and Weatherquest Christmas dinners over the years!

# Contents

# List of Figures

# List of Tables

# Chapter 1

# Introduction

The relationship between humans and the wind is as ancient as civilisation itself. The ancient Greeks had numerous wind gods including Aeolus, ruler of the winds and four others based on the cardinal directions, Boreas, god of the north wind, Eurus, east, Notus, south and Zephyrus, god of the west wind. It was well understood that different wind directions were associated with different types of weather, with Eurus considered unlucky because his (easterly) winds tended to bring blustery wind and storms. It is likely that the Greeks were the first to measure winds, around 430 BC (Jacobson, 2005) and the Greek scientist Theophrastus compiled a book on weather forecasting, called the Book of Signs, which remained highly influential in the study of weather and forecasting for nearly 2,000 years until substantial progress was made in meteorology in the 18th century. In 1806, Francis Beaufort introduced his system for classifying wind speeds, the 'Beaufort Scale'. The first known anemometer consisting of a swinging-plate placed perpendicular to the wind was developed in the 1450s by the Italian mathematician Leone Battista Alberti and in 1846 a simple four cup anemometer was invented by Dr. John Thomas Romney Robinson. This design was subsequently improved and reliable three cup anemometers (error of less than 3% up to 60 mph) were used by the mid-1930s. Cup anemometers are now widely used at surface monitoring sites alongside more sophisticated types including windmill and sonic anemometers. There have been/are many problems and limitations associated with surface monitoring instruments in general, with site instruments being relocated and updated but not calibrated properly, human error and inconsistencies with observing methods (e.g. conversion to automatic weather stations from manual during the 1990s). This has led to historical studies being based more on long-term trends of pressure gradients (e.g. the North Atlantic Oscillation (Cornes et al., 2013)), relatively insensitive to small measuring inconsistencies and location changes. The 1960 launch of the first successful weather satellite, TIROS-1, marked the beginning of the new age of meteorological observation, monitoring the major wind producing

storms on a global scale. Today, satellite-based monitoring of winds themselves is widely practised, through scatterometry for surface winds (estimating wind speed and direction through radar backscatter from sea surface waves) and cloud motion vectors for higher level winds (monitoring cloud movement to estimate winds).

Insurance is a form of risk management and has also had a profound effect on human civilisation. Simply helping each other is a form of insurance, aiding someone in a time of need means that you can expect the same treatment if and when you need it. Reinsurance is a more modern concept, where an insurer purchases insurance from other insurers to spread risk, allowing the original insurer to issue policies with higher financial limits than would otherwise have been possible. The performance of an insurance company can be made less volatile through reinsurance, absorbing larger losses and reducing the amount of capital needed to provide coverage. Insurance in the modern sense extends back to the Ancient Chinese and Babylonian merchants from as early as the 3rd millennium BC in terms of spreading risk on their cargo. The earliest known written legal code, the 'Code of Hammurabi', was developed by the Babylonians in ~1780BC and includes laws equating to a form of insurance, with a section ensuring that if a merchant's cargo was lost or stolen during transport, the state would reimburse them for their losses. Throughout ancient and modern history, it was the marine industry that made the most significant steps forward in (re)insurance and the first known (re)insurance contract was concluded in 1370 AD in Italy (SwissRe, 2002). Marine insurance was followed by insurance against fire as the earliest types of insurance; the oldest existing insurance company, the ‘Hamburger Feuerkasse’ (Hamburg fire fund) was founded in the 1670s following a number of intense fires in Hamburg. This gave rise to the development of the insurance industry, with the first reinsurer, the Cologne Reinsurance Company, founded in the 1850s (SwissRe, 2002). Today (re)insurance is a multi-trillion pound industry covering anything from David Beckham's right foot to the infamous payment protection insurance.

## 1.1 Wind in the UK and Europe

One of the key principles of (re)insurance is to limit (spread) the risk of large, or catastrophic, losses. This section briefly describes the UK wind regime, before

highlighting the importance of European extra-tropical cyclone (ETC) events, not only to the population of the affected areas, but to European (re)insurers. Windstorm Klaus of January 2009 is described in detail as an example of the damage and destruction seen during the passage of extreme ETCs.

### 1.1.1 UK wind regime

Located in one of the most common regions for atmospheric blocking, while also situated towards the end point of a major mid-latitude storm track, the UK has one of the most variable wind climates on Earth and NW Europe as a whole is a challenging region for prediction on all time scales (Barriopedro et al., 2006, 2008; Dacre and Gray, 2009; Woollings, 2010). Regional wind climate variability in the UK is large, governed by latitude (proximity to storm track), altitude and type of fetch (the UK has an exceptionally long coastline) as shown in Figure 1.1.

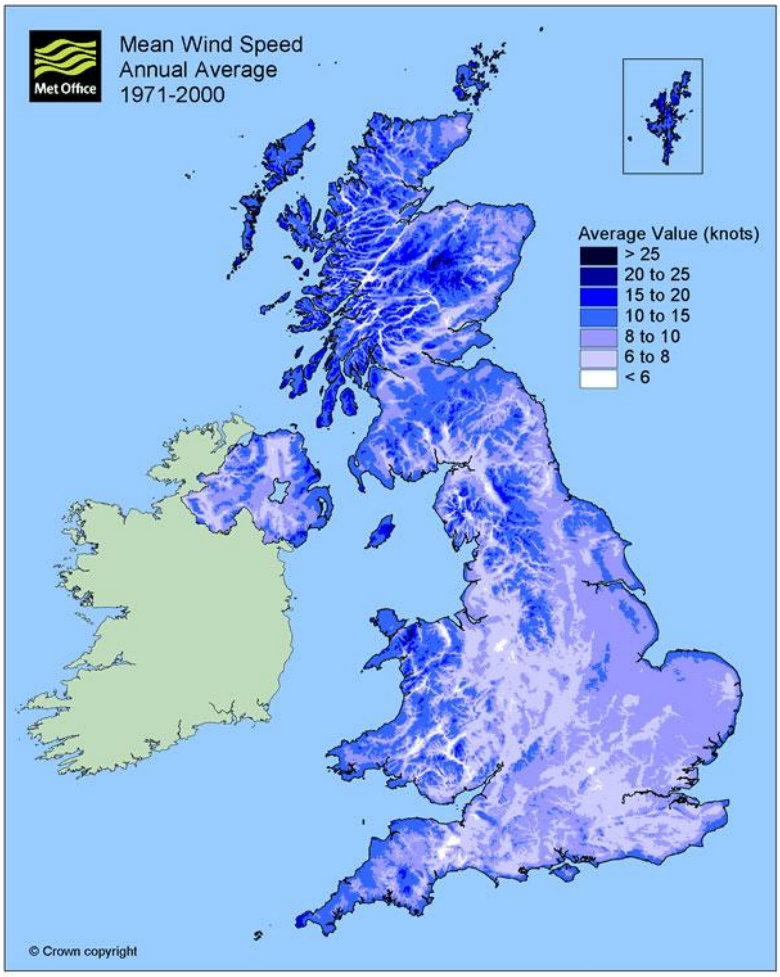


Figure 1.1– 1971-2000 Wind atlas of the UK (UK Meteorological office website; http://www.metoffice.gov.uk/learning/wind/windest-place-in-UK).

Seasons dominated by blocking (reducing losses) or cyclonic weather types (increasing losses), especially winter, can strongly skew the magnitude of annual insured losses (Munich Re, 2002), as well as have profound effects on the variability of wind power generated by the expanding UK wind energy sector (Sinden, 2007).

### 1.1.2 European wind extremes and associated (re)insurance risk

In Europe, windstorms remain the most economically significant weather peril when averaging over multiple years as exemplified by the Great Storm of 1987 (Hewston, 2008; Woodroffe, 1988; Browning 2004), Gudrun of 2005 (Baker, 2009) and Windstorm Kyrill of 2007 (Brönnimann et al., 2012; Hewston, 2008). From 1970-2011, 32 of the 40 most expensive world-wide insured loss events were weather related, 9 of which were located in Europe associated with ETCs, causing extreme winds and widespread flooding (Swiss Re, 2012). The winter storms of the early 1990s had some dramatic effects on the UK, the winter of 1989-90 being one of the most damaging on record (Pinto, 2012). This included the highly damaging Windstorm Daria of 1990 (Hewston, 2008; McCallum, 1990), which tracked across a large swath of England and Wales, causing widespread damage amounting to £1.9bn (equivalent to £3.2bn in 2010 values) of UK insured losses (Munich Re, 2002). A second storm, Vivian, buffeted the UK between 26th and 28th February 1990 and contributed to UK weather related property losses that year reaching their highest mark on record. In the winter of 1991-1992 the New Year's Day Storm affected northern Scotland and (far more severely) Norway (Gronas, 1995), producing stronger UK surface winds than Daria and Vivian, though causing less UK damage due to reduced vulnerability to insurance losses in the affected regions. ETCs have been categorised into three types based on the ratio of upper- (e.g. potential vorticity anomalies) and lower- level (e.g. diabatic heating) air forcing (Dacre and Gray, 2009). Type A cyclones are predominantly low-level forced, type B upper-level forced with low-level forcing that increases with time and type C have strong upper level forcing but weak low-level forcing throughout the life-cycle of the ETC. There is a higher proportion of type B and C ETCs in the east Atlantic affecting Europe, with type A ETCs less common.

Total annual losses attributed to windstorms depend, for example, on the precise track and intensities of storms, the relative vulnerability of the affected areas,

whether trees are in leaf or not and the relative dryness or wetness of the ground at the time of windstorm passage (Hewston and Dorling, 2011). Windstorms Klaus and Xynthia of January 2009 and February 2010 respectively were the most destructive ETCs to affect Europe over the last decade and section 1.1.3 provides a detailed description of Klaus, as an example to highlight the risk of ETCs to insurers and to the European population. Meanwhile winter storm Xynthia in February 2010 caused insured losses totalling almost $3bn in Germany, France and Spain, representing the world's 3rd most costly catastrophe of that year (Swiss Re, 2011), more costly than any 2010 North Atlantic hurricane. Indeed total European windstorm damage is considerable, equivalent to that of worldwide hurricanes when averaged over multiple years (Malmquist, 1999). ETC maximum wind gusts are generally not as high as those seen in tropical cyclones, however the area affected by high wind speed often has a larger footprint (Brönnimann et al., 2012), affecting a wider geographical area.

### 1.1.3 Windstorm Klaus

An example of a recent European ETC is Windstorm Klaus. Throughout the 23rd of January 2009, Klaus tracked north-eastwards towards Western Europe, having developed over the warm sub-tropical Atlantic waters during the preceding days. The ETC moved across the eastern Atlantic, moving at an average speed of 40 mph (64 km/h) and deepened explosively from 1001mb at 00:00 UTC on the morning of the 23rd to a central pressure of 969mb just 18 hours later (EQECAT, 2009). The low pressure centre tracked across the Bay of Biscay during the early hours of the 24th, as shown by the 00:00 UTC surface pressure analysis chart (Figure 1.2), where Klaus had deepened further to 963mb.

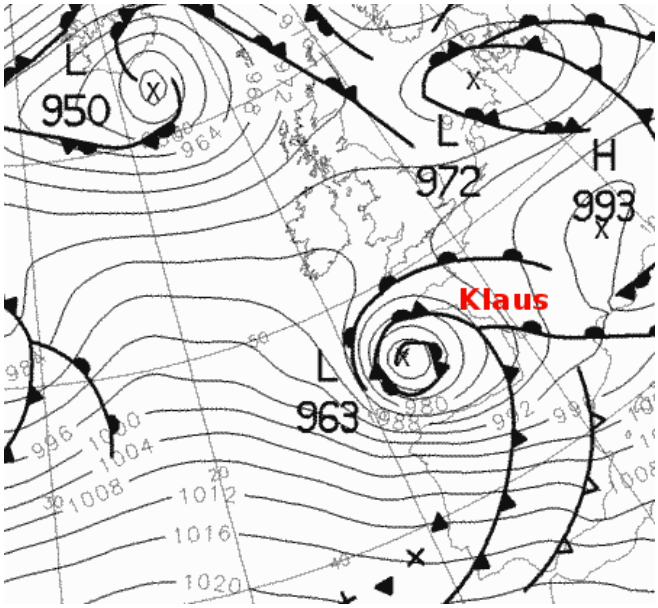


Figure 1.2 – UK Meteorological Office sea level pressure analysis chart at 00:00 UTC on the 24th January 2009 with ETC Klaus highlighted. Source: www.wetterzentrale.de

Klaus made landfall at 04:00 UTC in the south-west of France between La Rochelle and Bordeaux with gusts reaching well in excess of 100 mph (161 km/h) causing widespread damage. The storm tracked across the south of France, causing further damage and disruption here and in the north-east of Spain, reaching the Mediterranean by the early afternoon of the 24th (Figure 1.3).

Gust speeds of 99 mph (159 km/h) were recorded in Bordeaux, and up to 120 mph (193 km/h) in the northeast of Spain (RMS, 2009). The storm was still intense when it reached the Mediterranean coast with gust speeds of 114 mph (183 km/h) recorded at Perpignan (Figure 1.3), then began to weaken and as it tracked across northern Italy the winds had subsided to a maximum of 60 mph. These immense winds 'paralysed' southwest France and northeast Spain (Times Online, 2009), with damage experienced from the Dordogne region to the Pyrenees, leaving 25 people dead (14 in Spain and 11 in France). The swath and strength of the storm are illustrated by the widespread extreme maximum gust speeds seen throughout northern Spain and south-west France as shown in Figure 1.3.

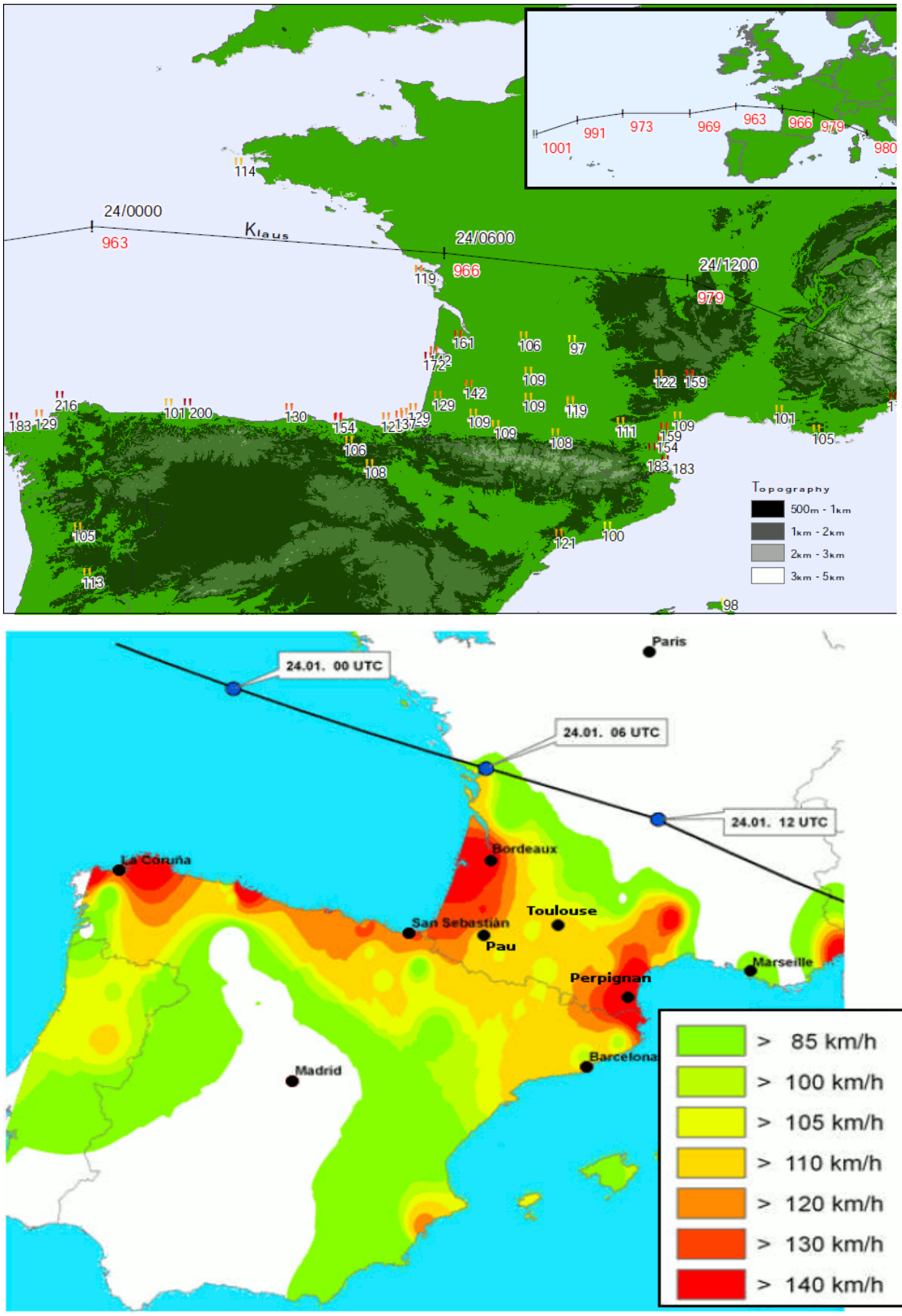


Figure 1.3 - Top – 6-hourly track of Klaus with central pressure in hPa and selected windspeed observations from France and Spain in km/h. Bottom – Maximum windspeed map (in km/h) from Klaus and affected cities (Adapted from Aon Benfield http://www.aon.com/impactforecasting/impact-forecasting.jsp).

The catastrophe modeller AIR Worldwide estimated that insured losses ranged from €350 (~£322) million to €700 (~£643) million in France, with significant losses also expected in Spain (Guy Carpenter, 2009) and according to the Swiss Re (2012) report, Windstorm Klaus caused insured losses totalling $3,418 (£2,362) million, the 35$^{th}$ most costly 1970-2011 event anywhere in the world. This was the 3$^{rd}$ most costly of 2010, more costly than any North Atlantic hurricane of that year. Météo France successfully predicted the strength, as well as the timing of the storm and issued a red alert warning, the highest level of alert (for the first time since this system has been in operation for the last eight years), and advised people to stay in their homes (Times Online, 2009). However, the forecasters did not expect the devastation to be as widespread as it was, with a less significant swath predicted, which highlights the difficulty/challenge associated with accurate extreme ETC forecasting.

## 1.2 Wind climate fluctuations in the NE Atlantic region

It is known that the wind in Europe is highly variable and that ETCs can cause major damage and fatalities, as explored in the previous section, but how and why do these variations occur? This section explores this variability in more detail from annual to decadal time-scales and highlights possible drivers.

Wang et al. (2009) demonstrated that storminess in the North-Atlantic-European region, based on atmospheric sea-level pressure gradients, undergoes substantial decadal and longer time scale fluctuations and that these changes have a seasonality and regionality to them. In particular, these authors showed that winter storminess reached an unprecedented maximum in the early 1990s in the North Sea and showed a steady increase in the north-eastern part of the North-Atlantic-European region, significantly correlated with variability in the North Atlantic Oscillation (NAO) index. The link to the NAO is found in all seasons except autumn. As the NAO swings from one phase to the other, large changes to windstorm intensity, track and to mean windspeed and direction are observed over the Atlantic (Hurrell et al., 2003). Both Atkinson et al. (2006), analysing the period 1990-2005, and Boccard (2009), 1979–2007, showed that the NAO gives good approximations for wind indices over Northern Europe. The same cannot be said however for synoptic weather types classifications including the Grosswetterlagen (Hess and Brezowsky, 1952; James, 2007) and the

Jenkinson-Collison weather type classification (Jenkinson and Collison 1977; Jones et al., 1993; Jones et al., 2013), with the decrease since early-1990s northern European windiness, seen in observational studies (e.g. Vautard et al., 2010; Earl et al., 2013), not so apparent. By considering the longer term Grosswetterlagen and Jenkinson variability through the 20th century, these authors concluded that care is needed in selecting the most appropriate long-term period on which to base wind energy investment decisions. Also, access to reliable and longer term windspeed measurements is highly desirable, an issue which the 'Twentieth Century Re-analysis' project and its successor 'ERA-20C' (see section 1.5.1) are addressing.

As greater reliance on wind power for electricity generation needs increases, so will the magnitude of risk due to exposure of the performance of the turbines to climate change (Harrison et al., 2008). The cold European winter of 2009-10 and the extreme cold of December 2010 have prompted much discussion about long-term climate variations and their possible impacts. However, Cattiaux et al. (2010) show that the cold European surface temperature anomaly of up to 6˚C for winter 2009-10 was in fact not as great as might have been expected given the associated record-breaking NAO and blocking frequency indices. In winter, blocking (usually associated with strong negative NAO) high pressure usually brings cold and calm conditions to the UK. These authors concluded that the event was a cold extreme which was not in any way inconsistent with an otherwise generally warming climate.

Focusing on predictability at the monthly, seasonal and decadal timescale, many forcing agents are thought to modulate European climate, for example sea surface temperatures, stratospheric circulation and solar variability (Rodwell et al., 1999; Lockwood et al., 2010, 2011; Woollings et al., 2010). Regional responses also arise from the dynamical reaction of the climate system to this forcing (Woollings, 2010; Jung et al., 2011) and internal atmospheric dynamics can be an important source of atmospheric inter-annual variability. Solar activity in 2009/10 fell to values unknown since the start of the 20$^{th}$ century and Lockwood et al. (2010), linking this to the occurrence of recent cold European winter months, estimate an 8% chance that the decline, which began around 1985, could continue to Maunder minimum levels within 50 years, from the previous grand solar maximum. However, ECMWF experiments

(Jung et al., 2011), testing the sensitivity to reduced ultra-violet radiation of the onset of the cold 2009-10 European winter, show that the unusually low solar activity contributed little, if any, to the observed NAO anomaly and that internal atmospheric dynamical processes were responsible. However, this study only reduced the ultra-violet of the solar radiation spectrum, rather than the solar constant, which is now incorporated in models spectrally, with associated knock on effects. Much research is ongoing to improve our predictive capability in Europe.

Hewston (2008) introduced for the first time an hourly windspeed database for a network of 43 UK surface stations, extending through the period 1980-2005 and providing good spatial coverage. Based on this they presented a climatology of the strongest wind gusts in the context of insurance weather perils. These authors presented evidence of an apparent downward trend in the strongest wind gusts over the UK since the early 1990s. In addition, Vautard et al. (2010), also using surface station data, reported that mean windspeeds have also been declining over the same period across most areas of the world, including Europe, a phenomenon which they termed “global stilling” and which they linked to changes in land-based biomass. However, while a decline was also found in Australian 2m windspeed observations by Troccoli et al. (2012), their equivalent 10m measurements actually showed a positive tendency.

Despite the improvements seen in numerical weather prediction (NWP) models and climate models over the past few decades, observations still play a key role in meteorology and climatology from operational forecasting to climatological studies dating back centuries. On a decadal time-scale the development of re-analysis projects (as discussed in section 1.5) have become increasingly important, however studies such as Vautard et al. (2010) and Smits et al. (2005) show that re-analysis can miss variability in surface winds for reasons such as changes in land-use. This highlights the sustaining importance and relevance of surface station observations, filling in knowledge gaps in this ever increasing computer modeling driven field.

## 1.3 Surface observations of mesoscale ETC features

It is clear from the previous sections that ETCs have a major impact on Europe, can generate hurricane force surface winds and possess considerable temporal variability. But what is it about these ETCs that generate such damaging winds? This section explores the mesoscale features within ETCs which can be associated with observed extreme surface winds.

There has been much research addressing the synoptic scale structure of ETCs since the development of the Norwegian cyclogenesis model, as reviewed by Henry (1922), developed at the Bergen Geophysical Institute, chiefly by Bjerknes in the late 1910s. It was the first conceptualised ETC life-cycle model, locating cyclogenesis along the polar front and dividing the cycle into stages of the typical life of a low pressure system in the extra-tropics, as explained in the literature (e.g. Parton et al., 2010). Development of the ETC life-cycle conceptual model culminated in the conveyer belt paradigm as summarised by Browning (1990) and the development of the Shapiro and Keyser (1990) cyclone life-cycle model (Figure 1.4). In addition, Schultz and Vaughan (2011) furthered the occlusion front paradigm within the Norwegian cyclogenesis model suggesting that viewing the occlusion process as wrap-up rather than catch-up resolves anomalies within the conceptual model and provides a better and more general fluid-dynamical description of the occlusion process. In this thesis the Shapiro and Keyser (1990) cyclone life-cycle model is applied to the identified storms to describe their development stage (Figure 1.4).

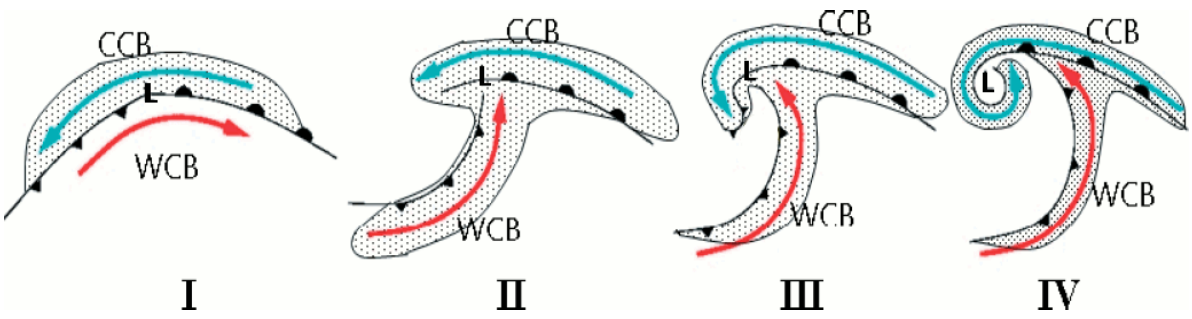


Figure 1.4 - Shapiro-Keyser conceptual model of the life cycle of an extratropical cyclone: (I) open wave, (II) frontal fracture, (III) bent-back front and frontal T-bone, and (IV) mature, frontal seclusion. The cold and warm conveyor belts (CCB and WCB respectively) are marked along with the low pressure centre (L) along with the cloud signature (Adapted from Baker, 2009).

This work however did not focus on the more localised most damaging winds seen within ETCs (Parton et al., 2009) and Browning (2004) identified the most extreme winds to be associated with a mesoscale feature at the end of the cloud head known as a sting jet (SJ), which was proved to be the case for the 1987 '16$^{th}$ October Storm' (Clark et al., 2005) and for Windstorm Jeanette in October 2002 (Parton et al., 2009) amongst others. The SJ is a short lived (a few hours) mesoscale feature associated with strong evaporation at the tip of the cloud head hook conceptualised by Browning (2004), described in Table 1.1. However Baker (2009) found that the strongest surface winds during Windstorm Gudrun of January 2005 were associated with the cold conveyer belt as it wraps around the low pressure centre and joins the momentum of the cyclone (rCCB). Meanwhile Clark (2011) developed a climatology of quasi-linear convective systems (QLCSs). These lines of organised and strong convection occur mainly along cold frontal boundaries in the UK, though a few occur in association with occluded fronts. Pre-frontal QLCSs were not included in Clark's (2011) climatology. This climatology was not constructed with surface wind gusts in mind; however they are well-known for producing strong winds, including intense downburst winds, a rear inflow jet (Weisman, 2001) and low-level mesovortices, all of which may produce damaging straight-line winds (Davis et al., 2004; Wheatly et al., 2006). The rear inflow jet and mesovortices usually travel perpendicular to the orientation of the line, as distinct from the winds within the parallel-flowing warm-conveyor belt (WCB), which is found ahead of many narrow cold frontal rain bands in ETCs (Browning, 2004). QLCSs are particularly common in the USA and are sometimes known as squall lines. QLCSs that present a strongly-bulging structure are referred to as bow echoes (Weisman, 2001). These systems have also been reported in Europe (Gatzen et al., 2011). Other mesoscale features occur during ETCs, such as troughs and other forms of convective systems, which can also result in damaging surface windspeeds, as shown below in Table 1.1 and in Figure 1.5.

Figure 1.5 displays the conveyor belts and other sub-storm features and their respective locations, within ETCs, where the highest surface impacts are likely during transition from stage III to stage IV of the Shapiro-Keyser conceptual model of the life cycle (Figure 1.4). The warm-conveyor belt (WCB) for example starts at low levels before rising above the warm front, with cold air below, so is most likely to affect the

surface in the warm sector as indicated in Figure 1.5, rather than nearer the warm front where it has been forced upwards. The a-b cross section in Figure 1.5 (right) shows the relative vertical positions of the SJ, rCCB and the DCB in ETCs which possess a well developed SJ that reaches the surface. Not all ETCs will follow the Shapiro-Keyser conceptual model life cycle, depending on whether the ETC is embedded in diffluent or confluent large-scale flow in the upper-levels and, if the former, will follow a life-cycle more akin to the Norwegian life-cycle model as explored by Schultz et al. (1998). Also, many ETCs will not contain all of these features, some for example not producing a SJ due to not deepening explosively enough (Browning, 2004). Furthermore, features may be present in many ETCs but have no observable effect on the surface winds. However all features shown in Figure 1.5 have been observed to cause extreme surface windspeeds within ETCs.

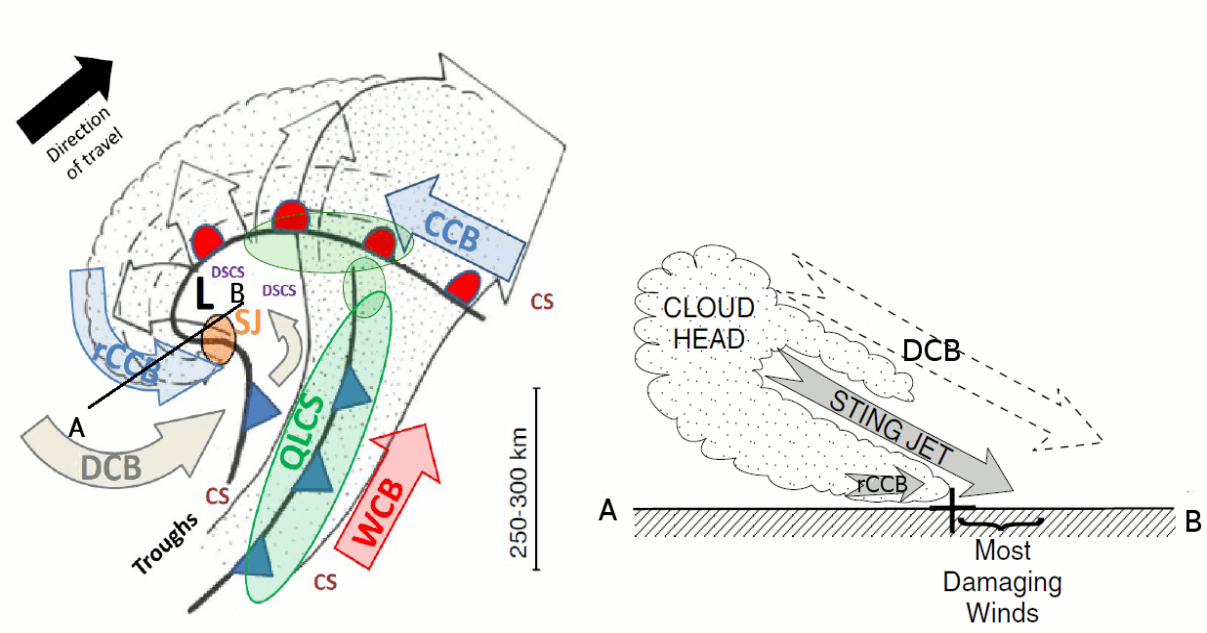


Figure 1.5 - (Left) Conceptual model of sub-storm features within an ETC, during transition from stage III to stage IV of the Shapiro-Keyser conceptual model of the life cycle of an extratropical cyclone (in Figure 1.4 ; adapted from Browning 2004). Features are marked as follows: CCB - cold conveyor belt; rCCB – returning cold conveyor belt; WCB - warm conveyor belt; DCB - Dry conveyor belt; QLCS – Quasi-linear convective systems; SJ – Sting Jet; DSCS – Dry slot convective systems; CS - Convective systems: (Right) Vertical cross-section of the A-B line (in left), displaying the relative positions of the conveyor-belts seen during sting jets and the region of cloud (adapted from Clark et al., 2005).

| | **Description of features associated with extreme surface gusts as depicted in Figure 1.5** |
|---|---|
| Cold conveyor belt (CCB) | Flows cyclonically around the cyclone centre at low levels and rises slowly (thermally indirect) along the cold side of and parallel to the warm front (Carlson, 1980). Typically travels against the flow of the system, with respect to the surface, often dampening its surface impact. |
| Returning cold conveyor belt (rCCB) | As the CCB rotates around the centre of low pressure, forming a secondary cold-front and the hook to the west of the cloud head, it rejoins (returns from the western side of the low pressure centre) the direction of ETC travel and often descends to the surface (Clark et al., 2005; Baker, 2009) creating strong winds. Usually seen in stage IV of the Shapiro-Keyser life cycle model (Figure 1.4). The rCCB is also used to describe the strong wind often produced by a high pressure gradient seen in the latter stages of development (IV) in the cold air following in behind the system, equatorward of the low pressure centre. |
| Warm conveyor belt (WCB) | A broad region of usually moderately strong wind in the warm sector, originating at low levels, flowing pole-wards and rising as it approaches the warm front. Depending on the maturity of the ETC, it can rotate anti-cyclonically (stages I-III of Shapiro-Keyser) once over the warm front to join the direction of travel or rotate cyclonically around the low-pressure centre (stages III-IV) forming the cloud head with some flow travelling at low levels across the dry slot before rising above the bent back front (Browning, 2004). |
| Dry conveyor belt (DCB) | Also known as the dry intrusion, the DCB contains cold, dry air descending from the upper troposphere or lower stratosphere, forming a dry slot, producing a region of clearing skies behind the cold front. The cloud free dry intrusion penetrates into the frontal cloud separating the cloud head from the polar front cloud band to form the comma pattern seen in stage II-III and as the cyclone develops further the cloud head wraps around the dry slot and begins to dissipate (Dacre et al., 2012). Strong winds are often experienced at the surface associated with the lower part of this sinking air (Cotton and Anthes, 1989), though Gray et al. (2011) state that the dry slot of an ETC is not usually associated with strong winds. |
| Quasi-linear convective systems (QLCS) | Also known as squall lines or bow echoes (usually in the USA), QLCS are lines of organised and strong convection, which occur mainly along cold frontal boundaries in the UK, with the remainder along the warm front or during post-frontal situations (Clark, 2011). QLCS produce strong winds where the strongest precipitation occurs, as intense downburst winds, a rear inflow jet (Weisman, 2001) or low-level mesovortices producing damaging straight-line winds (Davis et al., 2004; Wheatly et al., 2006), usually travelling perpendicular to the orientation of the front line, as distinct from the parallel flowing WCB. Clark's (2011) threshold criteria include:<br><br>Dimensions - Length ≥ 100 km, at the time of maximum extent; length ≥ 10 x width.<br>Duration - A coherent line (meeting the below intensity criteria) must |

| | |
|---|---|
| | persist for ≥ 2 hours.<br>Intensity - A continuous, or near continuous, line of rainfall rates ≥4 $mmh^{-1}$ (equivalent to 32.6dBZ). |
| Sting Jet (SJ) | Short lived (a few hours) mesoscale feature associated with strong evaporation at the tip of the cloud head hook, enhancing the dry slot windspeeds, dubbed the 'sting in the tail' or Sting Jet (SJ) (Browning, 2004; Clark et al., 2005). Latent heat release from the evaporation of cloud droplets and rainfall within this region of slantwise descent results in strong gusts at the surface. Conditional symmetric instability (Gray et al., 2011) in, and upwind of, the dry slot region can produce mesoscale slantwise circulations, also contributing to the severity of the SJ. Only seen in stages II and III of the Shapiro-Keyser life cycle model and replaced by the rCCB in stage IV. Parton et al. (2010) identified just nine potential SJ cases in seven years passing over Aberystwyth, with Martínez-Alvarado et al. (2012b) suggesting that they are a generic feature of ETCs occurring in between 23 and 32% of the strongest ETCs. |
| Dry slot convective systems (DSCS) | Convective systems occur within the dry slot and can produce damaging surface wind gusts. Browning (2004) suggests that these are generated by differential rotation with height around the cyclone centre, creating overrunning of low over high wet-bulb potential air in the dry slot releasing potential instability. |
| Convective systems (CS) | Small area of unorganised convection producing heavy showers and strong downdrafts down to the surface, triggered by localised upper-level divergence or low-level warm air advection associated with the passing of an ETC. This category also includes supercells and thunderstorms not associated with an ETC. |
| Pseudo quasi-linear convective systems | A line of strong wind and heavy rain producing organised convection which does not reach the status of QLCS as described by Clark (2011), but possesses the distinct characteristics. This includes troughs and frontal boundaries with a clear line of showers. |

Table 1.1 - Description of the ETC features responsible for surface gusts

So the natural question arising from this relates to the relative contributions of these mesoscale ETC features to associated extreme surface windspeeds, assessing whether SJs, receiving the most attention in the literature, are prominent, or whether it is another mechanism that causes the extremes.

## 1.4 Global forecasting models

The previous section explores the various features within ETCs that are associated with extreme surface wind speeds and discusses our understanding of them. But can they be forecasted operationally? This section introduces a forecast data archive that is available to the research community and describes how it can be harnessed for ETC studies.

The weather is chaotic in nature and has been a major challenge for forecasters to predict since the first ever attempt by Admiral Robert Fitzroy in 1861. Today, the tools available are far superior to those of the 19th century with the widespread use of supercomputers running state of the art global NWP models and high-resolution limited area NWP models based at numerous meteorological centres throughout the world, ingesting the latest in meteorological observation technology through state-of-the-art data assimilation systems (Inness and Dorling, 2012).

### 1.4.1 Global Forecast Models and ensembles

Models are initiated with a set of initial conditions, based on a combination of a previous forecast from an earlier model run and the latest observations, from which to run the various physics and parameterisation schemes to produce the deterministic weather forecasts for time-steps from a few hours to seasons and on to centuries ahead (in the case of climate models). Small errors in the initial conditions of a forecast can grow rapidly and significantly affect predictability (Buizza et al., 2005). In addition, predictability is flow-dependent and limited by model errors linked to the inaccurate simulation of atmospheric processes in NWPs. These two sources of uncertainty limit the skill of single, deterministic forecasts in an unpredictable way, with the knock-on effects of a poor quality short-term forecast impacting on medium-range forecast accuracy, with no indication of the confidence in the simulation. Ensemble prediction is a powerful alternative way to complement a single, deterministic forecast with an estimate of the probability density function of a spread of possible forecast states.

Over the last two decades, major meteorological weather prediction centres, from around the world, have invested heavily in Ensemble Prediction Systems (EPS),

alongside their increasingly high-resolution deterministic models. Indeed these two forecasting approaches compete for IT resource. The coarser resolution ensemble forecasting is now generally accepted as a powerful approach which enables an estimate of forecast confidence, especially for extreme events (Bougeault et al., 2010) such as ETCs. The respective meteorological centres perturb their deterministic model analyses in a variety of ways to power their EPSs, for example the European Centre for Medium-Range Weather Forecasts (ECMWF) use singular vector perturbations aimed at sampling the fastest growing variations, as described in chapter 2.2.1. A suite of slightly different (but plausible) initial conditions and boundary conditions are produced and along with variable parameterisation settings, (since many small-scale features in the atmosphere cannot be resolved by the model) a spread of equally likely forecast outcomes is produced. Some major meteorological centres also perturb the physics schemes within their respective NWP models to produce a wider and a more representative spread of the forecast uncertainty. Perturbations of the initial state are consistent with the available observational data (Mureau et al., 1993) and are particularly useful for assessing the confidence of extreme event forecasts due to their varied and unpredictable nature and high potential impact (Jung et al., 2005). Initial conditions, parameterisation and model physics schemes are discussed in Chapter 2.2.1. Both modelling approaches use nests embedded within the coarser parent domain (usually global model), which allows an area of interest to be viewed at significantly higher resolution rather than running at high resolution for the whole globe, saving significant time and computer power (see section 2.3.2).

EPS are especially useful for medium range forecasts, revealing the degree of predictability in the forecast. The ECMWF and National Centers for Environmental Protection (NCEP) began to use the ensemble approach as early as 1992 (Froude, 2010), with other leading meteorology centres soon to follow. In early validation of the ECMWF ensemble, Buizza et al. (1999) found that there was an evident improvement in the skill of the ensemble mean with respect to the control forecast after about day 4. When ECMWF first implemented model physics perturbations, the effect was to increase the ensemble spread (Buizza et al., 1999), indicating a need to compare models which do perturb physics schemes and those which do not. This is also the case for multi-model investigations, with Weigel et al. (2008) of the Swiss

meteorological centre ‘MeteoSchweiz', finding that that the use of a multi-model approach widens the forecast spread, but generally moved the mean closer to the truth. With many centres running their own independent EPSs, alongside their deterministic forecasts, meteorologists in the research community were naturally keen to compare and combine them to produce a multi-model ensemble. However, the difficulty was for the research community to access and coordinate the vast amounts of associated EPS output data. Some studies comparing the EPSs were undertaken in the early 2000s (Buizza et al., 2005; Bourke et al., 2004; Mullen and Buizza, 2001), however, comparing data in contrasting formats, resolution and computational grids is complex and problematic. Therefore, something needed to be done to facilitate extensive inter-centre forecast comparison.

### 1.4.2 THORPEX Interactive Grand Global Ensemble (TIGGE)

In 2005 a World Weather Research Programme, The Observing System Research and Predictability Experiment (THORPEX) Interactive Grand Global Ensemble (TIGGE), was conceived at a workshop at ECMWF (Richardson et al., 2005).

Early TIGGE-based studies included Pappenberger et al. (2008) who used TIGGE for early flood forecasting and warning, Park et al. (2008) who analysed forecast performance of the different models in the upper troposphere and Matsueda (2009) who assessed the predictability of atmospheric blocking events. Other TIGGE studies, particularly related to this project, include Froude (2010) who analysed the prediction of Northern Hemisphere ETCs, using a feature tracking methodology to identify and track the cyclones along the forecast trajectories, and Johnson and Swinbank (2009) who verified whether a multi-model ensemble combining ECMWF, NCEP, and the UK Met Office (UKMO) EPSs was superior to the respective single-model ensemble. Wiegand et al. (2011) investigated the forecast quality and predictability of synoptic and mesoscale aspects of a high-impact precipitation event, causing flooding on the southern side of the European Alps, in operational ensemble predictions from nine of the TIGGE meteorological centres. Meanwhile Keller et al. (2011) examined the TIGGE forecast characteristics of the extra-tropical transition of tropical cyclones and their impact on the mid-latitude flow. These examples highlight the wide range of research activities possible with the wealth of forecast data available within TIGGE.

Generally, the results favour the multi-model approach. Johnson and Swinbank (2009) show that the multi-model ensemble gives an improvement in comparison with a calibrated single-model ensemble for mean-sea-level pressure, 500hPa height and particularly for surface temperature, though do not mention the reason why other TIGGE members were left out of their investigation. Keller et al. (2011) conclude that the full TIGGE suite of ensemble members has more variability and thus offers a broader range of possible development scenarios during an ETC event than ECMWF alone, which is advantageous. Matsueda and Endo (2011) also suggest that the multi-model is beneficial, predicting the Madden-Julian Oscillation better than individual centre models, though it must be noted that the importance of this equatorial region is weighted differently from the extra-tropics in the various models. Froude (2010) however suggests that ECMWF has the most skill for storm intensity and track, though this is highly dependent on whether the 'truth' is considered to be the analysis of the ECMWF or that of the other respective models; Wiegand et al. (2011) concluded that there were surprisingly large discrepancies between different analyses and suggested that these should be more routinely accounted for and this point is addressed in the third set of research aims (section 1.6).

### 1.4.3 TIGGE-Limited area model (TIGGE- LAM)

Shortly after the establishment of TIGGE, a TIGGE-LAM panel of experts was established to support the development of the Limited Area Model (LAM) EPS component of TIGGE, aiming to create a database of limited-area ensemble products, similar to that of the global TIGGE database. Other objectives were to encourage a coordinated approach to LAM EPS, recommend solutions to allow better collaboration between meteorological centres, formulate proposals to facilitate the 'interoperability' of the contributing modelling systems and relocate existing LAM EPS systems, already tested and applied on specific regions, in other areas not covered by these forecasting systems (Bougeault et al., 2010; www.smr.arpa.emr.it/tiggelam/). Unfortunately, TIGGE-LAM has somewhat stalled over the last two years, which means that it has not developed as a key resource for this thesis. However TIGGE-LAM is still in the plans of numerous European meteorological centres; a recently updated plan is available at http://www.wmo.int/pages/prog/arep/wwrp/new/documents/THORPEX_17_TIGGE_LAM.pdf. The TIGGE-LAM plan acknowledges the difficulties involved, due

to the fundamental nature of LAM preventing centres from contributing to global studies, due to the limited geographical coverage of each contributor, but there are enough instances of overlapping spatial domains to warrant a continuation of the project in the future.

## 1.5 Atmospheric modelling

The previous sections have explored wind in the UK and Europe, with an emphasis on (re-)insured loss generating ETCs, and examined the available data for forecasting such events. This section investigates the research projects providing data for past ETC events, along with assessing the available modelling tools for simulating these events and comparing the recent developments in this ETC field with the ongoing tropical cyclone field, determining the extent to which tropical cyclone research can be of use in this study.

### 1.5.1 Re-analysis and HiGEM

Since the 1990s, major international efforts have led to the development of climate datasets called retrospective analyses or 're-analyses' as a substitute for the absence of reliable long term observational data. Both the NCEP/ National Center for Atmospheric Research (NCAR) and the ECMWF have constructed re-analysis datasets, with the objective of producing a comprehensive global atmospheric circulation dataset over an extended time period (Compo et al., 2011; Dee et al., 2011). ERA-Interim is the third global atmospheric re-analysis produced by the ECMWF evolving from ERA-15 and ERA-40 as described in detail by Dee et al. (2011), and forms the basis for many climatology studies (e.g. Hewston and Dorling, 2011) as well as providing the boundary conditions for higher-resolution mesoscale modelling. Limitations to this re-analysis dataset with regard to wind speed include the fact that variables such as maximum wind gusts may not be properly simulated due to insufficient resolution to capture local-scale variations of the terrain that are important for deriving reliable wind fields (Frank and Majewski, 2006), though reanalysis is often used to drive higher-resolution models to negate this limitation. ERA-interim, spanning from 1979-present, is not long enough to contain a large sample of extreme storms for a given region (Brönnimann et al., 2012) a reason for numerous studies to opt for observational data (e.g. Wang et al., 2009). Some of these

issues are partly addressed with the latest NCEP/NCAR re-analysis offering, a global 'Twentieth Century Re-analysis' (Compo et al., 2011) stretching back to 1871 supporting analyses of historical events (e.g. Brönnimann et al., 2012) consisting of 56 ensemble members, each of which is physically consistent and equally likely, helping to quantify uncertainty. This project assimilates only surface pressure reports unlike the shorter re-analysis projects which also ingest daily or 5-daily SST, sea-ice, radiosonde, satellite, temperature and humidity data. Unfortunately the latest version of the 'Twentieth Century Re-analysis' was initiated too late to be of great use in this thesis, however it could be of use in work succeeding this project, along with its successor ERA-20C (run from 1900 with updated NCEP model, available in 2014), to assess how faithfully it simulates the recent ETCs compared with surface station observations.

The U.K.'s first High Resolution Global Environmental Model (HiGEM) has been developed as part of a project partnering the Natural Environment Research Council (NERC), the U.K. academic community and the UKMO Hadley Centre. The main objective is to improve the resolution in both the atmosphere and ocean of the latest climate configuration of the UKMO Hadley Centre Global Environmental Model version 1 (HadGEM1) and HiGEM forms a major part of the UK–Japan Climate Collaboration (Shaffrey et al., 2009). For the first time, scientists from many different areas of NERC are working together in a concentrated effort to improve state-of-the-art global environment modelling, which has been fragmented in the past. As the resolution of HiGEM becomes higher, the gap between modellers and scientists specialising in particular processes and phenomena has been narrowed, as well as between models and observations of the Earth system. The success of HiGEM, as evaluated by Shaffrey et al. (2009), indicates what can be achieved through collaboration and sharing of information, somewhat lacking between high-resolution operational forecasters and the research community. Re-analysis plays a role in this high resolution project, with ERA-interim is used to drive the HiGEM model. This dynamical downscaling of re-analysis data approach has also been used in the 2004-2009 ENSEMBLES project, a climate change research project involving 66 partners from across Europe (ENSEMBLES website: http://www.ensembles-eu.org/). The project's main objective was to allow the uncertainty in climate projections to be

measured, so that a clearer picture of future climate could be formed. Re-analysis driven (both ERA-40 and ERA-interim) dynamical downscaled hindcasts were used to assess the quality of global/regional climate model runs in assessing uncertainty, with the time sequence in the re-analysis the same as in reality. This highlights how re-analysis products can be very useful despite the limitation of a coarse grid.

### 1.5.2 High-resolution windstorm modelling

With the absence of a TIGGE-LAM co-ordinated resource, researchers have turned to running high resolution models based within their respective institutions. For example, the Consortium for Small-scale Modelling (COSMO) was formed in October 1998, by a collaboration between the German and Swiss national weather services, the 'Deutscher Wetterdienst' (DWD) and 'MeteoSchweiz' (MCH) respectively, with the aim to develop, improve and maintain a non-hydrostatic limited-area atmospheric model, used both operationally and for research purposes by the members of the consortium. Many other European national and regional weather services have since joined COSMO and high-resolution modelling research is ongoing at numerous institutions throughout Europe using the COSMO-model (http://www.cosmo-model.org/). Similarly, the Weather Research and Forecasting (WRF) system, released in December 2000, is a mesoscale NWP and atmospheric simulation model designed for operational forecasting and research alike, promoting better links between the two communities (Michalakes et al., 2001). WRF is a collaborative effort, originating in the United States, whose developers include divisions of the NCAR and NCEP among many others (Skamarock et al., 2008) and has a more global user-base than the more European based COSMO model (http://www.wrf-model.org/). In the UK, most of the research community use the Unified Model (UM), which is the UKMO's NWP and climate modelling software suite, with coupled ocean and atmospheric models, run independently or sequentially (Davies et al., 2005). The UM is also used and adapted by many global forecasting centres and research institutions around the world. (http://www.metoffice.gov.uk/research/modelling-systems/unified-model).

All of the aforementioned NWP systems (or mesoscale modelling systems) are used, operationally or in research mode, to simulate European ETCs at high resolution for a variety of specific research purposes, focusing on certain aspects of ETCs. Extreme

wind related objectives range from the simulation of specific small scale transient features within ETCs, to decadal long climatologies of ETC tracks. The sub-storm mechanisms within European ETCs (as discussed in section 1.4) have been simulated in high-resolution to varying degrees. The SJ has been investigated widely using high-resolution NWP systems (e.g. Clark et al., 2005; Baker, 2009; Martinez-Alvarado et al., 2012) and indeed must be modelled with both high horizontal and vertical resolutions to reproduce realistic simulations, as highlighted by Martinez-Alvarado et al. (2010) for SJ simulation.

The extent to which high-resolution has been used to specifically model QLCSs over the UK is lacking, however WRF has been used to successfully simulate the mechanism over the USA; Atkins and Laurent (2009) found, by analysing quasi-idealised simulations of the 10 June 2003 bow echo event over St. Louis, USA, that the strongest ground-relative wind speeds were produced by mesovortices that formed near the descending rear-inflow jet rather than the often assumed rear-inflow jet itself or tornadoes causing the most extreme surface winds (Weiseman, 2001). The larger sub-storm mechanisms are naturally simulated more successfully with low-resolution NWP model output data due to their much larger scale as displayed by the Eckhardt et al. (2003) 15 year climatology of WCBs using $1^{o}$ x $1^{o}$ ERA-15 output.

Nevertheless, for forecasts and accurate simulations, it is not just small scale transient features within ETCs that benefit from high horizontal and vertical resolutions, but ETCs themselves. Froude (2010) shows that these are necessary to accurately simulate the tilted structure of baroclinic systems, which are critical to the growth and decay of cyclones. Furthermore, recent climatological studies are being undertaken using mesoscale modelling as indicated by Born et al. (2012) using the COSMO model to simulate 158 1972-2008 ETCs, comparing three wind gust estimation methods against surface observations in Germany. The COSMO model is also used by Kruschke et al. (2012) to compare downscaling approaches from 100 winter ETCs, finding that statistical downscaling is as good as dynamical for short lead times.

WRF, usually used on tropical storms as discussed in section 1.5.3, has recently been used to simulate ETCs. Odell et al. (2012) used WRF to model the deepest ETC ever

recorded (the Braer Storm of January 1993) assessing the effect of Greenland's topography on storm tracks including a sensitivity study of neglected diabatic processes and finding that latent heat release accounted for 30mb of the cyclone's deepening. Baker et al. (2012) used WRF to simulate an ETC from the 13th November 2009 (named windstorm Hans, section 4.1.3), investigating the impact of changing the microphysics schemes, and found that the advanced double-moment Morrison and Thompson schemes show 12-hour mean 10m winds about 50% higher than the simpler WSM3 (WRF single moment) scheme in the rCCB (Figure 1.5), suggesting that ice processes play an important role in the downward transport of momentum within the rCCB. Addressing the impact of microphysics schemes on the simulated surface winds is an objective of the study, as seen in the third set of research aims in section 1.6.

UK-based European ETC simulations have mainly been undertaken using the UM, as is the case with the work carried out on SJs (Clark et al., 2005; Baker, 2009; Martinez-Alvarado et al., 2012b; among others). Studies which use and compare multiple high-resolution NWP systems have been conducted, including work done by Martinez-Alvarado et al. (2010) using both the COSMO model and the UM to simulate a SJ during the passage of a cyclone over the UK on 26 February 2002, finding that both models are capable of reproducing sting jets with similar, though not identical, features. Martinez-Alvarado et al. (2012a) also uses the COSMO model and the UM, both initialised at 0600 UTC 23 November 2009 from ECMWF operational analysis fields, to investigate the diabatic processes and the structure of the WCB for an ETC case study (23rd-25th November 2009, named windstorm Max (section 4.1.3)), with results pending. (For list of low pressure systems see Institute of Meteorology of the Free University of Berlin, available from http://www.met.fu-berlin.de/adopt-a-vortex/)

### 1.5.3 Tropical cyclones

This thesis does not exclusively benefit from studies relating to the simulations of ETC events, but can also make use of research concerning the simulation of cyclones in tropical regions. Shaffrey et al. (2009) describe the improvements of the performance in the tropics of the increase of resolution of the coupled climate model HadGEM1.2,

and this is true for the high-resolution simulation of cyclones in tropical areas. The ability of NWP systems to predict tropical cyclone tracks has improved greatly over time compared with the corresponding intensity prediction, with mesoscale models being no exception to this rule. Hill and Lackmann (2009) found that the intensity of an idealised tropical cyclone was greatly amplified by increasing resolution from 36km, to 12km and 4km in the WRF-ARW model, comparable to empirical estimates of maximum intensity in the 4km grid spacing run. This is consistent with other literature for Hurricane NWP model research (Persing and Montgomery, 2003; Braun et al., 2006) resolving storm dynamics better at higher resolution and resulting in more intense wind speeds. Hill and Lackmann (2009) also found intensity sensitivity to surface layer and planetary boundary layer parameterisation schemes, most significantly in the 4km run. This is true, not just with idealised cases, but with examples using real data, with Pattanayak and Mohanty (2008) conducting a diagnostic analysis of a very severe cyclonic storm `Nargis' over the Bay of Bengal, using the WRF-ARW system, focusing on forecasting the cyclone track rather than its intensity. The system's track was difficult to predict operationally due to the cyclone not following the climatological path, making landfall on the Myanmar coast (East of the Bay) rather than the usual Indian or Bangladeshi coast (North/Northwest of the Bay). WRF was run at 27 km and 20 km resolution to get the real time forecast of 'Nargis', using initial conditions from the analysis up to four days prior. The model simulated the system well with an improvement, again, in the higher resolution run, more accurately reproducing the storm track. However the time delay of landfall was more severe.

Sensitivity studies of tropical cyclones are also of use to this study, be it, for example, the sensitivity of storm simulations to different boundary-layer or cloud microphysics schemes in studies such as Nolan et al. (2009), who examined two boundary-layer schemes in the WRF Model, (the Yonsei University and the Mellor– Yamada– Janjić schemes). They examined the relative effects on the mature hurricane stage, concluding that although there were many differences in detail between the schemes, all the simulations were ‘in good agreement with the detailed analyses of in-situ data’. The current WRF system includes several different microphysics options and Tao et al. (2011) compared four different cloud microphysics options for the performance of

these schemes for the Hurricane Katrina case study and found that microphysics schemes do not have a major impact on track forecasts but do on the wind intensity. They also found that simulated hurricanes had the strongest deepening or intensification when using only warm rain physics because all of the simulated precipitating hydrometeors are large raindrops that quickly fall out near the centre, hydrostatically producing the lowest pressure of all schemes. This sensitivity to microphysics schemes is in accordance with Baker et al. (2012), for ETCs, and is clearly an area which needs further work, and forms part of the research aims of this study (section 1.6).

## 1.6 Summary and research aims

Chapter 1 has introduced the ancient relationships that the human race has had with the wind and insurance, before describing the wind regime of the UK and Europe, linking this with related insurance risk and also mentioning concerns for the growing UK wind power industry, becoming increasingly sensitive to windspeed variations. Attention is drawn to ETCs as particularly impactful on the population of Europe and Windstorm Klaus of January 2009 is described in detail, showing just how destructive European ETCs can be. Fluctuations in wind climate of the NE Atlantic region are explored and the extreme surface wind producing mesoscale features within ETCs are identified, highlighting the need to quantify their relative contributions to extreme surface windspeeds. The operational weather forecast data is described, indicating the limits of accessing the data, along with the limits of using the available global model coarse resolution to resolve the mesoscale ETC features. The TIGGE database is introduced, along with related TIGGE research, emphasizing the use and importance of TIGGE despite only consisting of coarse global model data. The tools available for the high-resolution simulation of past ETC events are also presented, with the re-analysis and HiGEM projects explored and this is compared to the ongoing tropical cyclone research. Several studies highlight the need for high vertical and horizontal resolution to faithfully simulate the mesoscale ETC features, which have been known to cause extreme surface windspeeds.

The methods and data utilised to achieve the research aims below are presented and discussed in Chapter 2, with results presented in Chapters 3-5. Conclusions of the research and potential areas of future work are provided in Chapter 6.

This project aims to address the dearth of knowledge in the literature as highlighted in this chapter. The aims of this thesis are as follows, to be addressed in each of the three results chapters 3-5.

*Chapter 3*

- Update the analysis of temporal and spatial variability in the UK, using the 1980-2005 database first introduced by Hewston (2008), extending it through to the end of 2010.

- Extend the quality control conducted on these data. Deepen understanding of each station in the network by investigating the applicability of the Weibull distribution (see section 2.1.2) to each location, interpreting the results from a topographic perspective and testing a sub-sample the sites.

- Analyse variations of exceedences of a wide range of windspeed thresholds, both inter- and intra-annually, of interest to both the insurance and wind energy sectors, compare these with the larger-scale findings of Vautard et al. (2010) and discuss them in the context of key features of the regional-scale atmospheric circulation, such as the NAO.

- Quantifying the impact of the observed spatial and temporal variations on wind power energy production, both inter- and intra-annually, is an objective of this thesis.

*Chapter 4*

- Investigate the 1980-2010 variability of extreme daily maximum gusts, both top 1% and 0.1% and assess the relative contribution of each year.

- Compare the 2008-2010 period (overlap from the start of the TIGGE database and the end of the observation data respectively) with the longer term (1980-2010) variability and produce a set of surface extreme (top 1%) gust causing events and highlight their various characteristics.

- Construct a 2008-2010 climatology of the sub-storm mechanisms, discussed in section 1.3, to assess the proportion of surface extreme windspeeds that are associated with each mechanism.

- Highlight whether the extensive concentration of research, in the literature, on certain sub-storm mechanisms is warranted and whether other relatively overlooked features justify more attention.

*Chapter 5*

- Produce a sub-set of events, from those identified in chapter 4, which include surface extreme gusts that occur near the timings of analyses/forecast time-steps in the TIGGE database, from which to examine the TIGGE centre's forecasts.

- Examine the sensitivity of changing the analyses from ECMWF to each respective centre's analysis, assess the effect of grouping the model EPSs by those which perturb their physics schemes and those which do not and determine whether there is any forecast value gained from using the TIGGE compared to the ECMWF EPS in forecasting each event at distinct forecast time-steps.

- Determine how well the sub-storm mechanisms (introduced in section 1.3) are simulated by the ECMWF analyses and assess capability of the TIGGE centres to forecast them.

- Identify the characteristics of the TIGGE models, highlighting those which limit their ability to simulate ETCs faithfully; to be examined using high-resolution modelling sensitivity analysis, to assess how well an example ETC is simulated when these limits are removed, comparing with the observation network measurements (introduced in section 2.1).

- Assess the effect of improving the vertical and horizontal resolutions, along with quantifying the sensitivity to microphysics scheme selection, known to affect the simulated strength of ETC surface winds.

# Chapter 2

# Data, methods and tools

The data, methods and tools used to achieve the project's research aims, highlighted in section 1.6, are described and examined in this chapter. Details of updating the analysis of temporal variability to 2010 of the historic UK wind regime established by Hewston (2008) are provided in section 2.1, along with extending the data quality and applying the data to be of use to the wind power industry. A description of the methods behind the establishment of the set of ETC events for a mesoscale ETC feature climatology, and for forecasting experiments, is also provided in section 2.1. The diverse range of global models contained within the TIGGE database, and TIGGE experiment methods, applied to address the research aims, are described and each model's distinct attributes highlighted in section 2.2. The WRF model is described in section 2.3, with a focus on describing the model physics and parameterisation schemes and the method for the high resolution modelling experiments.

## 2.1 Updating the observed Wind Data, data quality and applications

This study extends the 1980-2005 database established by Hewston (2008) of hourly surface windspeed observations (measured at the standard 10m height) from UKMO stations across the UK, to the end of 2010, incorporating the anomalous European winter months in 2010. Wind data for all 31 years were extracted from the MIDAS (Met Office Integrated Data Archive System) Land Surface Observations Station database (UKMO, 2011), archived at the British Atmospheric Data Centre (BADC). Unfortunately, three of the 43 sites used in the original network (Coltishall, Durham and St Mawgan) have been discontinued since 2005 and have been removed from the database. Future updates of this database will have to include new sites to counteract these closures because there will always be closures and new stations opening in the

UK observation network. The hourly mean (consisting not of an average of the whole hour, but a 10-minute average, recorded from 20 to 10 minutes prior to the hour in question; hereafter HM) windspeeds and daily maximum gust speeds (DMGS; maximum 3 second average), with their associated wind directions, are extracted as described in detail by Hewston (2008) and Hewston and Dorling (2011). The site at Ringway (Manchester Airport) no longer records gust speeds, only HM windspeeds, leaving a 31 year (1980–2010) UK network of 40 sites for HM windspeeds and 39 sites for DMGSs whose geographical locations are displayed in Figure 2.1.

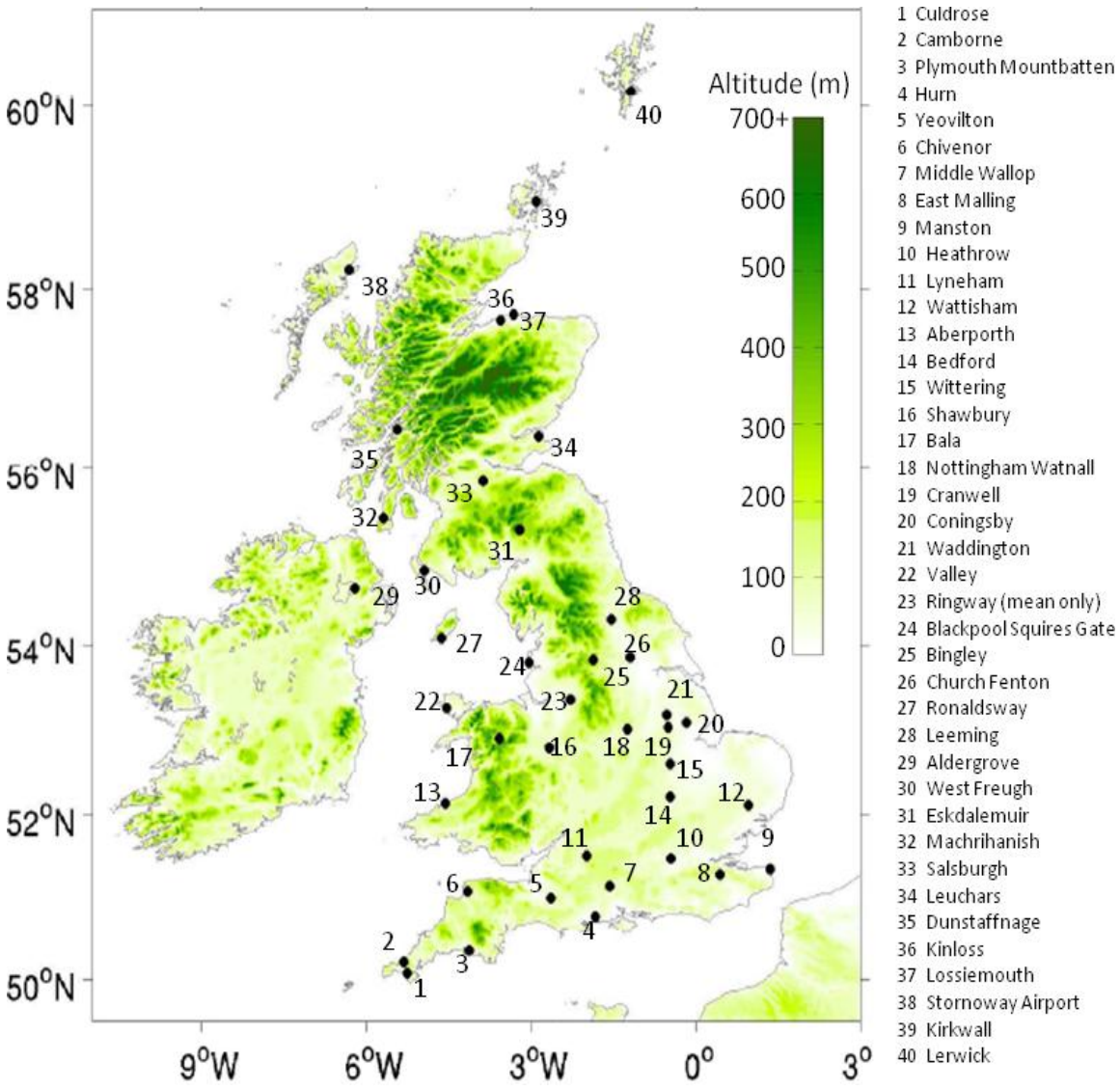


Figure 2.1 - Location of observation stations in the network. Note that Ringway (23) has no DMGS data, only recording HM windspeed.

The 40 sites used in this study have on average 98.5% HM data completeness, substantially higher than previous studies using HM MIDAS data (e.g. Sinden 2007, 77% HM data completeness). All of the sites used in this study meet the stringent UKMO site exposure requirements (available at http://badc.nerc.ac.uk/data/ukmo-midas/ukmo_guide.html). Since the sites in this study possess such a wide variety of topographies and therefore wind regimes, it is thought that when averaged together they give a good representation of the UK wind regime as a whole.

### 2.1.1 Data quality

The windspeed and direction data has undergone rigorous quality control, with checks on the equipment and raw data performed at the UKMO and the BADC. Further information on quality control performed on the MIDAS database and other possible sources of error is available at the BADC website (http://badc.nerc.ac.uk/data/ukmo-midas/ukmo_guide.html; UKMO, 2011) and in Hewston and Dorling (2011). Once downloaded, a series of steps were followed to further test the reliability of the information, removing duplicate data, detecting missing values and checking data consistency. Analysis of Weibull distributions, discussed below, was also helpful in highlighting potential anomalies. The MIDAS data does not normally include an HM value of 1 knot (0.515 $ms^{-1}$) and often uses a value of 2 knots (1.03 $ms^{-1}$), when the wind vane indicates gusty conditions (BADC website), to represent a mean speed of 0 or 1 knot. This leads to an over-representation of HM wind values of 2 knots and an under-representation of 0 and especially 1 knot at many sites. No attempt has been made to re-distribute these extra 2kt values into neighboring bins.

### 2.1.2 The Weibull distribution

Both the wind energy and insurance industries are sensitive to windspeed distributions. The Weibull distribution function has become widely used in meteorology to estimate how observed windspeeds tend to vary around their mean at sites where only a long term average is known, and is therefore helpful in the quality control of long term observational data. Originally used to describe the size distribution of particles, the Weibull distribution has numerous applications, including to model reinsurance claim sizes for the insurance industry (Kremer, 1998). The use and importance of the Weibull distribution has grown immensely in the wind power

industry and has been used to help site many thousands of wind turbines (Petersen et al., 1998).

The Weibull distribution came to prominence in meteorology during the 1970s (Takle and Brown, 1977). As a two-parameter density function it can be calculated as

$$P(U) = 1 - \exp\left[ -\left( \frac{U}{A} \right)^{k} \right] \quad (1)$$

Where P(U) is the probability distribution of windspeed U, A is the Weibull scale parameter and k is the shape parameter (Pryor and Barthelmie, 2010). For a narrow distribution, with a marked peak, k will take a relatively high value (e.g. > 2.5). Numerous statistical methods have been proposed to calculate Weibull scale and shape parameters (e.g. Pryor et al., 2004). Seguro and Lambert (2000) recommend the maximum likelihood method when windspeed data is available in a time series format. When the Weibull shape parameter has a value of 2, it is known as the Rayleigh distribution, and this is often used as the standard for wind turbine manufacturers' performance figures (Weisser, 2003). The Weibull distribution, however, has been found to produce a better fit to observed windspeeds than the simpler Rayleigh distribution (Celic, 2004).

Nevertheless it is problematic fitting a Weibull distribution at low windspeeds, as highlighted by Justus et al. (1976) who assessed potential output from wind-powered generators. On the other hand, it is generally accepted that sites with regular moderate or high windspeeds can almost always be approximated by the Weibull distribution (Petersen et al., 1998); Jamil et al. (1995) estimated a moderate windspeed threshold to be 12 $ms^{-1}$ or higher. It would therefore be expected that a Weibull distribution would more realistically simulate a DMGS distribution than an HM distribution.

Both the 31 year UK HM windspeed and DMGS data can be used to assess whether the Weibull distribution function is a good fit to these observations. The HM data contains periods of low windspeeds (including many calm hours/periods) which have been highlighted as not being well represented by the Weibull distribution. The DMGS

set however, by definition, should be more Weibull compatible. This study examines the capability of the Weibull distribution to represent the variance of land-based wind monitoring sites, by calculating the 31-year shape parameter at each site for both HM windspeed and DMGSs. This also reveals how well the commonly used Rayleigh distribution approximates the sites' windspeed variance. There have been numerous methods and modifications to the Weibull distribution to deal with zero and low windspeed values, however it is not the intention here to assess which of these best represents the DMGS and HM datasets. Therefore this study simply uses the commonly adopted basic maximum likelihood method (Seguro and Lambert, 2000). It must be noted that the basic method used is unable to accommodate calm conditions with windspeeds of 0ms$^{-1}$, although the approach can be modified to account for these (Wilks, 1990). Tests were carried out assigning a negligible value (0.00001 ms$^{-1}$) to reports of 0 ms$^{-1}$, however the results for HM windspeeds (not shown) displayed strong positive skewed, poorly fitting Weibull distributions and k values as low as 0.3, so the values of 0ms$^{-1}$ (sites ranging from 0.2% and 10.2% and averaging 2.1% of the HMs) were ignored.

### 2.1.3 Wind turbine power

The 31 year UK HM windspeed database allows an assessment of the potential impact of spatial and temporal variations in the UK wind regime on the wind energy sector. As greater reliance on wind power for electricity generation needs increases, so will the magnitude of risk due to exposure of the performance of the turbines to climate change (Harrison et al., 2008), as highlighted in the research aims (section 1.6). Power generated is proportional to the cube of the windspeed and the variability of the wind around the mean is therefore critical to the amount of power produced. Wind power generation potential can be quantified using the concept of energy density (strictly power density)

$$E = \frac{1}{2}\rho U^3 \qquad (2)$$

where E is energy density (W m$^{-2}$), ρ is air density (kg m$^{-3}$) and U is the hub-height windspeed (ms$^{-1}$) (Pryor et al., 2012). For this study, the energy density for each of the 40 HM observation sites is calculated with equation (2), using an air density of 1.225

kg $m^{-3}$ (15˚C at sea level) and is converted to hub height of 100m using the power law approximation in equation 3. This assumes negligible density variations (Pryor et al., 2004; Jamil et al., 1995), ignoring altitude and temperature variability between sites (which could theoretically lead up to an associated ±8% air density variation compared to the average value adopted, based on the altitudes of the sites and surface UK temperature range). A limitation of the applicability of the energy density quantity is that even the most modern wind turbines cannot harvest power below and above specific windspeed thresholds, as shown in Table 2.1.

Outside this range, the windspeed is either too low to turn the blades or too high, forcing the turbine to be shut down in order to prevent damage (AEA, 2011). Based purely on the cubic relationship between windspeed and power generation, energy density returns an overestimation of wind turbine performance, especially during stormy periods such as the early 1990s (Wang et al., 2009). For comparison, another method is also used to quantify wind turbine performance, including cut-in and cut-out windspeed thresholds and sensitivity to windspeed variations within that range (Oswald et al., 2008). For each of the 40 HM observation sites, a synthetic state of the art 3.6MW wind turbine is considered for the duration of the recorded observations and the 10m winds are adjusted to the typical hub height of 100m using the power law approximation, ignoring the important effect of variable atmospheric stability and surface roughness ($z_0$) for this simple estimate (Petersen et al., 1998; Motta et al., 2005).

$$\frac{U(z_1)}{U(z_2)} = \left(\frac{z_1}{z_2}\right)^p \qquad (3)$$

Where $U(z_1)$ and $U(z_2)$ are the windspeeds at heights $z_1$ and $z_2$, respectively, and p is the power law exponent taken to be equal to 0.14 (Petersen et al., 1998) (giving $U_{100}$ = $U_{10}$ x 1.38) . The value of p typically ranges from 0.05 (very unstable atmosphere with $z_0$=0.01m) to 0.69 (stable atmosphere with $z_0$=3m), the adopted value 0.14 represents a neutral atmosphere for a small $z_0$ (0.01-0.1m) and a typical value for areas with variable stability (Irwin, 1979). Once the height conversion has been performed, the power output is then estimated for each hour at each site based on the power output

curve of the 3.6MW wind turbine (Table 2.1). Energy density and power output are calculated for each site and averaged across the network, weighting for any missing data, and the observed temporal variability is discussed in section 3.6.

| Surface windspeed m $s^{-1}$ | Windspeed m $s^{-1}$ at 100m | Power kW | Energy Density W $m^{-2}$ |
|---|---|---|---|
| 0 | 0 | 0 | 0 |
| 1 | 1.38 | 0 | 1.61 |
| 2 | 2.76 | 0 | 12.88 |
| 3 | 4.14 | 102 | 43.46 |
| 4 | 5.52 | 361 | 103.02 |
| 5 | 6.90 | 770 | 201.21 |
| 6 | 8.28 | 1386 | 347.69 |
| 7 | 9.67 | 2175 | 553.84 |
| 8 | 11.04 | 2965 | 824.16 |
| 9 | 12.42 | 3411 | 1173.47 |
| 10 | 13.80 | 3565 | 1609.69 |
| 11 | 15.18 | 3595 | 2142.50 |
| 12 | 16.56 | 3600 | 2781.55 |
| 13 | 17.95 | 3600 | 3542.42 |
| 14 | 19.33 | 3600 | 4423.86 |
| 15 | 20.71 | 3600 | 5440.59 |
| 16 | 22.09 | 3600 | 6602.27 |
| 17 | 23.47 | 3600 | 7918.54 |
| 18 | 24.85 | 3600 | 9399.08 |
| 19 | 26.23 | 0 | 11050.50 |
| 20 | 27.61 | 0 | 12888.75 |
| 21 | 28.99 | 0 | 14920.34 |
| 22 | 30.37 | 0 | 17154.93 |
| 23 | 31.75 | 0 | 19602.18 |
| 24 | 33.13 | 0 | 22271.77 |
| 25 | 34.51 | 0 | 25173.35 |
| 26 | 35.89 | 0 | 28316.59 |

Table 2.1 - Power produced by a present-day state of the art 3.6MW wind turbine and Energy Density (from equation 2) for windspeeds in the range 0-26 $ms^{-1}$ converted to 100m (typical hub height) using the power law approximation (equation 3).

### 2.1.4 NAO

The HM and DMGS 1980-2010 windspeed database presents an excellent opportunity to investigate the relationship between the NAO index and UK windspeeds, as mentioned in the research aims (section 1.6), and assess the impacts of the phase

changes of the NAO on land based wind measurements and wind energy output estimates. This extends the work of Cheng et al. (2011) who used satellite observations to investigate inter-annual variability of high wind occurrence in the North Atlantic over the period 1988-2009. The particular NAO index used for this study is based on normalized sea-level pressure observations made at Gibraltar and Reykjavik in Iceland, with homogeneous records that date back to the 1820s, allowing for a long term monthly NAO index (Jones et al., 1997) [available on the University of East Anglia's Climatic Research Unit (CRU) website: http://www.cru.uea.ac.uk/~timo/datapages/naoi.htm; hereafter CRU website]. There are numerous methods to calculate the NAO index, however this monthly index has the advantage of the longest record, helping place the 1980-2010 UK HM wind variability into context (see http://www.cru.uea.ac.uk/cru/info/nao/ for more detail). It must be noted here, however, that this NAO is mainly of use in winter (DJFM) and that there is another in the Azores better suited to summer NAO, though for continuity reasons this study will use the aforementioned NAO data.

### 2.1.5 Establishing the set of ETC events

Chapter 1.3 describes the mesoscale features experienced during the passage of the European ETCs and the research aims in chapter 1.6 showed the need to quantify the proportion of these individual features which cause extreme surface windspeeds over an extended time-period. The observational database runs from 1980-2010 and the TIGGE database, which runs with a full complement of centres from February 2008 (see section 2.2.1), which also uses the ETC set established here for forecast performance assessment, overlap from February 2008 to December 2010. It was therefore decided to establish the set of ETC events from January 2008 to December 2010, allowing for a provisional-climatology comprising of 3 full years (as three years is too short a time period for a definitive climatology), with the intra-annual variability of ETCs in mind as indicated by Earl et al. (2013), so January is not under-represented.

It was decided to use the DMGS part of the observational database (despite TIGGE only outputting mean winds) when selecting the most damaging events as it is gusts which record the strongest winds and therefore best represent the most damaging ETC events. Firstly the DMGSs are ranked in order of intensity for each of the network

sites and the top 1% of each site for the whole 1980-2010 period. This means taking the strongest 114 DMGSs as there are 11,323 days from January 1980 to December 2010, but this value is often more due to the windspeeds being reported in integer values (knots) and regularly the same DMGS value occurs many times, for example, Eskdalemuir had the highest number of top 1% DMGSs because the value 51kn was ranked 109$^{th}$, but there were 33 individual examples (between 1980 and 2010), so a total of 142 (109 +33) DMGSs represent the top 1% for this particular site. The inter- and intra-annual variability of the top 1% (hereafter, eDMGS) is explored in chapter 4.1. In that chapter the top 0.1% DMGSs are also examined, which utilises the same method, but uses the strongest 12 DMGSs (along with any extra values tied for 12$^{th}$ rank) for each site.

Once the eDMGSs have been established, the dates of each are taken and the events occurring in 2008-2010 are retained, to set the 3-year period in the context of the longer climatological record of 1980-2010. Each of the 2008-2010 dates are then grouped together for those occurring on the same or adjoining days. These are then compared to surface pressure charts (available at www.wetterzentrale.de) and each eDMGS is then associated with a corresponding synoptic feature and that feature's name, given at the Free University of Berlin, if applicable, is then used for each eDMGS (incidentally all of the features associated with eDMGSs were ETCs). Some of the ETCs passed slowly over the UK over a maximum of 3 days. The number of times each ETC was associated with an eDMGS is counted, which includes multiple counts for the same network site if an eDMGS occurred on consecutive days at that same site and was associated with the same ETC event.

Despite all of the quality control conducted by the UKMO and in this study (see section 2.1.1), observational data quality concerns still arise. An example of this occurs in the data from Machrihanish (site 32), where a 63 knot (joint 78$^{th}$ ranked) DMGS was recorded on 29$^{th}$ November 2010 and was an isolated eDMGS, with no other sites recording an eDMGS on that particular, preceding or following day. Further investigation shows that the gust was recorded between 9 - 10am and that the preceding 3 hour (6-7am, 7-8am and 8-9am) hourly maximum gust speeds were 9, 14, and 15 knots respectively, while the following 3 hour (10-11am, 11am-12pm and 12-

1pm) hourly maximum gust speeds were 16, 16 and 15 knots respectively, with all of the gust measurements receiving the best score for quality control. This gust speed was also compared to the corresponding gust speeds at the network sites situated nearest to Machrihanish, none of which recorded values of a similar magnitude to the eDMGS in question and along with assessing surface pressure charts, radar images and satellite observations (not shown), it was decided that the gust was likely caused by an error and was omitted from the database. Checking all of the eDMGS examples is not possible here due to time constraints, so only ETC events which are associated with more than 1 eDMGS are included in the study.

Categorising each of the eDMGS to associated sub-storm features (see section 1.3) is done by subjective estimation, using surface pressure charts (courtesy of www.wetterzentrale.de), Nimrod radar images (downloaded from the BADC, source http://badc.nerc.ac.uk) and satellite images (courtesy of the University of Dundee Satellite Receiving Station, source http://www.sat.dundee.ac.uk/), along with the data from the surface observation network (see section 2.1). The surface pressure charts are only available for 00:00 UTC at www.wetterzentrale.de however, the UKMO have provided (on request) the required 12:00 UTC pressure charts. The satellite images are taken from Advanced Very High Resolution Radiometer (AVHRR) and Moderate-resolution Imaging Spectroradiometer (MODIS) onboard polar orbit satellites which produce images of the UK around ten times intermittently every day at a variety of channels in the visible or infrared part of the electromagnetic spectrum, allowing for images during the day or night. The Nimrod radar images are output every 15 minutes so they can be used to track precipitation producing features identified in the pressure charts and satellite images. Chapter 4 shows the process of this categorisation method for each of the sub-storm features indicating how each observation tool is used.

Once all of the sub-storm feature causes for all eDMGS have been categorised, they are then brought together in the development of the 2008 to 2010 provisional-climatology. A limiting factor of this method however is the biased weighting of events which strike close to mid-night, as they may be double counted if the extreme winds occurred either side of the change of day, and therefore counting as two DMGSs as opposed to one if it occurred at mid-day for example, as Hewston and

Dorling (2011) found. This fact will affect the results, however but is not much of a concern because when considering eDMGS winds, they are almost exclusively related to organised European ETCs, which are relatively unaffected by diurnal cycles (Hewston, 2008) and therefore give no specific sub-storm mechanism any unfair weighting.

## 2.2 The TIGGE Database

To assess the performance of the international forecasting centres to predict European ETCs, as stated in the third set of research aims (section 1.6) the TIGGE is utilised.

A major goal of THORPEX is to accelerate improvements in the accuracy of 1-day to 2-week high-impact weather forecasts for the benefit of humanity (Bougeault et al., 2010), with the key objectives as follows:

• To increase fundamental understanding of dynamics and predictability of the atmosphere.

• To make significant, quantifiable, worldwide improvements in decision making skills and consequent measurable reduction in societal distress.

• To promote and fully exploit advances in NWP, observations, communications and data-assimilation techniques.

• To deliver improved global and regional forecasting system with active involvement of developed, developing and least developed nations

Enhancing collaboration between operational centres and universities and increasing the availability of EPS data for research were among the main TIGGE objectives with a view to aiding the development of EPSs. By 1$^{st}$ February 2008, 10 operational weather forecasting centres were delivering near-real-time ensemble forecast data to the TIGGE database (not quite real-time to avoid commercial sensitivity).

The TIGGE is a centralised archive of ensemble model forecast data, from ten international meteorological centres, designed for data sharing to improve the accuracy of 1-day to 2 week high-impact weather forecasts and create research opportunities. Each contributing centre's model has many ensemble members which are model runs with slightly adjusted initial conditions and some centres also perturb their model physics schemes. The ten contributing partners are the Australian Bureau of Meteorology (BoM), the Brazilian Centre for Weather Prediction and Climate Studies (CPTEC), the Chinese Meteorological Agency (CMA), the Canadian Meteorological Centre (CMC), ECMWF, MeteoFrance, the Japan Meteorological Agency (JMA), the Korean Meteorological Administration (KMA), the UKMO and the American NCEP. All meteorological centres interpolate their forecast and analysis output data onto common regular grids, in a standardised format to aid usability for researchers (Bougeault et al., 2010) and also supply default data, on a horizontal grid of their choice, as close as possible (identical if possible) to the grid of their global model, which are stored in the database without any modification to guarantee the best precision. Both the control and perturbed ensemble model outputs are available in the TIGGE database.

### 2.2.1 Ensembles

Ensemble prediction is a powerful complement to a single, deterministic forecast providing an estimate of the probability density function of the spread of possible forecast developments, as discussed in section 1.4.1. This allows for an estimate of forecast confidence, especially for extreme events (Bougeault et al., 2010) such as ETCs. Small errors in the initial conditions of a forecast can grow rapidly and significantly affect predictability (Buizza et al., 2005), so the use of ensembles is widespread. Each centre's global model includes a variety of perturbed members, ranging from 11 to 51, along with runs per day ranging from 1-4, as summarised in Table 2.2. This equates to over 500 ensemble forecast runs per day, an unprecedented amount of forecast data contained in a single place, in a uniform format.

| Centre | BoM* Aus | CMA Chi | CMC Can | CPTEC Brazil | ECMWF Europe | JMA Jap | KMA Korea | Meteo-France | NCEP USA | UKMO UK | Total |
|---|---|---|---|---|---|---|---|---|---|---|---|
| No. of ensemble members | 33 | 15 | 21 | 15 | 51 | 51 | 17 | 11 | 21 | 24 | 259 |
| No. of model runs per day (UTC) | 2 (00) (12) | 2 (00) (12) | 2 (00) (12) | 2 (00) (12) | 2 (00) (12) | 1 (12) | 2 (00) (12) | 2 (06) (18) | 4 (00) (06) (12) (18) | 2 (00) (12) | 21 |
| No. of ensemble members per day | 66 | 30 | 42 | 30 | 102 | 51 | 34 | 22 | 84 | 48 | 509 |

Table 2.2 – Number of ensemble members (including control forecasts) for each TIGGE centre and number and times of model runs per day and the resulting total of ensembles per day before the termination of Australia's BoM. *BoM terminated 20th July 2010 (http://tigge.ecmwf.int).

The models vary greatly in characteristics, be it forecast length, horizontal resolution or vertical resolution, before any perturbation of initial conditions has been conducted and there are many different methods that are used to perturb the initial conditions. This leaves a wide variety of global models present within the TIGGE database. Table 2.3 shows the characteristics of all ten TIGGE contributing models. The horizontal resolution ranges from $0.45^{o}$ to $1.5^{o}$, though after the January 2010 update, the ECMWF model had a resolution of $0.2816^{o}$, and the vertical ranges from 19 to 62 levels. The first model data available in TIGGE is from October 2006, when the ECMWF, Japan's JMA model, and the UKMO model were the only contributors with the others soon to follow and by February 2008, Brazil's CPTEC joined, meaning a full set of 10 centres, until Australia's BoM model was discontinued. A new system, AGREPS (Australian Community Climate and Earth-System Simulator (ACCESS) Global and Regional EPS, an implementation of the Met Office Global and Regional Ensemble Prediction System (MOGREPS)) is under development and will be included in TIGGE, but it is anticipated that there could be a gap of a year or more before AGREPS is operational (TIGGE website, tigge.ecmwf.int/tigge/d/show_archive/table=news/). Australia's BoM model output that is available in TIGGE does not include analyses, which means that any experiment which involves comparing centres with their own analysis cannot include this model. It is necessary to note that all of the TIGGE contributing models are continuously being developed and improved, so the major

2008-2010 changes have been highlighted in Table 2.3's caption, though many other smaller updates may have been implemented during this time that will have slightly affected the model characteristics.

| | **Initial Perturbation method (area)** | **Physics perturb-bation?** | **Horizontal resolution (degrees)** | **No. of Vertical resolution** | **No. of Forecast length** | **Available on TIGGE from** |
|---|---|---|---|---|---|---|
| **BoM * (Australia)** | Singular Vectors (NH,SH) | No | TL119 (1.5$^{o}$) | 19 | 10 | September '07 – July'10 |
| **CMA (China)** | Bred Vectors (globe) | No | T213 (0.5625$^{o}$) | 31 | 10 | May'07 - present |
| **CMC (Canada)** | Ensemble Kalman Filter (globe) | Yes | TL149 (1.2$^{o}$) | 28 | 16 | October'07 - present |
| **CPTEC (Brazil)** | Empirical orthogonal function - based (40S:30N) | No | T126 (0.9474$^{o}$) | 28 | 15 | February'08- present |
| **ECMWF (Europe)** | Singular Vectors (globe) | Yes | TL399** (0.45$^{o}$) TL255** (0.7$^{o}$) | 62 62 | 0-10 10-15 | October'06 - present |
| **JMA (Japan)** | Bred Vectors (NH+TR) | No | TL319 (0.5625$^{o}$) | 40 | 9 | October'06 - present |
| **KMA (Korea)** | Bred Vectors (NH) | No | T213 (0.5625$^{o}$) | 40 | 10 | December'07 - present |
| **Meteo-France** | Bred Vectors (local) | No | TL358 (0.5$^{o}$) | 41 | 2.5 | October'07 - present |
| **NCEP (USA)** | Bred Vectors (globe) | No | T126 (0.9474$^{o}$) | 28 | 16 | March'07 - present |
| **UKMO (UK)** | Ensemble Kalman Filter (globe) | Yes | N144*** (1.25$^{o}$ x0.83$^{o}$) | 38*** | 15 | October'06 - present |

Table 2.3 – Characteristics of all of the TIGGE EPSs2008-2010, details of the perturbation approaches are given in section 2.2.2. NH – Northern Hemisphere, SH – Southern Hemisphere TR – Tropics. T – Spectral, N – Grid points.

*BoM terminated 20th July 2010

**ECMWF resolution upgraded from T399/T255 (0.45$^{o}$/0.7$^{o}$)to T639/T319 (0.2816 $^{o}$/0.5625$^{o}$) on the 26th January 2010

***UKMO resolution upgraded to N216 (0.83°) from N144 (1.25°) and 70 levels from 38 on the 9th March 2010

*Initial perturbation methods*

For the initial-condition perturbations a variety of methods are being used in TIGGE as seen in Table 2.3. BoM, ECMWF, and JMA use singular vectors, which aim to find those perturbations to a given initial state which grow most rapidly, as described by Bourke et al. (2004). China's CMA model, Korea's KMA model and MeteoFrance's model use bred vectors, which are created by adding a random initial perturbation, comparing the perturbed run with the control, measuring the difference (the bred vector) and adding the vector back to the control to create a new perturbed initial condition, hence described as a 'breeding' method (Toth and Kalnay, 1997). NCEP's model uses the ensemble transform technique (Wei et al., 2008), a version of the breeding vector technique, using previous ensemble forecasts to obtain the growing components of the analysis error, whereas the UKMO uses an ensemble transform Kalman filter approach, which is a form of square root filter and differs from the Kalman filter by using normalisation to obtain the prediction error rapidly to a particular set of observations (Bishop et al., 2001). Canada's CMC model uses an ensemble Kalman filter, perturbing the assimilated observations with pseudo-random numbers and this added 'noise' in the system then represents observational error. Brazil's CPTEC model uses a method based on empirical orthogonal functions to find the fast growing error in the initial state (Zhang and Krishnamurti, 1999).

Table 2.3 also indicates that some centres apply perturbations globally, while others just use their respective initial perturbation method in certain regions or hemispheres. MeteoFrance applies perturbations over 4 areas namely, the extra-tropics in the Southern Hemisphere, the tropical region, the North Atlantic Ocean and Western Europe (16 SVs) and extra-tropical North hemisphere except the previous area. The NH extra-tropical region is not the focus in the construction of the Brazilian CPTEC model and does not perturb the initial conditions in latitudes above 30N.

*Physics perturbations*

As well as applying perturbations to the initial state, some centres, namely CMC, ECMWF and the UKMO, also apply perturbations to the model physics as shown in Table 2.3 to represent imperfections in the physics schemes. The ECMWF applies random perturbations to the parameterised physical processes known as stochastic

physics and described by Buizza et al. (1999), whereas the UKMO uses the Shutts (2005) kinetic energy backscatter algorithm. The CMC use a similar approach to both of the above schemes, alongside several different physical parameterisation schemes, investigated by Houtekamer and Lefaivre (1997). When ECMWF first implemented model physics perturbations, the effect was to increase the ensemble spread (Buizza et al., 1999), indicating a need to compare models which do perturb physics schemes and those which do not.

### 2.2.2 Data assimilation techniques

It is fundamental in NWP to incorporate observed data, be it from surface observation stations, radar, satellites, radiosondes or dropsondes. Data assimilation is the process by which these observations are incorporated into the model's analyses, by combining all available observations in a given time window, producing an estimate of the atmospheric conditions, for a certain analysis time. There are a variety of methods for this used by the TIGGE contributing models.

Table 2.4 lists the data assimilation methods used by all of the contributing TIGGE models. Five of the ten models use 4D-VAR with the Korea's model using 3D-VAR. The basic goal of the 3D-VAR is to produce the best possible estimate of the true atmospheric state at the relevant analysis time through the repetitive solution of a prescribed 'cost function' as explained by Ide et al. (1997). 3D-VAR ingests all observations simultaneously, whereas 4D-VAR ingests observations that are distributed in time, especially useful for assimilating data from irregular polar orbiting satellites. The main reason for using 3D-VAR rather than 4D-VAR is because 3D-VAR is computationally cheaper to run and can also achieve a similar standard to 4D-VAR by using a rapidly updating cycle. However, 4D-VAR provides more accurate analyses under various situations; for example, Whitaker et al. (2009) found it to be much better for producing analyses when/where observations are sparse, using data from the 1930s. 3D-VAR was originally described as an important intermediate milestone to 'ultimate goal' of 4D-VAR (Courtier et al., 1998). China's CMA and NCEP use gridded statistical interpolation which is based on 3- and 4D-VAR, but is often considered less accurate. Buizza et al. (2005) found that the NCEP ensemble performance is negatively affected in the short range by the relatively low quality of the ensemble of data

assimilation systems. The other TIGGE centres use simpler assimilation methods, with Australia's BoM applying a multivariate statistical interpolation approach (GenSI), as described by Seaman et al. (1995), and Brazil's CPTEC simply uses the NCEP analysis. These different approaches inevitably lead to differences in analysis quality and the ECMWF analysis is widely regarded as being the most accurate, using the highest vertical and horizontal resolutions, the state of the art data assimilation method 4D-VAR and is used to represent 'truth' in many studies, for example (Froude, 2010; Wiegand, 2011). ECMWF analysis is used in this study to represent 'truth' in the majority of TIGGE forecast assessments in chapter 5.

| | **Data assimilation techniques in TIGGE** |
|---|---|
| **BoM * (Australia)** | Generalized multivariate statistical interpolation (GenSi) |
| **CMA (China)** | Gridded statistical interpolation (GSI) |
| **CMC (Canada)** | 4-dimensional variational data assimilation (4D-VAR) |
| **CPTEC (Brazil)** | NCEP analysis |
| **ECMWF (Europe)** | 4-dimensional variational data assimilation (4D-VAR) |
| **JMA (Japan)** | 4-dimensional variational data assimilation (4D-VAR) |
| **KMA (Korea)** | 3-dimensional variational data assimilation (3D-VAR) |
| **Meteo-France** | 4-dimensional variational data assimilation (4D-VAR) |
| **NCEP (USA)** | Gridded statistical interpolation (GSI) |
| **UKMO (UK)** | 4-dimensional variational data assimilation (4D-VAR) |

Table 2.4 – Data assimilation techniques used by each TIGGE contributing model.

### 2.2.3 The TIGGE centre forecast performance assessment

To test the extreme windspeed forecast performance of the TIGGE contributing models, the set of ETCs named using the methodology in section 2.5.1 are used. The timing of each eDMGS is examined for each event and the only gusts that can be used for forecast assessment are those which fall within a short time from the analysis/forecast time-step, namely 00:00 UTC and 12:00 UTC. Table 2.2 shows that NCEP and Meteo-France's models include analyses/forecast time-steps for 06:00 UTC and 18:00 UTC, however these are alone in analysing these times of day, so this project concentrates on the 00:00 UTC and 12:00 UTC analysis/forecast time-steps. Japan's model only produces output for 12:00 UTC, so any experiment concentrating on 00:00 UTC will not include this model's control or EPS forecasts.

Some of the eDMGSs are observed at times which do not correspond to the timing of the analyses. For example if a gust is observed at 04:00 UTC, the nearest time for an analysis is for 4 hours previous at 00:00 UTC, which means that there is a strong chance that the gust causing feature is not represented in the analysis 4 hours earlier, especially for the shorter time-scale features such as SJs and QLCSs). For this reason, only gusts observed within 2 hours of the analyses (10:00-14:00 UTC for the 12:00 UTC analysis and 22:00-02:00 UTC for the 00:00 UTC analysis) will be included for forecast assessment. The main forecast times to be used in this study are 48 hour and 120 hour, which means that Meteo-France's model is excluded because this forecasts are only run up to 60 hours, which is not long enough for use in this study as it is too short to cover the full life cycle of the majority of European ETCs (Dacre and Gray, 2009).

All of the TIGGE models interpolate their data onto common grids as already mentioned. The resolution options are 0.5˚x 0.5˚, 1˚x 1˚, 1.5˚x 1.5˚, 2˚x 2˚, 2.5˚x 2.5˚ and 3˚x 3˚; each centre's default resolution also available. Kipling et al. (2011) found that their TIGGE study, regarding 500-hPa geopotential height and 2 metre temperature, was not overly sensitive to different interpolated resolutions. Other TIGGE studies focussing on meteorological features in Europe use the 1˚x 1˚ interpolated resolution (e.g. Keller et al., 2011; Wiegand et al., 2011) and as this is a central resolution, compared with the TIGGE centres (Table 2.3), it seems that 1˚x 1˚

interpolated resolution is overall the most representative of the centres and is therefore used in this study.

To all eDMGSs for each event, that occur within the four hour time window for the 00:00 UTC and 12:00 UTC analyses/forecast time-steps, a representative grid point is assigned. The windspeed of this will be used to represent the eDMGS in the TIGGE forecast assessment. For eDMGSs which occur ≤ 2 hours from the nearest analysis time, the feature causing the extreme gust(s) is tracked using the relevant 15-minute Nimrod radar images and assigned their representative grid point from there.

An example event will be simulated that uses high-vertical and horizontal resolutions. The modelled coarse and high-resolution surface winds are then compared to the observations. Furthermore, the sensitivity of the model results to the choice of the microphysics scheme will be evaluated. The storm chosen for these tests is Windstorm Emma, identified in chapter 4. Windstorm Emma has the most eDMGSs represented by single analysis/forecast time-step (occurring within the 4-hour time-window) of any 2008-2010 event. This analysis/forecast time-step is on the 1st March 2008 00:00 UTC, and is modelled at high resolution as described below.

## 2.3 The WRF modelling system

A comprehensive technical review of the Advanced Research WRF Version 3 is provided by Skamarock et al. (2008), in which the system's attributes are described in detail. This section gives a concise summary of some of the important model characteristics, before the nesting options and various microphysics schemes are explained.

### 2.3.1 WRF System

The WRF system is a mesoscale NWP and atmospheric simulation model designed for operational forecasting and research alike, promoting better links between the two communities (Michalakes et al., 2001). WRF is the result of a collaborative effort; the main developers are several divisions of the NCAR and the NCEP but substantial input has been provided by many additional groups (Skamarock et al., 2008). WRF was released with Version 1.0 in November 2000, and has been actively developed since.

Version 3.0 was released in April 2008 and the latest version, 3.4.1, was released in August 2012 (WRF website, http://www.wrf-model.org). A positive aspect of WRF is the fact that, as with many of its predecessors, e.g. the Fifth-Generation NCAR / Penn State Mesoscale Model (MM5), it is an open source community model, continuously being improved by contributions from users internationally, utilising knowledge and experience from the broad scientific community. This keeps it up to date and with its single-source flexible code, it is efficient in a range of computing environments, including the UEA cluster, and can be used for a wide range of applications. This, along with WRF's flexible physics and parameterisation packages, including 13 different microphysics options, makes it an ideal tool to be utilised in this project.

The WRF system consists of WRF Pre-processing System (WPS), Software Framework (WSF), and Post Processing Verification software (Figure 2.2). WPS prepares WRF for the input of real data simulations, with three separate programs, Geogrid and Ungrib outputting into Metgrid before the data are ready for the model run. The Geogrid program defines map projection and domain locations, Ungrib reads the grib data containing the meteorological fields, producing an intermediate file and these feed into the Metgrib program which interpolates the horizontal meteorological data to the domains chosen by the user. The vertical interpolation is done using these metgrid files, converting the data onto the number of levels chosen for the WRF model run. There are two dynamical cores in WRF, the Advanced Research WRF (ARW), from NCAR, and the Non-hydrostatic Mesoscale Model (NMM) developed at NCEP. The cores have some different physics options. The NMM is less complex, faster and used primarily for forecasting, whereas ARW is used both operationally and for climate research, indicating that ARW is more suited to this project.

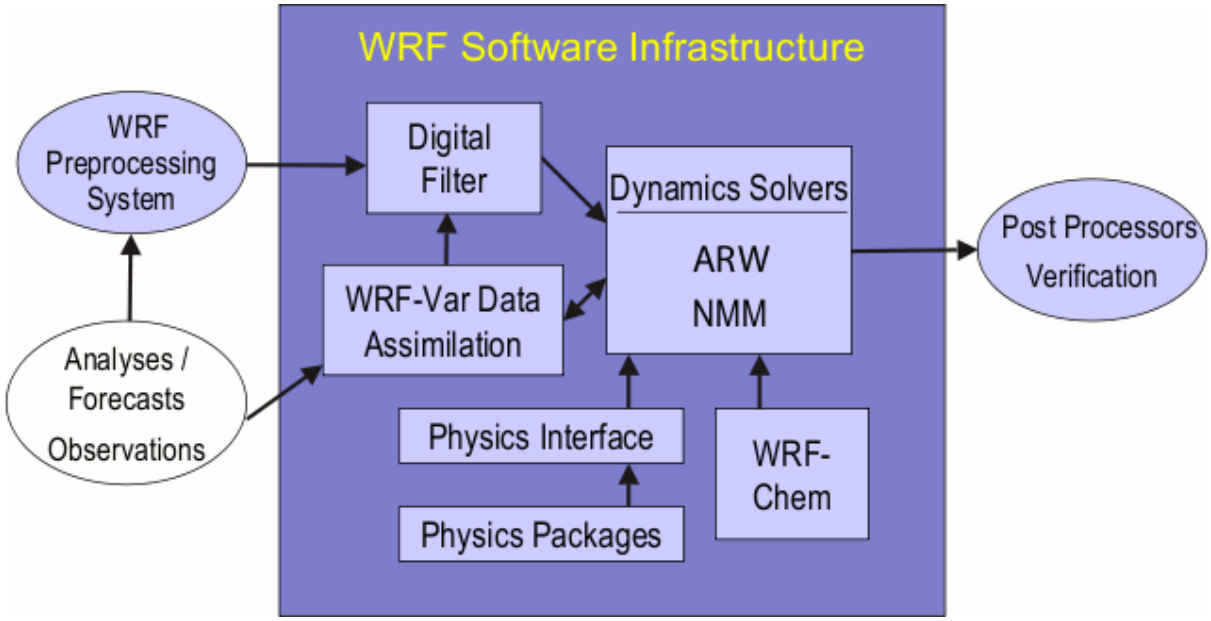


Figure 2.2 - The WRF Software Framework (Skamarock et al., 2008).

### 2.3.2 WRF Nesting

Nesting in NWP models was a significant breakthrough, allowing only part of a grid, rather than all, to run at higher resolution, saving significant time and computer power. Nesting in WRF is a relatively new development, first included in Version 2.0.1, released in 2004 (Wang et al., 2006). Nesting allows an area of interest to be viewed at significantly higher resolution, taking the boundary conditions from the coarser mother domain, with boundary conditions driving only the outer domain model run, ingesting data either from real data sources, ECMWF Re-analysis data for example, or run in an idealised environment. This is very important when examining European ETCs, with damaging wind speeds often localised, needing fine grid resolution to resolve small scale features. The system possesses two types, one-way and two-way nesting.

It is best to think of one-way nesting as a sequence, where the fine nested grid receives input from the coarse parent, though not returning any information. Two-way nesting involves both the coarse and fine grid domains to interact with each other. Nests are embedded within the parent coarser model and run simultaneously, with the feedback shut off for one-way nesting during the run. Another option for one-way nesting is to run the coarse model first, and then use the output from this for the fine grid's initial conditions. This is summarised in the diagram (Figure 2.3). It is

uncertain which is the most favourable nesting scheme for ETCs, however with one-way nesting requiring more computing time (from our own experience of running this model at UEA), two-way nesting is used in this study, using two nests described in section 2.3.4.

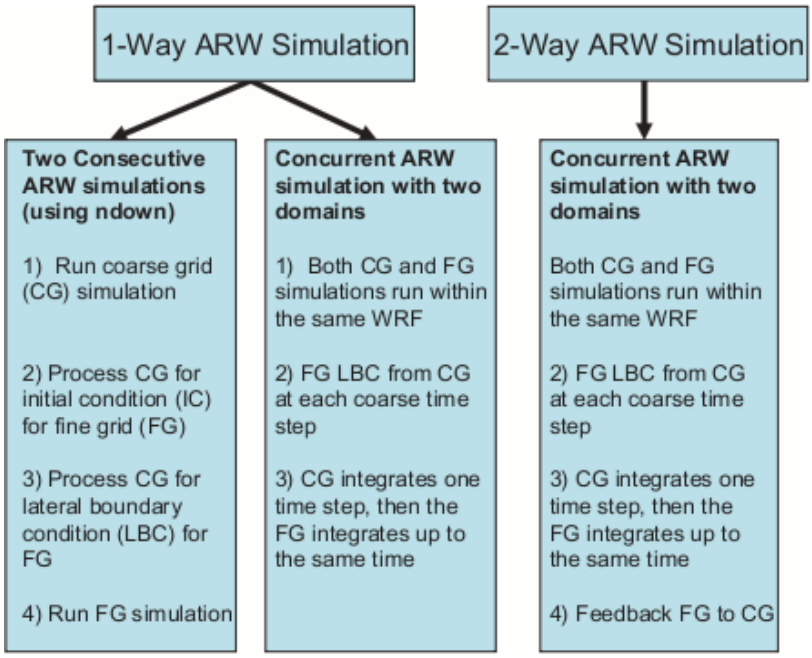


Figure 2.3 - WRF one-way and two-way nesting options (Skamarock et al., 2008).

### 2.3.3 WRF physics and parameterisation schemes

The most important components of NWP models are, arguably, parameterisation schemes, which represent sub-grid scale physical processes that are not explicitly represented, as stated and explored in detail by Stensrud (2007). Only the schemes relevant to this study are explained here, see Skamarock et al. (2008) for a description of all options. The suite of WRF physics schemes includes numerous options for microphysics, cumulus parameterization, planetary boundary layer, land-surface model, radiation and diffusion schemes, which can be combined in any way, all with between 3 and 13 different options. These options range from simple and efficient, to computationally demanding sophisticated schemes, and from newly developed, to well-tried schemes such as those in current operational models. This means that are thousands of ways of combining the different physics and parameterisation schemes, on top of the resolution and nesting options. Using previous research and the

knowledge of WRF gained through experience within UEA regarding many of the WRF options, this study aims to examine the sensitivity of two contrasting (simple and sophisticated) microphysics schemes, which is known to have a large impact when simulating surface winds during European ETCs (Baker et al., 2012), through a different representation of latent heat exchanges from evaporation and melting of hydrometeors. The nine schemes available in WRF are shown in Table 2.5, for some more than one version is available (e.g. the Thompson scheme).

| Scheme | Number of Variables | Ice-Phase Processes | Mixed-Phase Processes |
|---|---|---|---|
| **Kessler** | 3 | N | N |
| **Purdue Lin** | 6 | Y | Y |
| **WSM3** | 3 | Y | N |
| **WSM5** | 5 | Y | N |
| **WSM6** | 6 | Y | Y |
| **Eta GCP** | 2 | Y | Y |
| **Thompson** | 7 | Y | Y |
| **Goddard** | 6 | Y | Y |
| **Morrison 2-Moment** | 10 | Y | Y |

Table 2.5 – The different microphysics schemes available in WRF (from Skamarock et al., 2008)

It was decided that the most useful contrasting schemes to compare were the WRF Single-Moment 3-class (WSM3) and the Morrison 2-Moment. The WSM3 is not the simplest of all WRF schemes, this is the Kessler scheme, though the Kessler scheme only simulates water clouds, which is unrealistic when simulating European ETCs, while the WSM3 produces ice below $0^{o}$C. The WSM3 scheme is described in detail by Hong et al. (2004) and consists of three species of water (vapour, cloud water/ice (depending on temperature) and rain/snow), which is a so-called simple-ice scheme. The more sophisticated Morrison scheme is based on the two-moment bulk microphysics scheme of Morrison et al. (2005), consisting of six species of water, vapour, cloud droplets, cloud ice, rain, snow, and graupel/hail, and is described by Morrison et al. (2009).

### 2.3.4 Description of experiments

With ETC Emma selected for detailed investigation, as identified by the method described in 2.2.3, the track of the storm will be explored to indicate where best to place the WRF domains. The aim is to place the WRF domains to capture the developing storm as it tracks towards the UK, with domain 1 covering a large area on a synoptic scale, with the nested domains 2 and 3 covering progressively smaller areas on the mesoscale. There are two main sources of real data to act as the initial and boundary conditions for WRF; NCEP's Global Forecasting System (GFS) and the ECMWF analysis. As the ECMWF analysis has been used throughout this study, it would be logical to use this to drive the WRF model runs. However, from experience, it is clear that the WRF is more numerically efficient when driven by the GFS data, as GFS and WRF have been developed by the same groups so the model/data structure is the same between the two systems, which means 'they work well together '(Dudhia pers. comm. 2009). ECMWF outputs its own terrain following eta levels (normalised pressure levels) but an essential WRF input variable is pressure, which WRF then converts onto its own eta levels. The method for terrain following eta levels used in WRF is described by Skamarock and Klemp (2008). This means that the WRF model has to convert the ECMWF eta levels onto pressure levels, whereas the GFS data is already available as pressure variable, so it is less computationally intensive to use GFS data as the initial conditions. Therefore this study will use GFS data as initial and boundary conditions for straightforward running of WRF and for computational efficiency. The available GFS data is at 1˚x 1˚ resolution.

WRF is computationally more efficient when the resolution ratio of nests is in multiples of 3. Furthermore, WRF is less effective when the resolution difference between the parent and child domains is too large (Dudhia pers. comm. 2009). Therefore the following horizontal resolutions have been chosen: domain 1 - at 27km resolution, domain 2 - 9km and domain 3 - 3km. Again for computational efficiency, WRF is run using the 2-way nesting method, with separate 1 and 2 domain runs conducted for resolution comparison, because when using domain 1 from a 2-way nested method, the feedback from the nested finer domains has an impact on the coarse grid. These horizontal resolution comparison runs are conducted with 70 WRF eta levels, while vertical sensitivity tests are carried out using 105 levels (105 levels

are used because initial WRF runs based at UEA were conducted with 35 eta levels so it was natural to use multiples of 35 for the subsequent model runs, spaced evenly between the existing levels). In turn, the ETC simulation sensitivity tests for the two microphysics schemes are conducted for the high horizontal resolution runs for both 70 and 105 levels to highlight any difference in vertical interactions between the schemes in creating strong surface windspeeds.

Figure 2.4 shows the positions of the three domains, 1 modelled at 27km resolution, domain 2 at 9km and domain 3 at 3km. Windstorm Emma tracked over the North Atlantic (section 4.1.3), so domain 1 covers the synoptic scale area of development while domain 2 simulates the ETC at a mesoscale as it approaches the UK, with the highest resolution simulations conducted over the UK in domain 3, with results analysed in chapter 5.

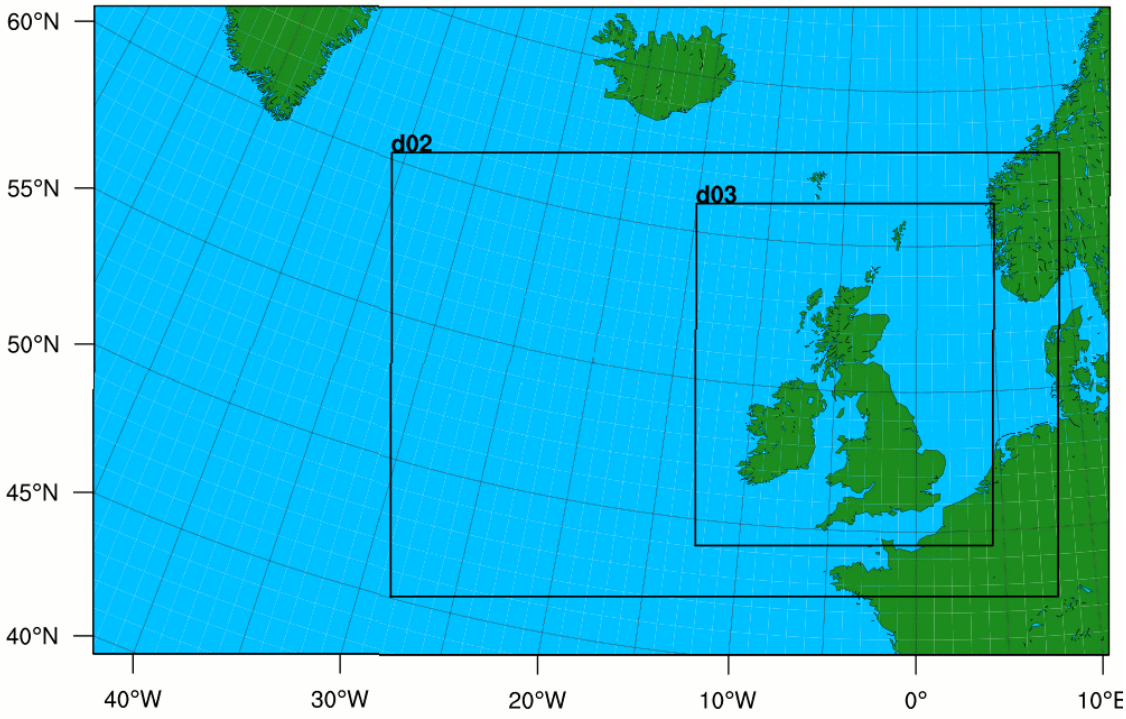


Figure 2.4 – Domain 1 (whole map) and nested domains 2 (marked d02) and 3 (marked d03) for simulation of Windstorm Emma.

## 2.4 Summary

The various methods and datasets utilised in this project, to address the research aims described in section 1.6, are described in this chapter.

In section 2.1, the surface monitoring station network data is introduced, with the data quality tests explained, along with how this database provides the opportunity to test whether the Weibull distribution function provides a good approximation to long-term observational wind data. The methodology behind quantifying the impact of the observed spatial and temporal variations on wind power energy production is described along with the data used for comparisons with the NAO. The methodology and data required for the establishment of a set of ETC events for a mesoscale ETC feature provisional-climatology completes the section.

In section 2.2 the global models contributing to the TIGGE database are described, with the details of the ensemble members for each meteorological centre, together with the various initial condition and physics perturbation methods. The range of data assimilation methods is also explored. The difficulties involved in devising a useful methodology to test the extreme windspeed forecast performance of the models contributing to TIGGE are highlighted, the diverse range of global NWP models contained within TIGGE explained and the various EPS perturbing methods considered.

A modelling system that best suits the requirements of the dynamical downscaling part of the project is the WRF model and is described in section 2.3. The WRF system and its nesting capacity are explained including physics and parameterisation schemes. WRF's ability to allow for the sensitivity testing of microphysics scheme selection is highlighted. The method for high resolution modelling experiments is described, along with justifying the use of NCEPs GFS analysis data, rather than the previously used ECMWF, for the initial and boundary conditions of the numerical experiments.

# Chapter 3

# 1980-2010 variability in UK surface wind climate

The results presented in this chapter address the first set of research aims discussed in section 1.6. These include analysis and discussion of windspeed threshold exceedence frequencies, the proportion of time that the HM winds or DMGSs are above a set of specific speeds, at individual sites and on average across the network of 40 (39) hourly windspeed (DMGS) sites first introduced by Hewston (2008), subsequently used by Hewston and Dorling (2011) and Earl et al. (2013), as described in section 2.1. This follows the approach adopted by Vautard et al. (2010) but provides detail for the UK rather than a more general continental or global scale. The further novelty of the chapter comes from using hourly data, rather than 6-hourly, by considering a high spatial density of stations in the UK, by incorporating gusts and wind directions and by including the anomalous conditions of 2010. Furthermore, the implications of a variable wind climate for wind energy density and wind power output are presented, building on the work of previous UK wind resource studies (e.g. Sinden, 2007). This chapter also includes the investigation of the applicability of the Weibull distribution to each location, as part of the quality control and to deepen understanding of each station in the network, along with sub-sampling sites to determine whether the patterns seen in the results are dominated by a selection of specific sites. Discussing the variability in the context of key features of the regional-scale atmospheric circulation, such as the NAO is also carried out in this chapter.

## 3.1 Inter-annual variability

Declining windiness across Europe between the early 1990s and the mid 2000s has previously been identified by Atkinson et al. (2006), Boccard (2009) and Wang et al.

(2009). Vautard et al. (2010) showed that this is not confined to Europe, but world-wide phenomena as discussed in chapter 1. Hewston and Dorling (2011) showed that this trend is affecting the UK, presenting evidence of a downward tendency in the strongest wind gusts over the same period, along with significant spatial variation, with the west coasts and northern areas experiencing higher windspeeds. This section quantifies the variability of the updated to 2010 network average from year to year, through windspeed averages, percentiles and threshold exceedences, as highlighted in the first set of research aims (section 1.6), along with assessing sensitivity of the selection of sites may be towards these results.

Figure 3.1 shows a time-series of the 40-station network average UK HM annual average windspeeds. The 5-year moving average exhibits peaks in the early 1980s and early 1990s, with the subsequent general declining tendency also visible. Network average windspeeds in the mid to late 2000s began to recover, however the anomalously low winds of the most recent year, 2010, discussed in detail below, contrasts with this increase. The windspeed variability is clear with network average windspeeds ranging from ~ 4.4ms$^{-1}$ in 2010 to ~5.4ms$^{-1}$ in 1986, with some rather large year to year variability. It must be noted that analysis of the annual network average acts to smooth extremes, ignores spatial variability and masks intra-annual variations; the winter storminess of the early 1990s, highlighted by Wang et al. (2009), is for example not revealed. In this chapter spatial percentiles are used (e.g. the 10$^{th}$ percentile of annual mean is calculated from the 4$^{th}$ and 5$^{th}$ lowest values of the 40 sites (4 values below and 36 above), weighted exactly between the two), while in chapter 4, temporal percentiles are used (e.g. 99$^{th}$ percentile calculated at each site by taking on the top 114 DMGS values from the 31-year long timeseries (11,323 days)).

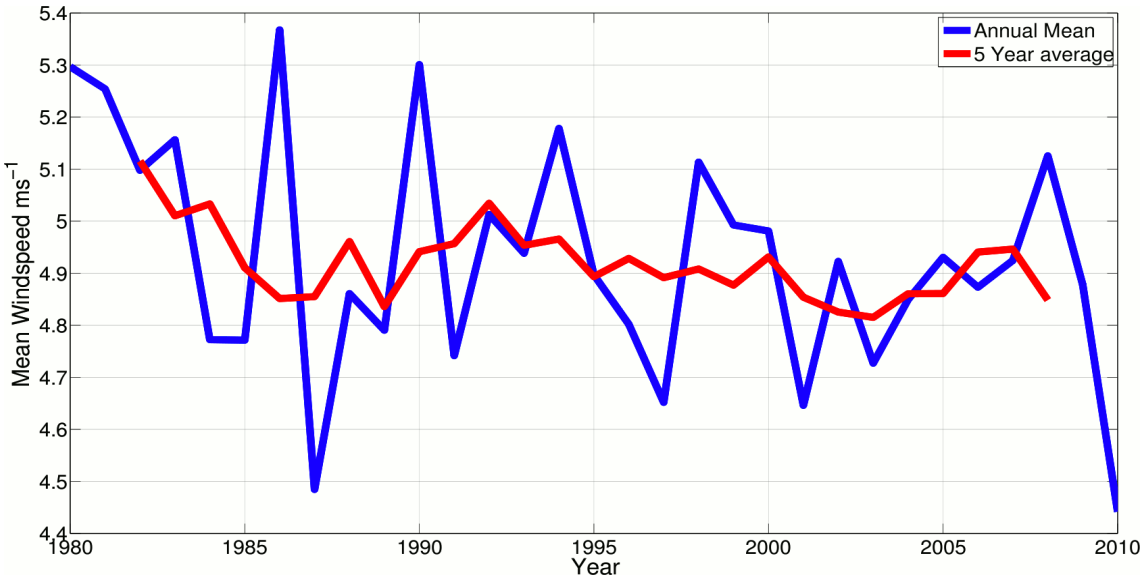


Figure 3.1 - Network average annual HM windspeeds ($ms^{-1}$), 1980-2010

Figure 3.2 shows a time-series of annual average 10m HM windspeeds in the form of the 10th, 50th and 90th percentiles, quantifying the inter-site variability to describe the data distribution in more detail. The 10th and 50th percentile 5-year moving averages exhibit peaks in the early 1980s and early 1990s, with a statistically significant decrease visible over the full 1980-2010 period (confidence levels of 99.9% and 95% for the 10th and 50th percentiles respectively; using ordinary least squared linear regression analysis). The 90th percentile shows a much more pronounced early 1990s peak, without the general decline seen in the 10th and 50th percentiles, but with a statistically significant decrease since 1990 (at the 99% level). The 10th and 50th percentiles show that in the mid-late 2000s windspeeds began to recover (as seen in the network average in Figure 3.1), however the anomalously low winds of 2010, discussed in detail below, are again at odds with this recovery. The large year-to-year variability is again apparent, for example the median varying from 4.3 to 5.3 $ms^{-1}$, not dissimilar from the network average results (Figure 3.1). These results and those of other authors mentioned highlight the presence of decadal variability and the linear trend analysis is conducted here only for completeness.

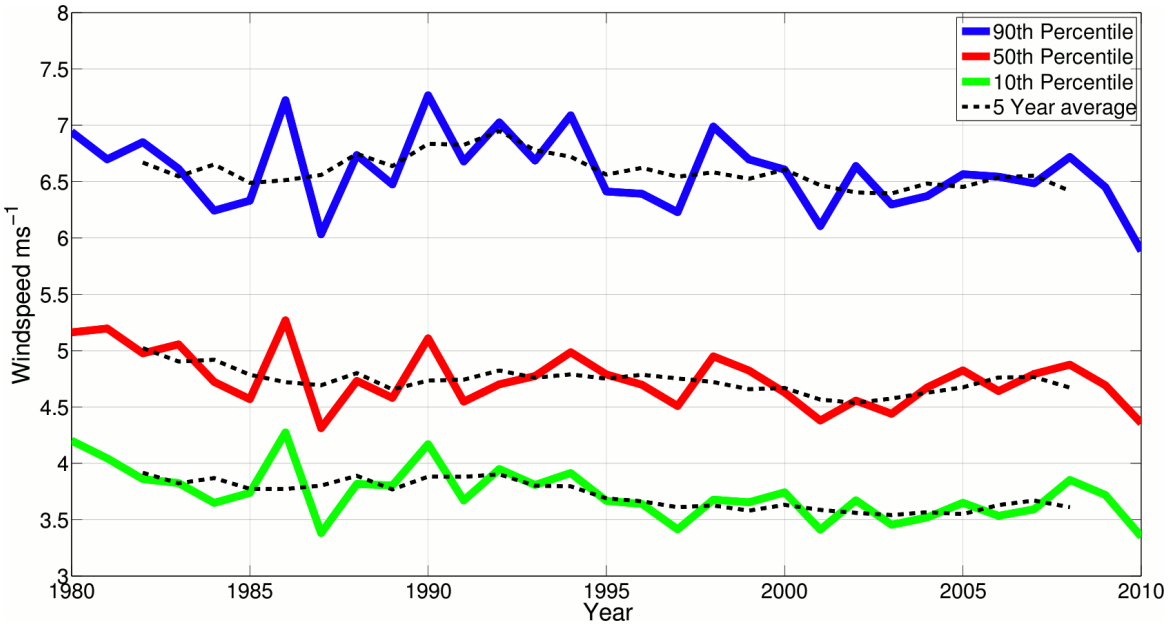


Figure 3.2 - 10th, 50th and 90th percentiles of annual average HM windspeeds (ms$^{-1}$), 1980-2010, from the 40- station network.

The level of significance for the decrease in the 10$^{th}$ percentile in Figure 3.2 is somewhat surprising, and is not seen so clearly in the literature (e.g. Vautard, 2010). Further investigation shows that this is due to decreases seen in the 3 dominant contributor sites to the 10$^{th}$ percentile. With a 40 site annual mean network, the 10$^{th}$ percentile value is calculated from the 4$^{th}$ and 5$^{th}$ lowest annual mean values (4 values below and 36 above), weighted exactly between the two. This means that in each of the 31 years, two sites contribute to the 10$^{th}$ percentile. Of these 62 (2 x 31 years) contributions to the 10$^{th}$ percentile, Nottingham (18) contributes on 17 occasions, Eskdalemuir (31) 12 times and Bala (17) 10. These inland sites are widely distributed geographically, however all show considerable decreases over the time-period as shown in Figure 3.3, and therefore have a big influence on the observed 10$^{th}$ percentile decrease.

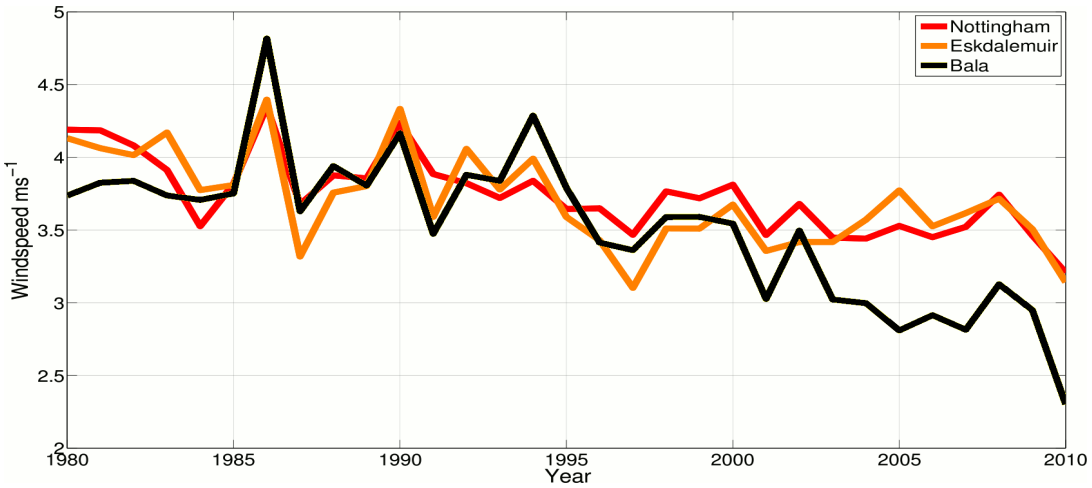


Figure 3.3 - Annual HM windspeeds (ms$^{-1}$) for the sites of Nottingham, Eskdalemuir and Bala, 1980-2010.

Other sites which also contribute to the 10$^{th}$ percentile, but not as extensively as the sites discussed above, do not exhibit such a clear decrease over the period as shown by Figure 3.4. The site for which the decline is most dramatic is Bala (17). Located in a south-west to north-east orientated valley in Snowdonia, Bala has seen a marked decline since the mid-1990s indicating that the site could be becoming more sheltered. Such a dramatic decline is not seen in any of the other network sites and will need to be investigated in future updates to the database to decide whether this decline is due to local land-use changes, making the site characteristics non-homogeneous, which subsequently may lead to its removal from the network. It is therefore interesting to examine the data presented using a different selection of percentiles.

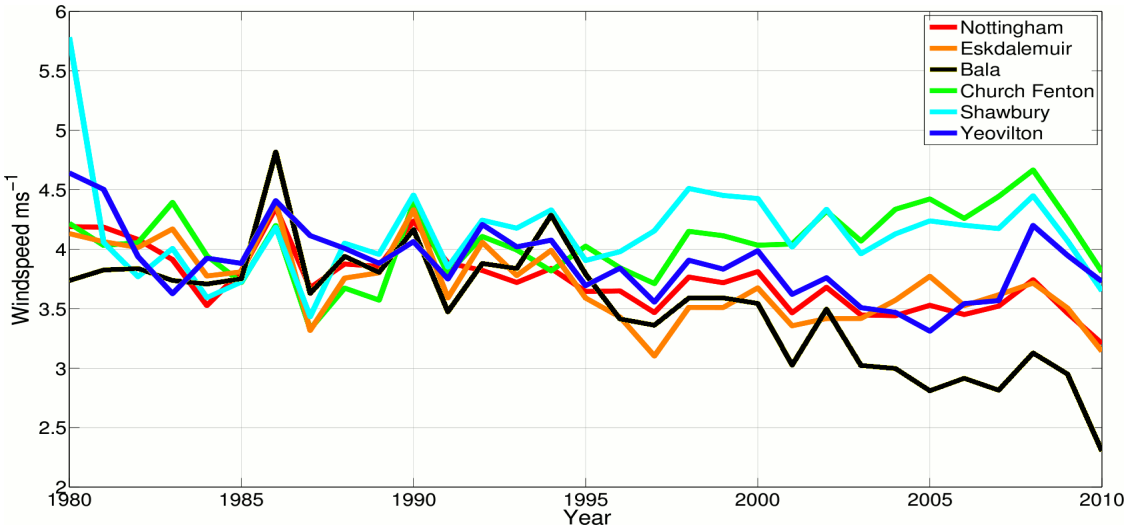


Figure 3.4 - Annual HM windspeeds (ms$^{-1}$) for the sites of Nottingham, Eskdalemuir, Bala, Church Fenton, Shawbury and Yeovilton 1980-2010.

Figure 3.5 shows a time-series of annual average 10m HM windspeeds, similar to that of Figure 3.2, but with the 20th, 50th and 80th percentiles. While the 20th percentile shows a decrease and displays similar annual variability to the 10th percentile (Figure 3.2) the decline is not statistically significant. It could therefore be said that the observed 10th percentile decline is perhaps not wholly representative of the lower wind speed range described by this network, drawing attention to the dangers of jumping to conclusions based on a single percentile. The upper percentiles (90th and 80th in Figure 3.2 and Figure 3.5 respectively) also show differences, with the early 1980s peak not seen so prominently in the 90th percentile compared with the 80th, but possessing a stronger early 1990s peak.

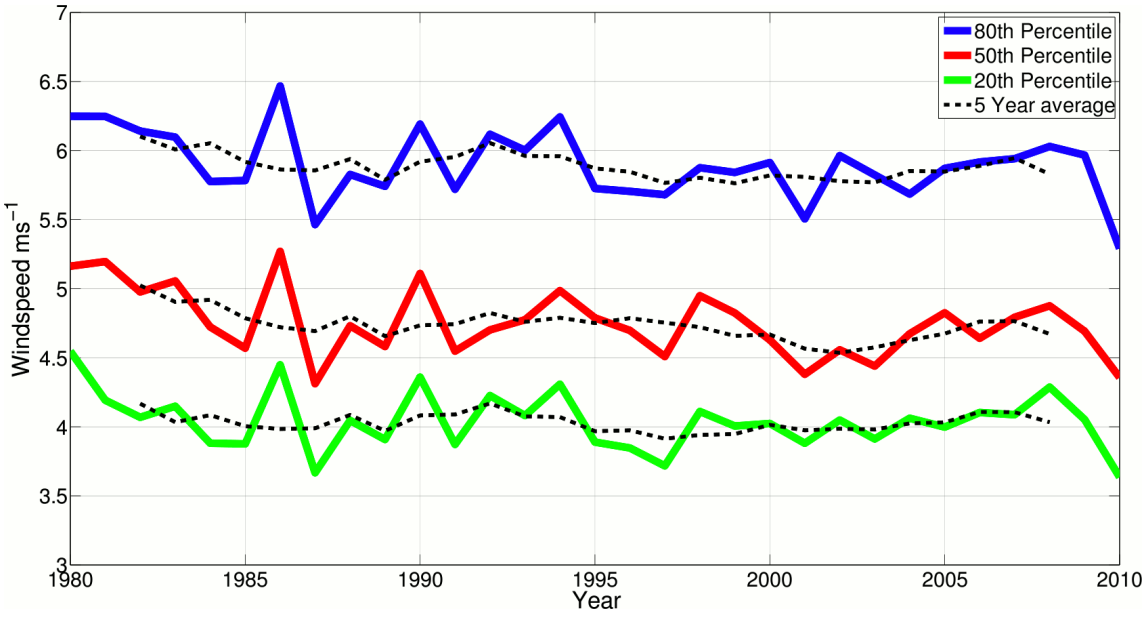


Figure 3.5 - 20th, 50th and 80th percentiles of annual average HM windspeeds (ms$^{-1}$), 1980-2010, from the 40- station network.

Behind these results from the network as a whole, it should be noted that 32 of the 40 sites display a decrease in annual mean windspeed over the full period, 15 of which are statistically significant (95% confidence level), while 8 show an increase, 2 of which are statistically significant. There is no clear geographical pattern to the distribution of stations exhibiting statistically significant changes.

To learn more about the nature of winds experienced in the UK over the 1980-2010 period, several HM windspeed exceedence thresholds were selected and the

frequency of exceedence at each site calculated. Figure 3.6 displays results, expressed as a network average, for three particular thresholds, 11ms$^{-1}$, 13ms$^{-1}$ and 15ms$^{-1}$ a 'strong breeze' on the Beaufort scale for 11 and 13ms$^{-1}$ and 'high wind' or 'near gale' for 15 ms$^{-1}$. These thresholds have been chosen here because when adjusted to wind turbine hub height, 3.6MW wind turbines begin to work at full capacity (Table 2.1) and 15ms$^{-1}$ is generally accepted as the speed at which insured property damage begins.

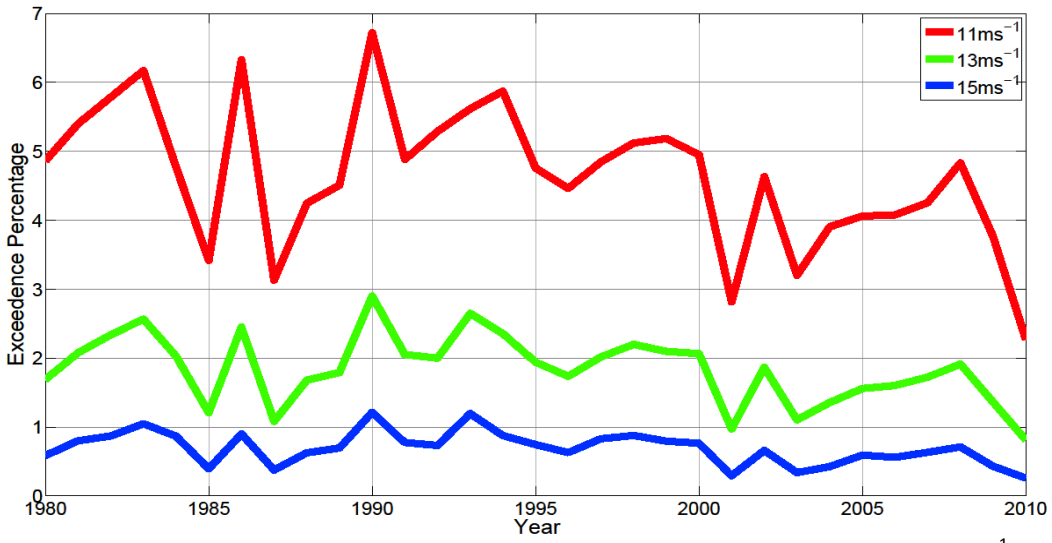


Figure 3.6 - Network average threshold exceedence percentages for 11, 13 and 15ms$^{-1}$ HM windspeeds.

Furthermore, all of the 40 sites in the network experience such windspeeds, unlike for higher thresholds which are only exceeded at a minority of sites. Throughout this chapter, the focus is on wind speed thresholds which are both consistent with those highlighted by Vautard et al. (2010) and, especially, on those for which it is known that building damage of varying degrees would be expected. It is acknowledged however that the latter actually vary with geography according to build quality as shown by Klawa and Ulbrich (2003) and so the implication of the threshold results should be seen as indicative only.

The proportion of time when the network average HM windspeed exceeds the 11ms$^{-1}$ threshold ranges from just over 2% of the time in 2010, due to the cold and relatively calm months of January and December that year (see 2010 windspeed and direction in Figure 3.7(d)), to 6.7% in 1990, associated with the storminess of January and February. The inter-annual variation is striking with, for an extreme example, 1986

experiencing winds in excess of 11ms$^{-1}$ for twice as many hours as in the previous and following years, a feature also reported by Vautard et al. (2010) for Europe as a whole, though less pronounced. The 13ms$^{-1}$ and 15ms$^{-1}$ threshold exceedences exhibit a similar pattern to that of 11ms$^{-1}$ with the 13ms$^{-1}$ (15ms$^{-1}$) ranging between just below 1% (just above 0.25%) and just below 3% (just below 1.2%) also in 2010 and 1990, respectively. The early 1980s and early 1990s, particularly the latter, have the highest proportion of HM windspeeds over each threshold, with a statistically significant decrease from 1980 for 13ms$^{-1}$ and 11ms$^{-1}$ exceedences (95% and 99% confidence respectively). The peak seen in the early 1980s is less apparent in the 15ms$^{-1}$ exceedence threshold and does not exhibit a statistically significant decrease since 1980 but has a strong decline (≥99% confidence) since the peak in 1990. The more intense the threshold exceedence, the more marked the peak in the early 1990s compared with that of the early 1980s, which is in keeping with the 90$^{th}$ and 80$^{th}$ percentiles of the HM annual average windspeed shown in Figure 3.2 and Figure 3.5 respectively. This reinforces the findings of Wang et al. (2009), suggesting a more volatile wind regime in the early 1990s with more 10m winds reaching in excess of 15ms$^{-1}$ but with a lower average windspeed compared to the early 1980s.

Figure 3.1 -Figure 3.6 all reveal a large change between the adjacent years 1986 and 1987, 1986 recording far higher windspeeds. To further investigate this difference, network average wind roses were produced for both years (Figure 3.7 (a) and (b), 1986 revealing a much more pronounced tendency for south-westerly winds. This is to be expected with stronger south-westerly winds associated with the ETC storm track approaching the UK from the west or south-west (Dacre and Gray, 2009). Increased south-westerly winds are positively correlated with the NAO (Cheng et al., 2011) and the monthly NAO index is significantly more positive in January, October, November and December in 1986 than in the equivalent 1987 months as discussed in section 3.2. The extreme high and low wind years of 1990 and 2010 (Figure 3.7 (c) and (d)) respectively also display the same pattern with 1990 possessing dominant strong south-westerly flows and 2010 relatively weak and evenly spread, associated with record breaking negative NAO values as discussed in section 3.2.

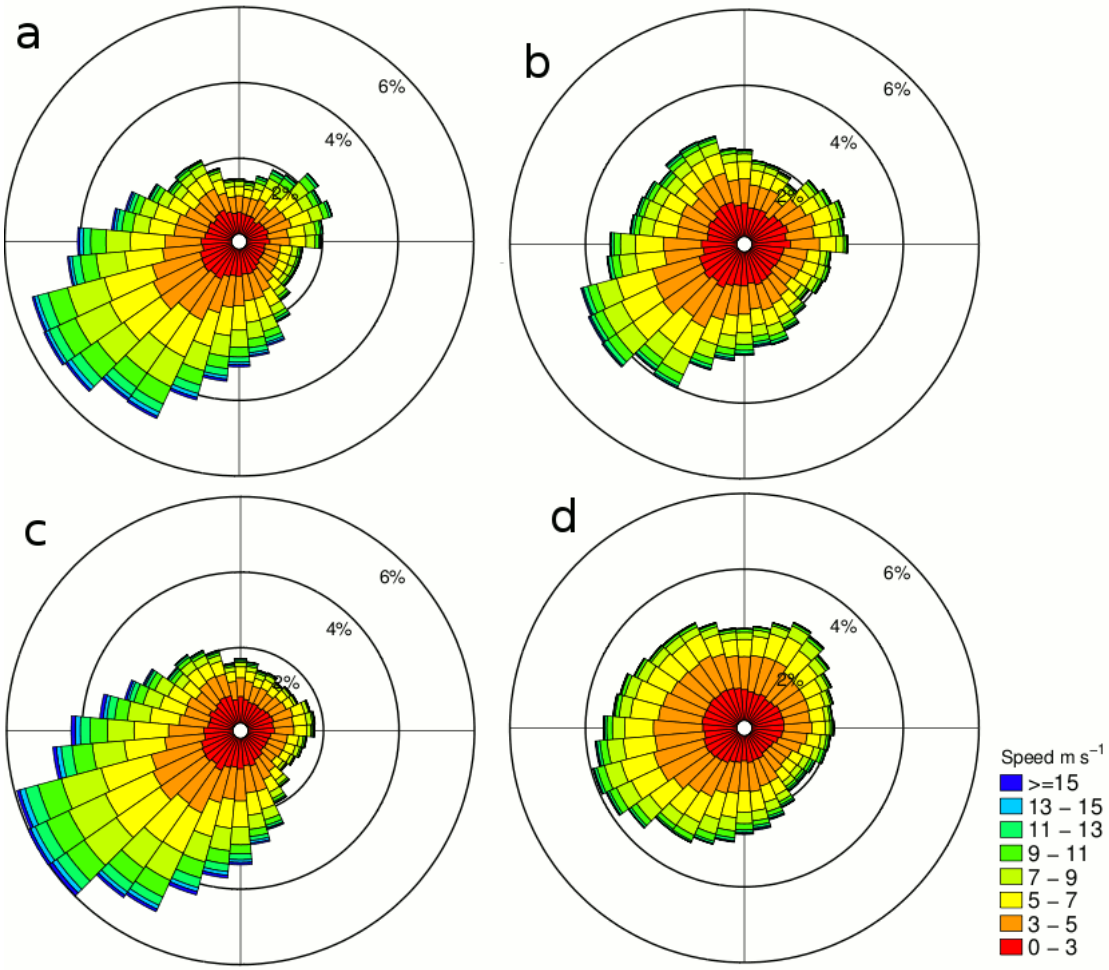


Figure 3.7 - Network average HM wind roses for 1986 (a), 1987 (b), 1990 (c) and 2010 (d).

The peaks of the early 1980s and early 1990s are further highlighted by the five year running mean of network average HM windspeed threshold exceedence shown in Figure 3.8, though the early 1980's peak is not as pronounced as in the 10$^{th}$ and 50$^{th}$ percentiles of site HM windspeeds shown in Figure 3.2. In Figure 3.8, in addition to the 11ms$^{-1}$, 13ms$^{-1}$ and 15ms$^{-1}$ exceedence thresholds shown in Figure 3.6, further thresholds of 3ms$^{-1}$, 5ms$^{-1}$, 7ms$^{-1}$ and 9ms$^{-1}$ are also included. Although the logarithmic scale somewhat reduces the visual impact of the variability, nevertheless a statistically significant decrease (≥99% confidence) over the last 20 years remains visible for exceedence thresholds in the range 7-15ms$^{-1}$. As expected, the contribution of individual sites to the total exceedence percentage varies throughout the network, especially as the exceedence thresholds rise and become of interest for the insurance sector. This is discussed in detail below (section 3.4), with Figure 3.16(a) highlighting the site contribution variations for the 15ms$^{-1}$ threshold.

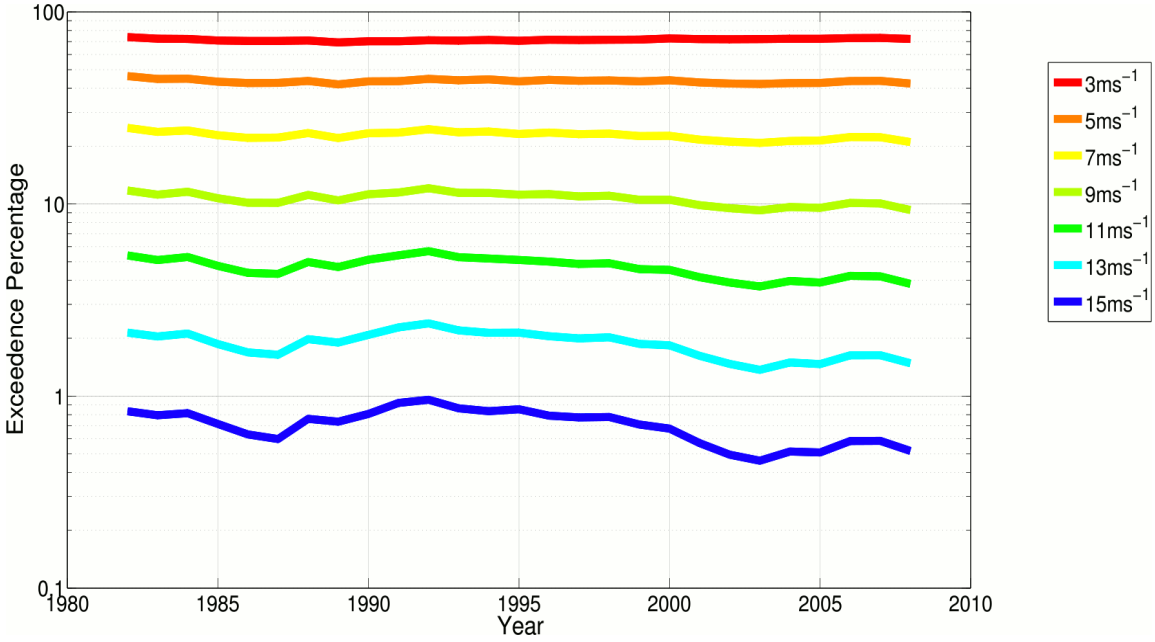


Figure 3.8 - Network average 5-year running mean HM threshold exceedence percentages for 3, 5, 7, 9, 11, 13 and 15ms$^{-1}$ HM windspeeds.

One of the findings of Vautard et al. (2010) was a general decline in European windspeeds over the last 30 years, especially for extreme winds, whereas UK results presented here more strongly emphasize an early 1990s peak and a marked decline over the last 20 years, highlighting the importance of not assuming a simple overall linear trend. We might not be surprised by this difference due to the UK's location on the edge of Europe, more exposed to the Atlantic, compared to the continental scale of the Vautard et al. (2010) study. Results presented here extend and are consistent with the UK, NAO and Grosswetterlagen indices presented by Atkinson et al. (2006) and with the broader spatial scale findings of Wang et al. (2009) and Boccard (2009).

The DMGS exhibits a similar long-term variability to that of the HM as depicted by the five year moving average of network average DMGS threshold exceedence shown in Figure 3.9. Higher thresholds are included here compared with the HM analysis, ranging from 9ms$^{-1}$ - 35ms$^{-1}$, revealing peaks in the early 1980s and early 1990s with the exception of the highest 35ms$^{-1}$ exeedence threshold which does not have such a marked peak in the early 1980s but a more extreme maximum in the running mean around 1991/2. The 35ms$^{-1}$ 1980-2010 decline is statistically significant (with 99% confidence) accommodating a peak in 1993, with the windspeed exceeding the threshold 0.5% of days (at all sites), compared to 2001 and 2010 when this threshold

was not breached at all (not shown). Lerwick (station 40) and Kirkwall (39), in the Northern Isles (Figure 2.1), contributed to 16 and 15 days respectively of the total 69 DMGS values in excess of this extreme wind threshold in 1993 (not shown). Note that 20ms$^{-1}$ is generally accepted as a starting wind gust (~15ms$^{-1}$ for associated HM) threshold for minor structural damage in connection with insurance claims.

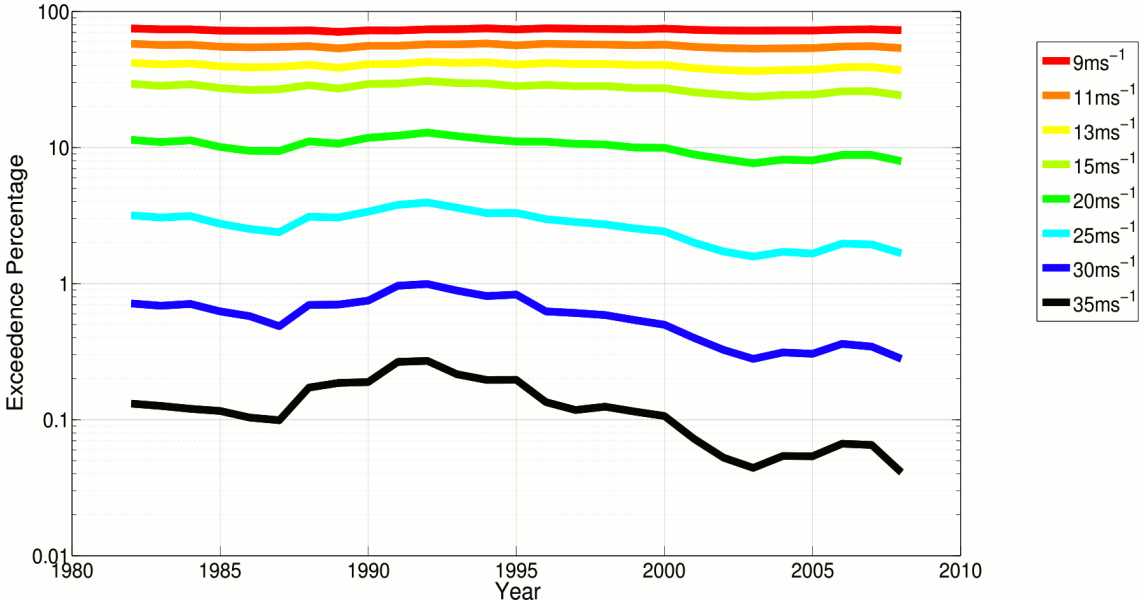


Figure 3.9 - Network average 5-year running mean threshold exceedence percentages for 9, 11, 13, 15, 20, 25, 30 and 35 ms$^{-1}$ DMGS.

### 3.1.1 Sub-sampling sensitivity tests

It is well known that extreme winds are not evenly distributed throughout the UK (Wheeler and Mayes, 1997) and the results here show that threshold exceedences are not equally distributed amongst the stations making up the observation network as discussed in section 3.4. With this and the data quality research aim (section 1.6) in mind, sensitivity tests of the inter-annual variability of threshold exceedences to the network configuration have been carried out. This was based on the removal of the five most significant contributor stations to the 15ms$^{-1}$ HM and 25ms$^{-1}$ DMGS exceedence thresholds in Figure 3.8 and Figure 3.9 respectively. This is, in effect, re-sampling 35 out of the 40 stations for the HM and 34 out of the 39 DMGS stations, removing the stations which make the largest contribution to the exceedence of these thresholds. In doing this, the largest possible impact on the results of removing 5 stations from the analyses is quantified.

The most significant contributor stations were identified from the 15ms$^{-1}$ threshold results (as seen in Figure 3.16-a in section 3.4) and were the sites of Lerwick (40), Aberporth (13), Valley (22), Kirkwall (39) and Salsburgh (33) contributing 17.2%, 9.6%, 8.9%, 8.7% and 6.4% respectively. Figure 3.10 shows the remaining 35 out of the 40 HM network sites and is essentially a re-working of Figure 3.8. While the removal of these five stations leads to inevitable quantitative changes of exceedence percentage, the year to year variations remain similar to the corresponding original with the peaks of the early 1980s and early 1990s prominent and the strengthening of the early 1990s peak as the thresholds rise.

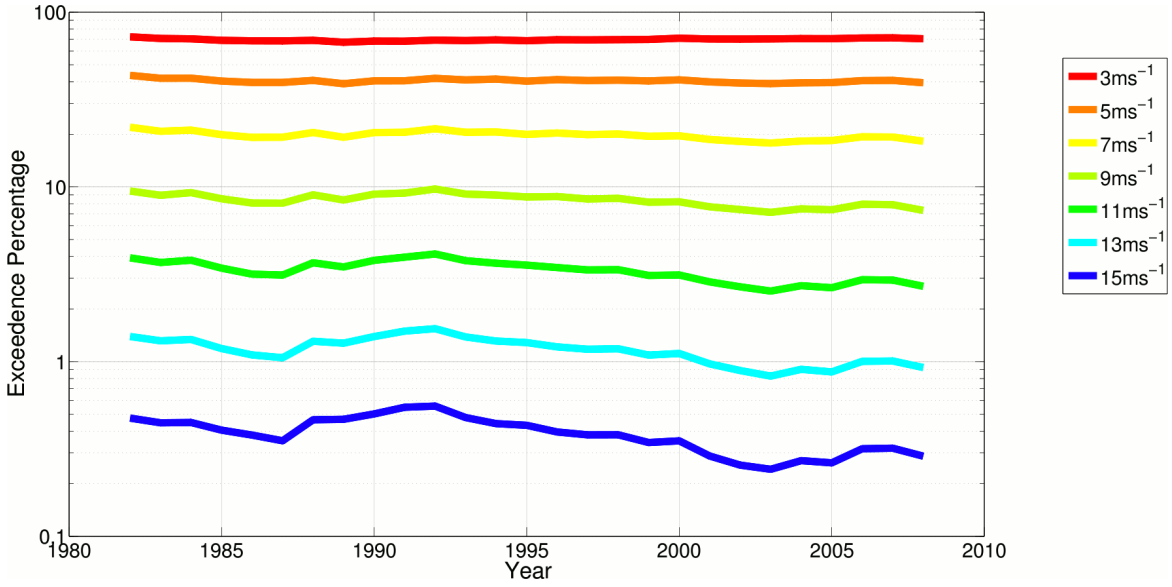


Figure 3.10 - 35 out of the 40 HM network sites with Lerwick (40), Aberporth (13), Valley (22), Kirkwall (39) and Salsburgh (33), the biggest, 2nd , 3rd , 4th and 5th biggest contributors respectively to the 15 ms$^{-1}$ threshold (see Figure 3.16(a)), removed.

For the DMGSs, the most significant contributor stations were Lerwick (40), Kirkwall (39), Aberporth (13), Stornoway (38) and Culdrose (1), identified from the 25ms$^{-1}$ threshold results contributing 9.5%, 6.7%, 6.5%, 5.9%, and 5.6% respectively. Figure 3.11 shows the remaining 34 out of the 39 DMGS network sites and is again a re-working of the original, Figure 3.9. As with the HMs there are quantitative changes of exceedence percentages but the variations between thresholds are similar and the interpretation of the periods of enhanced and reduced exceedence remains unchanged. These results enhance the confidence of the observation network, to give

a suitable and accurate portrayal of the UK wind regime, indicating low sensitivity to specific station choice.

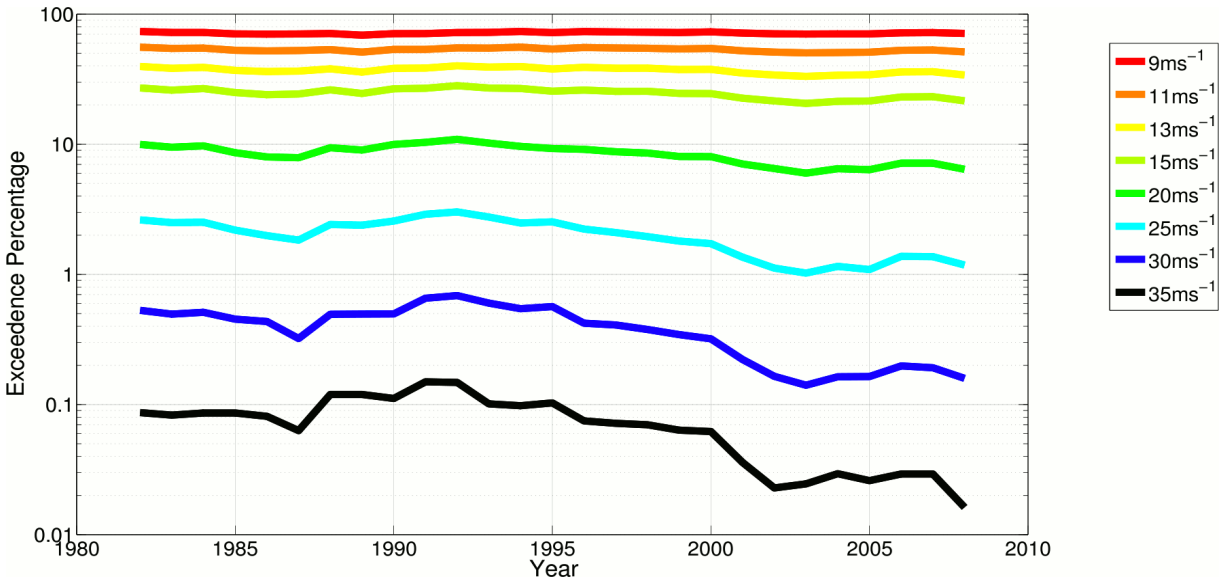


Figure 3.11 - 34 out of the 39 DMGS network sites with Lerwick(40), Kirkwall(39), Aberporth(13), Stornoway(38) and Culdrose(1), the biggest, 2nd , 3rd , 4th and 5th biggest contributors respectively to the 25 ms$^{-1}$ threshold, removed.

## 3.2 NAO – driver of temporal wind climate variations

The specific evolution of the UK wind regime, both inter- and intra-annual, is heavily dependent on the phase of the NAO (Hurrell et al., 2003), as discussed in section 1.2, and it is an aim of this research to discuss these results in the context of key features of the regional-scale atmospheric circulation (section 1.6). A high NAO winter means a strong storm track with a north-eastward orientation, which brings depressions and strong winds into NW Europe, whereas a low NAO winter produces a weaker, east-west oriented storm track, taking depressions into Mediterranean Europe, leaving the UK with relatively low winds (see CRU website http://www.cru.uea.ac.uk/cru/info/nao/ for more detail). This section explores how the NAO phase affects the HM network as a whole, also putting the 1980-2010 database into a far longer (1823-2011) context.

The index shown in Figure 3.12 represents the NAO in the winter months (DJFM; Cornes et al., 2013), but is calculated throughout the year. The locations of the sites are closer then to the respective ‘centres of action’ during winter, however it remains

informative during the other seasons. Winter often sees more negative extremes and summer positive extremes. The monthly index (the difference between the normalised sea level pressure over Gibraltar and the normalised sea level pressure over Southwest Iceland) ranges between -1 and 1 ~42% of the time, with more extreme values of ≤-2 and ≥2 occurring ~12% and ~14% of the time respectively (CRU website). Monthly extremes range from -6.05 to 6.66 over the whole 189 years.

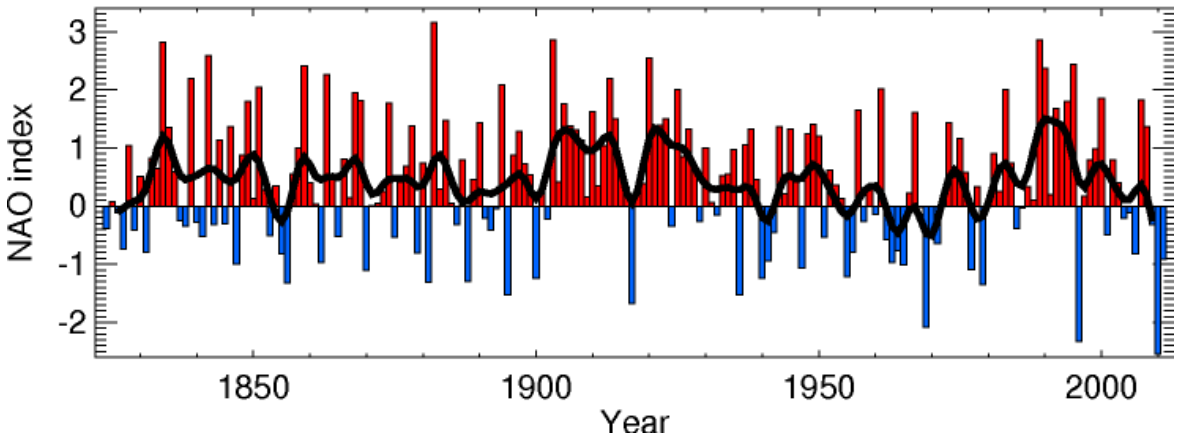


Figure 3.12 - Winter (DJFM) NAO index normalised sea-level pressure observations at Gibraltar and southwest Iceland 1823-2011 with 10-year Gaussian-weighted filter (Osborn website http://www.cru.uea.ac.uk/~timo/datapages/naoi.htm)

A more positive NAO is associated with enhanced storm activity over the Icelandic low region, experiencing not necessarily more frequent but more intense storms (Serreze et al., 1997). This leads to the UK being more affected by the extreme westerly winds. The long-term record of the NAO index in winter (DJFM) is shown in Figure 3.12. The inter-annual variability is clear, with the 10-year Gaussian-weighted filter highlighting the longer term fluctuations. Positive NAO (strongest westerlies) peaks in the early 1980s and particularly the early 1990s are apparent, with the all-time 10-year Gaussian-weighted filter peak in the early 1990s associated with the unprecedented storminess described by Wang et al. (2009). The decrease since the early 1990s is clear, and goes a long way to explain the declining trends in HM UK wind observations and DMGSs over the last 20 years, as can be seen in Figure 3.1 -Figure 3.6. The winter of 2009/10 had a substantially more negative NAO index than any other winter measured during the record (Osborn, 2011), explaining the anonymously low windspeeds observed. The consecutive winters 1994/5 and 1995/6 produced the greatest year to year contrast since the series began in 1823, however this was not seen in the station observations (Figure 3.1 - Figure 3.6) showing that winter NAO

index is not the only important factor contributing to the UK wind regime and hence the importance of studying intra-annual variability as discussed below. However, a more useful comparison with the winter NAO is the observed winter windspeeds, as discussed in section 3.3.

To investigate the effects that the NAO index variations have on the observed UK wind climate, two network average wind roses are presented in Figure 3.13, highlighting the difference in windspeed and direction observed during months (throughout the year) when the NAO index is in strong negative (≤ -2) and strong positive phase ( ≥2). When the NAO is in strong positive phase, observed winds are stronger and very much dominated by the south-west sector, whereas during periods of strong negative phase, the speeds are more often lower and the direction much more evenly spread, with a greater tendency for north-easterlies. During negative NAO phase, the anomalous increase in pressure over Iceland suppresses westerly winds, diverting the storm track southwards over the Mediterranean and encouraging a more northerly and easterly flow over the UK (Hurrell et al., 2003).

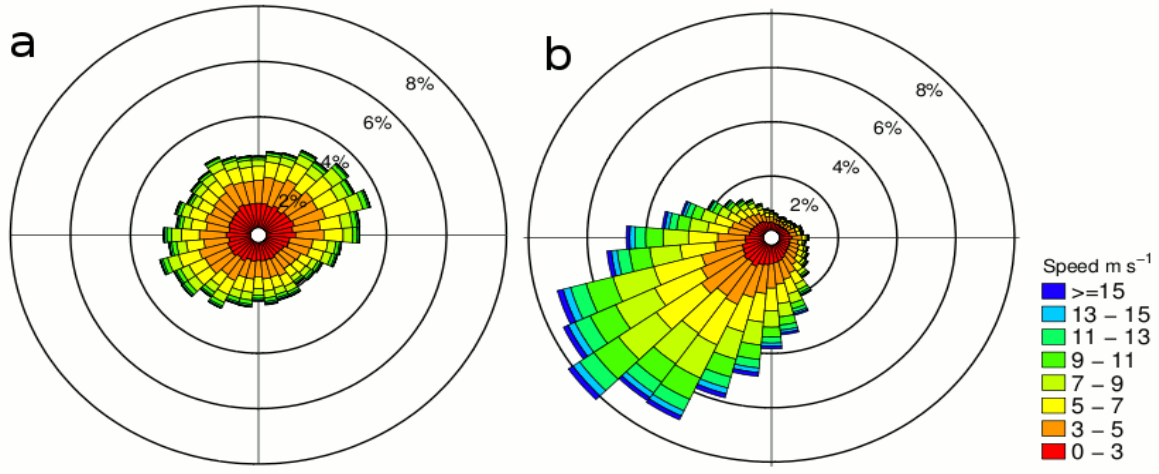


Figure 3.13 - 1980-2010 network average HM wind roses when NAO index is ≤-2 (a) and ≥2 (b).

## 3.3 Intra-annual variability

The extensive HM dataset established here has been used to investigate inter-annual variability, giving no indication of what is going on within each separate year. The aim of this section, as mentioned in the research aims (section 1.6), is to investigate the intra-annual variability by splitting the years into their respective seasons as Vautard et al. (2010) did at a continental scale. Separating the winter months also presents the opportunity for more direct comparison with the winter NAO time-series.

The considerable intra-annual wind variation in the UK is highlighted in Figure 3.14 by the seasonal network averages and 5-year seasonal averages of HM windspeed for 15ms$^{-1}$ threshold exceedences. The winter peak of HM windspeeds exceeding 15ms$^{-1}$ during the early 1990s is apparent, displaying the impact of the associated intense winter storminess (Wang et al., 2009), especially in the 5 year moving winter average. The statistically significant winter decline since 1990 (99% confidence) is particularly marked, generally following a similar progression to that of the NAO winter index series (Figure 3.12); strongly positively correlated with an 'r' value of 0.54. The winter of 1989/90 witnessed the highest 15ms$^{-1}$ threshold exceedence percentage of ~3.5%, with the lowest (complete) winter being in 2009/10, exceeding 15ms$^{-1}$ just 0.3% of the time, lower than in most autumn and spring seasons.

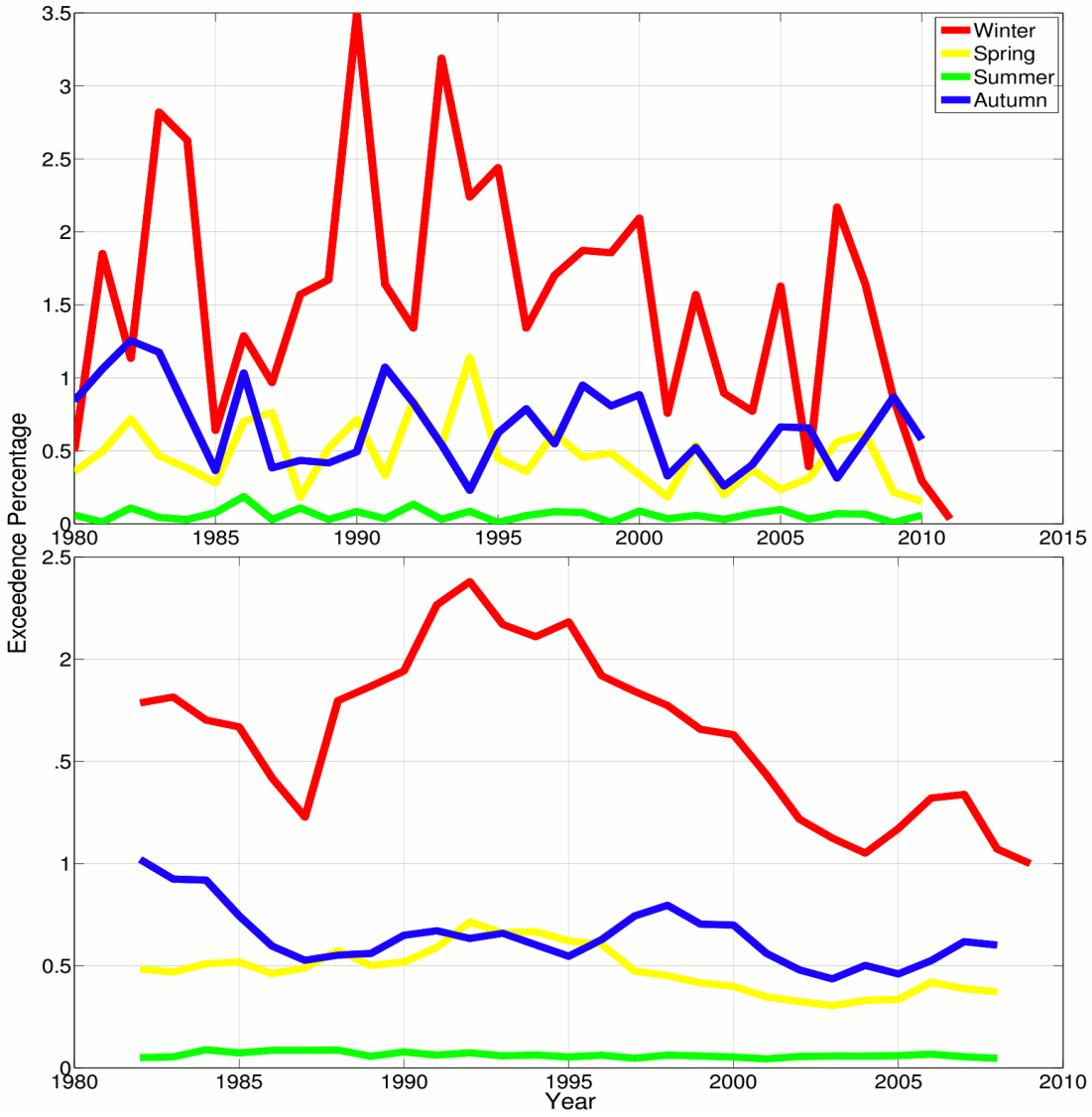


Figure 3.14 - Network average (top) and 5 year average (bottom) threshold exceedence percentages for 15 $ms^{-1}$ HM windspeeds during each season, winter (DJF), spring (MAM), summer (JJA) and autumn (SON) (note that the winter of 1980 only includes Jan and Feb 1980 and the winter of 2011 only includes Dec 2010).

The spring 15$ms^{-1}$ exceedence percentage (Figure 3.14) generally hovers around 0.5%, peaking at over 1% in 1994. Autumn meanwhile does not reveal a peak during the early 1990s, but was more extreme instead at the start of the observation period during the early 1980s and also peaked in the late 1990s before declining once more. This result is partially consistent with the findings of Vautard et al. (2010) who found that between 1979 and 2008, the most substantial linear decrease in Europe occurred in the autumn season. The relatively high 15$ms^{-1}$ exceedences of the early 1980s in autumn is consistent with the early 1980s peak in UK observations (Figure 3.1 -Figure 3.6) are not as apparent in the NAO winter time series. Meanwhile, summer season

threshold exceedences remain low and relatively consistent throughout the observation period. From this we can deduce that the threshold exceedence peak of the early 1980s is associated with higher winds in both winter and autumn seasons, whereas the early 1990s peak is caused mainly by the winter storminess alone.

Figure 3.14 shows the extent to which sub-annual variability can fluctuate independently of other parts of the year with, for example, winter seeing a large decline towards the end of the 31 year dataset, whereas the over 15ms$^{-1}$ HMs during the autumn seasons began to recover during this period. There are numerous factors which are contributors to this variability, with sea surface temperatures and NAO phase playing important roles as discussed in the previous section, along with other synoptic and global scale processes, including the Madden–Julian oscillation (MJO) phase and the phase of the El Niño–Southern Oscillation (ENSO). The MJO is the dominant mode of intra-seasonal variability in the tropical atmosphere and is characterised by an eastward propagation of large areas of both enhanced and suppressed tropical rainfall, observed over the Indian and Pacific Oceans, with the enhanced convection and precipitation phase followed by a dry phase in a cycle of 30 - 60 days. There is high inter-annual variability in MJO activity and it is linked to ENSO. Strong MJO is often experienced in the Pacific 6 - 12 months prior to the onset of El Niño, but not during the El Niño maxima, while MJO activity is typically greater during La Niña. The downstream effects of increased MJO activity produces coherent extratropical circulation anomalies including increased westerly flow extending across northern Europe (Matthews et al., 2004) affecting the wind regime of the UK on an intra-annual timescale. Further work is required to assess the relative importance of these mechanisms on the UK wind regime.

As the seasonal variation of the HM wind exceedence threshold of 15 ms$^{-1}$ is so strong, especially between winter and summer; Figure 3.15 displays the network average wind direction distribution for each season over the 1980-2010 period. All of the seasons are dominated, on average, by winds from the south-west quadrant, winter unsurprisingly having the strongest such winds, associated with the storm track moving south during the northern hemisphere winter (Dacre and Gray, 2009). Autumn has a similar looking wind rose to that of winter, whereas summer and spring have

different appearances, summer having a more influential north-west quadrant (and lower windspeeds overall) and spring a more significant north-easterly component. During summer the Atlantic westerlies are less dominant with the storm track pushed north by the Azores High, leading to climatologically more high pressure systems centred to the west of the UK producing comparatively more north-westerly winds. This means that summer winds are generally less extreme in speed despite the increase in thunderstorm activity seen in the summer and the associated potential for damaging downdrafts (Wheeler and Mayes, 1997). Conditions during spring and early summer are more favorable for blocking situations over northern Europe (Barriopedro et al., 2006), leading to comparatively more wind with a north-easterly component as confirmed in Figure 3.15(b).

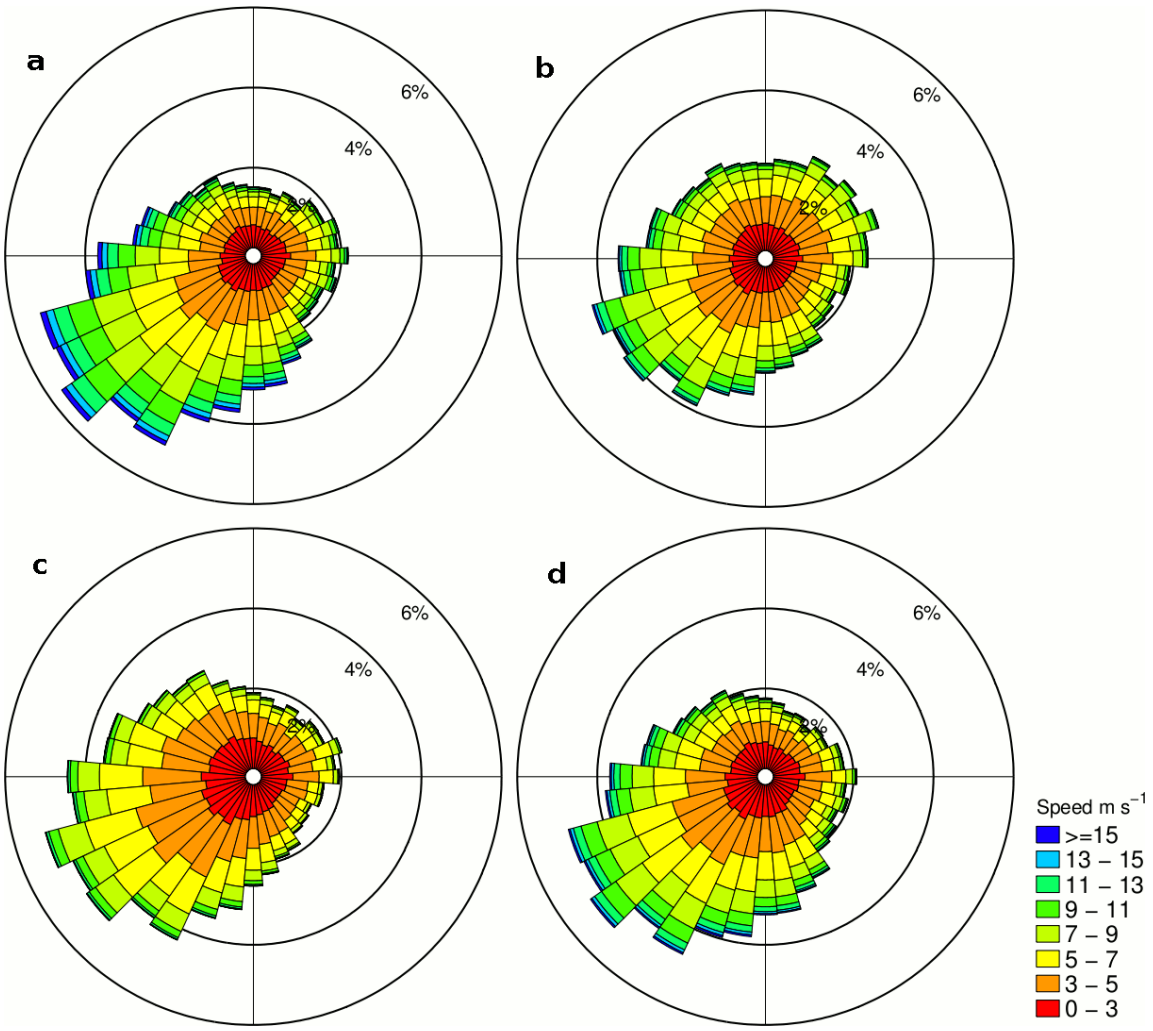


Figure 3.15 - Network average HM seasonal wind roses, 1980-2010, winter (a), spring (b), summer (c) and autumn (d).

## 3.4 Spatial variability

In the previous sections, the sites have been treated as a network average, which favours sites located in more exposed parts of the UK, as mentioned in the sensitivity testing in section 3.1. Here, in this section, the network is broken into individual site contributions and wind directions are explored in more detail, both as a network as a whole and on an individual basis, satisfying the spatial variability aspect mentioned in the research aims (section 1.6).

When dealing with the network average of exceedence thresholds, spatial variability is hidden. Spread across the UK, the network sites possess characteristics that vary considerably, both in topography and exposure to the storm track (Figure 2.1). Exposure to fetch over the Atlantic Ocean and Irish Sea is important, along with the latitude and altitude; the higher and further north a site is, the stronger the wind due to reduced friction at exposed high altitude sites and greater a proximity to the higher storm track density region to the south and east of Iceland (Dacre and Gray, 2009) in the north of the UK. Surface roughness and vegetation also play key roles as highlighted by Vautard et al. (2010). These points in mind, the relative contributions of each site to threshold exceedence, especially for higher thresholds, are expected to vary significantly. Figure 3.16 shows the relative contributions of each site to the exceedences of HM 15ms$^{-1}$ (speed at which insured property damage begins) and 25ms$^{-1}$ windspeed thresholds over the period 1980-2010, the circle size representing the contribution percentage. The 15ms$^{-1}$ site contributions are dominated by the west coast sites exposed to the Atlantic and Irish Sea, for example Aberporth (station 13 – Figure 2.1) and Ronaldsway (27), while the two sites furthest north, Kirkwall (39) and Lerwick (40), also make up more than 25% of the exceedences. This is unsurprising considering that the latter areas, closer to the Icelandic low, are susceptible to more intense storms, especially during positive NAO (Serreze et al., 1997). Meanwhile the west coast stations experience reduced friction when flow is onshore. This is further highlighted in the 25ms$^{-1}$ site contribution map (Figure 3.16(b)) with even more weight towards exposed sites and the most northerly Kirkwall (39) and Lerwick (40) stations.

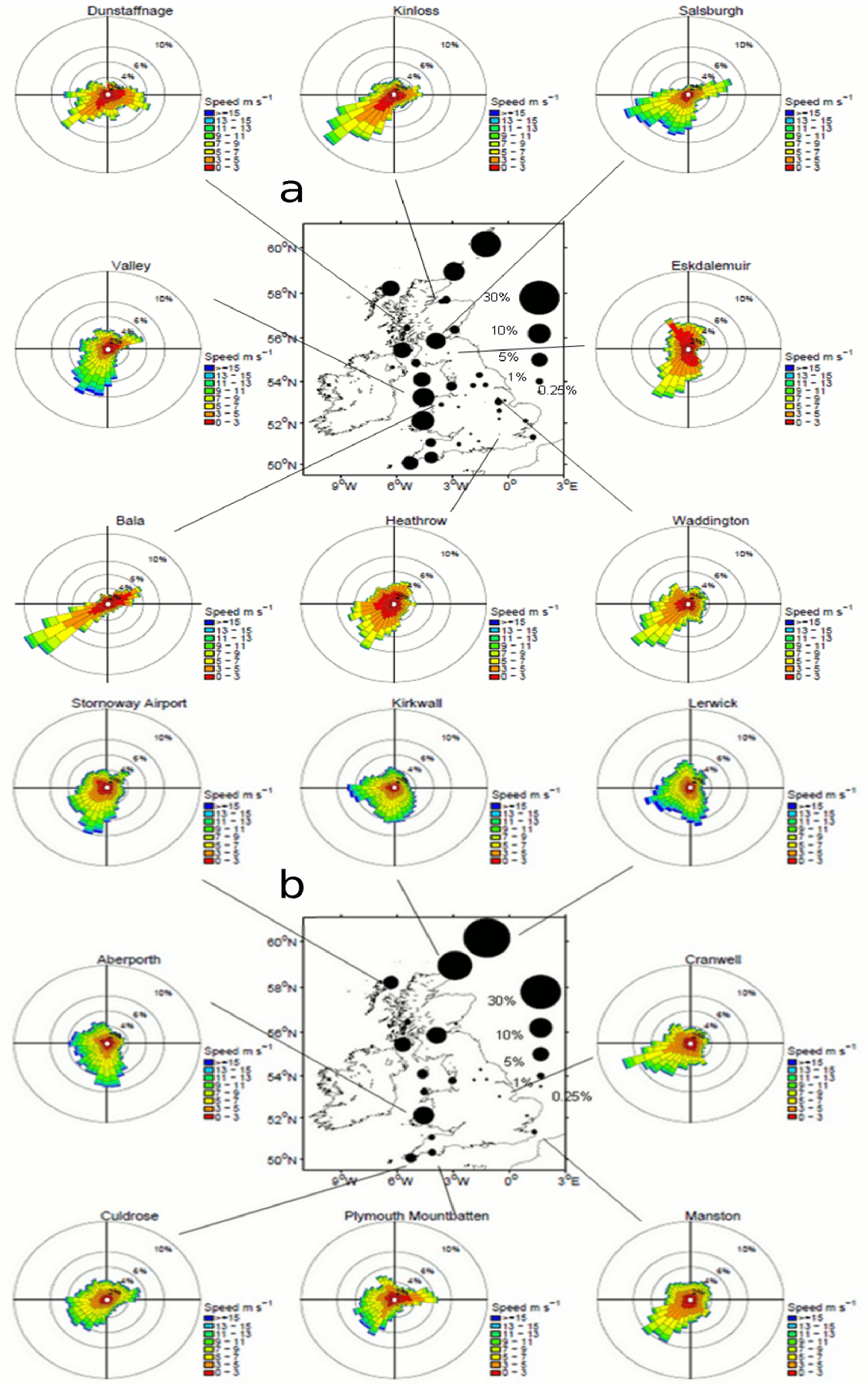


Figure 3.16 - Contribution (percentage) of each site to 15 $ms^{-1}$ (a) (total counts 74154) and 25 $ms^{-1}$ (b) (total counts 323) HM windspeed threshold exceedence plus selected all-windspeed 1980-2010 individual site wind roses.

Inland sites rarely contribute to either exceedence threshold compared with their more coastal neighbours. The inland northern sites of Eskdalemuir (31) and Salsburgh (33) are situated only 50 miles from each other and have similar altitudes of 242 and 277m respectively, however Salsburgh contributes far more to the $15ms^{-1}$ and $25ms^{-1}$ exceedence thresholds (just under 10% for each), with Eskdalemuir not exceeding $25ms^{-1}$ at all during the 1980-2010 period. Eskdalemuir is situated in a north-south orientated valley, with tree covered ridges on either side, whereas the Salsburgh monitoring site is located on an exposed grass covered hill with a large flat top to the north and east. Centrally located in Scotland's heavily populated central belt, Salsburgh is broadly representative of the insurance risks associated with windstorms transitioning across this important area. The Salsburgh- Eskdalemuir contrast is highlighted in the 1980-2010 HM wind roses in Figure 3.16, with wind direction distribution affected by the site characteristics, meaning that Eskdalemuir is somewhat sheltered from the strong westerly winds. Many of the site characteristics are highlighted by their respective wind roses, with Bala (17) located in a south-west to north-east orientated valley in Snowdonia, dominated by south-westerly and north-easterly winds, whereas the relatively flat and open site of Heathrow possesses a similar wind direction distribution to that of the network average with a prevailing south-westerly (Figure 3.17). Whiteman and Doran (1993) found that in the south-west to north-east orientated Tennessee Valley, the wind is constrained by topography, driven by the along-valley pressure-gradient, and often blows along the valley's axis despite a contrasting wind direction above the valley. This goes some way to explain the wind directions of Bala and Eskdalemuir, however, a more detailed study is required to confirm this.

It is generally stated that the prevailing wind in the UK is south-westerly, though there is a surprising lack of information available regarding this parameter in the literature. The HM windspeeds, for the 1980-2010 period, including all 40 UK measuring stations considered here, provide the opportunity to test this assertion using long-term observations. Figure 3.17 displays the network average direction over the full period, showing that that south-westerly wind is indeed the most common with the compass bearing (to the nearest $10^{O}$) of $230^{O}$ the most dominant (5.15%) and $120^{O}$ (1.75%) the least.

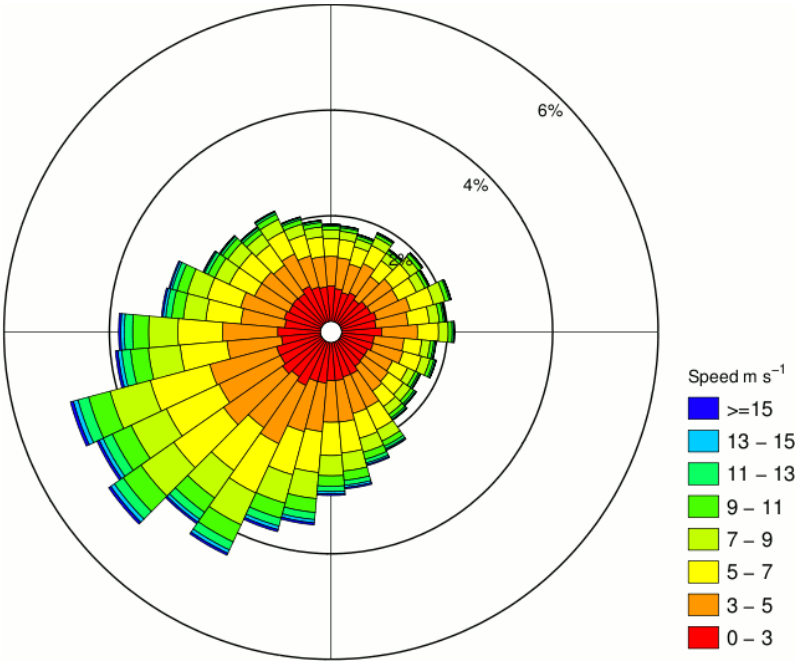


Figure 3.17 -1980-2010 network average wind rose

Table 3.1 shows the network average proportion of wind direction for each quadrant of the compass, revealing the south-westerly predominance of just under 40%. Despite this UK wind south-westerly orientation; there is an easterly component to the UK HM wind 38.1% of the time.

| Quadrant of wind direction | Percentage of Wind Direction | Percentage of Energy Density | Percentage of DMGS Wind Direction |
|---|---|---|---|
| North-east (10° - 90°) | 17.9 | 11.1 | 17.5 |
| South-east (100° - 180°) | 20.2 | 17.8 | 19.6 |
| South-west (190° - 270°) | 39.8 | 51.8 | 40.2 |
| North-west (280° - 360°) | 22.2 | 19.3 | 22.7 |

Table 3.1 - Network average HM wind direction, Energy Density and daily maximum gust direction divided into compass quadrants.

With the strongest winds in the UK occurring during times of positive NAO producing strong westerlies (Hurrell et al., 2003), wind roses are shown for the directions of HM winds exceeding the thresholds of 15ms$^{-1}$, 20ms$^{-1}$ and 25ms$^{-1}$, to confirm where the strongest winds originate (Figure 3.18). The 15ms$^{-1}$, 20ms$^{-1}$ and the 25ms$^{-1}$ thresholds are dominated by south-westerly winds with the south-west quadrant (190˚ - 270˚)

accounting for 59.9%, 70.2% and 78.9% respectively, as Hewston and Dorling (2011) found for extreme (top 2%) DMGSs.

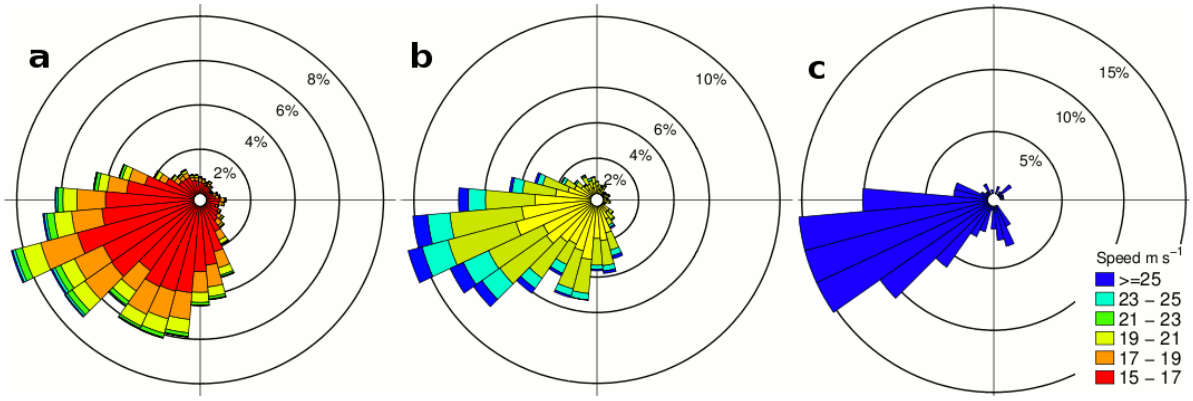


Figure 3.18 -1980-2010 HM wind roses for exceedences of 15ms$^{-1}$ (a - total counts 74154), 20ms$^{-1}$ (b - total counts 6059) and 25ms$^{-1}$ (c - total counts 323) thresholds (all sites).

The DMGS 1980-2010 39-site network average wind rose (Figure 3.19) is similar to that of the HM (Figure 3.17), with the proportion of wind direction for each quadrant (Table 3.1) also extremely similar. This is the same when comparing individual site HM wind roses (Figure 3.16) with equivalent DMGS wind roses (not shown). This suggests that the factors, be it site aspect, local scale flow or synoptic scale flow which contribute to the direction of HM winds, are the same for DMGSs.

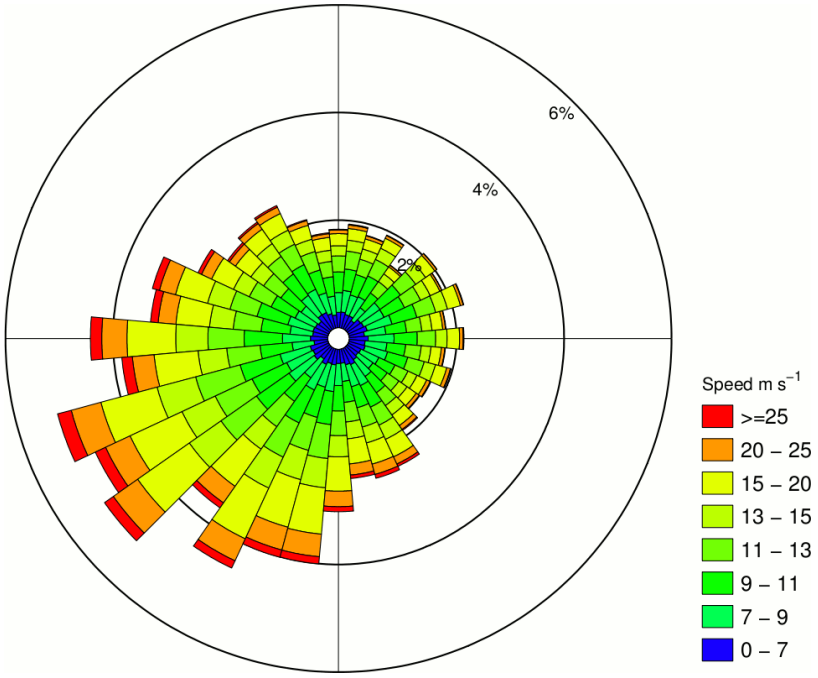


Figure 3.19 -1980-2010 DMGS network average wind rose

## 3.5 Application of the Weibull function to describe windspeed distributions

The Weibull distribution function came to prominence in meteorology during the 1970s (Takle and Brown, 1977) and has become widely used in meteorology to estimate how observed windspeeds tend to vary around their mean at sites where only a long term average is known as discussed in section 2.1.2. This section aims to deepen understanding of each of the stations in the network by investigating the applicability of the Weibull distribution across locations for both HMs and DMGSs, interpreting the results from a topographic perspective as stated in the first set of research aims in section 1.6.

The spatial variation of windspeeds in the UK is considerable, as shown above, and this contrast is also seen when the Weibull distribution is fitted to the HM and DMGS data. Figure 3.20 shows the relationship between the Weibull shape parameter (k) and mean windspeed at each of the 40 HM locations, along with histograms for some prominent sites. Generally there is a slight positive correlation (not statistically significant) between mean windspeed and k. The spread of k ranges from ~1.45–2.1, values similar to those reported in the literature by Celik (2004) based on hourly observations in Turkey (1.1-1.89), and by Pryor et al. (2004) for buoy measurements around the coast of North America (1.4-2.5). Different Weibull parameter calculation methods and ways of dealing with zero values have an effect (see section 2.1.2), along with the fact that the locations used in this study are geographically heterogeneous leading to highly varied wind regimes. Just 6 out of the 40 sites have k values of more than the commonly used Rayleigh distribution value of 2 and the majority of sites range from 1.7 - 1.9 highlighting the dangers of simply using the Rayleigh distribution to describe wind distributions for wind farm siting (Earl et al., 2013).

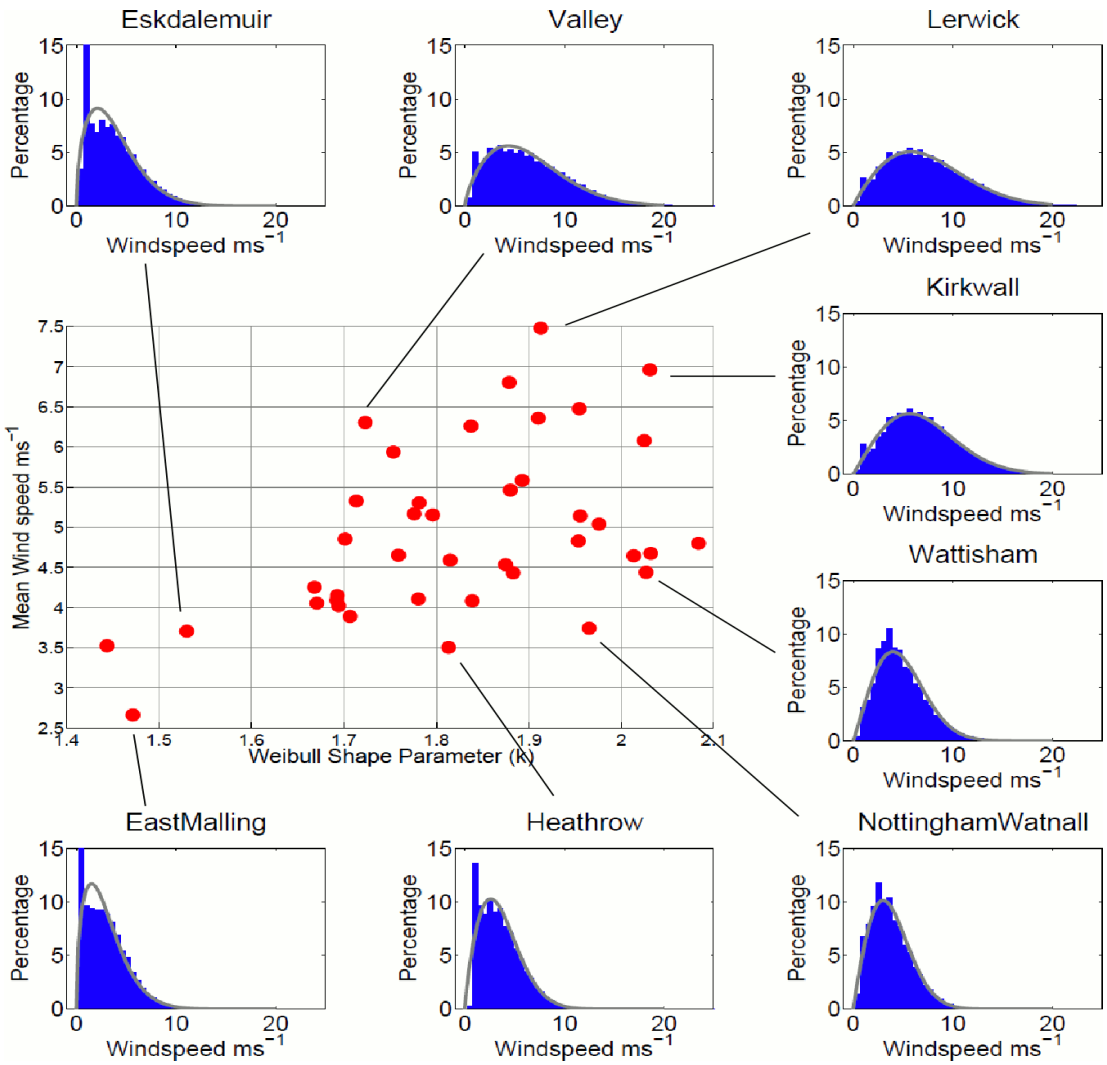


Figure 3.20 - HM windspeeds compared with Weibull shape parameter, k, for each site plus selected site wind distributions.

The Weibull distribution describes the observed HM winds well as shown by the histograms in Figure 3.20. The Weibull distribution provides a better fit to the sites with comparatively few low windspeeds (Jamil et al., 1995), as shown when comparing the sites of Lerwick (40) and Kirkwall (39) to Eskdalemuir (31) and East Malling (8). This is partly due to the method of low value recording in the MIDAS database producing an overrepresentation of 2 knots (1.03ms $^{-1}$) at certain sites (e.g. Eskdalemuir (31) and Heathrow (10)). This slightly negatively skews the Weibull distribution and affects the k values. It is also due to the nature of the Weibull distribution best approximating well measured sites with moderate or high windspeeds (Petersen et al., 1998).

Weibull shape parameter (k) values seem to be a function of both the strength of the mean wind and the impact of site characteristics. Sites with very low windspeeds such as East Malling (8) produce low values of k, due to the high counts of low wind values, however other sites with higher means but with anomalous wind roses (varying greatly from that of the network average (Figure 3.17), affected by local site characteristics – Figure 3.16) such as Bala (17) and West Freugh (30) also have low k (not shown), associated with topographic effects such as local valley flows. Sites with low means but evenly distributed (similar to network average) wind roses like Heathrow (10) (Figure 3.16) and Nottingham (18) (not shown) have relatively high k with regard to mean wind (Figure 3.20). Valley (22) has a high mean windspeed but is located in a valley, so local topography affects the wind direction and windspeed distributions.

The Weibull distribution does not approximate the DMGS distribution as accurately as for the HM winds as shown by Figure 3.21. The k values are much higher than for the HMs, ranging between ~2.4 and ~2.9, which is unsurprising given that the use of the DMGS metric eliminates many low values. The windspeed threshold of 12 $ms^{-1}$ required for good Weibull fit according to Jamil et al. (1995) seems not to be reliable for DMGSs, with sites possessing averages above and below 12$ms^{-1}$, being underestimated for the most frequent values and overestimated for the lower windspeeds (Figure 3.21). Generally the tails of the distributions are well approximated for the higher average DMGS sites and slightly overestimated for the sites with lower average DMGS.

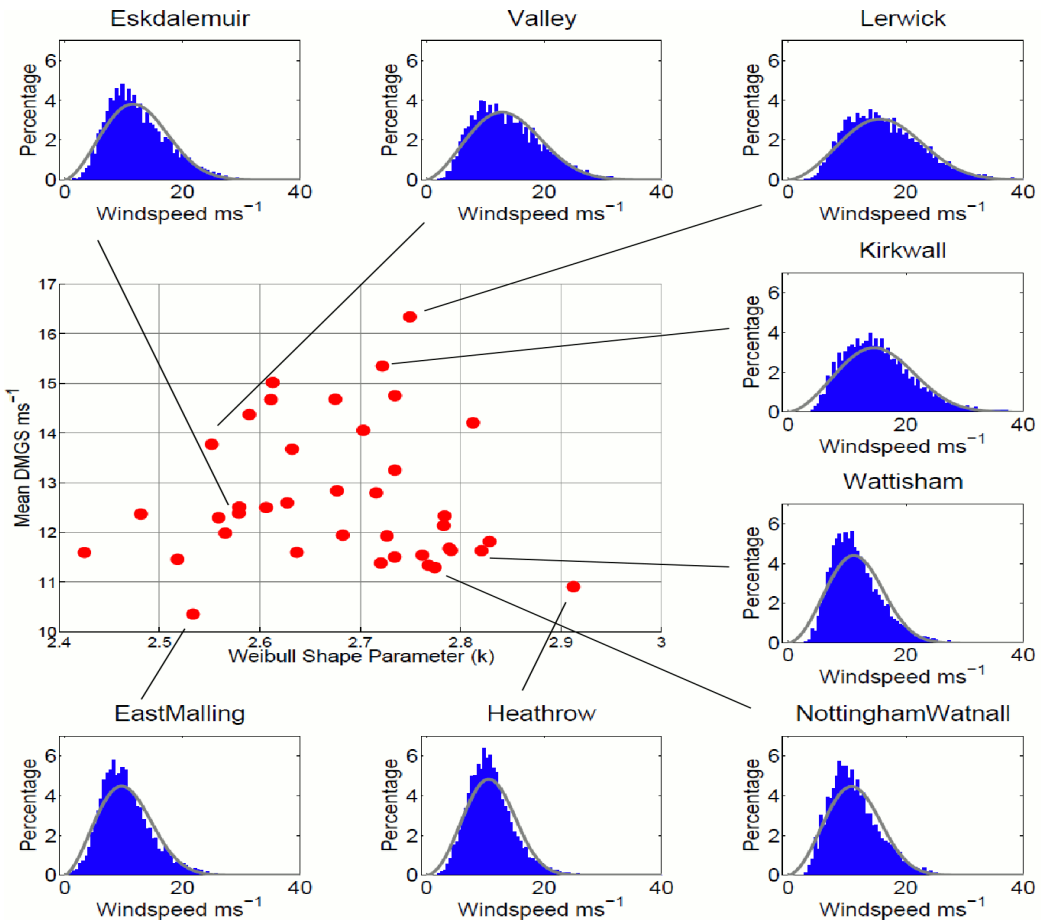


Figure 3.21 - DMGSs compared with Weibull shape parameter for each site, along with selected site DMGS distributions.

## 3.6 Wind energy implications

Wind power (both onshore and offshore) is expected to make a significant contribution to the decarbonisation of the UK's electricity supplies (AEA 2011), meaning increasing exposure to variations in windspeeds. Therefore understanding how these windspeeds variations affect wind power production is crucial. This section utilises the HM dataset, used throughout this chapter, to quantify the knock on effect that variation in UK winds has on energy production.

The HM windspeeds have been converted into network average energy density and potential power output (PPO) of a synthetic wind turbine network. Table 3.1 highlights just how important the SW quadrant is for wind power production. Both methods show significant year to year variability of power output over the 1980-2010 period (Figure 3.22), as originally seen in the annual network average HM windspeeds (Figure

3.1), percentiles (Figure 3.2 and Figure 3.5), in the HM threshold exeedences (Figure 3.6 and Figure 3.8), in the DMGS threshold exceedences (Figure 3.9) and in the NAO index (Figure 3.12). Peaks in energy density and PPO are seen in the early 1980s and early 1990s and are clearly displayed by the 5 year moving averages. The anomalous year of 2010 stands out in both energy metrics, representing the lowest values of the whole 1980-2010 period. The extreme variability of consecutive years 1986-7 as discussed in section 3.1, is also clear in both. The main difference between the two methods is the more marked peak in the early 1990s in energy density. The unprecedented storminess described by Wang et al. (2009) of the early 1990s produced the most extreme winds of the period in the UK, often above the cut-out speed of even the most modern and largest turbines. The 10m windspeeds of above 18ms$^{-1}$ are too high to be captured by the 3.6 MW turbines in the PPO, but account for extremely high levels of energy production in the energy density output (Table 2.1) due to the cubic relationship with windspeed. The PPO results are in accordance with those of Sinden (2007) during corresponding years of study. In addition the load factor of 30% is in keeping with the predetermined value used in the Sinden (2007) study. This load factor was found by Sinden to approximate the UK wind power output figures well, especially since 1997.

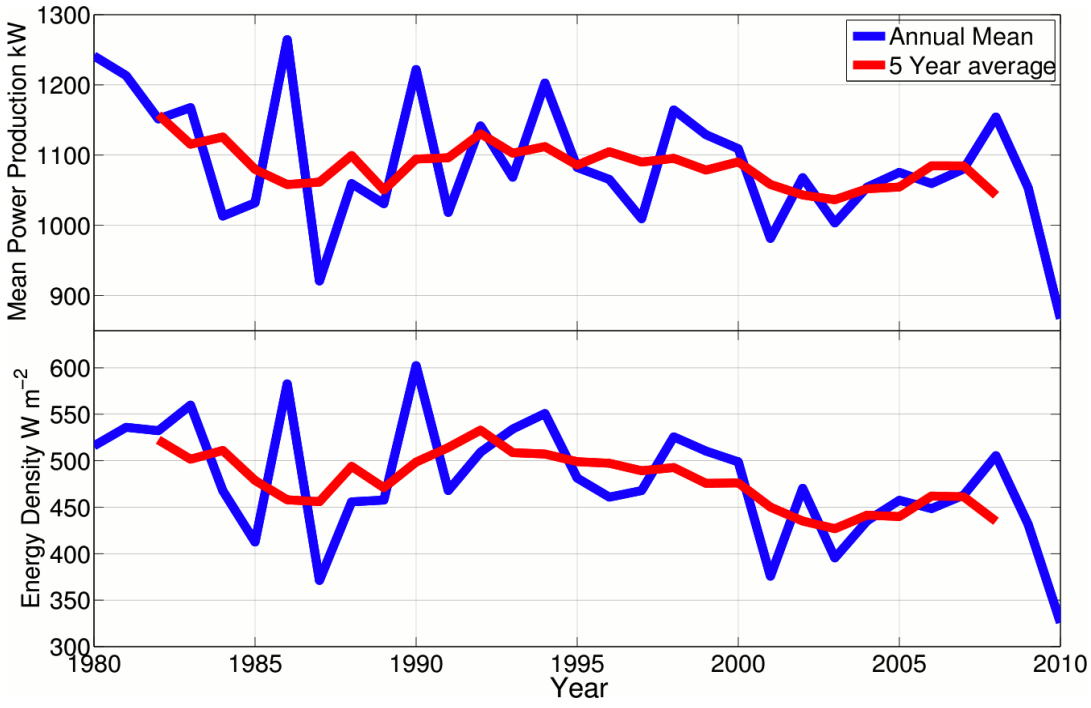


Figure 3.22 - Bottom – Network average energy density (W m$^{-2}$). Top - network average potential power output (kW) of a synthetic network of 100m hub height 3.6MW wind turbines.

The range of annual mean PPO is large, 867-1265kW (2010 and 1986 respectively) with an average of 1087 kW. During the highest production year, the synthetic 3.6MW wind turbine network was working on average at 35% efficiency (aka load factor; with the assumption of steady winds) and at 24% efficiency for the lowest production year. The year 1986 saw 16 % more energy generated than the 1980-2010 average whereas 2010 was 20% below. The energy produced in 1987 was just 73% of that of 1986, a much larger difference than the inter-annual variability in wind energy density that Petersen et al. (1998) found across many regions in Europe (±10 –15%). This shows that basing wind farm decisions on a single year of monitored data can be a dangerous practice (Brayshaw et al., 2011).

The demand for electricity in the UK fluctuates strongly, varying from hourly to annual timescales (Pöyry, 2011). Users need electricity at different times of the year for different reasons (e.g. summer cooling demand and warming in winter) (Sinden, 2007), which may not match the periods of low and high wind output (AEA, 2011). Winter is the season when electrical power output is most important, with colder temperatures and shorter days, domestic and commercial users require energy for heating and lighting, so how does the synthetic wind turbine network simulate seasonal PPO variation over the 1980-2010 period? Figure 3.23 shows the evolution of seasonal mean PPO and seasonal 5-year average PPO, highlighting the prominence of the winter season, though not as dominant in power production as might be expected given the dominance of winter windiness (Figure 3.14), likely to be due to the power curve and cut-out speeds of wind-turbines (Table 2.1). The efficiency of synthetic power harnessed is at its greatest in winter 1995 (47% efficiency), and at its lowest (18%) in summer 1983. The 5-year average indicates the winter decline in power production towards the end of the 2000s, as the summer rises to the highest point in the last 20 years, highlighting the impact of the intra-annual independent long term fluctuations as seen in Figure 3.14. PPO is very low in the winter of 2009-10 and comparable to the summer averages. This shows that storage and backup generation schemes will become crucial to energy suppliers in the future, with ever increasing reliance on wind power and other renewable sources.

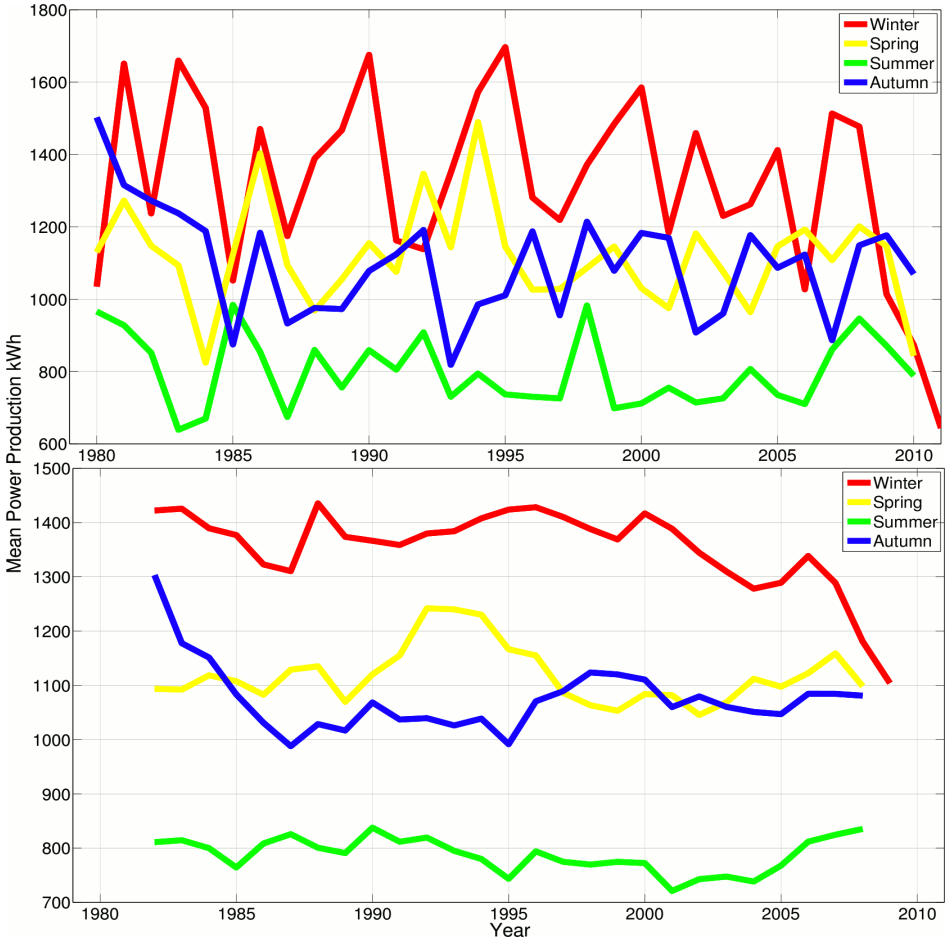


Figure 3.23 - Network average seasonal and 5 year average seasonal mean potential power output (kW) of a synthetic network of 100m hub height 3.6MW wind turbines (note: the winter of 1980 only includes Jan and Feb 1980 and the winter of 2011 only includes Dec 2010).

## 3.7 Summary

The characteristics of the UK HM and DMGS wind regimes, with applications to the insurance and wind energy industries, are presented and analysed in this chapter, covering the research aims of section 1.6, based on data from a 40 (39) hourly windspeed (DMGS) monitoring network over the continuous 1980-2010 period. This section provides a summary of the main findings as follows.

- Annual mean windspeed ranges from 4.4 to 5.4 $ms^{-1}$.

- The average, $10^{th}$ and $50^{th}$ (but not the $90^{th}$) percentile HM windspeeds have declined significantly over this specific period, whilst still incorporating a peak in the early 1990s. 2010 recorded the lowest annual $10^{th}$ and $90^{th}$ percentile

and second lowest (behind 1987) 50$^{th}$ percentile windspeed over the whole 1980-2010 period. This is all, however, in the context of longer term decadal variability.

- As the HM exceedence thresholds rise, the early 1980s peak in exceedence frequency diminishes, while the early 1990s peak becomes more apparent, with a declining tendency since, confirming the early 1990s unprecedented peak in NE Atlantic winter storminess reported by Wang et al. (2009). This is not fully consistent with Vautard et al. (2010) who highlighted a temporally broader decline for the whole of Europe over the period 1979-2008.

- The DMGS exceedence thresholds exhibit similar variations to those of the HM, with the highest thresholds (30 and 35 ms$^{-1}$) displaying the most marked early 1990s peak and a decline since, indicating that the decrease of extreme DMGSs highlighted by Hewston and Dorling (2011) has continued through to 2010, contributing to the reduction in UK storm-related insurance claims.

- The network average 1980-2010 HM prevailing wind direction is in the south-west quadrant (40% of the time), which translates into a 51% proportion of energy in the wind. However significant seasonal and inter-annual variation is apparent in the relative frequency of all wind directions and this needs to be accounted for in wind energy assessments.

- The Weibull distribution is more suited to representing HM winds rather than DMGS distributions at typical land-based sites, the former revealing site-specific shape parameter values ranging from 1.4-2.1 somewhat in contrast with the often assumed k=2 Rayleigh distribution, with associated implications for turbine site selection.

- The range of network average annual mean Potential Power Output is significant, from -20% to +16% around the average, with the synthetic energy produced in 1987 just 73% of the previous year, 1986, and 2010 the lowest producing year of all.

# Chapter 4

# Sub-storm features associated with extreme surface gusts in UK ETC events

An analysis of the historical wind regime of the UK, as described by 10m station measurements, was presented in Chapter 3, with an emphasis on the inter-annual variability of windspeed threshold exceedence frequencies, the spatial distribution of damaging windspeeds and the relative downstream effects of the NAO phase. This chapter focuses mainly on the final 3 (2008-2010) years of the 31 (1980-2010) year observation database, overlapping with the availability of the full TIGGE database from early 2008, as described in section 2.2.3. The emphasis of this chapter is on damaging surface windspeeds; although mean windspeeds can play a role in structural damage through loading, it is usually wind gusts which are the most destructive (Hewston, 2008), so the 39-site DMGS database introduced in section 1.2 of this thesis is utilised. As highlighted in chapter 1, it is essential to understand the processes behind extreme UK surface winds, since they cause widespread damage to insured property and infrastructure and pose a risk to the well-being of the public. When considering the extreme winds that breach certain exceedence thresholds, there is a spatial dominance of a few sites as shown in Figure 3.16. To avoid this geographical bias when identifying the set of ETC events of 2008-2010 events, percentages from each site are used.

Initially this chapter focuses on examining significant features of the last 31 years of the UK wind regime, in terms of eDMGS (top 1%) and top 0.1% (or $99^{th}$ and $99.9^{th}$ percentiles) of DMGSs at each of the monitoring stations. It then proceeds to focus on the final 3 years and identify sub-storm mechanisms associated with the extreme

gusts, with the intention of creating an associated provisional climatology to meet the research aims stated in section 1.6. The set of European ETCs on which to base this climatology and experiments of the models contained within the TIGGE database presented in chapter 5 are also identified in this chapter.

## 4.1 Extreme windstorm events

During the development of a windstorm loss model, Hewston (2008) found that it was only the top 2% of local DMGSs that resulted in damage to insured property. Concentrating here on the top 1% and 0.1% of DMGSs places even further emphasis on damaging and life threatening winds. This approach is distinct from previous climatological studies, for example Parton et al. (2010), Clark (2011) and Martínez-Alvarado et al. (2012b), who used mid-tropospheric observations, radar imagery and ERA-Interim data respectively, without reference to the effect of the relevant mechanisms on windspeeds at the surface.

### 4.1.1 Inter and intra - annual variability of extreme DMGSs 1980-2010

Results presented throughout chapter 3 showed that the years 2008-2010 saw a well below average frequency of high mean winds, but before analysing the extreme DMGS observations from this period, they must first be placed into the longer term context of the full surface station measurement database to highlight their contribution to eDMGSs and the top 0.1% of DMGSs.

Figure 4.1 displays the inter-annual distribution of eDMGS observed at all of the 39 network stations. There is a large annual range, lowest in 2010 with just 19 (0.4% of the total 4854) occurrences of eDMGSs, while the highest value of 371 (7.6%) occurred during 1993, with all of the 16 above average (~156 counts) years being pre-2001. The early 1980s and early 1990s stand out as periods of extreme windspeed, the final decade much less so. These results are in accordance with those presented in chapter 3 and in the literature for the UK and Europe as a whole (Earl et al., 2013; Wang et al., 2009; Vautard et al., 2011). Of course they are also consistent with the

extreme DMGS (top 2%) results of Hewston and Dorling (2011), this thesis providing an update to those findings which covered the shorter 1980-2005 period.

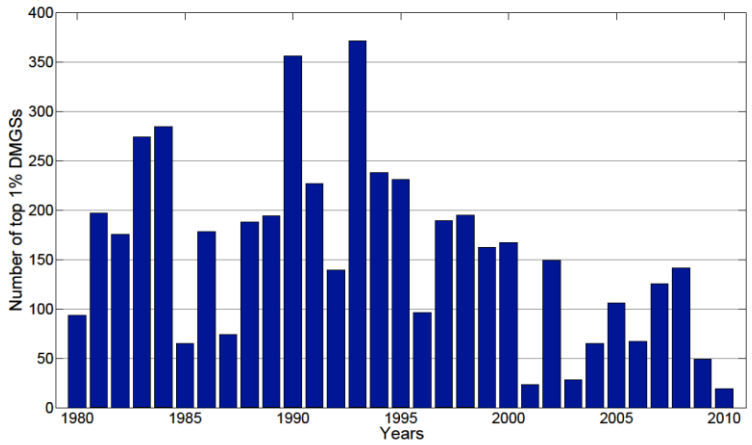


Figure 4.1 - 1980-2010 inter-annual variability in the frequency of eDMGS (of 4854) counts.

Generally 2008-2010 was a low-wind period, each year with below the average count value of ~156; 2008 represented the 18$^{th}$ highest contributor year to eDMGSs, while 2009 was 28$^{th}$ and 2010 provided the fewest examples. The year 1987 is also far below average despite including the '16th October Storm', which set records for insured loss in the UK with widespread structural damage, Munich Re (1999) reporting that the storm cost insurers just under £1.85bn (equivalent to £4.06bn in 2010). The low incidence of high wind gust events immediately prior to this storm may well have contributed to the high degree of damage experienced during the storm itself, with structures and trees, still in leaf, not recently exposed to high windspeeds (Hewston and Dorling, 2011; Browning, 2004).

Figure 4.2 displays the inter-annual distribution of top 0.1% DMGSs observed at all of the 39 network stations, providing an insight into the periods of site-specific extreme storminess. This again highlights 2008-2010 as a low-wind period, with a total of just 3 (0.6% of the 513) occurrences of top 0.1% DMGSs, contrasting with 77 alone in 1993 (15%). The unprecedented storminess of the early 1990s (Earl et al., 2013; Wang et al., 2009), discussed in chapters 1 and 3, can be seen to be largely due to exceptional

years in 1990 and 1993, neighbouring years being much closer to the 16.5 31-year average (3.2%).

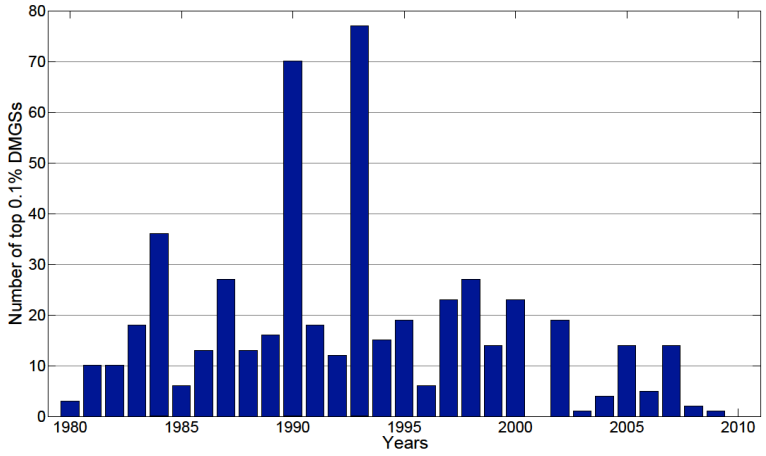


Figure 4.2 - 1980-2010 annual distribution of Top 0.1% DMGSs (of 513 – not quite 1/10$^{th}$ of the figure in the Figure 4.1 caption) counts.

The year 2008 accounted for double the number of eDMGS occurrences compared with 1987, whereas the 1987 top 0.1% occurrences far outweigh those attributed to 2008, 27 (5.3%) to 2 (0.4%), indicating that there was no 2008-2010 storm of a comparable magnitude to the record breaking '16th October Storm'. Interestingly, 36.4% of 1987's eDMGS occurrences were also in the top 0.1% bracket, by far the highest proportion of any year. Further investigation of 1987 reveals that the '16th October Storm' only produced 7 of the 27 top 0.1% occurrences that year and that an event on 27$^{th}$ March produced top 0.1% DMGSs at 18 of the 39 sites, affecting southern England and Wales. These March and October events transformed the otherwise low-wind 1987 into a perceived legendary UK wind year. However examination of the intra-annual trends in extreme DMGSs reveals that these are largely driven by winter variability rather than autumn or spring, as shown in Figure 4.3.

Winter months (DJF) account for 66.2% of eDMGSs and 75.2% of the top 0.1% DMGSs, with January the dominant contributor to both percentiles followed by February and then December, which is unsurprising because winter is the time of year when synoptic conditions best accommodate extreme ETCs to track across the UK (Dacre and Gray, 2009). The months of March and October, so influential in 1987, are less

prominent, though they account for more DMGS extremes than November for both percentiles. The months from April to September rarely contribute to the extreme DMGSs. January experienced 202 (39.3%) of the total of 513 top 0.1% events, with January 1993 the stormiest of all, accounting for 58 of them, including the mid-January Braer Storm producing 23 top 0.1% DMGSs, while on January 25th 1990, Windstorm Daria produced 22 top 0.1% DMGSs on a single day. Other prominent UK windstorms causing heavy insured losses and impacting the top 0.1% DMGS climatology include Jeanette of late October 2002 (12 top 0.1% DMGS occurrences), Erwin (12) in January 2005 and Windstorm Kyrill on 18th January 2007 (14). With high profile storms featuring so prominently in the extreme DMGS part of the observation database, additional confidence can be placed in its ability to accurately represent the UK's extreme wind regime.

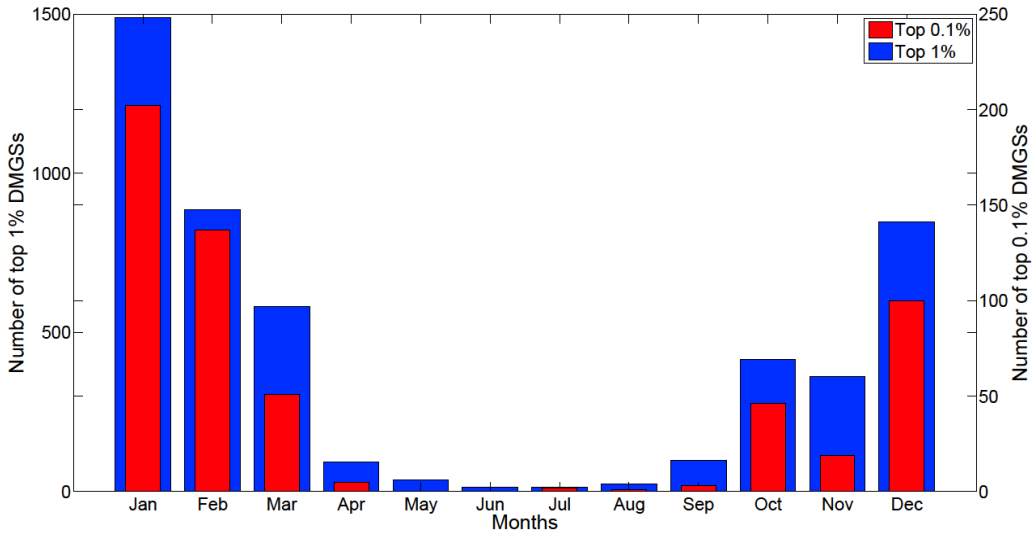


Figure 4.3 - 1980-2010 monthly distribution of eDMGSs and top 0.1% DMGSs.

### 4.1.2 2008-2010 wind characteristics

This section focuses mainly on the characteristics of the 2008-2010 eDMGSs as there were so few top 0.1% occurrences during this period. The 3 examples of top 0.1% DMGS occurrences were recorded at Machrihanish (site 32 in Figure 2.1) on the 8th and 31st of January 2008 and at Manston (site 9) on the 14th November 2009 and are explored in more detail in section 4.4. Of the 209 2008-2010 eDMGSs, 141 (67.4%) were experienced in 2008, 49 (23.4%) in 2009 and just 19 (9.1%) in 2010.

Figure 4.4 shows that the 2008-2010 monthly distribution of the eDMGSs is again dominated by January, however February and December are not so prominent, the latter especially, due to the anomalously low wind years of 2009 and 2010. March was the 2nd most stormy month over the 3 years, slightly above its 31 year average, with November also contributing strongly to the total well above its 31 year average, showing that the 2008-2010 period was not entirely "low-wind", and was indeed more extreme than average, for some months of the year. July experienced more eDMGS occurrences than any other April-September month, all occurring in the lowest windiness year of 2010, indicating that mid-summer can stand out in times of otherwise "lean" storminess, impacts being potentially enhanced when trees are still in leaf (Hewston, 2008), and that intra-annual variability can be in contrast to the annual-variability as discussed in section 3.3.

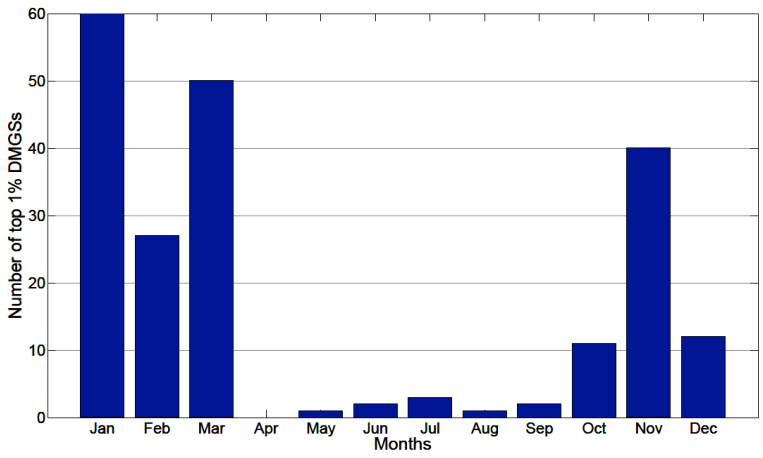


Figure 4.4 - 2008-2010 monthly distribution of eDMGSs

### 4.1.3 2008-2010 storm set identification

In the previous section, the final 3 years of the database have been shown to be generally "low-wind" compared with the 1980-2010 period of analysis as a whole. Nonetheless there are still 209 (/4854) examples of eDMGSs experienced at the 39 network sites during this period from which to identify a set of windstorm events. This section aims to associate each DMGS with a particular ETC sub-synoptic feature, using the parent ETC name allocated by the Free University of Berlin, using the method described in section 2.1.5.

All of the DMGSs were associated with an ETC. A total of 28 unique ETC events were identified, each accommodating at least 2 occurrences of eDMGSs (using the method described in section 2.1.5), as shown in Table 4.1 and Figure 4.5. The ETC allocation method ruled out 13 eDMGSs which were isolated (no other eDMGSs at any other site on that or connecting days) and these were therefore not assigned a parent ETC due to data quality concerns. Each event is described in detail in Table 4.1 and UK geographical extent highlighted in Figure 4.5. The isolated eDMGSs, which were removed for data quality concerns, would be an interesting set of gusts to investigate in themselves, and this is a potential avenue for future related work.

Table 4.1 displays the names and dates of the 28 identified ETC events which were shown to contribute to the eDMGS climatology in the UK between January 2008 and December 2010. As previously shown, this was a period of lower than average strong ETC activity over the UK. Despite this, there were many newsworthy events which caused widespread damage and disruption across the UK. Table 4.1 would also benefit from an assessment of the associated classification Type, A, B or C to each event, as discussed by Dacre and Gray (2009), regarding baroclinicity/upper air forcing and western/eastern Atlantic formation area. Due to time constraints, this is a recommended avenue for further study.

| **Storm Number and Name** | **UK impact start/end date** | **No. of eDMGS observations (no. of different sites)** | **Brief description (and Shapiro-Keyser development stages) adapted from the Low pressure descriptions at the Institute of Meteorology of the Free University of Berlin. Available from http://www.met.fu-berlin.de/adopt-a-vortex/** |
|---|---|---|---|
| **1 Christine – 07/01/08 - 4 (4)** - Formed an open wave (I) between the Azores and Ireland, developed into a T-bone (III) on the 6th and matured, travelling across Wales and England on the 7th with a low pressure centre (LPC) of 985mb, bringing strong westerlies just south of the LPC to southern Wales and southern England. The ETC then moved over Denmark on the 8th, before decaying. | | | |
| **2 Eliane – 08/01/08 to 09/01/08 - 10 (9)** - Generated just south of Iceland throughout the 8th and reached maturity (III-IV), with a LPC of 970mb over the Western Isles, at 0000 UTC on the 9th, producing strong south-westerlies, veering into westerlies over the northern UK, before tracking towards Scandinavia and decaying over Finland on the 12th. | | | |
| **3 Karin/Louisa – 17/01/08 to 18/01/08 - 2 (2)** - On the 15th Karin developed over the sea area off Newfoundland and reached the UK on the 17th (LPC of 977mb) followed by Louisa 24 hours later (973mb), both producing strong westerlies to the whole of the UK. Karin tracked over Scotland before first turning north over the Faroe Islands and Iceland and then moving over Scandinavia and eventually to Russia on the 23rd. Louisa, a secondary ETC, followed behind further south, before overtaking Karin, tracking to southern Norway on the 19th and decaying over eastern Scandinavia on the 20th. | | | |

**4 Paula – 24/01/08 to 26/01/08 - 5 (4)** - Developed over Newfoundland on the 23rd and reached the Scottish Western Isles by 0000 UTC of the 25th and possessed a well developed T-bone (III) structure (LPC 971mb). The low pressure centre then moved rapidly to Scandinavia, leaving a strong pressure gradient throughout the UK on the 25th, before moving on to Russia by the 27th.

**5 Resi – 30/01/08 to 01/02/08 - 23 (20)** - Formed between the Canadian Labrador Peninsula and the southern tip of Greenland on the 29th and tracked rapidly north of Iceland through to between Orkney and the mainland at 0000 UTC on the 1st, where the storm was already fully mature (IV) featuring an intense LPC of 955mb generating extreme south-westerlies/westerlies all over the UK. She then tracked over southern Scandinavia before weakening on the 2nd and dissipating on the 4th in north-western Russia.

**6 Winni – 08/02/08 - 2 (2)** – Generated on the 7th into an open wave (I) in the Azores, tracked and developed north-eastwards to the west of the UK, passing just north of Scotland at 1200 UTC on the 8th as a well developed cyclone (III-IV) with an LPC of 996 bringing localised strong winds to northern Scotland. Winni then moved onto the Baltic region and decayed in north-western Russia on the 13th.

**7 Zizi/Annette – 21/02/08 to 22/02/08 - 8 (7)** - Zizi formed over the Canadian Labrador Peninsula on the 20th and tracked over Iceland on the 21st (LCP 946mb) and north toward the Arctic. High-pressure (1033mb) over the Azores created a strong pressure gradient over the UK throughout the 21st and 22nd, where Annette formed from a frontal wave off the west coast of Ireland on the 22nd. Annette tracked rapidly and developed over southern Scandinavia and on to Siberia before weakening.

**8 Carmelita – 26/02/08 - 3 (3)** - Formed off the east coast of the United States on the 23rd and tracked across the North Atlantic to between Iceland and the Scottish Western Isles by 0000 UTC on the 26th (LPC 962mb), by which time the storm was fully mature (IV) and produced strong westerlies over northern England and Scotland. Carmelita then tracked across to Scandinavia and eventually decayed over Siberia on the 1st.

**9 Emma – 29/02/08 to 01/03/08 - 25 (18)** - Formed over Newfoundland on the 28th and tracked across the North Atlantic while deepening rapidly reaching the Faroe Islands late on the 29th fully mature (IV) and particularly intense with a LPC of 959mb accompanied by high-pressure over Spain as high as 1034mb. The low split in two on the 2nd, one tracking north along the Norwegian coast and the other across Denmark and the Baltic, before moving towards Russia on the 3rd where it weakened.

**10 Johanna – 10/03/08 -11 (11)** - Developed south of Greenland and deepened (II-IV) explosively and tracked towards southern UK on the 9th. The storm reached the UK fully mature on the 10th with a deep LPC (946mb) and tracked across the Midlands splitting in two, with one low pressure centre moving north over Scotland and towards Iceland on the 11th and weakened. The other low pressure centre moved into the North Sea before weakening and reached southern Sweden where it re-intensified into a small system and continued on to northern Russia.

**11 Kirsten – 11/03/08 to 12/03/08 - 16 (16)** - Formed off the east coast of the United States, tracked and developed across the North Atlantic arriving over the UK directly behind Johanna late on the 11th fully mature (IV), with the deep LPC of 961mb located over western Scotland at 0000 UTC on the 12th generating strong westerlies over Wales and southern England. Kirsten moved over the North Sea and southern Scandinavia, across the Baltic Sea to eastern Europe and dissipated.

**12 Melli – 21/03/08 - 2 (2)** - Appeared over the western North Atlantic on the 17th and tracked north-east along the east coast of Greenland and was mature (IV) by 0000 UTC on the 20th located north-east of Iceland. Melli moved quickly towards Central Europe and at 0000 UTC on the 21st was centred over northern Denmark (LPC 973mb), bringing strong northerly/north-westerly winds to the UK before moving over to the Baltics and eventually dissipating over the Barents Sea on the 29th.

**13 Naruporn – 22/06/08 - 2 (2)** – A small cyclone formed over the Atlantic north of the Azores on the 19th and tracked north to reach Ireland at 0000 UTC of the 22nd possessing a well developed T-bone (III) structure with a LPC of 992mb, bringing localised strong winds to the Irish Sea and Wales. Naruporn then moved slowly north-eastward over Scotland onto Norway on the 23rd and weakened over eastern Scandinavia by the 28th.

**14 Wilhelmine/Xevera – 23/10/08 to 25/10/08 - 10 (6)** - Wilhelmine appeared off the south-east coast of Greenland on the 22nd and tracked towards Iceland, splitting into numerous deep low pressure centres. By the 24th at 0000 UTC three intense LPCs (978mb, 953mb and 944mb) were located between the southern tip of Greenland and to the north of the Faroe Islands, producing a marked pressure gradient across the UK generating strong westerlies. One of the centres transferred to Scandinavia during the 24th, whereas another remained north of Iceland, with the third remaining off the southern tip of Greenland and eventually decaying. On the 25th Xevera, having formed over the western North Atlantic the day before, passed Wilhelmine's 2nd and 3rd LPSs to the south and tracked just north of Scotland with a T-bone (III) structure (LPC 965mb) before breaking into numerous LPCs itself, which tracking over northern Scandinavia on the 26th.

**15 Chanel – 10/11/08 - 2 (2)** - Formed off the southern tip of Greenland on the 8th and moved rapidly eastward and became a deep low centred just off the Scottish Western Isles fully mature (IV) at 0000 UTC on the 10th, with a LPC of 959mb, generating strong westerlies over the UK. During the 10th Chanel split in 2, with one centre moving swiftly into southern Scandinavia, while the other settled over Scotland before finally moving off during the 12th towards southern Norway and decaying over Sweden on the 13th.

**16 Zimone – 19/12/08 to 20/12/08 - 6 (5)** - Formed off Newfoundland on the 18th and moved rapidly across the North Atlantic and by 0000 UTC on the 20th was maturing (III-IV) with a LPC of 972mb over Shetland producing strong winds over Scotland and northern England. Zimone then moved on to southern Scandinavia and dissipated over north-eastern Europe on the 21st.

**17 Antje – 21/12/08 - 5 (5)** - Appeared over the western North Atlantic on the 19th, moved swiftly towards Europe and was located just north of Scotland by 1200 UTC on the 21st as a mature (IV) cyclone with a LPC of 970mb, bringing strong westerlies to Scotland. Antje subsequently moved eastwards over Norway and onto Sweden and dissipated over the Barents Sea on the 24th.

**18 Frank – 17/01/09 to 18/01/09 - 16 (15)** - Formed off the North American coast on the 16th and moved quickly across the North Atlantic to be centred over the ScottishWestern Isles on the 18th at 0000 UTC and was extremely large, deep and intense (LPC 946mb), bringing severe westerlies to the whole UK. The storm then moved north-westward to Iceland before migrating south-west and dissipated on the 22nd off the tip of Greenland.

**19 Caesar – 07/03/09 to 08/03/09 - 3 (3)** - Formed off the east coast of Greenland on the 6th and then tracked to Iceland. During the 7th the storm developed further while moving south-eastward and was centred over the Faroe Islands at 1200 UTC on the 8th fully mature (IV; LPC 962mb) bringing strong westerlies to Scotland and Northern Ireland. Caesar then tracked north-eastward into the Norwegian Sea and weakened on the 10th.

**20 Jochen – 08/09/09 - 2 (2)** - Formed on the 7th in the mid-North Atlantic from an open wave (I) and moved towards the UK, possessing T-bone (III) structure on the 8th at 0000 UTC centred just west of Ireland with a LPC of969mb. The storm then tracked north-eastward over the Western Isles producing localised severe winds to northern Scotland, while being pushed north by building high pressure over the southern UK and tracked to northern Scandinavia and had weakened by the 10th.

**21 Berti – 01/11/09 - 2 (2)** - Formed over the North Atlantic from a wave disturbance on the 30th and moved towards the Azores before tracking north-east towards the UK. During the 1st Berti tracked from south of Ireland over Wales, northern England and over Scotland, developing and deepening all the time from frontal facture (II) at 1200 UTC (LPC 980mb) on the 1st to a mature deep cyclone at 0000 UTC on the 2nd (LPC 965mb) bringing strong winds to the UK, especially eastern England. The ETC then moved north to the Norwegian Sea, merged with another low pressure system and dissipated on the 4th.

| |
|---|
| **22 Hans – 13/11/09 to 14/11/09 - 8 (7)** - Appeared over the mid-North Atlantic on the 12th and tracked to the north-east of the Azores and on towards the southern UK, centred over southern Ireland at 1800 UTC on the 13th, with a T-bone structure (III; LPC 974mb) having deepened explosively, bringing strong southerlies to southern England and Wales. Winds of 100mph were reported on the Isle of Wight and sea transport was disrupted across Southern England and Wales, with the port of Dover being closed just after 1200 UTC on 14th due to high winds. Hans split into multiple LPCs and tracked north during the 14th over the UK, with winds veering to a south-westerly flow, and continued to track north past Iceland on the 16th and carried on towards the Arctic. |
| **23 Klaus* - 18/11/09 to 19/11/09 - 3 (3)** - Formed off Newfoundland on the 17th and tracked east and was located south of Iceland and west of Ireland at 1200 UTC on the 18th with a LPC of 956mb, where the low pressure centre, detached from its fronts (IV), produced strong south-westerlies over the UK. Klaus then moved north to Iceland on the 19th, lingering for a while, before tracking north to northern Norway, dissipating on the 24th. |
| **24 Max – 24/11/09 to 25/11/09 - 7 (6)** - Appeared over the mid-North Atlantic on the 23rd, tracked towards the UK and was centred over northern Scotland at 1200 UTC on the 25th as a mature (IV) cyclone (LPC 958mb), generating strong south-westerlies, veering to westerlies over the UK. Max shifted north-east and by the 27th was weakening centred over the Norwegian Sea. |
| **25 Ohm – 29/11/09 - 2 (2)** – A small cyclone formed off Newfoundland on the 27th and tracked across to southern England. At 0000 UTC on the 29th Ohm was centred over Cornwall (England) with a classic T-bone (III; LPC 971mb) structure bringing strong winds to south-west England. The ETC then tracked very slowly towards the English Channel, weakening significantly, and dissipated over southern France on the 1st. |
| **26 Petra – 15/07/10 to 16/07/10 - 2 (1)** - A small cyclone formed an open wave (I) at 0000 UTC on the 15th, south-west of the UK, tracked north-eastward and was centred over north Wales at 0000 UTC on the 16th with a classic T-bone (III; LPC 988mb) structure bringing localised strong winds (especially for Summer) to north Wales and the Irish Sea. Petra then weakened and tracked northward via the Faroe Islands and dissipated between Svalbard and northern Norway on the 21st. |
| **27 Becky – 07/11/10 to 08/11/10 - 3 (3)** - Formed over the Labrador Sea on the 6th becoming a strong low over the south of Greenland and was mature (IV) on the 8th at 0000 UTC, located just west of the Scottish Western Isles with a LPC of 956mb, bringing strong southerlies to the UK ahead of the low pressure centre. During the 8th, the storm weakened somewhat and tracked south-eastward over Ireland, southern England and France, dissipating over Germany on the 10th. |
| **28 Carmen – 11/11/10 to 12/11/10 - 12 (9)** - Formed off the northeastern United States on the 9th, tracked eastward and was mature (IV) and intense on the 11th at 1200 UTC with a deep LPC of 948mb, located just west of the Western Isles, generating strong westerlies over Ireland, Wales and central and southern England. The storm split in two, with one centre tracking north-east along the Norwegian coast, weakening over the next few days. The other centre maintained extreme winds, moving rapidly over southern Scandinavia to the Baltic Sea and weakened over Russia on the 15th. |

Table 4.1 - Set of 2008-2010 ETC events associated with eDMGS. * Note - Klaus refers to a separate event from the January 2009 event discussed in chapter 1.

Figure 4.5 shows the geographical extent of the eDMGSs for each ETC, highlighting the localised nature of some ETCs, for example Berti and Naruporn, compared to events which stand out on a national scale, such as Resi, Emma and Frank. The most intense

and damaging storms to affect Europe between 2008 and 2010 were Windstorms Klaus and Xynthia, which occurred in late January 2009 and early March 2010 respectively as described in section 1.1.3. Both of these events caused most damage and disruption in France and Spain, leaving the UK unscathed in terms of eDMGSs at any of the network sites.

Figure 4.6 shows the maximum 2008-2010 gust seen at each site, highlighting the sites most susceptible to extreme winds, corresponding well with the 1980-2010 >15ms$^{-1}$ and >25ms$^{-1}$ HM exceedence threshold maps shown in figure Figure 3.16. Inland sites, especially in central and southern England, experienced far lower maximum gust speeds than their coastal counterparts, with all sub-28ms$^{-1}$ maxima occurring in this region as discussed in Earl et al. (2013) and in section 3.4 of this thesis. Exposure to fetch over the Atlantic Ocean and Irish Sea is clearly influential, with no sub-28ms$^{-1}$ maxima occurring on the western UK coast. Latitude and altitude are also important, the higher and further north a site is, the stronger the maximum DMGS due to reduced friction at exposed high altitude sites and closer proximity to the region of higher storm track density to the south and east of Iceland (Dacre and Gray, 2009). Some differences are apparent, however, between the 1980-2010 >15ms$^{-1}$ and >25ms$^{-1}$ HM exceedence threshold maps shown in Figure 3.16 and the maximum 2008-2010 gusts shown here (Figure 4.6), with the sites of Manston and Machrihanish standing out more in the latter, due to being the only two sites to experience top 0.1% DMGSs over the 2008-2010 period.

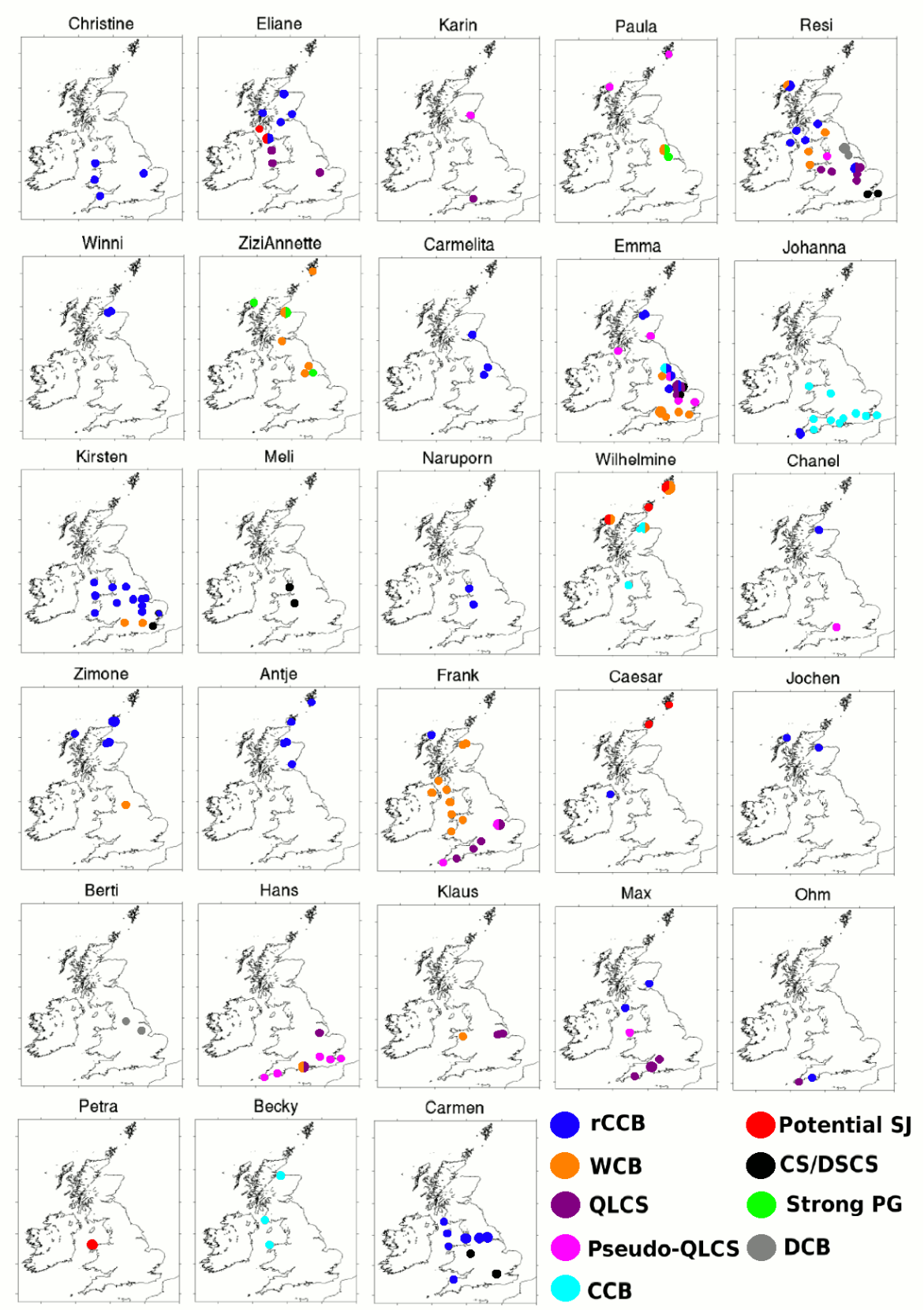


Figure 4.5 - Sites affected by each ETC event. Small circles indicate a single eDMGS per site, larger circles indicate consecutive days of eDMGS. Mechanisms are marked as in Figure 1.5.

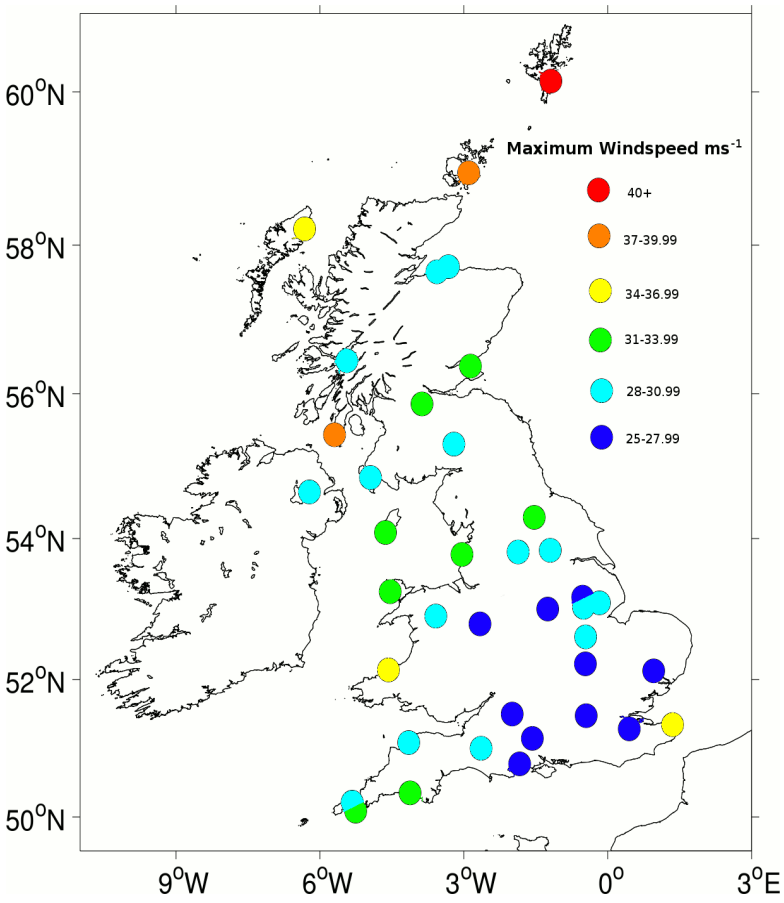


Figure 4.6 – 2008-2010 maximum DMGS at each of the network sites.

## 4.2 Sub-storm mechanisms

The previous section has identified and described the 2008-2010 events which caused eDMGSs in the UK network of observation sites and has shown geographically which areas are most susceptible to extreme winds. We know that these DMGS observations were all associated with an ETC, however there are many different types of sub-storm mechanisms which cause extreme gusts as discussed and described in chapter 1 (Figure 1.5, Table 1.1). This section uses Windstorm Emma as an example to demonstrate the adopted methodology, due to its severity and widespread impact on the UK, producing the most eDMGSs of any 2008-2010 event, with any sub-storm mechanisms not represented during the passage of Emma demonstrated using other diagnosed events. It must be stated here that the responsible sub-storm features are diagnosed subjectively so the results must be taken with caution (see section 2.1.5).

Local characteristics, such as topography and vegetation can also have a major effect on the wind at the monitoring sites (section 3.4), potentially exacerbating or dampening the eDMGS values.

### 4.2.1 Sub-storm mechanisms experienced during Windstorm Emma

The life-cycle of Emma led to two separate cold fronts, the storm having already split into two low pressure centres (LPCs) over the UK. Emma also had a major impact downstream across mainland Europe as described by Dotzek and Forster (2011), who showed that severe weather over France and Germany, reported on the European Severe Weather Database, was almost exclusively associated with the line of the secondary cold front, leading to bands of severe storm reports at the surface. This, however, does not demonstrate whether this was also the case for the UK and does not give an indication of which specific sub-storm processes were involved in Emma's extreme surface DMGSs.

Figure 4.7 shows Emma bringing strong winds to the UK at 00:00UTC on 1$^{st}$ March 2008, as indicated by the tightly spaced isobars, and highlights the frontal boundaries, with a surface warm front extending from northern Belgium to north-west Spain, the surface cold front in the English Channel and the secondary surface cold front across central England and Wales. Using the method described in section 2.1.5, similar to that used by Parton et al. (2010) to give synoptic context to their feature finding algorithm, it is possible to identify the individual sub-storm features responsible for the 25 eDMGSs which occurred during Emma.

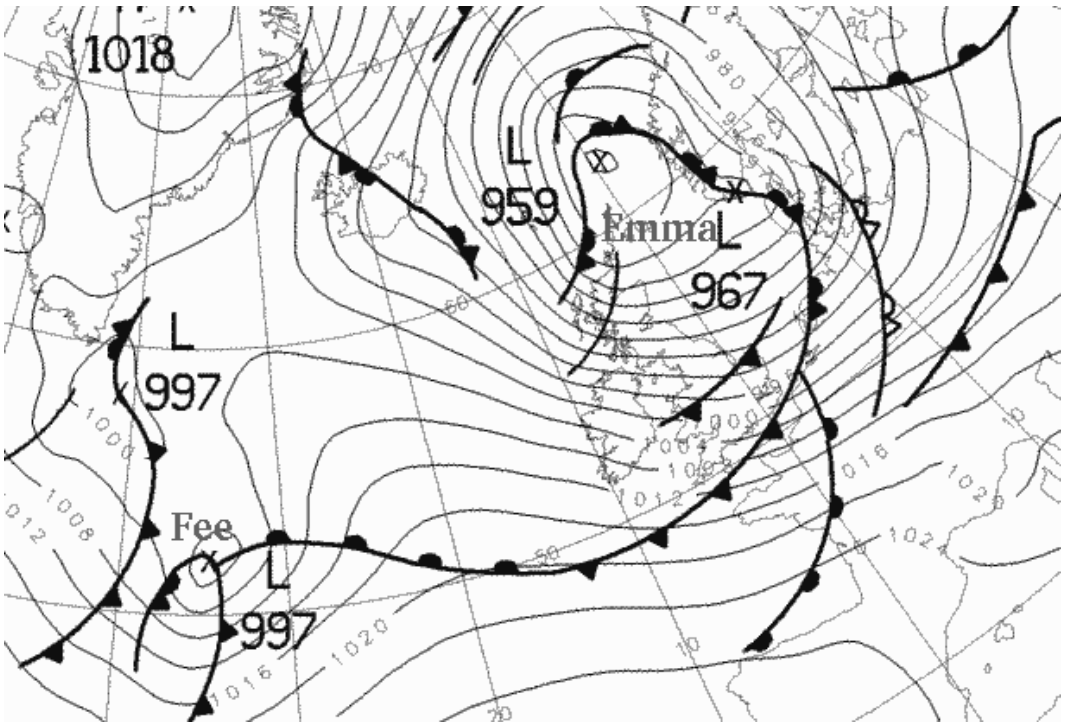


Figure 4.7 – UKMO sea-level pressure analysis chart from 1st March 2008 00:00 UTC showing Windstorm Emma affecting the UK (courtesy of the UKMO via wetterzentrale, www.wetterzentrale.de).

Table 4.2 and Figure 4.8 show the locations, times and wind directions of each eDMGS experienced at any of the 39 network observation sites, along with the subjective diagnosis of responsible sub-storm features, based on the schematic Figure 1.5. Emma displays a wide range of sub-storm mechanisms diagnosed as generating eDMGSs, providing the opportunity to investigate many mechanisms in the context of a single event. It is not common for a single ETC to contain, let alone produce extreme surface winds associated with, all sub-storm mechanisms. However windstorm Emma is an exception and those features are examined below by way of example, before mechanisms not contained in Emma are examined from other identified ETC events.

| Site location (station number) | Date and time of DMGS | Compass bearing (degrees) and speed ($ms^{-1}$) of DMGS | eDMGS Gust causing mechanism |
|---|---|---|---|
| Leeming (28) | 29th - 14.19 | 230 / 30 | CCB |
| Leuchars (34) | 29th - 14.51 | 250 / 27 | preQLCS |
| Machrihanish (32) | 29th - 16.09 | 270 / 33 | preQLCS |
| Church Fenton (26) | 29th - 18.38 | 260 / 27 | preQLCS |
| Lyneham (11) | 29th - 20.47 | 250 / 25 | 2nd WCB |
| Bingley (25) | 29th - 20.57 | 270 / 30 | 2nd WCB |
| Cranwell (19) | 29th - 23.32 | 260 / 26 | QLCS |
| Waddington (21) | 29th - 23.33 | 300 / 28 | QLCS |
| Coningsby (20) | 29th - 23.45 | 300 / 26 | QLCS |
| Wittering (15) | 29th - 23.47 | 260 / 26 | QLCS |
| Lyneham (11) | 1st - 00.43 | 260 / 26 | 2nd WCB |
| Heathrow (10) | 1st - 01.11 | 260 / 24 | 2nd WCB |
| Coningsby (20) | 1st - 01.13 | 300 / 27 | 2nd CS behind QLCS |
| Bedford (14) | 1st - 01.15 | 270 / 26 | postQLCS |
| Middle Wallop (7) | 1st - 01.40 | 280 / 25 | 2nd WCB |
| Wittering (15) | 1st - 01.43 | 280 / 28 | 2nd CS behind QLCS |
| East Malling (8) | 1st - 01.53 | 280 / 26 | 2nd WCB |
| Wattisham (12) | 1st - 01.55 | 290 / 27 | postQLCS |
| Leeming (28) | 1st - 02.04 | 270 / 28 | rCCB |
| Waddington (21) | 1st - 02.31 | 280 / 26 | rCCB |
| Nottingham (18) | 1st - 03.35 | 280 / 26 | rCCB |
| Church Fenton (26) | 1st - 03.41 | 270 / 30 | rCCB |
| Cranwell (19) | 1st - 05.17 | 270 / 29 | rCCB |
| Kinloss (36) | 1st - 00.42 | 270 / 27 | rCCB |
| Lossiemouth (37) | 1st - 03.29 | 310 / 29 | rCCB |

Table 4.2 – eDMGSs during windstorm Emma

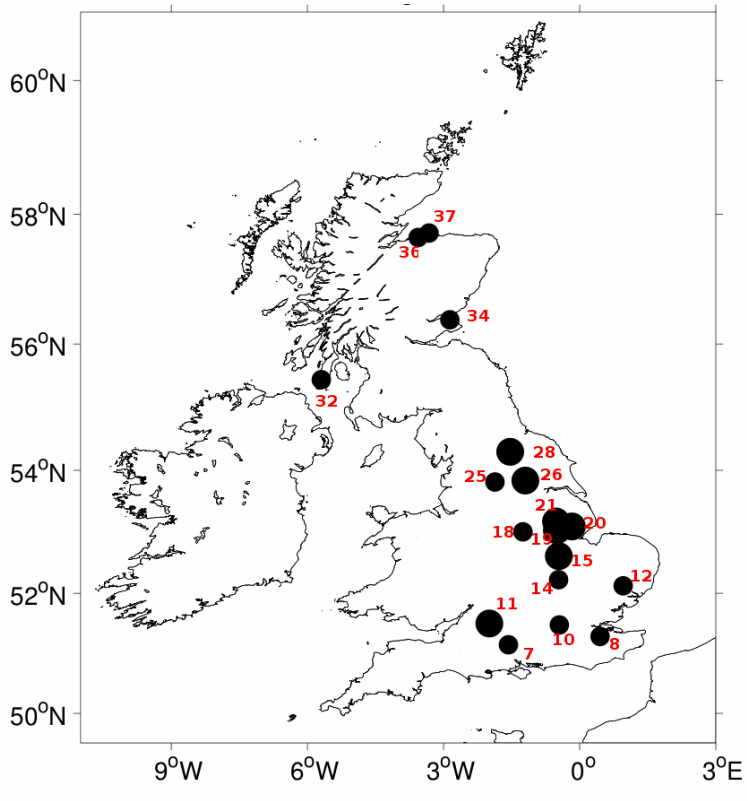


Figure 4.8 - Emma affected sites with site number (see figure Figure 2.1). Larger circles correspond to sites affected twice during Emma's passage.

*Cold-conveyor belt (CCB)*

Table 4.2 shows that the first DMGS recorded at Leeming was associated with the CCB (Figure 1.5). This interpretation was made with the aid of observation tools introduced in section 2.1.5.

The sea-level pressure analysis chart in Figure 4.9 shows the locations of the surface fronts at 12:00 UTC on 29th February 2008, with Emma between stage III and IV of the Shapiro-Keyser life cycle (Figure 1.4). Leeming is located ahead of the oncoming surface warm front. Using 15-minute radar image updates the front locations were tracked and the surface warm front was located west of Leeming at the time of the DMGS (14:19 UTC) as shown by the radar image (Figure 4.9 (right)), with the rain ahead of the surface warm front clearly visible over Wales (orographically enhanced), the Midlands and East Anglia. With this information along with the wind direction of this gust being almost parallel to the warm front, it was concluded that the gust was most likely to be associated with the CCB.

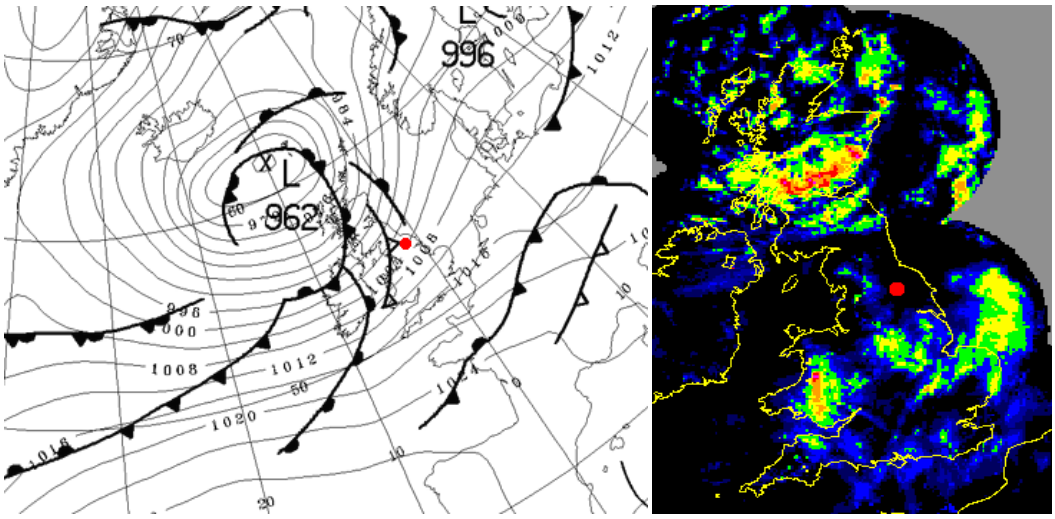


Figure 4.9 - Sea-level pressure analysis chart (courtesy of the UKMO) for 12:00 UTC February 29th 2008 (left) and 14.15 Nimrod radar image (courtesy of the BADC/UKMO, source http://badc.nerc.ac.uk) with Leeming's location highlighted (red spot).

*Quasi-linear convective system (QLCS)*

Table 4.2 shows that the DMGSs recorded at Cranwell, Waddington, Coningsby and Wittering, at 23:32, 23:33, 23:45 and 23:47 respectively on the 29th February were judged to be associated with a QLCS. These DMGSs coincided with a QLCS as diagnosed by Clark (2011) along the secondary cold front as seen in the surface analysis chart (Figure 4.7). This, along with the radar image in Figure 4.10, indicating heavy rain directly over the sites at their respective eDMGS times, led to the conclusion that the gust was most likely to be associated with a QLCS. The mechanisms marked as preQLCS and postQLCS in Table 4.2 refer to DMGSs associated with the same organised system of which a QLCS occurred, but which did not strictly adhere to the QLCS selection criteria of Clark (2011) (also referred to as a pseudo-QLCS), an example of which is described later in this section.

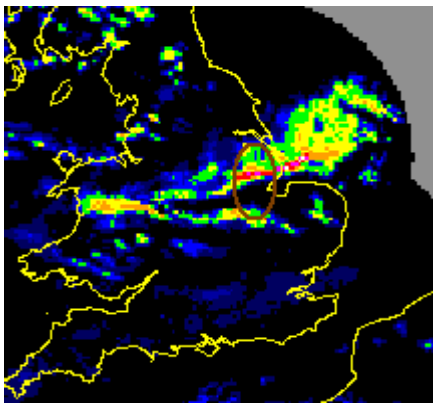

Figure 4.10 - 23:45 UTC 29th February 2008 from Nimrod radar image (courtesy of the BADC/UKMO, source http://badc.nerc.ac.uk) showing the affected sites (brown oval).

*Warm Conveyor Belt (WCB)*

Windstorm Emma did not produce any eDMGSs within the main WCB, however the sites of Lyneham (affected twice), Heathrow, Wittering and East Malling all experienced extreme DMGSs ahead of the 2nd cold front (Table 4.2), though clearly separated from the cold frontal QLCS as shown in Figure 4.11 for the site of Lyneham on the 1st March 2008. The isobars in the 00:00 UTC synoptic chart (Figure 4.7), along with surface air and dew point temperature observations (not shown), indicate that the section behind the initial cold front and ahead of the 2nd cold front (and associated QLCS) is, in effect, an extension of the main warm sector as the initial cold front weakens. These DMGS observations, in the warm sector, were therefore associated with a 2nd WCB. This example highlights the complexities involved in subjectively assessing sub-storm feature types for some eDMGSs.

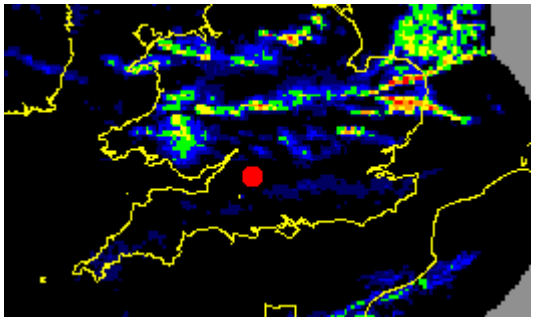

Figure 4.11 - 00:45 UTC 1st March 2008 from Nimrod radar image (courtesy of the BADC/UKMO, source http://badc.nerc.ac.uk) showing the affected site of Lyneham (red dot).

*Isolated convective systems and pseudo-QLCSs (CS and pseudo-QLCS)*

Table 4.2 shows that Coningsby and Wittering experienced eDMGSs from isolated convective systems. These occurred in the wake of the QLCS that passed over the sites in the preceding hours, and which by 01:15 UTC had moved further south to cause an eDMGS at Bedford despite no longer being classified as a QLCS according to Clark (2011) – it is therefore classified here as a post-QLCS.

Using the surface pressure analysis chart in Figure 4.7 and comparing it to the 01:15 UTC radar image (Figure 4.12), it can be deduced that the 01:13 UTC DMGS experienced at Coningsby occurred behind the secondary cold front and was associated with a small convective system producing a heavy shower as clearly visible in the radar image (red circle). It was therefore concluded that this eDMGS was most likely to have been caused by a downdraft from this isolated convective system.

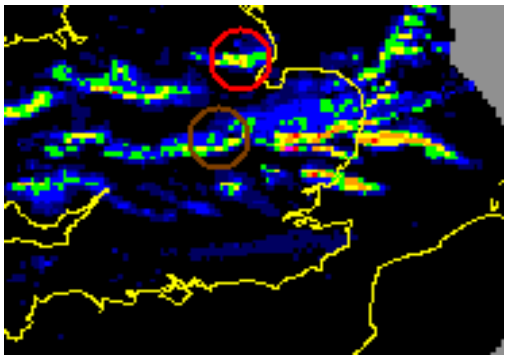

Figure 4.12 - 01:15 UTC 1st March 2008 from Nimrod radar image (courtesy of the BADC/UKMO, source http://badc.nerc.ac.uk) showing the affected sites of Coningsby (red circle) and Bedford (brown circle).

Two minutes after the gust at Coningsby another eDMGS was recorded 70 miles south at Bedford as shown by the brown circle in Figure 4.12. This gust coincided with the passage of the secondary cold-front, which ceased being classified as a QLCS at 0000 UTC on 1st March (just 1:15 earlier), but which was still able to produce the eDMGS - this was therefore classified as a pos-tQLCS (also referred to as a pseudo-QLCS).

*Returning cold conveyor-belt (rCCB)*

The rCCB which occurred during Emma is best indicated by the tight isobars stretching from east of Iceland to Scotland in the 00:00 UTC 1st March sea-level pressure analysis chart (Figure 4.7), where Emma is in stage IV of the Shapiro-Keyser life cycle (Figure 1.4). As the system migrated eastwards, the rCCB began to affect a large swath of the UK, producing eDMGSs at eastern UK sites as shown in Table 4.2 and Figure 4.8. Satellite and radar images (not shown) indicate that the cloud free dry intrusion had dissipated by this point, so these DMGSs are therefore most likely to be associated with the rCCB rather than the dry conveyor belt, following in behind the fully developed system.

### 4.2.2 Sub-storm mechanisms not experienced during Windstorm Emma

Some sub-storm mechanisms which can also be important contributors to surface extreme winds were not experienced during Windstorm Emma. These are examined here in detail, using other examples from the 28 windstorm set (all described in Table 4.1).

*Dry conveyor belt (DCB) during Berti (1/11/2009)*

The two eDMGSs experienced during Berti (Table 4.1) were both located within the dry section behind the surface cold front, at Waddington and Bingley at 13.07 UTC and 13.11 UTC respectively.

The radar and satellite images in Figure 4.13 indicate that the eDMGSs were not associated with the dry slot convective systems that had been triggered over Wales and were too far behind the surface cold front to have been caused by any frontal mechanisms. With the ETC in early development (stage II), the dry slot, between the cloud head and cold front, is clearly recognisable so it can therefore be deduced that the DCB was the most likely cause for Berti's two eDMGSs.

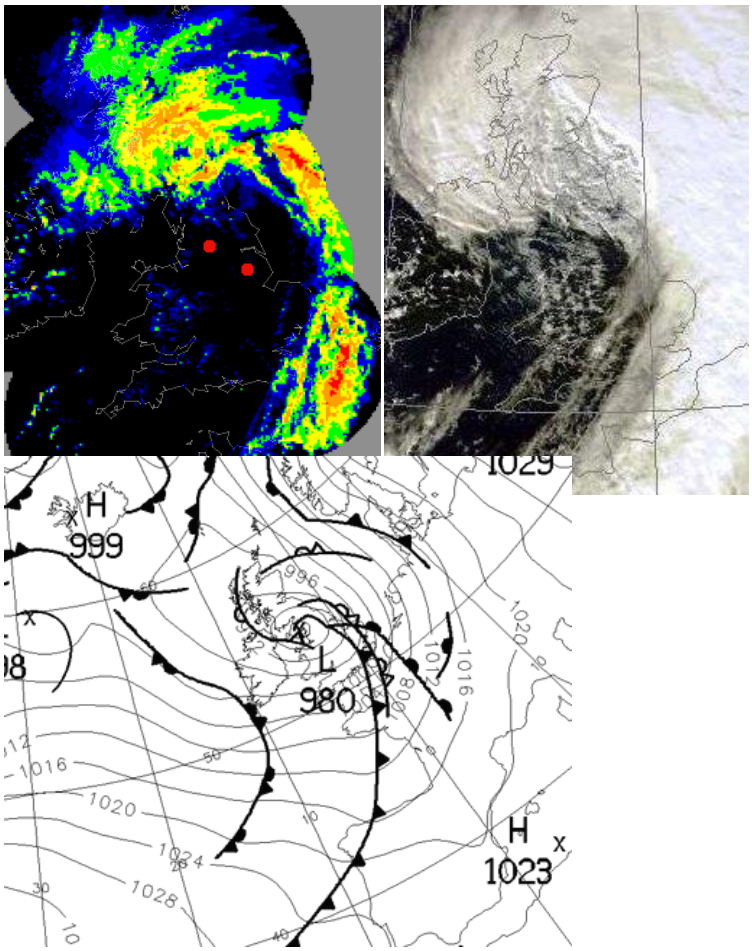


Figure 4.13 - Nimrod radar image (courtesy of the BADC/UKMO, source http://badc.nerc.ac.uk) from 1st November 2009 showing the affected sites of Waddington and Bingley (red dots) at 13:15 UTC, satellite (channel 37) at 13:12 UTC and 12:00 UTC surface pressure analysis chart (courtesy of the UKMO).

*Potential Sting Jet during Ohm 29/11/2009*

One of the eDMGSs experienced during Windstorm Ohm, at Culdrose on 29th November at 02:04 UTC, possesses the characteristics of a sting jet based on the observations.

The sea-level pressure analysis chart in Figure 4.14 shows that the ETC possessed a classic T-bone structure associated with stage III of the Shapiro-Keyser life cycle model, two hours before the observed eDMGS at Culdrose, the optimum part of the ETC life cycle for sting jet generation (Browning, 2004). The satellite and radar images, close to the timing of the eDMGS, clearly show the cloud and rain associated with the rCCB entering the dry slot at the 'hook' section of the cloud head, known to be the

preferred location for sting jets to form (Browning, 2004). Therefore, in conjunction with explosive deepening (24mb in 24 hours according to era-interim data (not shown)), the conditions are perfect for the development of conditional symmetric instability (CSI) release and development of a sting jet (Gray et al., 2011). There is also a degree of rainfall banding visible in the radar image (on the hook part of the echo), comparable to that seen in other sting jet studies, indicating the existence of multiple slantwise convective circulations (Paton et al., 2009; Browning, 2004). The event has therefore been classified as a potential sting jet in this study. This method of attempting to deduce genuine sting jets is also discussed in more detail in section 4.4.

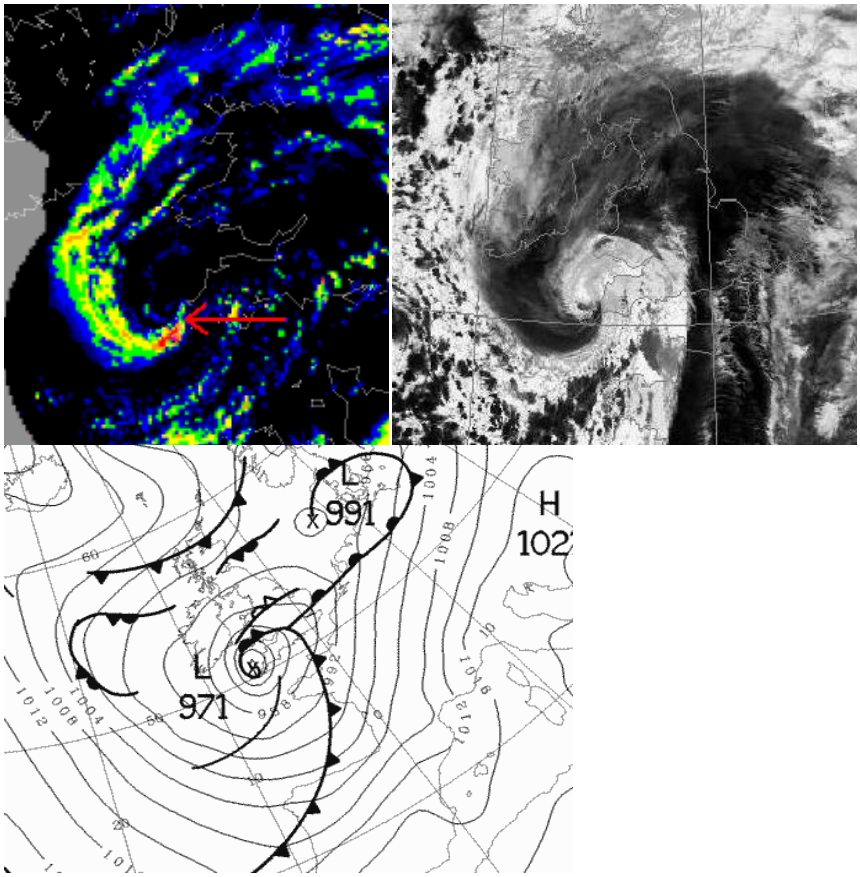


Figure 4.14 – Nimrod radar image (courtesy of the BADC/UKMO, source http://badc.nerc.ac.uk) from 29th November 2009 showing the affected site of Culdrose (red arrow) at 02:00 UTC, satellite at 02.22 UTC (courtesy of the University of Dundee Satellite Receiving Station, source http://www.sat.dundee.ac.uk/, MODIS satellite channel 31 (reversed image)) and 00:00 UTC sea-level pressure analysis chart (courtesy of the UKMO).

*Strong pressure gradient during Zizi and Annette (22/02/2008)*

Not all eDMGS occurrences are linked purely to frontal or conveyor belt or convective mechanisms and are instead caused by extreme pressure gradients and associated high velocity airflow. Three of the eight eDMGSs during the passage of Zizi and Annette were most likely to have been caused by strong pressure gradient, rather than any specific mechanisms within either of the two ETCs, for example Kirkwall at 11:51 on the 22nd February 2008.

The sea-level pressure analysis chart (Figure 4.15) shows how tightly packed the isobars were just after the passage of Annette at 12:00 UTC on 22nd February 2008, bringing strong winds to the UK, especially to exposed locations like Kirkwall (Orkney). With the surface pressure of 1028mb in the English Channel and 976mb over the Faroe Islands, the eDMGS experienced were labelled as being most likely caused by this strong pressure gradient associated with the ETC. A radar image is not shown here due to not indicating any features near the eDMGS location.

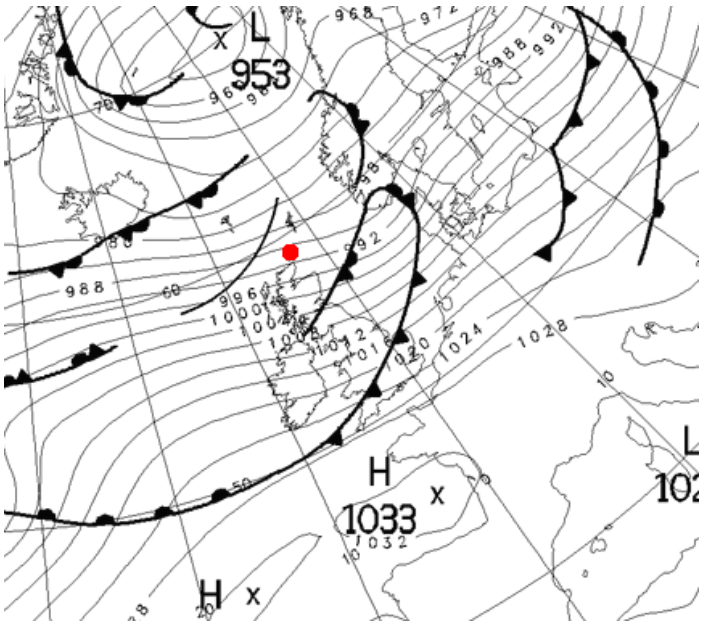


Figure 4.15 - 22nd February 2008 12:00 UTC sea-level pressure analysis chart (courtesy of the UKMO) showing the affected site, Kirkwall (red dot)

## 4.3 2008-2010 provisional-climatology for sub-storm mechanisms

The previous section describes the process behind determining which mechanism was most likely responsible for each eDMGS, with a selection of example results from windstorms Emma, Berti, Ohm and Zizi/Annette. Here, all the subjectively estimated causes for all eDMGS, from each of the 28 events, are brought together in the development of a 2008 to 2010 provisional-climatology (3 years is insufficient time for a definitive climatology). Table 4.3 displays the total numbers of eDMGSs caused by the different sub-storm mechanisms for each of the 28 identified 2008-2010 windstorm events (Table 4.1) and Figure 4.16 displays the location of each. This highlights the full UK spread of some mechanisms, namely the CCB, WCB and pseudo-QLCSs, and the regionality of others such as the potential SJ bias of western and northern sites and QLCS tendency for locations in the south. However, it must be stressed that there are too few examples to be definitive about the geography of this climatology.

| **eDMGS causing mechanism** | **Total (percentage)** |
|---|---|
| **rCCB** | 70 (35.7) |
| **WCB** | 33 (16.8) |
| **QLCS** | 26 (13.3) |
| **Pseudo-QLCS** | 17 (8.7) |
| **CCB** | 16 (8.2) |
| **Potential SJ** | 13 (6.6) |
| **Dry slot CS & Isolated CS** | 11 (5.6) |
| **DCB** | 5 (2.6) |
| **Strong PG** | 5 (2.6) |
| | **196** |

Table 4.3 - eDMGS causing sub-storm mechanisms from 1980-2010 which occur in the TIGGE period 2008-2010.

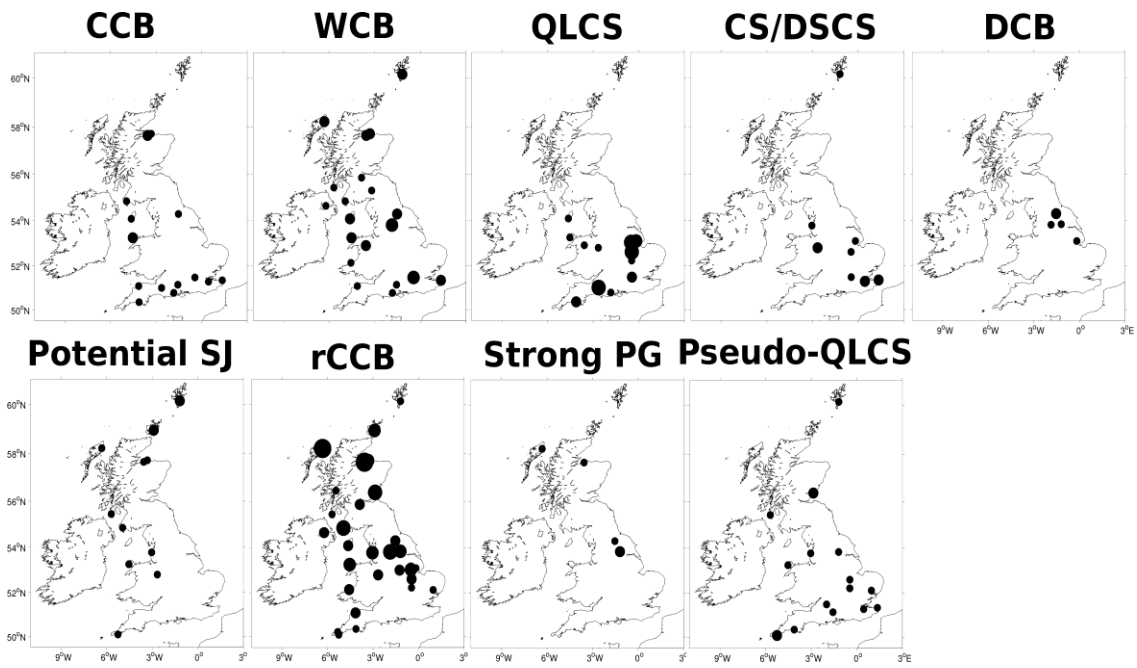


Figure 4.16 – Locations of eDMGSs for each of the ETC mesoscale mechanisms (larger circle denotes multiple observations).

Over this 3 year period, the returning cold-conveyor belt (rCCB) accounted for more than a third of all eDMGSs with the warm-conveyor belt (WCB) the second most influential. These conveyor belts are widely known to regularly cause extreme surface winds within ETCs (e.g. Browning, 2004) and the results are comparable, proportionally, to those of the Parton et al. (2010) 7 year climatology (1998-2005) of a mid-troposphere profiling radar located at Aberystwyth, when using the Shapiro-Keyser life cycle model. However, it must be kept in mind that theirs is an upper level climatology, during a windier period (Figure 4.1) and based on different classification methods. The spread of the rCCB is consistent throughout the UK apart from the southern coast of England, due to its sheltered location from westerly and north-westerly orientated rCCB. The WCB is associated with eDMGSs across the country, which is not of much surprise considering the typically large area of this feature (Figure 1.5).

Clark (2011) shows that QLCSs occur frequently in the UK during the autumn and winter months and the results here indicate that they are also influential in causing the more extreme surface winds, accounting for over 13% of 2008-2010 eDMGSs. QLCSs were also shown to be responsible for 71% of all ‘cool season’ (September-

February) tornadoes according to the 2003-2010 provisional climatology of Clark (2011), with 27% of the 103 identified QLCSs producing at least one tornado. Non-tornadic QLCSs can also produce strong surface winds through heavy precipitation creating downbursts, microbursts and the fragmentation of the line to form 'bow-echoes' (bow-shaped segments; Galvin and Willington, 2011). It is well documented that 'bow echoes' produce strong surface winds in the USA, posing a threat to life and property (Weisman, 2001), through rear inflow jets and low-level mesovortices producing damaging straight-line surface winds (Wheatly et al., 2006), which means that these processes are likely to be at least partly responsible for the QLCS eDMGSs seen in this study. However, there is no way of distinguishing between these non-tornadic and tornadic mechanisms behind the extreme surface winds using satellite, radar and surface observations alone, requiring high-resolution NWP simulations or eyewitness tornado observations to give a more accurate indication. Notwithstanding, QLCSs are of significant importance to production of damaging winds in the UK. Further discussion concerning the use of the Tornado and Storm Research Organisation (TORRO) records to extend this work is included in the recommendations for future work in chapter 6. Figure 4.16 shows the distribution of QLCSs (which is essentially a sub-set of Clark's (2011) climatology) to be solely located in the southern half of the UK as Clark (2011) also highlights; the latter do not propose a reason for this, though do acknowledge that deficiencies in radar detection may play a part in some areas of apparent low QLCS frequency.

Features with similar characteristics to those of QLCSs, but not included in the Clark (2011) climatology, including pre- and post-QLCSs, troughs, surface fronts and QLCS occurrences outside of the 'cool season' have been similarly categorised as pseudo-QLCSs. Pseudo-QLCS-produced eDMGSs accounted for just under 9% of the allocated eDMGSs, including a total of 9 frontal, 2 troughs and 6 pre-/post-QLCSs (not shown) in windstorms all occurring during the 'cool season'. These events were not wide enough spatially, long enough temporally or intense enough to feature in Clark's (2011) climatology, however still produced extreme surface wind speeds, indicating that the Clark (2011) threshold criteria may be too rigid for the UK. The latter is further supported by the geographical distribution here being less weighted towards the

south of the UK, implying that QLCSs do occur in northern locations, just not as regularly.

As yet there are no examples of SJs in the literature between 2008 and 2010. Here, however, 13 of the 196 eDMGSs were diagnosed as potentially being caused by SJs in 7 separate events within the 3 year period, a rate similar to that reported by Parton et al. (2010), whose study was outside the 2008-2010 period. However, as mentioned previously, 2008-2010 was a relatively "low-wind" period compared to that analysed by Parton et al. (2010) and the respective adopted methodologies were different, so comparison between the two must be made with caution. Furthermore, it has not been possible here to effectively distinguish between SJs and the rCCB during T-bone development (stage III and between III-IV) using the observational and relatively coarse model output tools available, hence the category being titled 'potential' SJ. Martínez-Alvarado et al. (2012b) suggested SJs are a generic feature of ETCs occurring in 23-32% of the strongest ETCs, so it must also be kept in mind that many of the storms may have contained a SJ even if the impact of such was not recorded by the surface observing network. A western UK bias of potential SJs is suggested by Figure 4.16, which may not be much of a surprise considering that SJs occur fairly early in an ETC's life cycle (section 1.3), during or just after the rapid deepening of ETCs that form in the genesis region in the relatively warm waters of the eastern Atlantic; ETCs are more likely to form and develop over the sea than over land (Dacre and Gray, 2009). This implies less rapid deepening and therefore less SJ potential over eastern UK locations, with eastward tracking ETCs losing their energy source once they reach the western UK. However, Browning (2004) found that for the October 1987 storm, a SJ formed in eastern England, though the exceptional SW-NE orientation of this track may have added to the low-level forcing (type A) of this ETC and meant that it was still intensifying when it reached the south coast of England, producing a SJ over the eastern UK, unlike the majority of east Atlantic forming storms that are usually forced from upper-levels (type B and C) and which have a more W-E track (Dacre and Gray, 2009). There is currently no study of the geographical spread of surface SJs, Martínez-Alvarado et al. (2012b) indicating the SJ precursor areas in relation to the ETC centre and all other SJ-related publications being case study based. Various indicators of SJs can be examined to determine the likelihood of a SJ event, as discussed by Browning

(2004). For a SJ to form, the ETC should have been or be in the process of deepening explosively (24mb in 24 hours; 1 Bergeron - also known as a meteorological 'bomb' in the terminology of Sanders and Gyakum (1980)). Furthermore the storm should exhibit cloud banding, visible in the satellite imagery or in precipitation intensity seen in the radar imagery, indicating the existence of multiple slantwise convective circulations, often seen in known sting jet cases (Browning, 2004).

Table 4.4 indicates that windstorms Winni and Naruporn were unlikely to contain surface affecting SJs as their respective deepening during development was not extreme enough and there was no obvious evidence of cloud banding, so the closely located rCCB (Figure 1.5) is the feature most likely responsible for the gusts. Furthermore, the table shows that Caesar and Petra are also unlikely to have contained surface gust creating SJs due to a lack of explosive deepening, however deepening was rapid and both examples show evidence of cloud banding, so are not ruled out here as potential SJ events, due to the 6 hourly temporal resolution limitation as noted in the Table 4.4 caption. The 3 other potential SJ events Eliane, Wilhelmine and Ohm are all likely candidates for surface affecting SJs, however high resolution modelling is desirable to achieve conclusive evidence of SJs (e.g. Browning, 2004), as with the QLCS case. Nevertheless, this indicates that 3 of the 28 (10.7%) ETC events contained a SJ (along with 2 unlikely, but not ruled out ETCs (a further 7.1%)), a result not inconsistent with the 23-32% found by Martínez-Alvarado et al. (2012b), considering the low-windiness of this period along with the surface observation selection methodology (not including mid-tropospheric observations but constrained to observed eDMGSs).

| Storm | System Start Date | Time (from start date) and pressure from ERA-interim and (in brackets) synoptic pressure charts | Max 24hr deepening in mb from ERA-interim and (in brackets) synoptic pressure charts | Max 12hr deepening in mb from ERA-interim and (in brackets) synoptic pressure charts | >= 1 Bergeron | Cloud banding evidence? |
|---|---|---|---|---|---|---|
| **Eliane** | 08/01/08 | +0 1000 (1000)<br>+6 993<br>+12 984 (976)<br>+18 974<br>+24 971 (970)<br>+30 967<br>+36 967 (972) | 29 (30) | 16 (24) | Yes | Yes |
| **Winni** | 07/02/08 | +6 1006<br>+12 1004 (1004)<br>+18 1001<br>+24 1000 (1000)<br>+30 997<br>+36 998 (996) | 9 (8) | 5 (4) | No | No |
| **Naruporn** | 21/06/08 | +0 1006 (1006)<br>+6 1003<br>+12 1002 (1001)<br>+18 997<br>+24 994 (991)<br>+30 991 | 12 (15) | 8 (10) | No | No |
| **Wilhelmine** | 24/10/08 | +12 992 (992)<br>+18 986<br>+24 980 (978)<br>+30 971<br>+36 967 (965) | 25 (27) | 15 (14) | Yes | Yes |
| **Caesar** | 07/03/09 | +0 983 (983)<br>+6 979<br>+12 975 (975)<br>+18 972<br>+24 971 (971)<br>+30 966<br>+36 961 (962) | 14 (13) | 10 (9) | No | Yes |
| **Ohm** | 27/11/09 | +12 1005 (1005)<br>+18 1002<br>+24 998( 994)<br>+30 992<br>+36 985 (982)<br>+42 978<br>+48 975 (971)<br>+54 973 | 24 (23) | 14 (12) | Yes | Yes |
| **Petra** | 15/07/10 | +0 1006 (1006)<br>+6 1001<br>+12 998 (996)<br>+18 994<br>+24 991 (988)<br>+30 989 | 15 (18) | 8 (10) | No | Yes |

Table 4.4 - Potential sting jet examples causing eDMGSs from the 1980-2010 period but which specifically occur in the 2008-2010 TIGGE period. ERA-Interim and 6-hourly surface pressure analysis charts are used for the LPCs and satellite and radar imagery to deduce cloud banding. (Note: the maximum deepening could have been 03-03 for example, so 6 hourly analyses may not capture this perfectly)

This further investigation of SJ events indicates that a revision of Table 4.3 is required. With windstorms Winni and Naruporn unlikely to contain surface affecting SJs, their eDMGSs have been re-categorised as shown in Table 4.5. Both events contained two eDMGSs, at Kinloss (site 36) and Lossiemouth (37) during Winni and at Blackpool (24) and Shawbury (16) during Naruporn, which were all decided as being more likely associated with the rCCB due to a lack of explosive deepening to produce a surface affecting SJ. This means that the maximum number of eDMGSs associated with SJ is 9 (4.6%), and the rCCB has even greater impact, with 37.8% of eDMGSs associated with this mechanism.

| **eDMGS causing mechanism** | **Total (percentage)** |
|---|---|
| **rCCB** | 74 (37.8) |
| **WCB** | 33 (16.8) |
| **QLCS** | 26 (13.3) |
| **Pseudo-QLCS** | 17 (8.7) |
| **CCB** | 16 (8.2) |
| **Dry slot CS & Isolated CS** | 11 (5.6) |
| **Potential SJ** | 9 (4.6) |
| **DCB** | 5 (2.6) |
| **Strong PG** | 5 (2.6) |
| | **196** |

Table 4.5 – Revision of Table 4.3 following further SJ investigation.

## 4.4 Top 0.1% DMGSs

The focus of the previous sections has been on eDMGSs (eDMGSs), here the three 2008-2010 top 0.1% examples are examined in detail to highlight the mechanisms involved in such extreme gusts during an exceptionally "low wind" three year period.

*Machrihanish 8th January 2008*

Windstrom Eliane affected a large swath of the UK and was especially extreme over southern Scotland as shown in Figure 4.5. The site of Machrihanish experienced a violent DMGS occurring at 23:47 UTC and was the joint 10th strongest gust experienced at the site between 1980-2010, recording a 3-second gust of 37.6 $ms^{-1}$. As Table 4.4 highlights, Windstrom Eliane has the potential to have contained a SJ, deepening at least 29mb over the preceding 24 hours (to the gust recorded at Machrihanish) and banding visible in the satellite and radar images (especially clear in the 02.31 image in Figure 4.17 to the west of Machrihanish). Figure 1.5 displays the location of a SJ in relation to the cloud signature, just east-wards of the cloud hook, indicating that a SJ would most likely have affected Machrihanish around the timing of the first satellite image shown in Figure 4.17 at 22.28, more than an hour prior to the recorded DMGS; at this stage the cloud head possessed a classic T-bone structure seen in stage III of the Shapiro-Keyser conceptual model of the life cycle (Figure 1.4). The radar image (Figure 4.17) in turn, shows that at the time of the gust, Machrihanish was located directly below the southern part of the hook cloud, a location more likely to be associated with the rCCB, with the typical swath of a SJ thought to be only a few kilometres across (Browning, 2004; Clark et al., 2005). It is unclear whether Eliane produced a SJ at this location and as previously mentioned, high resolution modelling is desirable to achieve conclusive evidence (e.g. Browning, 2004). Nonetheless, it is likely from the observations available here (Figure 4.17) that the violent DMGS seen at Machrihanish was caused by the rCCB as Baker (2009) found for Windstorm Gudrun from 2005, having analysed the event using model data output from the Met Office UM. (It could be argued here that Table 4.5 requires a further update, however, due to evidence being somewhat inconclusive, it was decided to leave this eDMGS as a 'potential' SJ.)

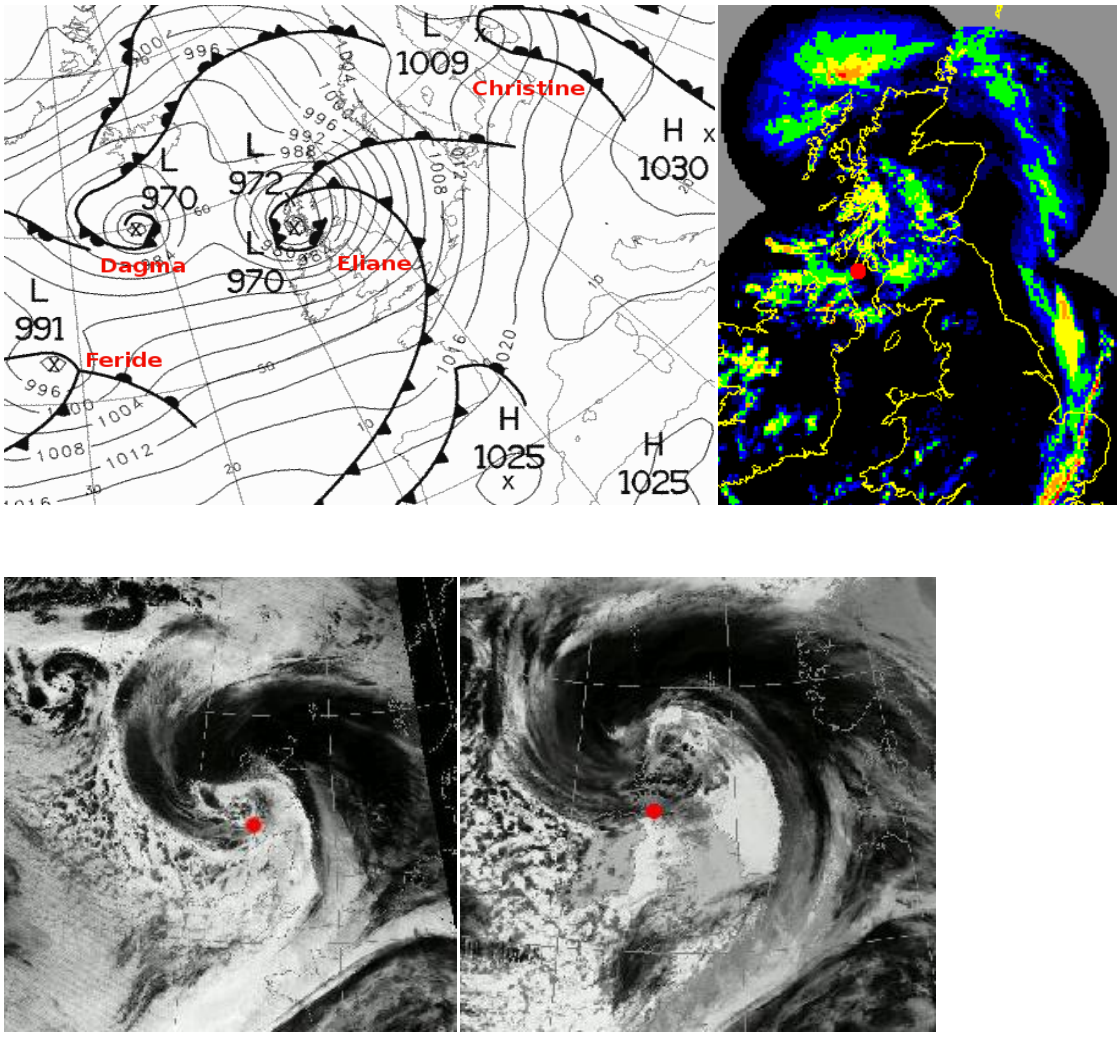


Figure 4.17 - 9th January 2008 00:00 UTC surface pressure chart (courtesy of UKMO) a Nimrod radar image (courtesy of the BADC/UKMO, source http://badc.nerc.ac.uk) showing Machrihanish highlighted (red dot) on the 8th January at 23:45UTC and two satellite images (courtesy of the University of Dundee Satellite Receiving Station, source http://www.sat.dundee.ac.uk/, MODIS satellite channel 31 (reversed images)) taken on the 8th January at 22.28 UTC and on the 9th January at 02:31 UTC.

*Machrihanish 31st Jan 2008*

Windstorm Resi produced eDMGSs at 20 separate network sites (Table 4.1), more than any other 2008-2010 event and also caused a top 0.1% DMGS at Machrihanish. The 3-second violent gust was recorded at 16:39 on the 31st January 2008 with a speed identical to that of Eliane, 37.6 $ms^{-1}$, another joint 10th strongest gust experienced at Machrihanish between 1980-2010. As Resi began to produce strong winds over the UK, the ETC was mature (Shapiro-Keyser stage IV) as shown in the

earlier satellite image in Figure 4.18 (bottom-left). This image and surface pressure chart present the conditions many hours (3.5 and 4.5 respectively) before the timing of the DMGS at Machrihanish but provide a useful insight into how the ETC developed prior to producing the violent DMGS. The radar image taken just 6 minutes after the DMGS indicates that Machrihanish was located beneath the southern part of the well developed cloud hook, highlighted by the bright colours in the image indicating heavy precipitation, and is highly likely to be associated with the rCCB, well known to regularly produce strong surface winds (Figure 1.5; Browning, 2004; Clark et al., 2005; Baker, 2009).

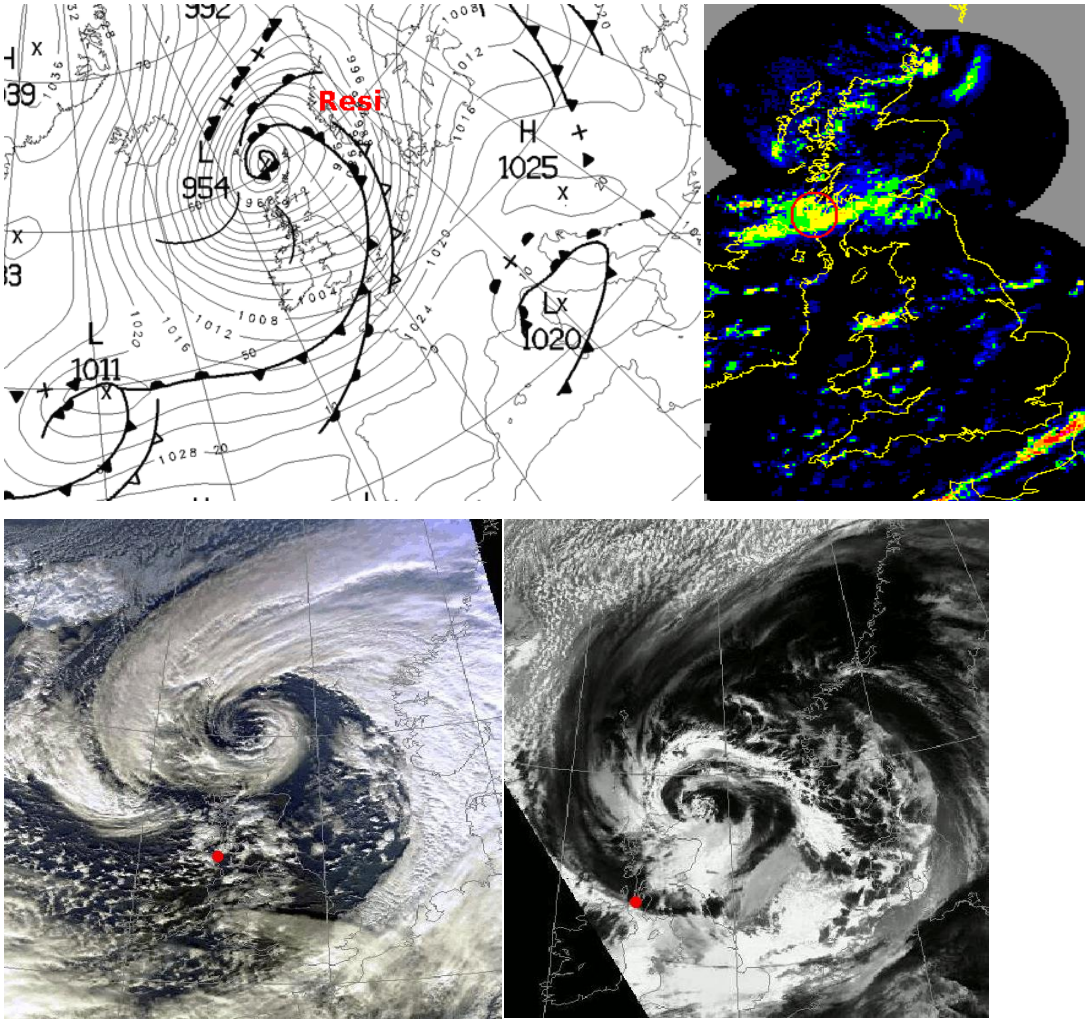


Figure 4.18 - 31st January 2008 12:00 UTC sea-level pressure analysis chart (courtesy of the UKMO) a Nimrod radar image (courtesy of the BADC/UKMO, source http://badc.nerc.ac.uk) showing Machrihanish highlighted (red dot) on the 31st January 2008 at 16:45 UTC and two MODIS satellite images (channels 37 and 31 (reversed image))(courtesy of the University of Dundee Satellite Receiving Station, source http://www.sat.dundee.ac.uk/) taken on the 31st January 2008 at 13:09 UTC and 20:57 UTC respectively.

*Manston 14th November 2009*

Windstorm Hans produced eDMGSs over a relatively small area of the UK, concentrated over southern England, due to strong southerly winds associated with the WCB and the occurrence of three separate QLCS over the two affected days, as identified by Clark (2011). The top 0.1% DMGS occurred at 14:40 UTC on the 14th November 2009 and was, on a site-specific basis, the strongest wind gust seen at any network site during 2008-2010, the 4th strongest 1980-2010 3-second gust experienced at Manston, a recorded speed of 35.5 $ms^{-1}$ (compared to the two joint 10th strongest DMGSs seen at Machrihanish during 2008-2010).

The 3 QLCSs associated with Hans affected central southern and south-east England between 13:00 UTC on the 13th and 05:00 on the 14th November and occurred along the warm and cold fronts seen in the surface pressure chart in Figure 4.19, displaying the already mature (Shapiro-Keyser stage IV) ETC, and along a secondary cold front behind the initial cold front. These had passed over the UK by the time of the DMGS recorded at Manston, however an organised line of convection formed at the southern tip of the occluded front as seen in the satellite image (taken 2 hours before the DMGS) and the radar image (observing the reflectivity field five minutes after the DMGS). The radar image indicates heavy precipitation associated with this line convection (however, not a sufficient convection line to meet the selection criteria of Clark (2011), for QLCS classification) over Manston at the time of the DMGS, highly likely to be responsible for the gust, either through strong downdrafts or a rear-inflow jet. The compass bearing of the gust was 200°, making it unlikely to be a rear-inflow jet, however again it is difficult to be conclusive without high-resolution modelling. Nonetheless, it is certain that this line convection feature was responsible for the violent DMGS seen at Manston, again indicating that the Clark (2011) QLCS threshold criteria may be too rigid for the UK.

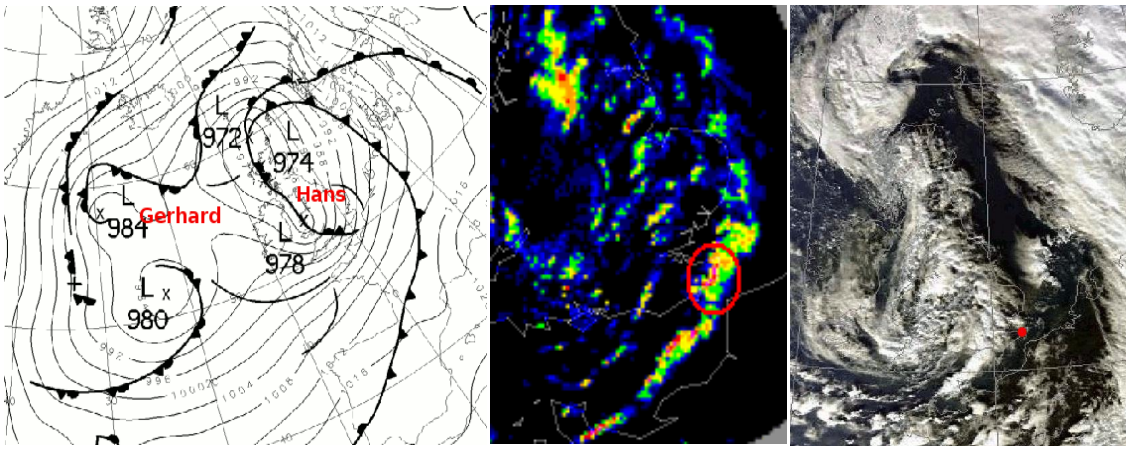


Figure 4.19 - 14th November 2009 12:00 UTC seal-level pressure analysis chart (courtesy of the UKMO) a Nimrod radar image (courtesy of the BADC/UKMO, source http://badc.nerc.ac.uk) showing Manston highlighted (red circle) on the 14th November 2009 at 14:45UTC and a MODIS (channel 37) satellite image (courtesy of the University of Dundee Satellite Receiving Station, source http://www.sat.dundee.ac.uk/) taken on the 14th November at 12.41 UTC.

These top 0.1% DMGS results highlight the importance of sub-storm mechanisms which are perhaps not given the attention that their surface impacts merit. There is currently much concentration of studies on the mechanisms behind SJs causing the strongest gusts during extreme wind producing ETCs (Browning, 2004; Clark et al., 2005; Martínez-Alvarado et al., 2012b). However, these results suggest that greater attention would also usefully be paid to the rCCB and QLCS/pseudo-QLCS mechanisms.

## 4.5 Summary

An assessment of how the most extreme DMGSs, both eDMGSs and the top 0.1% of DMGSs, vary over the 1980-2010 period, both intra and inter-annually, is made in chapter 5, placing the 2008-2010 period into longer term context. This period is used to construct a 3-year climatology of ETC sub-storm mechanisms associated with the highest surface gusts recorded in the station database.

- There is a wide range in annual variability of eDMGS and top 0.1% DMGS occurrences. eDMGSs are lowest in 2010 with just 19 (0.4% of the total 4854) and highest, 371 (7.6%), in 1993, while 2008-2010 is shown to be a “low-wind”

period. Top 0.1% DMGS also reveals 2008-2010 to be a “low-wind” period, with a total of just 3 (0.6% of the 513) occurrences, compared with 1993 alone recording 77 (15%).

- The 1980-2010 winter months (DJF) are shown to be the most dominant with 66.2% of the eDMGSs and 75.2% of the top 0.1% DMGSs. 2008-2010 eDMGSs are again dominated by January, however February and December are not so prominent, the latter especially, due to the anomalously low wind years of 2009 and 2010. March was the 2$^{nd}$ most stormy month over the 3 years, with November also contributing strongly, indicating that this period was not entirely uncommonly low, and was indeed more extreme, for some months of the year.

- The rCCB (described in section 1.3) accounts for more than a third (74 out of 196, 37.8%) of all 2008-2010 eDMGSs, with the warm-conveyor belt (WCB) the second most influential (33 out of 196, 16.8%).

- Quasi-linear convective systems (QLCSs), account for 26 out of 196 (13.3%) of eDMGSs, with pseudo-QLCSs (not reaching the threshold criteria of Clark (2011)) a further 17 (8.7%), indicating that QLCSs are of great importance in generating extreme surface winds.

- The QLCS threshold criteria of Clark (2011) are shown to be too rigid for the UK, omitting some extreme gusts during pseudo-QLCSs. The criterion of Clark which prevents most of the pseudo-QLCS DMGSs from being classified as QLCSs relates to rainfall intensity: ‘a continuous or near continuous line of rainfall rates ≥ 4 mmh$^{-1}$ (equivalent to 32.6 dBZ)’ (Clark, 2011), which needs to be lowered to capture more of the observed surface extreme windspeeds.

- There are no examples of Sting Jets (SJ) in the literature between 2008 and 2010, however 3 of the 28 identified ETC strong wind events are shown to be highly likely to have contained a SJ during their development.

# Chapter 5

# ETC global forecast model comparison and high resolution modelling

An assessment of the historical UK wind regime, as described by 10m station measurements, has been presented in Chapter 3, with an emphasis on the inter-annual variability of windspeed threshold exceedence frequencies, the spatial distribution of damaging windspeeds and the relative downstream effects of the NAO phase. An assessment of the extreme gusts experienced over the 1980-2010 period and specific responsible mechanisms (2008-2010) have been discussed in Chapter 4. This chapter focuses on how well these extreme eDMGSs are represented by global model wind analyses and how well they are forecasted by the global NWP models available in the TIGGE database. It then goes on to investigate the ability of the WRF model to simulate an example ETC, focusing on sensitivity to horizontal and vertical resolution and to choice of cloud microphysics scheme.

## 5.1 ECMWF analysis vs surface observations and TIGGE forecast quality

Figure 5.1 shows the UK split into 1˚x 1˚ grid squares (the resolution used in this study, see section 2.2.3) and presents the maximum mean (note the use of mean wind in TIGGE rather than gust) windspeed experienced at each corresponding grid point during the period 1st of January 2008 - 31st December 2010 according to the ECMWF analysis. 3 full years were analysed in this study, despite Brazil contributing only from the 1st February 2008 and Australia withdrawing in July 2010, and the ECMWF analysis

was used as 'truth' as discussed in section 2.2. In Figure 5.1 the grid points (at the centre of the grid squares shown) have been interpolated onto a regular 1˚x1˚ grid (one of the TIGGE resolution options) from the original N200 Reduced Gaussian grid resolution (Bougealt et al., 2010), also made available on the TIGGE database (http://tigge.ecmwf.int/).

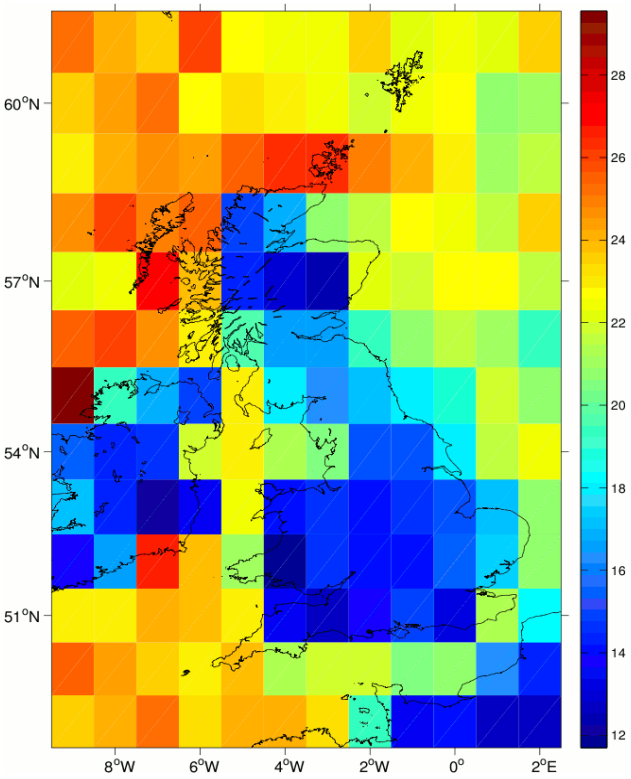


Figure 5.1 - Maximum ECMWF analysis 10m windspeed ($ms^{-1}$) for each 1˚x 1˚ grid square during the period 2008-2010 (grid points are located in the centre of each grid square shown).

The ECMWF maximum mean windspeeds in Figure 5.1 correspond well with the observed 2008-2010 maximum DMGSs shown in Figure 4.6 in terms of spatial variability, with the associated reduced amplitude due to mean winds being represented rather than DMGSs. Again, the inland southern areas generally experience the lowest windspeeds and exposure to fetch over the Atlantic Ocean and Irish Sea is influential, highest mean windspeeds occurring on the western coasts of Ireland and Scotland. The general rule of increased latitude and altitude being associated with stronger winds is shown to apply, due to reduced friction at exposed high altitude sites and closer proximity to the higher storm track density region to the south and east of Iceland (Dacre and Gray, 2009) in the north of the UK. However there is a noticeable maximum windspeed discrepancy with the Shetland Isles (north

Scotland) not seeing the highest winds, whereas the Shetland site of Lerwick (site number 40; see Figure 2.1) experienced the strongest DMGS (41ms$^{-1}$) over this period. A possible reason for this is the fact that the ECMWF analysis gives a snapshot of the mean wind at 00:00hrs and 12:00hrs, whereas the DMGS covers the whole 24 hour day and the DMGS at Lerwick in Figure 4.6 was experienced at 14:48 UTC on October 25$^{th}$ 2008, so was not represented in the ECMWF analysis. Also, the grid point is located just east (downwind from the strongest winds) of the Shetland Isles whereas Lerwick's monitoring station is relatively exposed at 82m above sea level. Another reason is that the relationship between mean winds and gusts is complex, as explained by Bechtold and Bidlot (2009), and it is a limitation of this study to have mean winds in TIGGE representing the set of windstorms identified using the eDMGSs observations (chapter 2.1.5). Nevertheless, the comparison shows that using the ECMWF analysis as 'truth' for much of this study is reasonable.

### 5.1.1 How was Windstorm Emma represented in TIGGE?

Windstorm Emma produced the most eDMGSs of any 2008-2010 ETC event and passed rapidly over the UK as shown in Table 4.1 and Table 4.2. Windstorm Emma was investigated in detail in section 4.2.1. Emma's passage over the UK coincided with an ECMWF analysis and corresponding TIGGE forecast time-steps (for 8 of the centres) for 1$^{st}$ March 2008 at 00:00 UTC, with 13 of the 25 eDMGSs occurring within 2 hours of this time (see Table 4.1) according to the methodology used in this study (section 2.2.3). The number of eDMGSs represented in this one analysis/forecast time-step is by far the largest, the next highest being associated with Windstorm Carmen (6 - not shown), indicating that Windstorm Emma is a good case study to investigate the forecasting capabilities of the TIGGE centres. The fact that the Japanese model does not output to 00:00 UTC (only to 12:00, section 2.2) is outweighed by the 1$^{st}$ March 2008 00:00 UTC analysis representing so many eDMGSs.

Figure 5.2 shows the windspeeds seen in the ECMWF analysis at 00:00 UTC on 1$^{st}$ March 2008 during the passage of Emma, expressed also as a percentage relative to the maximum windspeed in ECMWF analyses over the full 2008-2010 period shown in Figure 5.1. This highlights the relative ferocity of windstorm Emma, producing the

strongest 2008-2010 mean winds in the model in many parts of the country, supporting the focus here on Emma as a case study ETC.

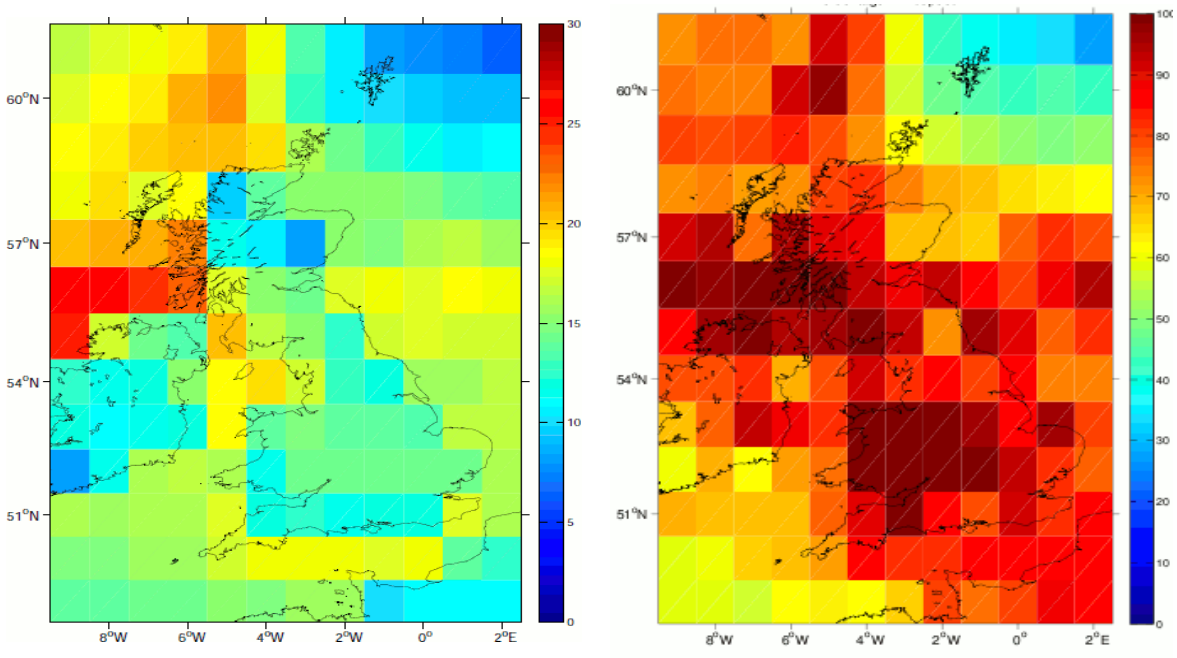


Figure 5.2 - Left - ECMWF analysis 10m windspeed ($ms^{-1}$) for each 1˚x 1˚grid point for 1st March 2008 00:00 UTC (grid points are located in the centre of each grid square shown). Right- 1st March 2008 00:00 UTC mean windspeed as a percentage of the 2008-10 maximum ECMWF analysis windspeed shown in Figure 5.1.

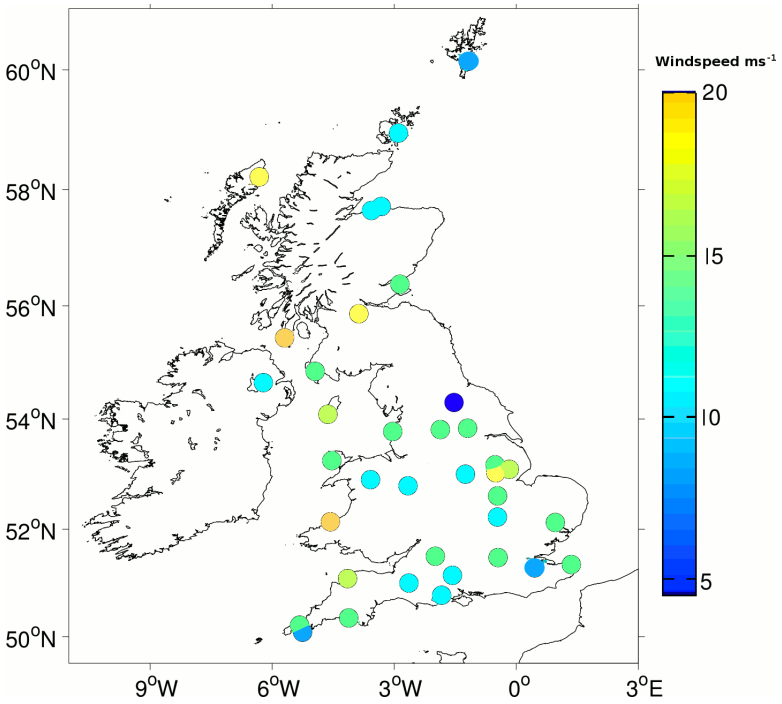


Figure 5.3 – Observed HM winds ($ms^{-1}$) (recorded from 23:40-23:50 UTC 29th February 2008) representing 00:00 UTC 1st March 2008. The sites of Dunstaffnage, Eskdalemuir and Ringway failed to report data, so there are 37 sites displayed here.

Figure 5.3 shows the HM windspeeds at the observation network sites at 00:00 UTC on 1st March 2008 (recorded from 23:40-23:50 UTC 29th February 2008), enabling comparison with the ECMWF analysis in Figure 5.2. With the analysis only representing the central point of each grid, varying geographically from the observation sites, local topographic effects (section 3.4) have to be expected. For example the two most south-western sites (Culdrose (site number 1) and Camborne (2)) are represented by the same grid square in the ECMWF analysis (Figure 5.2), however Culdrose is located on the south coast and Camborne in the north of Cornwall, leaving them more exposed to different wind directions, therefore often experiencing different windspeeds as occurs during windstorm Emma (Figure 5.3). This highlights the limitations of using a coarse model grid scale to represent individual locations, indicating the need for higher resolution modelling as conducted in section 5.5. However, even with finer resolution, comparing model grid squares with individual station locations is a fundamental challenge, due to local and micro-scale processes. Generally, the ECMWF analysis overestimates the surface winds, possibly for reasons highlighted by Vautard et al. (2010) regarding the misrepresentation of variations in surface vegetation by models, or due to the fact that the observations are from a ten minute average (from 20-10 minutes prior to the hour in question) and the ECMWF analysis is an instantaneous representation of mean winds on the hour (here 00:00 1st March 2008), with Emma's associated winds continuingly strengthening during this time. Nevertheless, the ECMWF analysis gives a good spatial reproduction of the observed winds, using the HM observations within the data assimilation process, and is widely expressed as being the best tool available as a representation of 'truth' in the North Atlantic and European region (Froude, 2009).

### 5.1.2 TIGGE control forecasts

The TIGGE archive contains the control forecasts of the contributing centres as well as the perturbed ensemble members. Here, a comparison is made between the TIGGE centres at various time-steps with regard to the spatial root-mean-square error (RMSE), a commonly used statistical tool to assess forecast accuracy (e.g. Wiegand et al., 2011; Park et al., 2008). The spatial area investigated covers the UK, including all grid points from 9°W – 2°E and 49-61°N, as previously seen in Figure 5.2.

Figure 5.4 shows the RMSE for 10m wind-speed (based on all grid points from 9°W – 2°E and 49-61°N) for 1-7 day forecasts valid at 1st March 2008 00:00 UTC for all TIGGE members other than MeteoFrance (due to only going out to T+60 as discussed in section 2.2) and Japan (who do not produce a forecast for 00:00 UTC), with respect to their own analyses (bottom - Australia is absent due to not providing analyses) and with respect to the ECMWF analysis (top). The grid used is the same 1˚x1˚ grid used in Figure 5.1 and Figure 5.2. It is not the intention here to assess which model control run performed best for each of the identified ETC events, but to give an indication of the multi-model spread for this most extreme 2008-2010 ETC example, Windstorm Emma. RMSEs generally grow with lead time, which is unsurprising as forecasts are likely to be increasingly accurate as lead times become shorter, giving less time for the model initial condition errors to grow. However, the error growth is clearly not linear or uniform amongst the models for this ETC. When compared against their respective analyses, the Canadian model out-performs all other models for predicting windstorm Emma's 10m surface winds at 00:00 UTC on March 1st 2008 at T+24, +72, +120 and +168, with the ECMWF performing to a similar standard at T+120 and better at T+144, along with the UKMO model performing best at T+ 96. These models use the state of the art 4D-VAR for data assimilation in the initial conditions. Johnson et al. (2006) suggests that the use of 4D-VAR is important for the Canadian model in preventing rapid error growth, compensating for the relatively low resolution model. From T+48 hours, the 3D-VAR powered Korean model begins to perform well, agreeing with suggestions that 3D-VAR can compete with 4D-VAR in areas of comprehensive data coverage (Whitaker et al., 2009). NCEP's model is relatively strong at longer lead time for this ETC example, though less so at shorter range. A possible reason for this is the low quality of data assimilation method used for providing the initial conditions, as Buizza et al. (2005) found, suggesting that the NCEP ensemble performance is negatively affected in the short range. This impact can also be seen in the Brazilian model which also uses NCEP analysis for initial conditions, with the highest RMSE of any model at T+ 24. However, this is only one event, in one small domain area, so care must be taken with these results and another ETC example could reveal quite different inter-model performance.

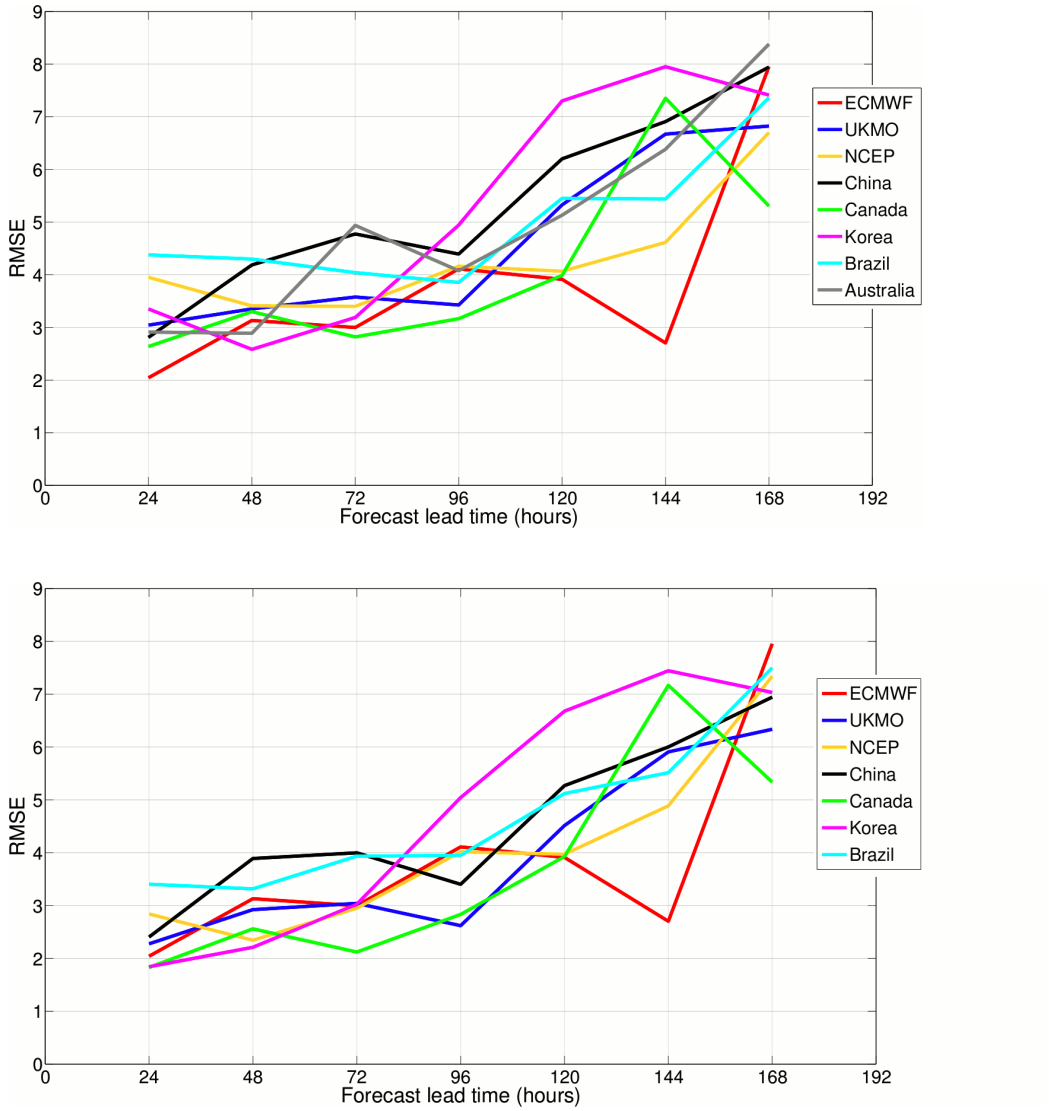


Figure 5.4 – Spatial (9°W – 2°E and 49-61°N) average root-mean-square error (RMSE) of the control forecast 10m windspeed ($ms^{-1}$) for (top) 8 TIGGE centres at increasing time-step compared to the ECMWF analysis, and (bottom) 7 TIGGE centres at increasing time-step compared to their respective analyses valid at 1st March 2008 00:00 UTC.

Figure 5.4 also shows the RMSE of each model's control forecast compared to the ECMWF analysis. The ECMWF model performs comparatively better when all centres use its analysis as 'truth', as expected due to forecast and analysis generated using the same model characteristic shown in Table 2.3. When using the ECMWF analysis, each centre's forecast RMSE is markedly increased, as Wiegand et al. (2011) found for upper-level potential vorticity over Western Europe and Morocco for a high impact flooding event in May 2008. This result confirms the suggestion made by Wiegand et al. (2011) that these discrepancies should be more routinely accounted for. Bougeault et al. (2010) also highlight this point, stating that the choice of the optimal verification

analysis is both a difficult and a sensitive one, and additional associated research is needed. It is surprising that the ECMWF fails to outperform many of the other models, especially the Canadian model, even when all models are compared to the ECMWF analysis in the Windstorm Emma example. It is not until T+24 that it possesses the lowest RMSE (Figure 5.4), having previously been lowest at T+144. It is unclear why this occurs, when the ECMWF has the highest horizontal and vertical resolutions and the best data assimilation scheme, though highlights that the multi-model can add value and that no one model will always produce the best forecasts. The control run is just one of the available ensemble members, no more likely to be correct than any of the other members from each centre, so how do the other EPS members perform for this ETC example?

### 5.1.3 TIGGE ensemble forecasts

TIGGE also provides the research community with the opportunity to assess the ensemble spread of each of the contributing centres, through the provision of all ensemble members. Each of the contributing centres perturb their initial conditions in a variety of ways as discussed in section 2.2.1. For example, the ECMWF uses singular vectors to achieve maximum perturbation growth for a given optimisation time (Palmer et al., 1995), while the NCEP use the ensemble transform technique (Wei et al., 2008), which is a version of the breeding vector technique as described by Toth and Kalnay (1993), using previous ensemble forecasts to obtain the growing components of the analysis error. Not all of the centres perturb their respective initial conditions on a global scale, instead for different regions which may therefore affect the forecast error of European ETCs. The ECMWF, NCEP and the Canadian model also perturb their model physics, which has been known to widen the spread of the ensemble (Buizza et al., 1999).

Figure 5.5 shows the RMSE for 10m wind-speed for 1-7 day forecasts valid at 1$^{st}$ March 2008 00:00 UTC for all available TIGGE members, as with Figure 5.4. Here, the RMSE of each model's control forecast (in relation to the ECMWF analysis; top) is compared with the ensemble mean of each member's EPS (bottom; also in relation to the ECMWF analysis). Again, RMSEs generally grow with lead time as expected, but the ensemble means are more linear than the control forecasts, especially the ECMWF.

This is of no surprise considering the control forecast is only one member, whereas the ensemble consists of up to 50 members (see section 2.2.1) therefore averaging out the individual member's variability. Generally each centre's ensemble mean performs better in the medium range than the control (beyond 120 hours) with less of a difference seen in the shorter range. The Canadian and UKMO models have most noticeable negative discrepancy between the control and the ensemble mean, with the Canadian ensemble mean RMSE at least 1ms$^{-1}$ higher than the control at each time-step apart from at 144 hours, while the UKMO ensemble mean is worse in the shorter range (up to 96 hours). It is difficult to explain these discrepancies without looking at the respective spreads of the EPS members.

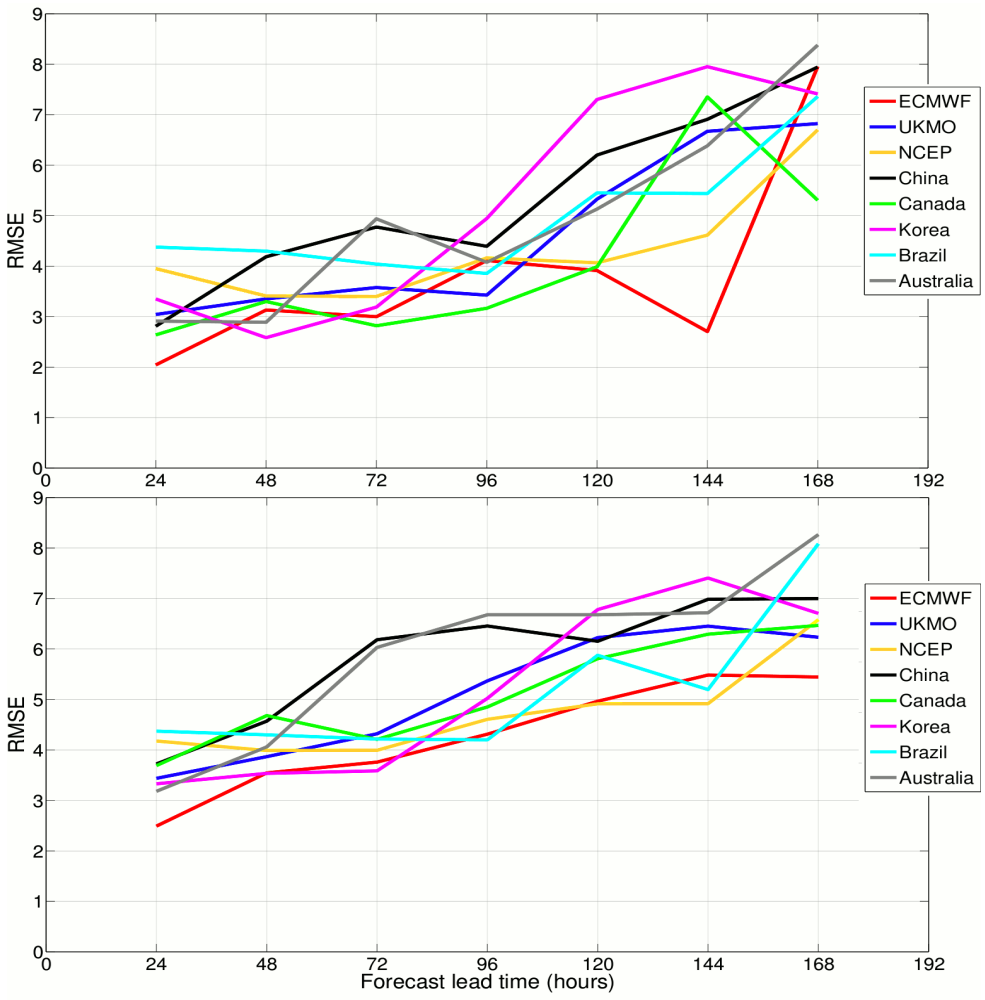


Figure 5.5 –Spatial (9°W – 2°E and 49-61°N) average root-mean-square error (RMSE) of the (top) control forecast 10m windspeed (ms$^{-1}$) and (bottom) ensemble mean forecast 10m windspeed (ms$^{-1}$) for 8 TIGGE centres at increasing time-step compared to the ECMWF analysis valid at 1$^{st}$ March 2008 00:00 UTC.

Figure 5.6 shows the spatial average RMSE (based on all grid points from 9°W – 2°E and 49-61°N) for 10m windspeed for 1-7 day forecasts valid at 1st March 2008 00:00 UTC for all TIGGE members other than MeteoFrance (due to only going out to T+60 as discussed in section 2.2.1) and Japan (who do not produce a forecast for 00:00 UTC), for each individual ensemble member. Each of the individual model EPSs are displayed along with the grand ensemble, incorporating all 189 available TIGGE ensemble members. The RMSEs are with reference to the ECMWF analysis rather than to the individual centre respective analyses. Again, it is not the intention here to assess which model's members performed best for each of the identified ETC events, but to give an indication of the multi-model ensemble forecast spread within TIGGE for the ETC Emma event.

Figure 5.6 shows the RMSE spread of 10m windspeeds for each centre and there is a large variety. The ECMWF possesses relatively low EPS spread until T+120, when the dispersion becomes much larger. The ECMWF EPS contains a member with the lowest RMSE at every time step, however it must be kept in mind that the comparison is with the ECMWF's own analysis. The Canadian model, with its perturbed physics, has a very wide EPS spread, which provides support for the statement made by Buizza et al. (1999) that perturbing model physics widens the ensemble spread, with at least one member's RMSE below 4 $ms^{-1}$ all the way out to T+144 for this extreme ETC example. However as shown in Figure 5.5, the Canadian model's ensemble mean is not as good. This raises the question about skill vs. spread of ensemble models, which for a good ensemble, need to be in balance. High skill is for example reflected in an ensemble mean close to the truth (Jolliffe and Stephenson, 2003), however, for extreme events, having at least one member which simulates this extreme at a relatively long range is important. It can therefore be argued that the Canadian model performs poorly with regard to the ensemble average, however despite this fact, the EPS has enough spread to capture this extreme event, with its members often having the lowest RMSE, so the opposite can also be argued.

The spread of the UKMO ensemble, which also implements model physics perturbations, has a relatively low range, with no member below 4 $ms^{-1}$ RMSE from T+120 onwards, despite using the same data assimilation and initial perturbation

scheme as the Canadian model, in addition to operating at higher horizontal and vertical grid resolutions. The two models, however, have different model physics perturbation approaches, which have a clear effect on the respective spreads in this case, indicating the relative importance of model physics parameterisation schemes compared to resolution for this ETC. The NCEP model has very low EPS spread for Emma and is one of only two EPSs, along with the Brazilian model, which see a decrease in RMSE from T+ 24 to T+96 for some ensemble members, again agreeing with Buizza et al. (2005) that the NCEP ensemble performance is negatively affected in the short range by the relatively low quality of the ensemble of data assimilations, with Brazil's model also affected since it uses the NCEP analysis. The Brazilian model has the lowest EPS spread and highest RMSE of the model's best performing member at all time-steps, which is unsurprising as the initial perturbations are not made at latitudes above $30^{o}$ north, therefore not perturbing the regions in which European ETCs occur. Having said that, the Brazilian model performs relatively well compared to the EPSs when considering the ensemble means in Figure 5.5. The Korean model performs well in the short range (especially with ensemble mean Figure 5.5.) and is among the best performers with at least one of its 16 EPS members with an RMSE below 3 $ms^{-1}$ until T+72 hours, whereas by T+120 it is being outperformed by the other models for this forecast. This indicates that the use of the bred vectors perturbation for the extra-tropics can produce a good quality short-range forecast. The Chinese model also uses bred vectors, producing a large EPS spread throughout, with at least one EPS member having an RMSE of below 3 $ms^{-1}$ until T+144 hours, one of the best EPS forecast performances of any TIGGE model for the Emma ETC. The Australian model also has a wide spread form the T+ 24 step, but contains some of the highest RMSEs in its members, which is perhaps unsurprising considering its use of a simple data assimilation technique and low resolution as described in section 2.2.2, which is possibly a reason behind its termination in July 2010. This model also performs poorly when considering ensemble mean at except at the shortest when it outperforms all but the ECMWF (Figure 5.5). RMSE, often also used over a set of events, gives a good overview of the accuracy of a forecast with respect to each grid point, however it does not indicate whether the forecast has under-estimated, overestimated or simply mistimed the passage of the ETC in question.

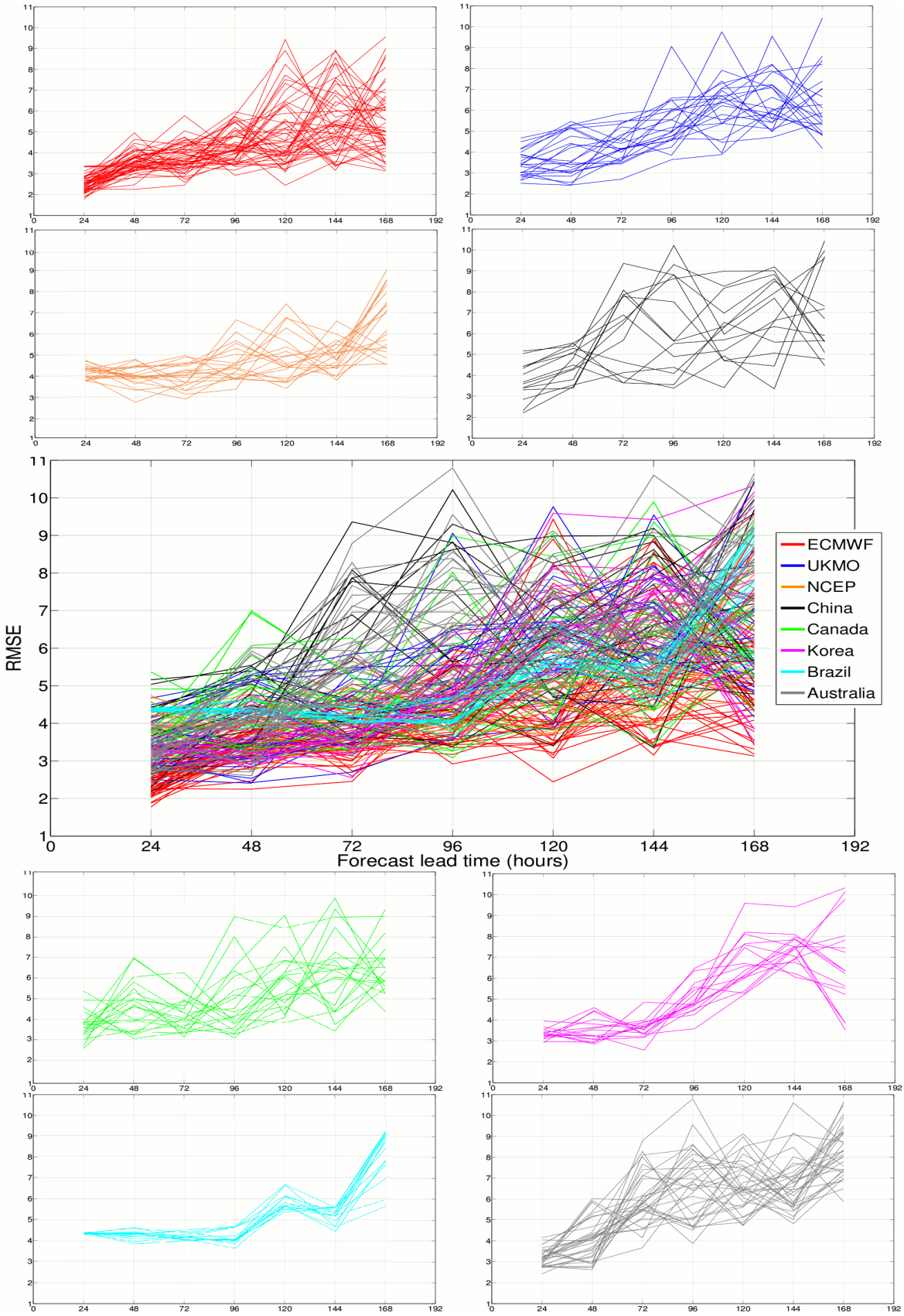


Figure 5.6 – Spatial (9W – 2E and 49-61N) root-mean-square error (RMSE) of 10m windspeeds ($ms^{-1}$) of the ensemble forecast for 8 TIGGE centres at increasing time-step compared to the ECMWF analysis, displayed separately and together for 1st March 2008 00:00 UTC (note variable y-axis scales)

The 15ms$^{-1}$ exceedence is shown to be widespread in Figure 5.2 for Windstorm Emma 1$^{st}$ March 2008 00:00 UTC. Figure 5.7 shows the grid squares that were over the 15ms$^{-1}$ exceedence threshold (left maps on each panel) in the ECMWF analysis and under the 15ms$^{-1}$ exceedence threshold (right maps on each panel). The forecast for a grid square is considered a 'hit' ('false alarm') if the windspeed was over (under) 15ms$^{-1}$ according to the ECMWF analysis and is also above 15ms$^{-1}$ in the forecast. The percentage of EPS members which recorded 'hits' (left maps on each panel) and 'false alarms' (right maps on each panel) in the T+120 (panels a, c and e) and T+48 (panels b, d and f) forecasts are shown. The models which perturb the physics schemes of their ensemble members (PetPhys) (ECMWF, Canada and UKMO – totalling 93 ensemble members) are highlighted (panels a and b) and those which do not (panels c and d) (unPetPhys) (Australia, Brazil, China and NCAR – totalling 96). All of the TIGGE EPSs are also shown (panels e and f), totalling all 189 available ensemble members.

Figure 5.7 shows that for the T+120 Windstorm Emma 1$^{st}$ March 2008 00:00 UTC forecast the PetPhys model EPSs have a slightly better 'hit' percentage (providing windspeed forecasts of ≥ 15 ms$^{-1}$ at grid points which breached 15ms$^{-1}$ in the ECMWF analysis) than the unPetPhys model EPSs , though the former also have a higher percentage of false alarms, (providing windspeed forecasts of ≥15 ms$^{-1}$ at grid points which did not breach 15ms$^{-1}$ in the ECMWF analysis) but not over the UK mainland. The area where the PetPhys model EPSs perform better for the T+120 forecast is over the North Sea, with the PetPhys model EPSs having a wide 'hit' area of over 50%, whereas the corresponding grid points for unPetPhys model EPSs were around 40%. The TIGGE shows that generally the ≥15 ms$^{-1}$ windspeed areas over land were missed by many members, especially over the Central Belt and south-west of Scotland and northwest England where the 'hit' percentages were below 10%, whereas the Western Isles of Scotland TIGGE 'hit' percentages are around 50%.

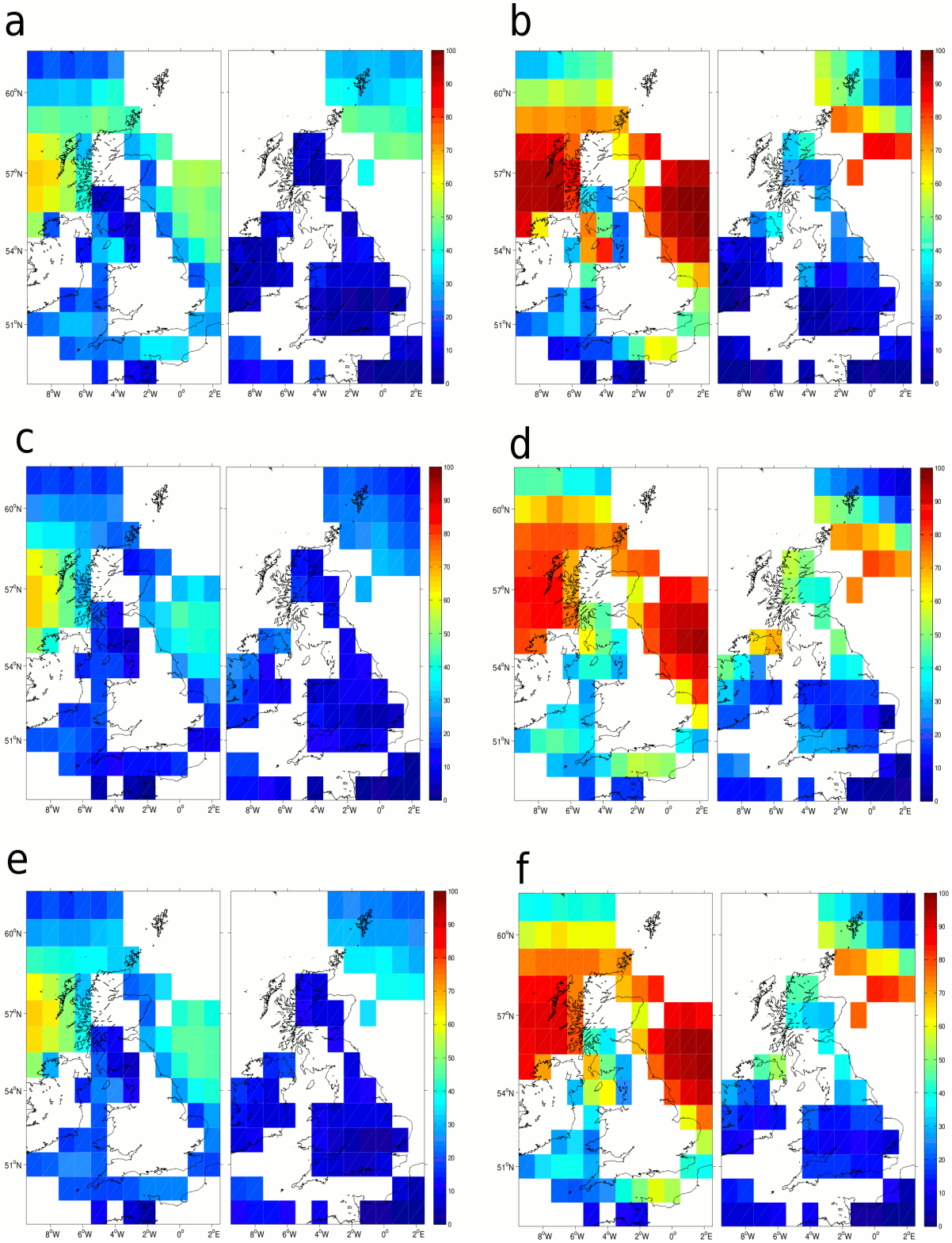


Figure 5.7 – UK 10m windspeed hit (left maps) and false alarm (right maps) percentages of ensembles for the 120 hour forecast (a,c and e)and 48 hour forecast (b, d and f) for the 15ms$^{-1}$ exceedence threshold for 1$^{st}$ March 2008 00:00 UTC, compared with ECMWF analysis. (a) and (b) represent centres which perturb their respective physics schemes (ECMWF, Canada and UKMO), (c) and (d) represent centres which do not perturb their respective physics schemes and (e) and (f) represent all centres together. Grid points are located in the centre of each grid square shown.

The T+48 forecasts contain more EPS members recording ≥15 $ms^{-1}$ 'hits'. The TIGGE shows that ≥15 $ms^{-1}$ windspeeds over the Western Isles of Scotland are generally well forecasted at T+48, though the other land affected areas, such as south-west Wales and south-west England, have only around 25% of members recording a ≥15 $ms^{-1}$ 'hit'. The PetPhys models have a low number of members correctly simulating the magnitude of ETC Emma over the Central Belt and south-west of Scotland and northwest England where the 'hit' percentages are as low as 20%. These areas have relatively more successful EPS members from the unPetPhys models, where the respective 'hit' percentages range from 10% - 30% higher than the PetPhys, though again the unPetPhys model EPSs contain higher false alarm percentages of over 15 $ms^{-1}$ windspeeds over Scotland and Northern England. A possible explanation of this finding is that perturbing the model physics acts to widen the spread (Buizza et al., 1999), intending to represent a wider array of possible outcomes, meaning that the strong winds were not forecasted by many PetPhys members. Nevertheless the possibility is covered by some members, sufficient to prompt the attention of chief forecasters at meteorological centres with regard to issuing warnings.

An avenue for future work, to extend the findings presented here, would be to group the EPSs by data assimilation schemes or initial perturbation methods. Also, extending the domain of the analysed area would allow for tracking storms to assess differences in track locations and timing of strongest winds.

## 5.2 Extreme DMGSs represented by TIGGE

So far the focus has been on windstorm Emma in TIGGE, due to the 1st March 2008 00:00 UTC analysis/forecast time-step covering so many extreme DMGSs as discussed in section 5.1.1. This section assesses how well TIGGE represents the other identified ETC events from section 4.1.3.

Some of the observed eDMGSs occur at times which are relatively distant (≥2 hours) from the timing of availability of analyses, which are at 00:00 and 12:00 UTC. Only gusts observed within 2 hours of the analyses (10:00-14:00 UTC for the 12:00 UTC

analysis and 22:00-02:00 UTC for the 00:00 UTC analysis) are included in this TIGGE study as explained in section 2.2.3.

Table 5.1 displays the eDMGSs captured by the TIGGE analysis/forecast time-steps. 21 of the 28 storms are represented to a degree by TIGGE (>0% of an event's eDMGSs coming within 2 hours of the 00:00 and 12:00 UTC TIGGE analysis/forecast time-steps) and are assigned a 'TIGGE storm number') and 12 of the 28 events have ≥50% of their eDMGSs falling within two hours of the TIGGE analysis/forecast time-steps. The table also displays the sub-storm mechanisms (from Table 4.5) that are associated with each eDMGS and their respective locations are highlighted. Each eDMGS is assigned a representative grid square in the respective analyses and given a 'TIGGE gust number', with many of the eDMGSs represented by the same grid square as other eDMGSs, so are given the same 'TIGGE gust number'. For example, Windstorm Paula (start date 24/01/08) is the second 2008-2010 ETC captured in TIGGE (using the method described in section 2.2.3) so is assigned the 'TIGGE storm number' 2. The ETC has associated eDMGSs in two separate analyses/forecast time-steps, the T+24 (00:00 UTC 25/01/08 (24 hours after the start of the storm)) and T +36 (12:00 UTC 25/01/08 (36 hours after the start of the storm)), has 4 out of 5 eDMGSs covered within the respective two hour time allowance, which are all apparent in the ECMWF analysis (e.g. over 70% of the maximum in Figure 5.1, which is subjective value of windspeeds not being represented) and contains two eDMGSs, at Leeming (site 28) and Church Fenton (26), which are represented by the same grid square (which represents the nearest grid point) in the same analysis, hence given the same 'TIGGE gust number', 7. There are some eDMGSs which have not been represented by the ECMWF analysis, for example, the rCCB gust during Chanel (TIGGE storm number 12) at Kinloss (36) did not reach the necessary 70% of the maximum (of the 2008-2010 maximum wind, seen in Figure 5.1) to constitute representation of the eDMGS. Some strong winds seen in the analyses at the time of an eDMGS may not be related to the gust causing mechanism in question. For example, the DMGSs observed during Windstorm Frank (TIGGE storm number 15) were categorised as isolated convective systems (see chapter 4.2.1), and were counted as being represented in the ECMWF analysis, however may have been captured in the analysis by winds more likely associated with the WCB, but this is difficult to determine due to the coarse resolution, along with the

fact that the ECMWF analysis is representing mean wind speeds rather than 3-second gusts.

| **Storm name (TIGGE storm number)** | **ETC Start Date** | **eDMGSs covered by ECMWF analysis T+… no. of hours from start date** | **Proportion of eDMGSs covered by 2hours either side of available analyses** | **Represented by analysis? Yes (Y), No (N) and associated mechanism** | **'TIGGE wind number' in order of DMGS time (numbers occurring multiple times indicates grid square sharing) and locations** |
|---|---|---|---|---|---|
| Christine | 07/01/08 | | 0/4 | | |
| Eliane (1) | 08/01/08 | 24 | 4/10 | Y(QLCS)<br>Y(Potential SJ)<br>Y(Potential SJ)<br>Y(rCCB) | 1 Wittering<br>2.WestFreugh<br>3.Machrihanish<br>4.WestFreugh |
| Karin/Louisa | 17/01/08 | | 0/2 | | |
| Paula (2) | 24/01/08 | 24; 36 | 4/5 | Y(pQLCS-CF)<br>Y(pQLCS-CF)<br>Y(strong PG)<br>Y(strong PG) | 5.Stornaway<br>6.Lerwick<br>7.Leeming<br>7.Church Fenton |
| Resi (3) | 31/01/08 | 0; 12; 24; 36 | 8/23 | Y(WCB)<br>Y(CS)<br>Y(DCB)<br>Y(rCCB)<br>Y(DCB)<br>Y(DCB)<br>Y(rCCB)<br>Y(rCCB) | 8.Stornoway<br>9.Manston<br>10.Church Fenton<br>11.Leeming<br>12.Stornoway<br>11.Leeming<br>12.Stornoway<br>13.Cranwell |
| Winni (4) | 08/02/08 | 12 | 2/2 | Y(rCCB)<br>Y(rCCB) | 14.Kinloss<br>14.Lossiemouth |
| Zizi/Annette (5) | 21/02/08 | 12; 36 | 2/8 | N(WCB)<br>Y(strong PG) | 15. Leeming<br>16.Kinloss |
| Carmelita (6) | 26/02/08 | 12 | 1/3 | Y (rCCB) | 17.Leeming |
| Emma (7) | 29/02/08 | 24 | 13/25 | Y(QLCS)<br>Y(QLCS)<br>Y(QLCS)<br>Y(QLCS)<br>Y(rCCB)<br>Y(2$^{nd}$WCB)<br>Y(2$^{nd}$WCB)<br>Y(CS)<br>Y(postQLCS)<br>Y(2$^{nd}$WCB)<br>Y(CS)<br>Y(2$^{nd}$WCB)<br>Y(postQLCS) | 18.Cranwell<br>18.Waddington<br>19.Coningsby<br>23.Wittering<br>20.Kinloss<br>21.Lyneham<br>22.Heathrow<br>19.Coningsby<br>22.Bedford<br>21.MiddleWallop<br>18. Wittering<br>23.East Malling<br>24.Wattisham |
| Johanna | 10/03/08 | | 0/11 | | |
| Kirsten (8) | 11/03/08 | 12; 24 | 3/16 | Y(WCB )<br>Y(rCCB)<br>Y(CS) | 25.Lyneham<br>26.Shawbury<br>27.EastMalling |
| Meli (9) | 21/03/08 | 0 | 1/2 | Y(CS) | 28.Blackpool |
| Naruporn (10) | 22/06/08 | 12 | 2/2 | Y(rCCB)<br>Y(rCCB) | 29.Blackpool<br>30. Shawbury |
| Wilhelmine (11) | 23/10/08 | 60 | 4/10 | Y(CCB)<br>Y(CCB) | 31.Ronaldsway<br>32.Kinloss |

| | | | | | |
|---|---|---|---|---|---|
| | | | | Y(CCB)<br>Y(rCCB) | 32.Lossiemouth<br>33.Stornaway |
| Chanel (12) | 10/11/08 | 0; 12 | 2/2 | Y(trough)<br>N(rCCB) | 34.Lyneham<br>35.Kinloss |
| Zimone (13) | 19/12/08 | 24 | 4/6 | Y(rCCB)<br>Y(rCCB)<br>Y(rCCB)<br>Y(rCCB) | 36.Kinloss<br>36.Lossiemouth<br>37.Kirkwall<br>38.Kirkwall |
| Antje (14) | 21/12/08 | 12 | 4/5 | Y(rCCB)<br>Y(rCCB)<br>Y(rCCB)<br>Y(rCCB) | 39. Lossiemouth<br>40.Kirkwall<br>39.Kinloss<br>41.Leuchars |
| Frank (15) | 17/01/09 | 24 | 2/16 | Y(CS)<br>Y(CS) | 42.Culdrose<br>43.Wittering |
| Caesar | 07/03/09 | | 0/3 | | |
| Jochen | 08/09/09 | | 0/2 | | |
| Berti (16) | 01/11/09 | 12 | 2/2 | N (DCB)<br>N (DCB) | 44.Waddington<br>45.Bingley |
| Hans (17) | 13/11/09 | 24 | 1/8 | Y(QLCS) | 46.Cranwell |
| Klaus | 18/11/09 | | 0/3 | | |
| Max (18) | 24/11/09 | 24 | 3/7 | Y(QLCS)<br>Y(QLCS)<br>Y(QLCS) | 47.Yeovilton<br>48.Yeovilton<br>49.Lyneham |
| Ohm | 29/11/09 | | 0/2 | | |
| Petra (19) | 15/07/10 | 24 | 2/2 | Y(Potential SJ)<br>Y(Potential SJ) | 50.Valley<br>50.Valley |
| Becky (20) | 07/11/10 | 24 | 2/3 | Y(CCB)<br>Y(CCB) | 51.WestFreugh<br>52.Valley |
| Carmen (21) | 11/11/10 | 12; 24 | 7/12 | Y(DSCS)<br>Y (rCCB)<br>Y (rCCB)<br>Y (rCCB)<br>Y (rCCB)<br>Y (rCCB)<br>Y (rCCB) | 53.Shawbury<br>54.Chivenor<br>55.ChurchFenton<br>56.Blackpool<br>57.Bingley<br>58.Blackpool<br>58.Bingley |
| Total | | 28 | >0% 21/28<br>>=50% 12/28 | | |

Table 5.1 – Identified events (from chapter 4) that are represented by a relevant analysis/forecast time-step and assigned a TIGGE storm number. The 'Represented by analysis?' column provides a yes or no answer to whether the gust (which does fall within 2 hours of the analysis) is evident in the analysis, based on the percentage of maximum analysis windspeeds in Figure 5.1.

## 5.3 Added value using the TIGGE?

When comparing the TIGGE contributing model EPSs, including the ECMWF EPS, with the ECMWF analysis, a key question is how well do the other models compete? In the earlier assessment for ETC Emma, some models were very competitive, namely the Korean and Canadian. The ECMWF, as described in section 2.2.1, uses the most sophisticated data assimilation method to perturb the initial conditions (4D-VAR),

operates at the highest vertical and horizontal resolutions and has the largest number of EPS members of any TIGGE model. The ECMWF also perturbs the model physics, a practise only incorporated in two other models, shown to have a positive impact for the medium range (T+120) forecast for the ETC Emma example Figure 5.6, though not so much at shorter forecast time-steps. Section 5.1 shows that the other models can compete and even outperform the ECMWF forecasts, though this was for only one of the 21 2008-2010 events covered by the TIGGE database, but is this true for other events?

A powerful way to verify the skill of EPS forecasts is by utilising the relative operating characteristics (ROC) curve and ROC score (Jolliffe and Stephenson, 2003). The ratios between the hit and false alarm rates, that can be expected from use of different probability thresholds (e.g. strong wind thresholds to highlight an extreme event), are assessed by ROC score, indicating whether and to what extent the EPS has skill. ROC score and other skill scores (e.g. the Brier score) are only useful however if the base rate (climatology) of events or an unbiased sample of forecasts from which to identify false alarms is available. The method used in this study (section 2.2.3) is based on observed events, only allowing for the assessment of already known events, not providing data for 'false alarms' or 'well forecasted non-events' in the TIGGE. This means that skill scores are not possible to use in this section. Therefore, in the absence of 'false alarms' and 'well forecasted non-events', this section focuses on the 'hits' and 'misses' of each 2008-2010 event, comparing the TIGGE to the ECMWF EPS.

Figure 5.8 shows how well the ECMWF EPS and the TIGGE forecasted the windspeeds of each of the eDMGS representing grid squares in the ECMWF analysis. Each box and whisker represents the inter-quartile range and range respectively of the ECMWF EPS and the TIGGE T+120 and T+48 hour forecasts divided by the ECMWF analysis of eDMGS representing grid squares. This means that the low numbers represent an under predicted forecast, high numbers a false alarm, with forecasted winds higher than in the ECMWF analysis and a value of 1 represents a perfect forecast, with the forecast and analysis with the same windspeed value for the grid square in question. Where the spread of the inter-quartile range and range is large, the EPS spread is

large. The TIGGE storm number refers to the number assigned to each TIGGE represented storm in Table 5.1.

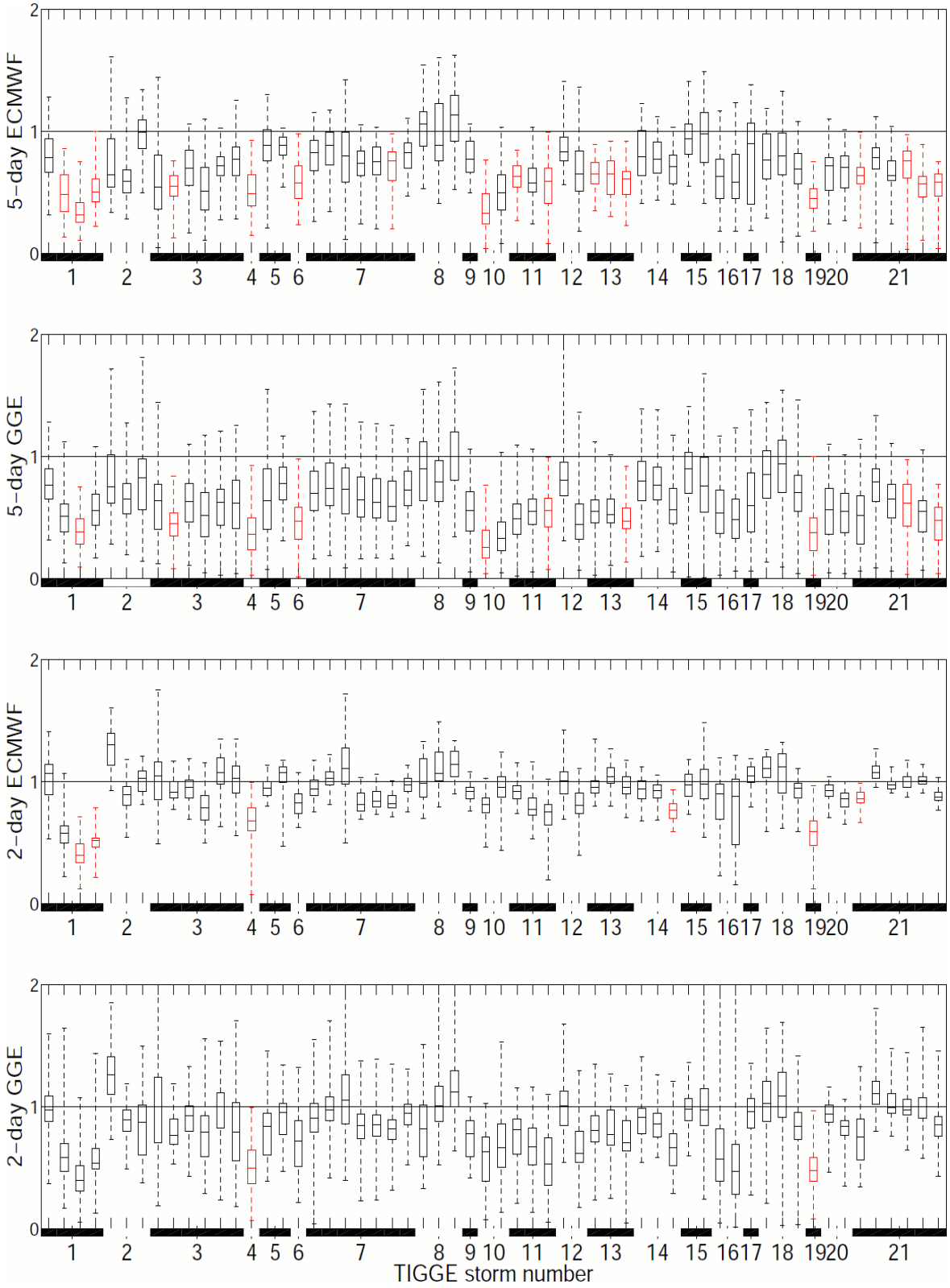


Figure 5.8 – Forecasts divided by analyses for the 58 specific eDMGS representing grid points (from Table 5.1) giving an ensemble spread for the ECMWF EPS and the TIGGE. Low numbers represent an underprediction in the forecast, 1 a perfect forecast and high numbers a false

alarm. TIGGE storm number refers to Table 5.1. Missed forecasts, by all ensemble members, (<1) are highlighted in red.

Generally, the TIGGE has a larger spread than the ECMWF EPS, which is of no surprise considering the ECMWF EPS is included in the TIGGE, and this larger spread is particularly pronounced at T+48. This is in agreement with the findings of Keller (2011) that the multi-model ensemble offers a broader range of possible development scenarios during an ETC event than the ECMWF EPS alone, which is beneficial when considering extreme events. The ECMWF EPS has no EPS member capturing the observed mean windspeed in 18 of the 58 eDMGS representing grid squares for the 120 hour forecast (highlighted red in Figure 5.8) and of these, 8 are captured by the TIGGE, leaving 10 which were not forecasted by any TIGGE model EPS member. This has improved by the 48 hour forecast with 6 of the eDMGS representing grid squares missed by the ECMWF EPS and of these, 4 are captured by the TIGGE, leaving 2 which were under-estimated by all TIGGE model EPS members. This again indicates the value of applying the TIGGE in forecasting, however Figure 5.8 does not reveal which TIGGE models were influential in the improved forecasts, this is seen for T+120 in Figure 5.9. There is one example (Antje (14)) where the observed intensity has been successfully captured within the spread of the T+120 forecasts in the ECMWF EPS, however by T+48, this is no longer the case and we have a missed forecast. This indicates that improvements in forecasts as forecast time horizon reduces are not monotonic, as also shown in the ECMWF control forecast in Figure 5.4.

Figure 5.9 displays forecast spread of the windspeeds for each of the eDMGS representing grid squares, however this time, highlighting each TIGGE centre's EPS individually and showing the absolute values (forecasts minus ECMWF analysis) of the forecasts performance at the T+120 time interval. This means that the negative numbers represent an under-predicted forecast (< 0) with forecasted winds lower than in the ECMWF analysis windspeed value for the grid square in question, positive numbers a false alarm of the severity of an event (>0) and a value of 0 represents a perfect forecast.

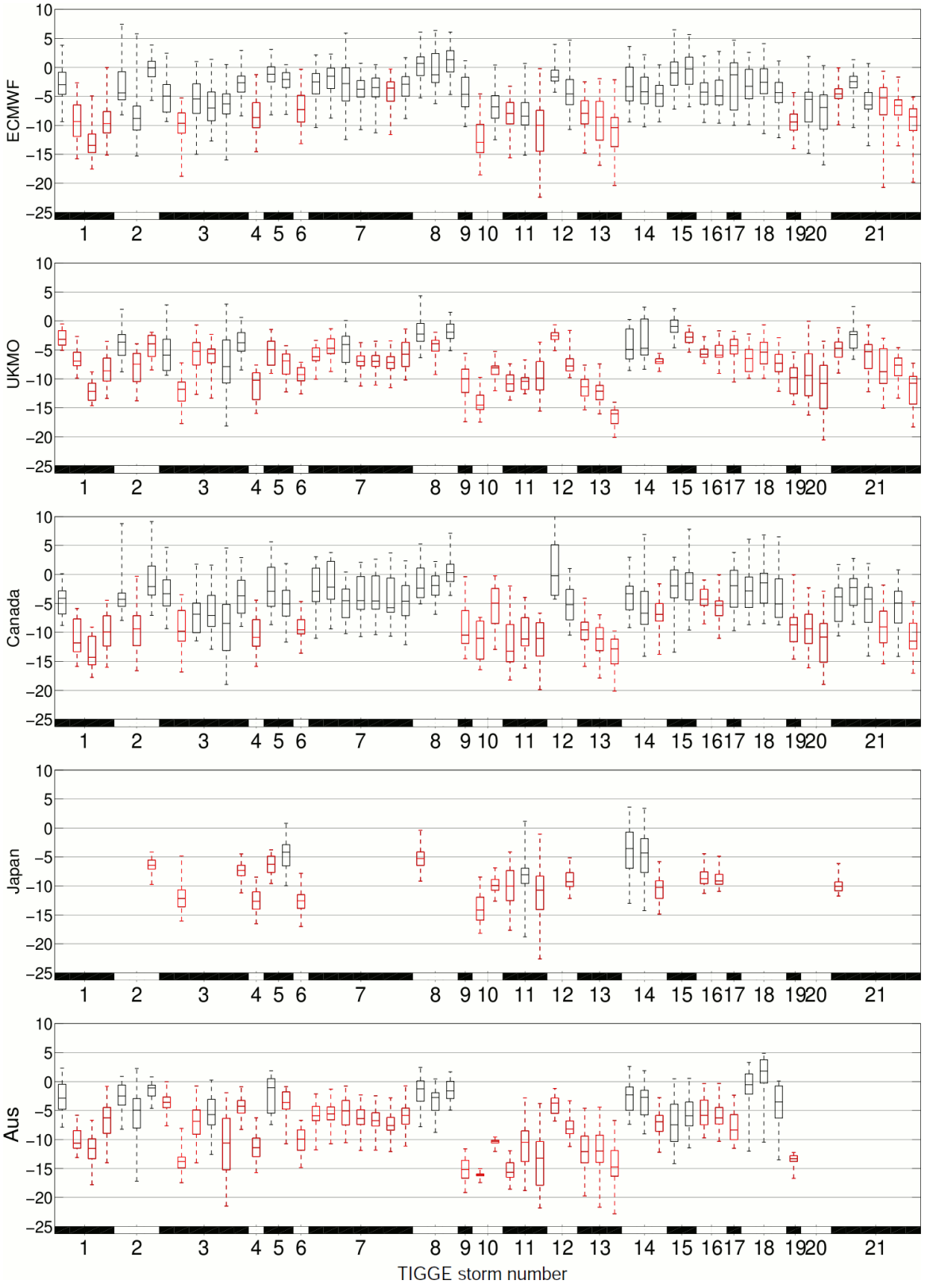
ECMWF
UKMO
Canada
Japan
Aus
10
5
0
−5
−10
−15
−20
−25
1 2 3 4 5 6 7 8 9 10 11 12 13 14 15 16 17 18 19 20 21
TIGGE storm number

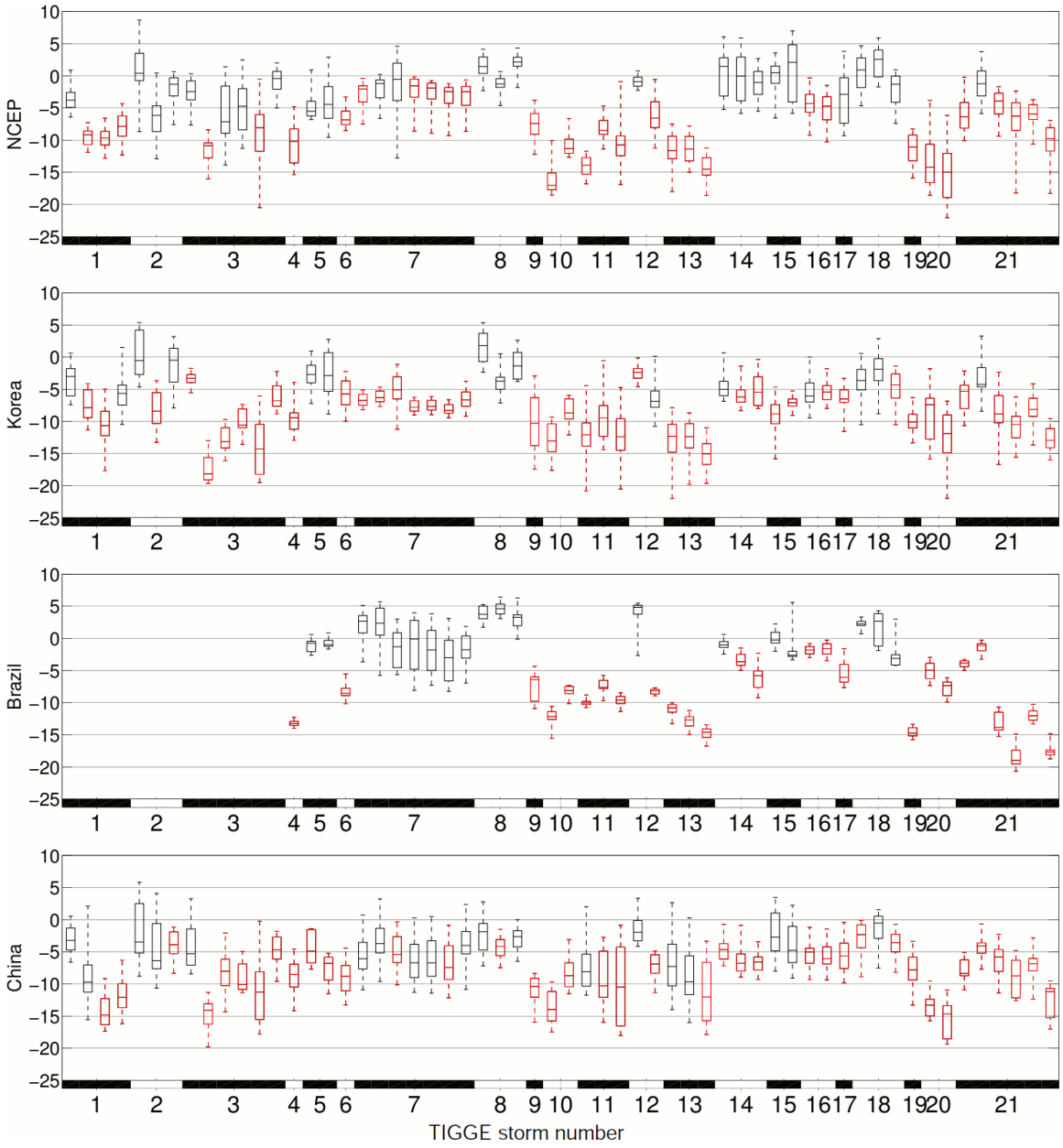


Figure 5.9 – Difference between forecasts and the analyses (forecasts minus analysis)in $ms^{-1}$ for the 58 specific eDMGS representing grid points (from Table 5.1) giving an ensemble spread for each EPS in TIGGE. Low numbers represent an underprediction in the forecast, 0 a perfect forecast and high numbers a false alarm. TIGGE storm number refers to Table 5.1. Missed forecasts, by all EPS members, (<0) are highlighted in red.

Figure 5.9 shows that the ECMWF EPS spread is relatively large and often the ensemble range captures the event, with at least one member with a positive value, however the ensemble median produces a value of up to 8 $ms^{-1}$ (TIGGE storm numbers 2 and 11) below the observed value, despite 'capturing' the event. This again raises the question about skill vs. spread of ensemble models with some meteorologists arguing that these forecast were successful as they 'raise the alarm' for a possible extreme event, however others would argue that the ensemble median

value is 8 $ms^{-1}$ too low meaning that this is an unsuccessful forecast (see Jolliffe and Stephenson, 2003). The ECMWF and Canadian models which perturb the physics schemes of their ensemble members have larger ranges, supporting Buizza et al. (1999), and therefore capture more events. However, the UKMO, which also perturbs its physics schemes, has a smaller range also seen in Figure 5.6, likely to be from the different perturbation approaches, again highlighting the importance of model physics schemes. In fact, the UKMO model captures the fewest events (with at least one member with a positive value) at T+120, just 19%, however also has the 2nd fewest (behind the ECMWF) ensemble medians underestimating the events by more than 10$ms^{-1}$, indicating that model can be argued as being the 2nd best performing.

Table 5.2 focuses on the missed forecasts of mean windspeeds by the ECMWF EPS for the particular 1˚x 1˚grid squares representing eDMGSs from Figure 5.8 and Figure 5.9, highlighting the examples that were successfully forecasted by any TIGGE member. The number of 'successful' (at least one member capturing the windspeed intensity) ensemble members is displayed, for both the total TIGGE (for that time step) and the successful EPS member's centre. Of the 8 examples, in the T+120 forecast, that were missed by all ECMWF EPS members but captured by various TIGGE members, 6 were only captured by 1 TIGGE member and 4 of these were members of China's 14 member EPS (see also Figure 5.9). This perhaps should be of no surprise when keeping Figure 5.6 in mind, showing such large spread of the ensemble members in the Chinese EPS, potentially due to the relatively low quality GSI data assimilation technique (Buizza et al., 2005). The Canadian model captured 3 of the 8 ECMWF EPS missed forecasts, including two occasions when 3 out of the 20 ensemble members made a successful forecast, which is again of no surprise considering the wide EPS member spread for RMSE evolution in Figure 5.6, however this is likely to be due to the perturbation of model physics for the different EPS members, known to widen EPS spread (Buizza et al., 1999), rather than a poor data assimilation technique as it uses the sophisticated 4D-VAR to obtain good quality initial conditions. 3 of the 14 Brazilian EPS members captured the missed forecast, 'TIGGE wind number' 23, during Windstorm Emma (TIGGE storm number 7), which may be explained by the relatively good medium range forecasts provided by Brazil (Figure 5.4 - Figure 5.6) when the lower quality NCEP initialising analysis (Buizza et al., 2005; used by Brazil's model for

initial conditions, before adding perturbations) has less influence. The Korean model also successfully forecasts a missed ECMWF EPS forecast, with 1 of the 16 EPS member predicting the magnitude of the windspeed in the relevant grid square ('TIGGE wind number' 4), during Windstorm Eliane (TIGGE storm number 1), complementing the performance seen in Figure 5.4, where this model had the lowest RMSE compared even to the ECMWF EPS, even when using the ECMWF analysis as 'truth', again confirming suggestions that models with 3D-VAR generated initial conditions can compete with 4D-VAR in parts of the world with comprehensive data coverage (Whitaker et al., 2009).

Table 5.2 shows that in the 48 hour forecast, of the 4 examples that were missed by all ECMWF EPS members but captured by various TIGGE members, 3 were captured by more than one other TIGGE centre's EPS. The unsuccessful forecast, by the ECMWF EPS, of 'TIGGE wind number' 53, during Windstorm Carmen (21), was well captured by both the Korean model, with 9 out of the 16 members reaching or exceeding the observed magnitude and 6 of the 20 Canadian members also 'successful'. 'TIGGE wind number' 41, during Windstorm Antje (14), is the only example that was forecast successfully by the ECMWF EPS at 120 hours but not at 48 hours as already mentioned, but was captured by the Canadian and NCEP models. 8 of the 20 NCEP EPS members forecasted the windspeeds strongly enough and, along with the NCEP EPS also capturing the missed forecast from Eliane (1), adds more quality to the multi-model T+48 forecast than to the T+120. This is not in line with Buizza et al's, (2005) statement that the NCEP ensemble performance is negatively affected in the short range by the relatively low quality of the ensemble of data assimilation, and is suggesting the opposite. The two of the 4 T+48 examples that were missed by all ECMWF EPS members but captured by various TIGGE members, during Eliane (1), were both captured by the Canadian EPS, with the Korean and NCEP (as just mentioned) also successfully forecasting 'TIGGE wind number' 4.

| TIGGE wind number (storm number) | Captured by ECMWF 5-day? | Captured by TIGGE 5-day? | Centres that captured | Captured by ECMWF 2-day? | Captured by TIGGE 2-day? | Centres that captured | Feature |
|---|---|---|---|---|---|---|---|
| 2 (1) | No | Yes 1/175 | China 1/14 | Yes | Yes | | Y (Potential SJ) |
| 3 (1) | No | No | | No | Yes 2/175 | Canada 2/20 | Y (Potential SJ) |
| 4 (1) | No | Yes 1/175 | Korea 1/16 | No | Yes 3/175 | Canada 1/20 Korea 1/16 NCEP 1/20 | Y(rCCB) |
| 9 (3) | No | No | | Yes | Yes | | Y(CS) |
| 14 (4) | No | No | | No | No | | Y (Potential SJ) |
| 17 (6) | No | No | | Yes | Yes | | Y (rCCB) |
| 23 (7) | No | Yes 6/189 | Brazil 3/14 Canada 3/20 | Yes | Yes | | Y (QLCS)/ Y (2nd WCB) |
| 29 (10) | No | No | | Yes | Yes | | Y (Potential SJ) |
| 31 (11) | No | Yes 1/239 | China 1/14 | Yes | Yes | | Y (CCB) |
| 33 (11) | No | No | | Yes | Yes | | Y (rCCB) |
| 36 (13) | No | Yes 1/189 | China 1/14 | Yes | Yes | | Y (rCCB) |
| 37 (13) | No | Yes 1/189 | China 1/14 | Yes | Yes | | Y(rCCB) |
| 38 (13) | No | No | | Yes | Yes | | Y (rCCB) |
| 41 (14) | Yes | Yes | | No | Yes 9/239 | Canada 1/20 NCEP 8/20 | Y (rCCB) |
| 50 (19) | No | No | | No | No | | Y (Potential SJ) |
| 53 (21) | No | Yes 3/207 | Canada 3/20 | No | Yes 15/207 | Canada 6/20 Korea 9/16 | Y (DSCS) |
| 56 (21) | No | No | | Yes | Yes | | Y (rCCB) |
| 57 (21) | No | Yes 1/157 | Canada 1/20 | Yes | Yes | | Y (rCCB) |
| 58 (21) | No | No | | Yes | Yes | | Y (rCCB) |

Table 5.2 – Missed ECMWF EPS forecasts (from Figure 5.8).Which of these examples were captured by the TIGGE in T+120 and T+48 forecasts?

This study indicates that for the T+120 forecasts, an ensemble consisting of just the ECMWF, Canadian, Chinese and Korean EPS members would capture the same eDMGS representing grid squares as the whole TIGGE, though the ensemble medians will be negatively influenced. For the T+48 forecasts, an ensemble consisting of just the ECMWF and Canadian models would suffice, indicating that there is value of using model physics perturbations for short term forecasts, despite not finding this earlier, for the Windstorm Emma example. The forecast performance of the Canadian model is consistent with the findings of Froude (2009) who concluded that this EPS performed best of all but the ECMWF EPS for intensity and the best of all for the propagation speeds of ETCs. Overall, this study shows that there is value in using the multi-model, with more EPS members producing a broader range of possible development scenarios during an ETC as Keller (2011) found, especially for medium range forecasts.

## 5.4 Sub-storm mechanism forecasts

Table 5.2 shows that the sub-storm mechanism, as seen in Figure 5.10, that associated wind speeds were the most challenging to predict by the ECMWF EPSs were the potential SJs, with all 3 examples covered by the TIGGE analysis/forecast time-steps (Table 5.1) not captured by the ECMWF EPS at T+120 and 1 in the T+48 forecast. Of the 3 missed by the ECMWF EPS in the T+120 forecast, 1 was captured by the TIGGE, a Chinese EPS model member, but the 1 missed in the T+48 forecast was not captured either by the TIGGE. This is of no surprise since TIGGE global models are working at resolutions ranging from $0.45^{o}$ to $1.5^{o}$ (~50-165 km) all interpolated onto a standard $1^{\circ}$x $1^{\circ}$ (~111 km) grid and SJs are sub-grid scale, thought to be only a few kilometres across (Browning, 2004; Clark et al., 2005). Clark et al. (2005) also found that a 90-level version of the UM (section 1.5.2) verified better, for a SJ event, than a 38-level version and the TIGGE global models range from having 19 to 62 levels (Table 2.2), generally insufficient to resolve a SJ. The fact that the only successful EPS members to forecast the $2^{nd}$ Eliane (1) potential SJ example ('TIGGE wind number' 3) were from the Canadian EPS is surprising, due to its low horizontal resolution ($1.2^{o}$) and lack of vertical levels (28), but this is not the first study to find this and Johnson et

al. (2006) suggests that perhaps the use of 4D-VAR for data assimilation compensates for this low resolution by providing a better initial state. Also, it is unlikely at such a coarse resolution that the windspeed simulated in the ECMWF analysis, correctly forecasted by the 2 Canadian EPS members, in the specific grid square (representing the observed potential SJ at Machrihanish (see Table 5.1)), is correctly simulating the SJ and is conceivably representing the larger rCCB, which typically occurs within a few kilometres of the SJ (Figure 5.10). That said, the data assimilated into the analysis may have captured the feature. This highlights the necessity for the TIGGE-LAM project (section 1.4.3) to allow comparisons with models designed to capture mesoscale features.

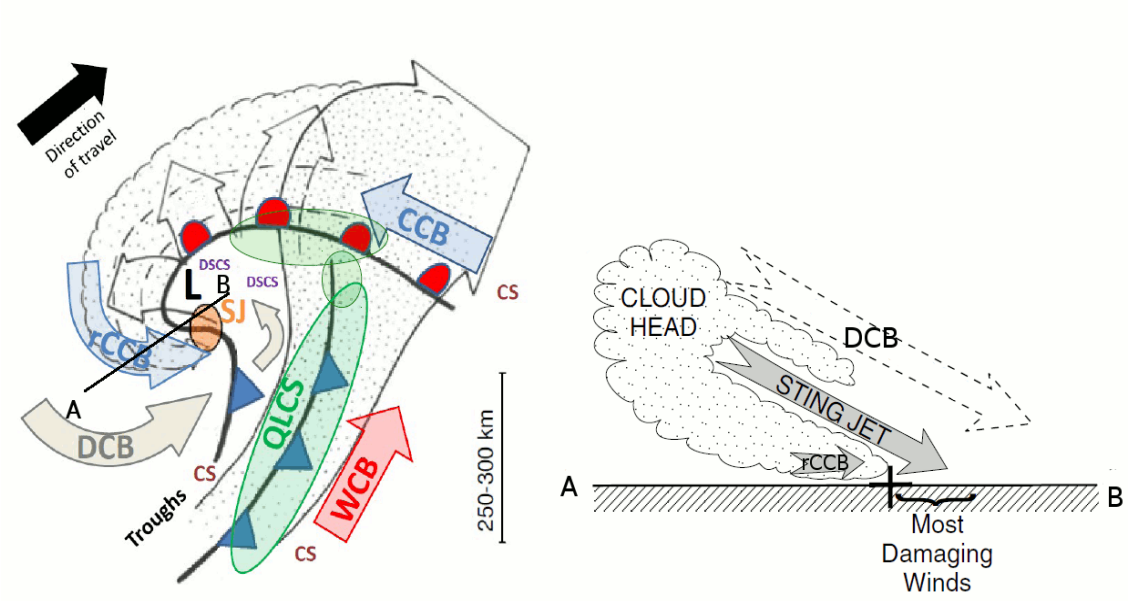


Figure 5.10 – Repeat of figure 1.5.

Table 5.2 also highlights that the other sub-storm mechanism that is prominent in the unsuccessful ECMWF EPS forecasts is the rCCB, where 11 out of the 22 represented examples (Table 5.1) are not forecast correctly at T+120 but this had fallen to 3 by T+48. This includes the ECMWF EPS forecast that was successful in the T+120 but not at T+48 ('TIGGE wind number' 41, during Windstorm Antje (14)) as mentioned earlier. It is unclear why the rCCB is so poorly forecasted by the TIGGE contributing centres at T+120, compared with the other features such as the WCB and QLCSs, though a possible explanation is that the rCCB position has much to do with the track of the ETC, whereas the WCB typically covers a wider area (section 1.3), so is less sensitive. Froude (2009) found that the centres vary greatly on the propagation speed and

position of European ETCs and that the T+48 hour prediction is markedly better in all models than the T+120, which provides an explanation of the poor 120 hour but reasonable 48 hour forecasts for rCCB. The good quality forecasts for QLCSs is somewhat surprising considering the relatively small scale of this feature, though this feature is always closely positioned to the WCB (Figure 5.10 – Repeat of figure 1.5.), so the coarse global models are not distinguishing between them; further work is needed to assess whether this is the case in this climatology by conducting and analysing higher resolution modelling as in the following section.

Another reason for the unrealistically successful forecasts is due to a limitation of the methodology used here (section 2.2.3), assuming the ECMWF analysis as 'truth' when it is unlikely all features have been correctly simulated with the associated coarse resolution, especially in small transient features such as isolated CSs. Table 5.1 showed whether each eDMGS is represented in the ECMWF analysis based on a percentage (≥70%) of the 2008-2010 maximum values (Figure 5.1) for the relevant grid points. An example of this percentage method is highlighted in Figure 5.2 where, for Windstorm Emma (7), the percentage values are shown to be high for all of the eDMGS representing grid squares, hence all being judged to be represented by the ECMWF analysis. Table 5.1 also shows that the eDMGSs seen during Windstorm Berti (16) were not represented in the associated ECMWF analysis, due to windspeeds being lower than (the subjective value of windspeeds not being represented) 70% level of the 2008-2010 maximum. This meant that the TIGGE EPSs produced good forecasts, of equal or stronger windspeeds than the analysis (Figure 5.8), providing a successful forecast compared to the ECMWF analysis, but not good in terms of being representative of the observed extreme surface windspeeds. This highlights the importance of accurate analyses to faithfully reproduce the ETC events which cause such surface extremes and which endanger lives and damage property.

## 5.5 WRF modelling

Understanding the dynamical processes within ETCs that cause the strongest and most significant surface winds, causing insured losses and endangering lives, is essential and the previous section shows that these are not always well simulated in the global forecast models. The need for a good analysis from which to compare these forecasts is crucial and in the absence of TIGGE-LAM (section 1.4.3), meteorologists in the research community are turning to running high resolution models based within their respective institutions, to conduct simulations of past events. In this section, the benefit of increasing model horizontal and vertical resolutions is assessed using the WRF modelling system, and the impact of applying two contrasting cloud microphysics schemes, proven to be important when simulating surface winds during European ETCs (Baker et al., 2012), is also determined.

### 5.5.1 Initial conditions

Two possible sources of real data to act as the initial conditions for WRF are the analyses from NCEP's Global Forecasting System (GFS) and from ECMWF operational model, as discussed in section 2.3.4. The GFS analysis was used here because GFS and WRF have been developed by the same groups, aiding their compatibility (Dudhia pers. comm. 2009).

Figure 5.11 shows the 10m windspeed data from the GFS and the ECMWF analyses for the 1$^{st}$ March 2008 00:00 UTC. Each model's attributes are described in section 2.2.1. The analyses vary considerably in places, by over 5ms$^{-1}$ for example off the coast of north-west Ireland and in the English Channel. Much of this variation is due to different interpolation methods used for the 1˚x 1˚ output, as the ECMWF model runs on a finer grid than the GFS, as well as deploying contrasting data assimilation techniques as described in section 2.2.2.

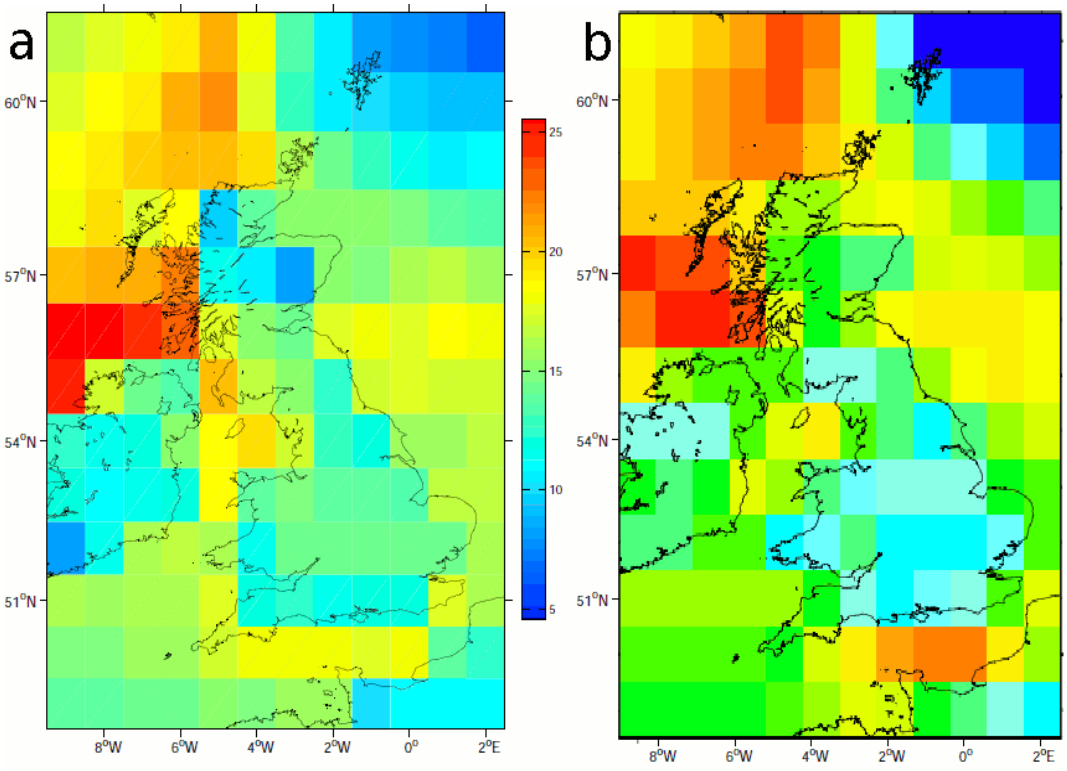


Figure 5.11 – 10m windspeed ($ms^{-1}$) in (a) ECMWF analysis (as in Figure 5.2) and (b) NCEP GFS analysis for 1st March 2008 00:00 UTC at 1˚x 1˚ resolution.

When compared to the observations in Figure 5.3, neither of the analyses agree with the values of the network observations particularly well. For example the ≥18 $ms^{-1}$ HM windspeed at Aberporth (site 13) is estimated at 9 and 15 $ms^{-1}$ by the GFS and ECMWF analyses respectively. The under-representation of this coastal site is likely to be dependent on the precise nature of the interpolation process, which itself is dependent on land/sea detail in each model, highlighting the difficulties involved in standardising different models onto a common grid point through interpolation and operating at relatively low resolution to represent areas of complex topography. Generally, the GFS estimations are on the low side for the ETC Emma analysis from the 1st March 2008 00:00 UTC, whereas the ECMWF windspeeds are too strong in many locations (as mentioned in section 5.1.1), especially in central England.

### 5.5.2 The impact of increasing resolution

NWP systems like the WRF model are increasingly being used, in the research community, to simulate European ETCs at high resolution for a variety of specific

research purposes, focusing on certain aspects of ETCs as discussed in section 1.3. It is widely shown that high resolution modelling produces more accurate simulations, not just for small scale transient features within ETCs, but for ETCs themselves (Froude, 2010). However, it can be argued that parameterisation schemes, that represent sub-grid scale physical processes that are not explicitly resolved, are the most important components of models, even more so than the highest resolutions, as explored in detail by Stensrud (2007) and as discussed in section 2.3.3.

Figure 5.12 shows the 10m windspeed output from the GFS analysis (as seen in Figure 5.11), which supplies the boundary conditions for the WRF model runs, domains 1, 2 and 3, which are also shown at increasing horizontal resolutions of 27km, 9k and 3km respectively. As the resolution increases, the windspeeds generally approach those seen in the observations (Figure 5.3), with the effects of the topography more faithfully reproduced in the high-resolution runs. For example, the Aberporth (13) observed HM windspeed of ≥ 18 $ms^{-1}$ is better represented with winds of a similar magnitude simulated off the coast of Wales. The strong 10m windspeeds associated with the rCCB of Emma, off the west coast of Scotland, vary greatly at each resolution, with the strongest winds contrasting in location, though it is not possible to verify which is most accurate, due to a lack of surface observation sites in this vicinity. The windspeed intensity increase seen between the 27km and 9km resolution, of the rCCB (off the west coast of Scotland), is consistent with literature for tropical cyclone NWP model research (Hill and Lackmann, 2009; Persing and Montgomery, 2003; Braun et al., 2006) which show better resolving of storm dynamics at higher resolution, resulting in more intense wind speeds, however this intensity increase is not maintained when moving between 9km and 3km resolutions. This is likely to be due to the WRF model not explicitly resolving the effects of convective and shallow clouds, relying on cumulus parameterisation schemes (retained for all domains here) to represent vertical fluxes due to unresolved updrafts and downdrafts and compensating motion outside the clouds (Skamarock et al., 2008) at 27km, whereas at finer resolution (domains 2 and 3), WRF can resolve these finer scale features explicitly. This leads to an improved simulation between 27km and 9km, but adding relatively less value between 9km and 3km. This indicates that for global forecasting centres, the very highest horizontal resolution is perhaps not vital for accurate

simulations of ETCs for their respective analyses for forecast comparison and that sub-10km resolution may suffice.

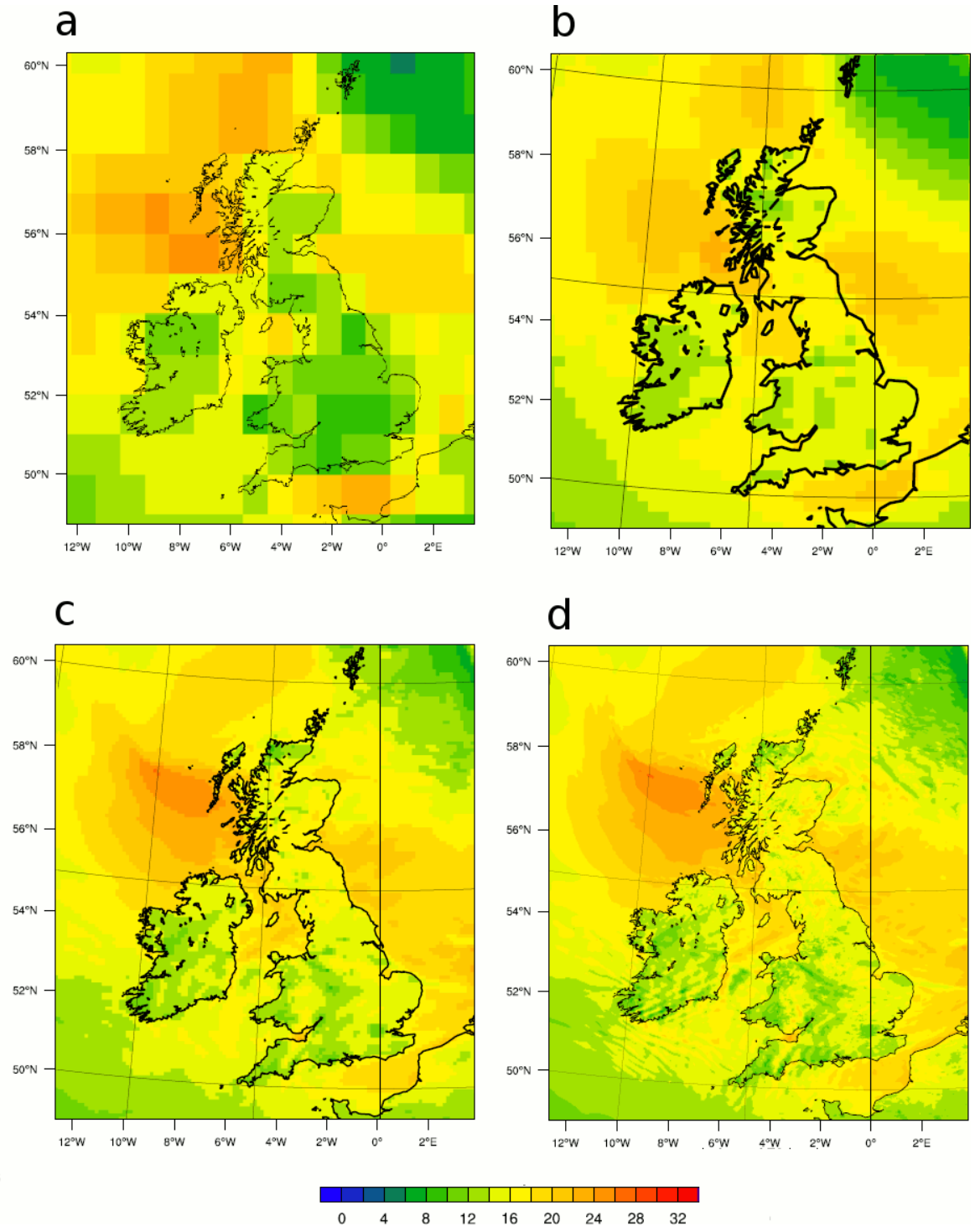


Figure 5.12 - 10m windspeed ($ms^{-1}$) for (a) NCEP GFS analysis, (b) WRF domain 1 (27km) (c) WRF domain 2 (9km) (d) WRF domain 3 (3km) for 1st March 2008 00:00 UTC (WRF run with 70 levels and WSM3 microphysics scheme).

### 5.5.3 Sensitivity of increased vertical resolution and two different microphysics schemes

Tao et al. (2011) evaluated four different cloud microphysics options in a Hurricane Katrina simulation case study and found that microphysics schemes have a major impact on wind intensity. This sensitivity was also demonstrated for European ETCs by Baker et al. (2012), as discussed in section 1.5.

Figure 5.13 shows the WRF 10m windspeed output at 3km resolution from 1st March 2008 00:00 UTC, highlighting the sensitivity to vertical resolution and choice of microphysics scheme. The WRF runs are conducted with 70 vertical levels (as used in Figure 5.12) and 105 vertical levels (extra 35 levels spaced evenly between the existing levels), while the microphysics schemes tested are the WRF Single-Moment 3-class (WSM3) and the Morrison 2-Moment, described in section 2.3.3. Figure 5.13(b) displays the difference in the 10m winds between the two vertical resolution runs (both run with microphysics scheme WSM3), indicating that WRF has generally low sensitivity to altered vertical resolutions during ETC Emma, however, there is some disagreement along the secondary cold front (see section 4.2.1 and in Figure 5.14(e)) indicating that frontal dynamics were sensitive to vertical resolution in this ETC example. Figure 5.13(e) displays the difference in the 10m winds between the two microphysics schemes, both run with 70 levels, showing that the Morrison scheme produces a larger area of rCCB associated strong surface winds (off the Western coast of Scotland) than the WSM3. This compliments the results of Baker et al. (2012) and Tao et al. (2011), who suggested that ice processes play an important role in the downward transport of momentum within the rCCB, with the Morrison scheme producing a more accurate reproduction. Figure 5.13(h) displays the difference in the 10m winds between the two microphysics schemes, both run this time with 105 levels, and again, this increase in levels made relatively little impact. However using 70 levels is perhaps too high a vertical resolution as a baseline, when other studies, namely Clark et al. (2005) and Parton et al. (2009) compare 90 levels with 38 levels in SJ sensitivity tests. This study suggests that the choice of microphysics scheme has more of an impact than the vertical resolution in the high resolution simulation of ETCs, once 70 levels have already been included.

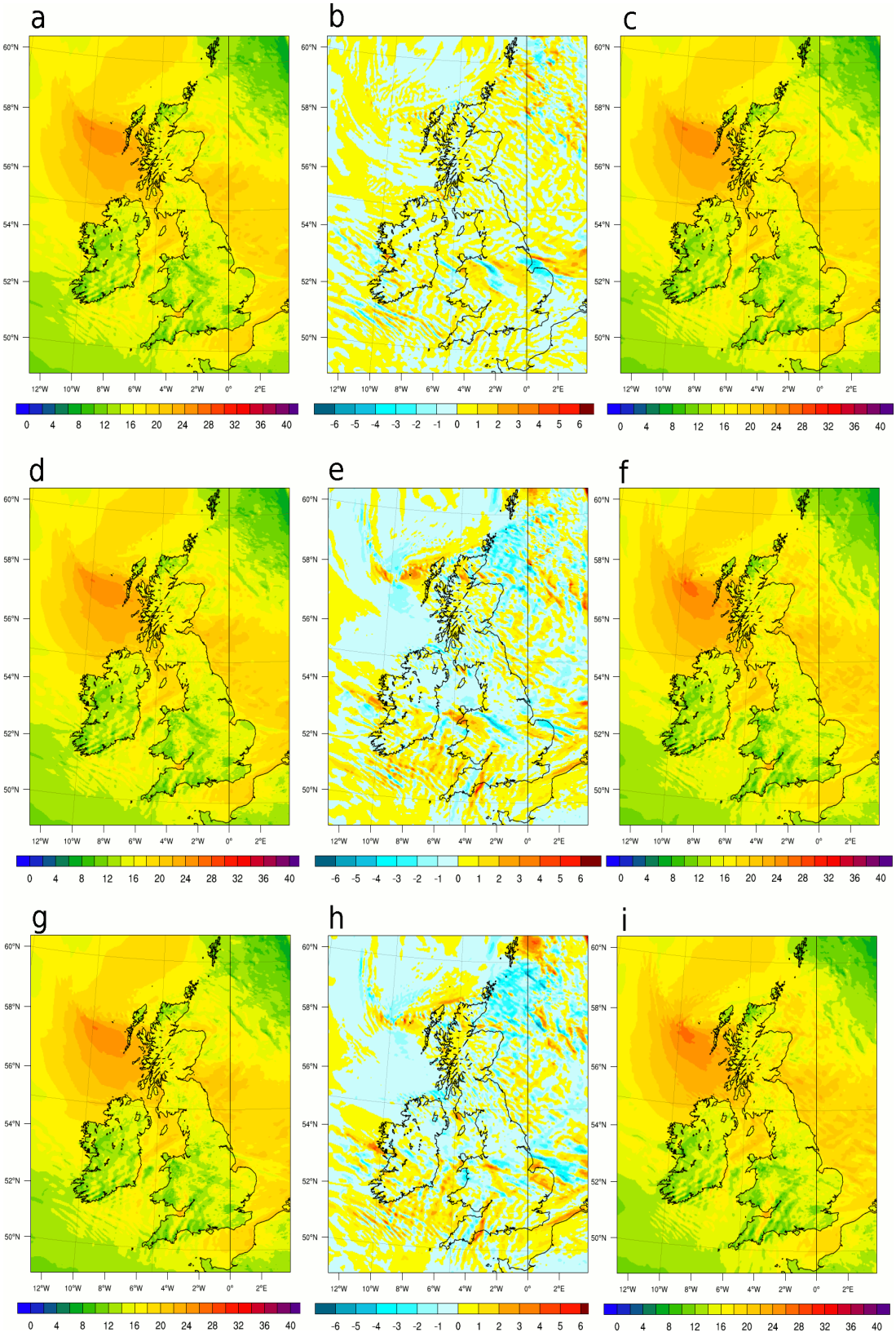


Figure 5.13 - 10m windspeed ($ms^{-1}$) for (a) and (d) WRF domain 3 run with 70 levels and WSM3 microphysics scheme, (c) and (g) WRF domain 3 run with 105 levels and WSM3 microphysics scheme, (f) WRF domain 3 run with 70 levels and Morrison microphysics scheme, (i) WRF domain 3 run with 105 levels and Morrison microphysics scheme, (b) difference between (a) and (c) (a minus c), (e) difference between (d) and (f) (d minus f) and (h) difference between (g) and (i) (g minus i) for 1st March 2008 00:00 UTC.

Figure 5.13 shows the variations in windspeed between the simulations, but it is unclear exactly what is different about the simulations to cause the distinct variations. It is known that the secondary cold front, as described in section 4.2.1 and depicted in the surface analysis chart (Figure 4.7), was responsible for numerous eDMGSs in central England (Table 4.2) during the time of these simulations and was diagnosed by Clark (2011) as a QLCS. The front is conspicuous in the Nimrod radar image (Figure 5.14(e)) with high reflectivity, indicating heavy rain, aiding an assessment of each simulation's representation of the front. Figure 5.14 demonstrates where the precipitation areas are in each of the four (the two microphysics schemes at the two vertical resolutions) simulations, representing the locations of the frontal areas, along with the radar image. Figure 5.14(a), the output from the 70 level WSM3 run, has a continuous line of reflectivity, however this is positioned further North and orientated differently than in the radar image, whereas Figure 5.14(c), the output from the 105 level WSM3 run, has a less coherent line of precipitation, though simulates the high reflectivity over Wittering (site 15) more faithfully. Figure 5.14(b), the output from the 70 level Morrison scheme run, has a less coherent but better positioned line of convection than (a), with the reflectivity band over Waddington (21) and north of East Anglia and the rain band over Wittering (15) well simulated. The 105 level Morrison scheme run (Figure 5.14(d)) is similar to the 70 level Morrison scheme run, however does not simulate the intensity of the rain bands over Waddington (21) and Wittering (15) as well. This again highlights sensitivity to microphysics schemes when simulating ETCs at high resolution, supporting the results of Baker et al. (2012) and Tao et al. (2011). The WRF run with 70 vertical levels and utilising the Morrison scheme (Figure 5.14(b)) appears to give the best representation of reflectivity and therefore frontal structure for Windstorm Emma. This is however, only one example ETC and it is an avenue for future work to run these tests on more of the identified ETC events to confirm this preliminary result.

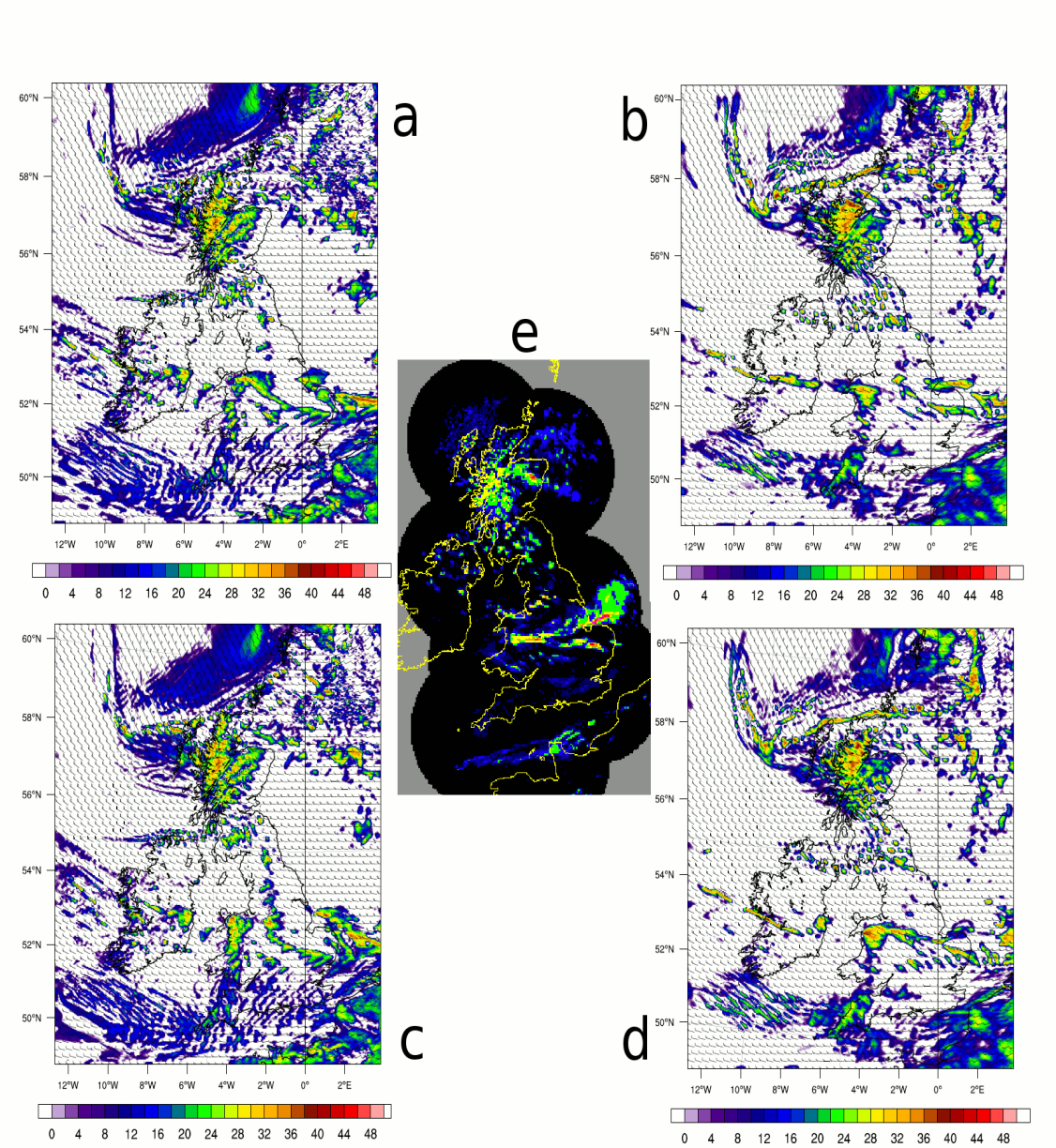


Figure 5.14 – Reflectivity in dBZ and 10m windspeed vectors for (a) WRF domain 3 run with 70 levels and WSM3 microphysics scheme, (b) WRF domain 3 run with 70 levels and Morrison microphysics scheme, (c) WRF domain 3 run with 105 levels and WSM3 microphysics scheme, (d) WRF domain 3 run with 105 levels and Morrison microphysics scheme and (e) Nimrod radar image for 1st March 2008 00:00 UTC.

So how well did the WRF 10m windspeed output compare to HM windspeeds observed at surface stations during the passage of Windstorm Emma?

Figure 5.15 displays the 10m windspeed model output from the GFS analysis and all of the WRF sensitivity runs (from nearest land based grid point to the respective sites) along with the HM windspeeds and hourly maximum 3 second gust observations at

the Leeming (28), Waddington (21) and East Malling (8) sites during the passage of Emma, from the 29th February to 1st March 2008. The respective eDMGSs, the reason for the event's inclusion in the study, are also highlighted. Each site represents different sub-grid mechanisms as the cause of the eDMGS as seen in Table 4.2, with Leeming's two eDMGSs during Emma coming courtesy of the CCB and the rCCB, while the eDMGS seen at Waddington was associated with a QLCS and that seen at East Malling was associated with the 2nd WCB.

For the CCB associated eDMGS at Leeming seen on the 29th, and related strong HM winds, all of the WRF 3km runs do a good job at simulating the strong winds, with the two lower resolution runs under-representing the magnitude. The mean winds are somewhat overestimated for the rCCB associated eDMGS on the 1st of March, by all but the domain 1 (27km) output. This is also true for the QLCS seen at Waddington late on the 29th, though the eDMGS was not reflected in the HM windspeeds for this mechanism, and the 3km 70 level WSMS scheme run produced the most accurate mean windspeed here, though this is perhaps through misrepresenting the position of the front (Figure 5.14(a)), rather than through accurate simulation. For the WCB associated eDMGS at East Malling recorded on the 1st March, all WRF simulations missed the associated strong mean windspeed. It must be taken into account however, that the model gives a snapshot on the hour, whereas the observations are recorded from 20-10 minutes prior to the hour in question along with the fact that the land based grid point nearest the observation site, especially for the coarser domains, may be many kilometres away.

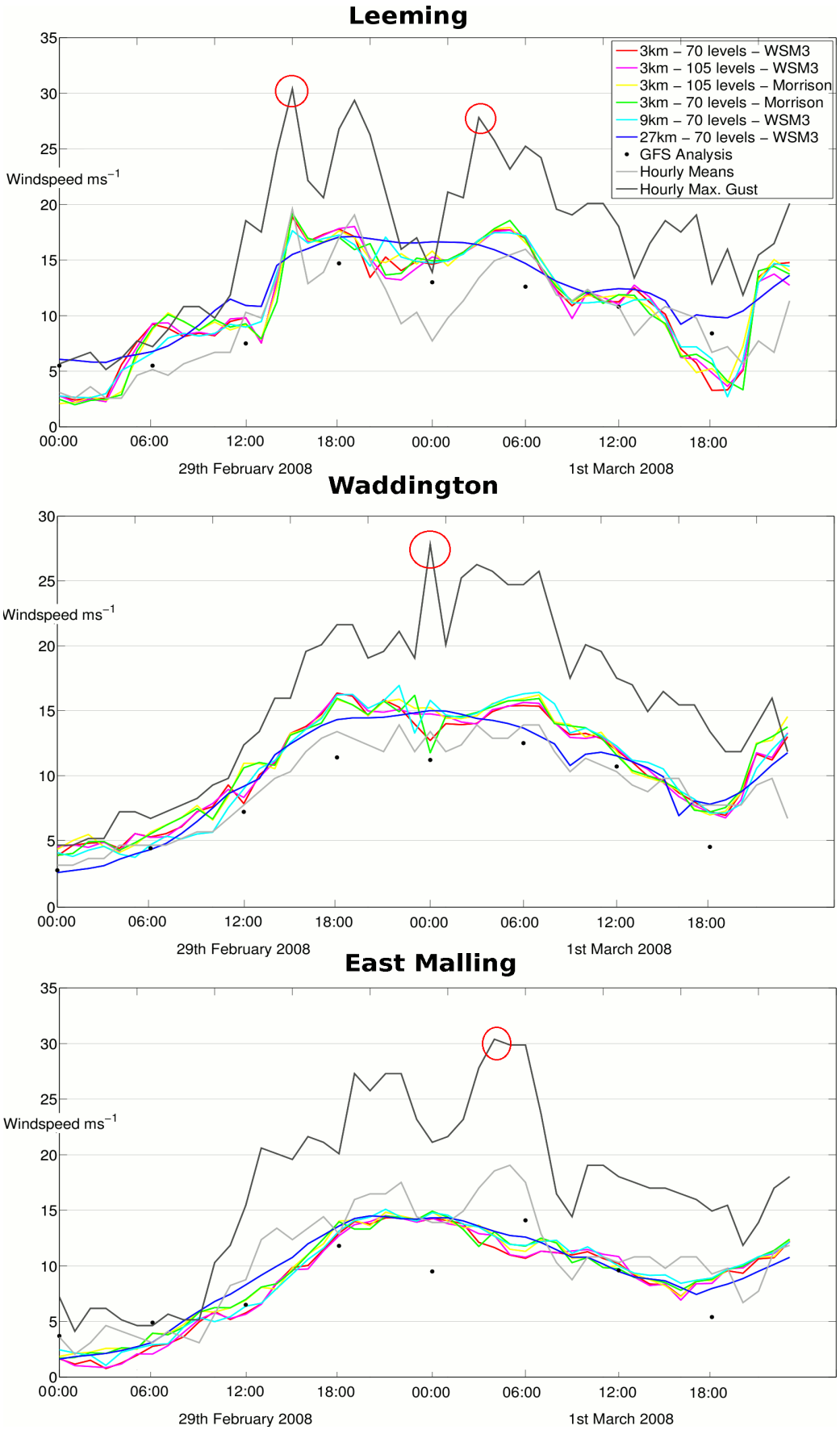


Figure 5.15 – 10m windspeed (ms$^{-1}$) at sites Leeming (28), Waddington (21) and East Malling (8), with WRF output (from nearest land based grid point) and surface HM and hourly gust observations, with the eDMGSs highlighted (red circles).

Generally the improvement of the 9km domain 2 from the 27km domain 1, especially for Leeming, is significant and any subsequent increase in resolution is relatively ineffective, even with changes in microphysics scheme. This again indicates that for global forecasting centres, the very highest horizontal resolution is perhaps not vital for accurate simulations of ETCs for their respective analyses and that sub-10km resolution may suffice, however, this is for only one ETC example. These results indicate that an avenue for future work includes the sensitivity of coarser, but still sub 10km resolution, WRF runs with numerous microphysics schemes, to assess whether these parameterisation schemes can improve ETC simulations more effectively than increasing resolution. Also, the exploration of gust options within WRF to see how well the eDMGSs are represented, not just the respective HM winds, provides another opportunity to move this work forward.

## 5.6 Summary

An assessment to whether there is any forecast value gained from using the TIGGE multi-model global ensemble compared to the solitary use of the ECMWF EPS is made in chapter 5 for the specific case of Windstorm Emma along with 20 other 2008-2010 windstorm events. The need for high-resolution modelling analysis is highlighted, expressing the need for the TIGGE-LAM project to come to fruition, and conducted here using the WRF model.

- For medium range forecasts (T+120), an ensemble consisting of just the ECMWF, Canadian, Chinese and Korean EPS members would capture (that is, at least one member forecasts a windspeed at least as high as that observed) the same set of eDMGS events as an ensemble consisting of all EPS members in TIGGE. However this would lower the ensemble mean compared to the solitary ECMWF EPS.

- In the shorter range (T+48), an ensemble consisting of just the ECMWF and Canadian models would suffice, indicating the value of using model physics perturbations for short range forecasts. These results highlight some value in

using the multi-model ensemble, with more EPS members producing a broader range of possible development scenarios during an ETC.

- The WRF surface wind simulations of ETC Emma (March 1st 2008) differ greatly in the size and position of the area of strongest surface winds between 27km and 9km horizontal resolution experiments, but not between 9km and 3km, suggesting, for this event at least, that the highest horizontal resolution is not vital to capture sufficient detail for a suitable warning system. In light of this it is interesting to note that ECMWF's plan is for increases in horizontal resolution to 10km and 20km respectively, by 2015, of their global deterministic and EPS models (Wedi et al., 2012).

- The WRF surface wind simulations for Emma display higher sensitivity to different microphysics schemes than to changes in the vertical resolution. This highlights the importance of investigating diabatic processes within extreme European ETCs, found to have a major influence on the explosive deepening of the most destructive ETC events (Fink et al., 2012).

# Chapter 6

# Conclusions and future work

## 6.1 Main findings of the project

A comprehensive assessment of the 1980-2010 UK wind regime is presented in this thesis, based on a 40-station network of 10m land-based HM windspeed and daily maximum gustspeed (DMGS) measurements first introduced by Hewston (2008) and Hewston and Dorling (2011), incorporating periods of both relatively low windspeed and times of extreme storminess. The regime is assessed in terms of long-term temporal trends, seasonality, spatial variation, distribution and extremes (Chapter 3). Also presented is a short climatology (2008-2010) of the sub-storm mechanisms related to those individual ETC events which were found to be associated with highest percentile windgusts (eDMGS) during this period (Chapter 4). This same set of ETCs then formed the basis of an assessment of forecast performance of 2-day and 5-day forecasts by global ensemble systems available through TIGGE (Chapter 5). These findings led to the selection of a particularly prominent ETC, Emma, comprising many of the sub-synoptic features of interest, to form the basis of a high-resolution model sensitivity analysis using WRF, considering the influence of horizontal and vertical resolution and of cloud microphysics scheme (Chapter 5).

The main research findings of this project, relating to the stated research aims in section 1.6, from each of the three results chapters 3-5, are as follows:

*Chapter 3*

The first set of project aims expresses the need to update the analysis of temporal and spatial wind variability in the UK, using the 1980-2005 surface station database first introduced by Hewston (2008), extending it through to the end of 2010, while also enhancing the data quality as well as adding analysis of HM windspeeds to the original DMGS focus. Output from this updated database is presented throughout the chapter,

along with data quality tests which include an assessment of the sensitivity of results to the distribution of stations in the network.

The network average annual (5-year running) HM windspeed ranges from 4.4 - 5.4ms$^{-1}$ (4.8 - 5.1 ms$^{-1}$) with the 5-year running mean windspeed peaking during the early 1980s and early 1990s and declining since. 2010, the final year in the climatology, experienced the lowest annual mean windspeed over the whole 1980-2010 period, attracting the attention of both the insurance and wind energy sectors, both highly exposed to windspeed variations. The associated HM windspeed variation leads to an annual potential power output range of -20% to +16% around the average, based on the power output curve of a state-of-the-art 100m 3.6MW turbine, highlighting the importance of storage and backup generation schemes in the future, with ever increasing reliance on wind power and other renewable energy sources.

The highest (30 and 35 ms$^{-1}$) DMGS exceedence thresholds display a marked early 1990s peak and a decline since, indicating that the decrease of extreme DMGSs highlighted by Hewston and Dorling (2011) has continued through to 2010, contributing to the reduction in UK storm-related insurance claims.

The network average 1980-2010 HM prevailing wind direction is in the south-west quadrant (40% of the time), but with significant spatial and seasonal/annual variations in the relative frequencies of all wind directions and this natural variation needs to be accounted for in wind energy assessments. The overall 40% frequency in south-west quadrant winds actually contains 51% of the overall energy in the wind, highlighting the relative vigour of winds in this quadrant. Despite this south-west wind focus, it should also be noted that there is an easterly component to the UK HM wind 38.1% of the time.

The Weibull distribution is more suited to representing HM winds rather than DMGS distributions at typical land-based sites, the former revealing site-specific shape parameter (k) values ranging from 1.4-2.1. This highlights that the common assumption of k=2 (Rayleigh distribution) is too simplistic, with associated implications for potential turbine site assessments.

*Chapter 4*

The main objective from the second set of project aims is to construct a 2008 to 2010 provisional climatology of ETC sub-storm mechanisms associated with the highest surface gusts recorded in the station database. This shows that the returning cold-conveyor belt (rCCB; described in section 1.3) accounts for more than a third (74 out of 196, 37.8%) of all eDMGSs, with the warm-conveyor belt (WCB) the second most influential (33 out of 196, 16.8%). Quasi-linear convective systems (QLCSs), account for 26 out of 196 (13.3%) of eDMGSs, with pseudo-QLCSs (not reaching the threshold criteria of Clark (2011)) a further 17 (8.7%), indicating that QLCSs are of great importance in generating extreme surface winds. The QLCS threshold criteria of Clark (2011) are shown to be too rigid for the UK, omitting some extreme gusts during pseudo-QLCSs. The criterion of Clark which prevents most of the pseudo-QLCS DMGSs from being classified as QLCSs relates to rainfall intensity: 'a continuous or near continuous line of rainfall rates ≥ 4 $mmh^{-1}$ (equivalent to 32.6 dBZ)' (Clark, 2011), which needs to be lowered to capture more of the observed surface extreme windspeeds. There are no examples of Sting Jets (SJ) in the literature between 2008 and 2010, however 3 of the 28 identified ETC strong wind events are shown to be highly likely to have contained a SJ during their development.

*Chapter 5*

A main aim of the thesis is to assess whether there is any forecast value gained from using the TIGGE multi-model global ensemble compared to the solitary use of the ECMWF EPS. For medium range forecasts (T+120), an ensemble consisting of just the ECMWF, Canadian, Chinese and Korean EPS members would capture (that is, at least one member forecasts a windspeed at least as high as that observed) the same set of eDMGS events as an ensemble consisting of all EPS members in TIGGE. In the shorter range (T+48), an ensemble consisting of just the ECMWF and Canadian models would suffice, indicating the value of using model physics perturbations for short range forecasts. These results highlight some value in using the multi-model ensemble, with more EPS members producing a broader range of possible development scenarios during an ETC.

The need for high-resolution modelling of an ETC event for sensitivity analysis is highlighted in the research aims. The WRF surface wind simulations of ETC Emma (March 1st 2008) differ greatly in the size and position of the area of strongest surface winds between 27km and 9km horizontal resolution experiments, but not between 9km and 3km, suggesting, for this event at least, that the highest horizontal resolution is perhaps not vital to capture sufficient detail for a suitable warning system. In light of this it is interesting to note that ECMWF's plan is for increases in horizontal resolution to 10km and 20km respectively, by 2015, of their global deterministic and EPS models (Wedi et al., 2012).

The WRF surface wind simulations for Emma also display higher sensitivity to different microphysics schemes than to changes in the vertical resolution. This highlights the importance of investigating diabatic processes within extreme European ETCs, found to have a major influence on the explosive deepening of the most destructive ETC events (Fink et al., 2012).

## 6.2 Recommendations for future work

This research has revealed numerous useful avenues for future related work. As an extension to the unique 40 station UK windspeed observation network (presented in chapter 3), updated and improved in this project, Irish observations could be added (given the necessary data access) improving the spatial coverage of the dataset in an area highly exposed to the strong south-westerly winds during the development and track of ETCs. This would support the solitary N. Irish station at Aldergrove (site 29). In addition, good quality (continuous and reliable) wind farm windspeed data could be used (if records date back far enough) along with buoy measurements and oil rig data. This would not only improve the spatial coverage, including off-shore locations, but provide the opportunity to investigate windspeeds at multiple vertical levels (at wind farms). However, getting access to these datasets is problematic due to the commercially sensitive nature of windspeed to the wind power industry. To further place the 1980-2010 period into longer term context, extending the observation network comparisons with the NAO, it is possible to examine long-term records of weather types or pressure triangles to analyse long-term changes in storm activity.

Cornes and Jones (2011), for example, analysed pressure triangles for the northeast Atlantic region over the period 1851–2003 and this database could be used to further strengthen our confidence in the data quality, comparing this with the 40 station UK windspeed observation network. Another way to strengthen the data quality could be to perform principal component analysis on the site's HM and DMGS data, annual/winter averages or focus on some of the extremes, to explain the variance highlighting coherent patterns and indicating anomalous sites or periods of data.

Threats going forward for the observational database include the fact that monitoring site locations are often changing and others being discontinued. For example Wick Airport was moved in 1993, which had to be proven by Hewston (2008) in the absence of available associated metadata, and the original network database sites of Coltishall, Durham and St Mawgan have been discontinued since 2005. As part of any future research, continuing to update, at least the basic version of, this unique observational database, due to its wide range of applications and the continued relevance of monitoring the UK's wind climate, is very important. For this to be possible however, the future contributors of this database must incorporate data from new observation sites.

Further work concerning the identification of ETC events and their respective sub-storm mechanisms associated with extreme surface wind events (chapter 4) would be beneficial, including an assessment of the associated classification Type, A, B or C to each event, as discussed by Dacre and Gray (2009), regarding baroclinicity/upper air forcing and western/eastern Atlantic formation area. This would enable further investigation of the types of ETCs responsible for the most extreme gusts, with the upper-level forced types B and C dominating the ETCs which affect the UK. Also, with Nimrod radar data availability, so crucial in identifying and tracking the relevant sub-storm mechanisms, dating back to 2002, there is an opportunity to extend the 3-year provisional climatology (2008-10) presented here, to a full decade long climatology. The Tornado and Storm Research Organisation (TORRO) records could also be utilised to further the understanding of sub-storm mechanisms, especially QLCSs, highlighting whether, and to what extent, the associated eDMGSs are caused by tornadic or non-tornadic mechanisms.

Another research focus going forward would be to extend the TIGGE forecast assessments, presented in chapter 5, by grouping the EPSs by data assimilation schemes or by initial perturbation methods, highlighting the relative importance of these NWP data assimilation approaches. TIGGE-LAM is still in the plans of numerous European meteorological centres as discussed in section 1.4.3, with enough instances of overlapping spatial domains to warrant a continuation of the TIGGE-LAM project. When this is up and running, related future work assessing the respective higher resolution output will be a priority. The WRF results indicate that future mesoscale modelling experimentation is essential and should include the sensitivity of coarser, but still sub-10km resolution, mesoscale model runs to choice of cloud microphysics scheme, to assess whether these parameterisation schemes can improve ETC simulations of wind fields more effectively than increasing resolution. Exploration of gust estimation options within WRF, to see how well the eDMGSs are represented, not just the respective HM winds, provides another opportunity to move this work forward.

## 6.3 The future of the UK wind regime

The recent variability in UK mean wind and gust climate, including the particularly anomalous atmospheric circulation patterns of 2010, quantified and discussed here, naturally leads to related questions about the future, both within the scientific community and from other sectors exposed to these variations, namely the insurance and wind energy sectors. These two industries are both highly exposed to wind extremes, however for opposite wind extremes. 2010 was an anomalously low wind year, a relatively bad year for wind energy production but a good year for the insurance industry in terms of reduced claims volumes. The two sectors are, however, also positively related if one considers the growing underwriting role that insurance is now playing, reducing the risk of weather-sensitive wind energy revenue streams. Since 2010, there is the perception that the 2010 experience has not been maintained, given the occurrence of some significant windstorm events such as ETC Friedhelm which affected a large area of Scotland on 8$^{th}$ December 2011. This is indeed the case for the sites of Wattisham and Wittering (not shown; updated for a

separate project) where 2011 and 2012 HM windspeed values have recovered from those of 2010. This provides further encouragement to continue to update the work presented in Chapters 3 and 4.

Numerous authors have been considering the possible impact of climate change over the 21st century on the wind climate of north-west Europe, in the context of the decadal variability seen over the last century (Brown et al., 2009; Ulbrich et al., 2009; Pryor et al., 2011). This is clearly a complex question and future climate projections have an especially large spread between models over Europe compared with other mid-latitude areas (Hawkins & Sutton 2009), highlighting Europe as being one of the hardest regions for which to predict weather and climate on all timescales (Woollings 2010; Ulbrich et al., 2009). Generally, storm location, frequency and intensity have shown considerable variability across Europe over the past century, confirmed over the last decades here in the UK by this study, making it difficult to identify clear trends, as highlighted in the recent European Environment Agency report (EEA, 2012). However, one point which models do seem to currently agree on for the future climate is an increasing frequency of intense cyclones in the region of the British Isles (Ulbrich et al., 2009) and increased winter storminess (Scaife et al., 2011). This is complemented by a recent study by Donat et al. (2011) involving 20 climate models, anticipating increased storminess over northern parts of central and Western Europe, and a decrease in extreme wind speeds in southern Europe.

Recent extreme events such as the cold European winter of 2009-10 have led to alternative causal interpretations, including an emphasis on the important role of recent declining solar output (Lockwood et al., 2010, 2011) and on internal dynamical responses to varied forcing (Jung et al., 2011). While further research seeks to improve models and reduce key uncertainties, both in the prediction of extreme event onset and of persistence, it seems wise to anticipate further significant variability in the UK wind climate and to concentrate upon building resilience to this.

# References

AEA, 2011: Evaluation of the climate risks for meeting the UK's carbon budgets. *Report for Committee on Climate Change ED56732*- 3. [Available online at http://hmccc.s3.amazonaws.com/Progress%202011/ED56732_FinalReport_FINALv2.pdf]

Atkins, N. T., and M. St. Laurent, 2009: Bow echo mesovortices. Part I: Processes that influence their damaging potential. *Mon. Weather. Rev.* 137(5), 1497-1513.

Atkinson, N., K. Harman, M. Lynn, A. Schwarz, and A. Tindal, 2006: Long-term Windspeed Trends in Northwestern Europe. Garrad Hassan. [Available online at http://w.bwea.com/pdf/28proceedings/Tindal%20paper.pdf]

Baker, L., 2009: Sting jets in severe northern European wind storms. *Weather*, 64(6), 143-148.

Baker, T., P. Knippertz, and A. Blyth, 2012: High Winds in Extratropical Storms: The Role of Microphysics. European Storms Workshop 3rd – 5th September 2012, University of Leeds, Leeds. [Available online at http://www.cgs.leeds.ac.uk/europeanstorms/]

Barriopedro, D., R. Garcia-Herrera, and R. Huth, 2008: Solar modulation of Northern Hemisphere winter blocking. *J. Geophys. Res.* 113, D14118. doi:10.1029/2008JD009789

Barriopedro, D., R. Garcia-Herrera, A. R. Lupo, and E. Hernández, 2006: A climatology of Northern Hemisphere Blocking. *J. Climate.* 19, 1042-1063.

Bechtold, P., and J. R. Bidlot, 2009: Parametrization of convective gusts. ECMWF Newsletter No. 119.

Bishop, C. H., B. J. Etherton, and S. J. Majumdar, 2001: Adaptive sampling with the ensemble transform Kalman filter. Part I: Theoretical aspects. *Mon. Weather. Rev.*, 129(3), 420-436.

Boccard, N., 2009: Capacity factor of wind power realized values vs. estimates. *Energ. Policy.* 37, 2679-2688.

Born, K., P. Ludwig, and J. G. Pinto, 2012: Wind gust estimation for Mid-European winter storms: towards a probabilistic view. *Tellus A*, 64.

Bougeault, P., Z. Toth, C. Bishop, B. Brown, D. Burridge, D. H. Chen, B. Ebert, M. Fuentes, T. M. Hamill, K. Mylne, J. Nicolau, T. Paccagnella, Y. Park, D. Parsons, B. Raoult, D. Schuster, P. Silva Dias, R. Swinbank, Y. Takeuchi, W. Tennant, L. Wilson, and S. Worley, 2010: The THORPEX interactive grand global ensemble. *Bull. Am. Meteorol. Soc.*, 91(8), 1059-1072.

Bourke, W., R. Buizza, and M. Naughton, 2004: Performance of the ECMWF and the BoM ensemble prediction systems in the Southern Hemisphere. *Mon. Weather. Rev.*, 132(10), 2338-2357.

Braun, S. A., M.T. Montgomery, and Z. X. Pu, 2006: High-resolution simulation of Hurricane Bonnie, 1998 : Part I: The organization of eyewall vertical motion. *J. ATMOS. SCI.,* 63(1):19–42,.ISSN 0022-4928.

Brayshaw, D. J., A. Troccoli, R. Fordham, and J. Methven, 2011: The impact of large scale atmospheric circulation patterns on wind power generation and its potential predictability: A case study over the UK. *Renew Energ.* 36, 2087-2096.

Brönnimann, S., O. Martius, H. von Waldow, C. Welker, J. Luterbacher, G. P. Compo, P. D Sardeshmukh and T. Usbeck, 2012: Extreme winds at northern mid-latitudes since 1871. *Meteorologische Zeitschrift*, *21*(1), 13-27.

Brown, S., P. Boorman, R. McDonald, and J. Murphy, 2009: Interpretation for use of surface windspeed projections from the 11-member Met Office Regional Climate Model ensemble. UKCP09 Tech. Note. 22 pp.

Browning, K. A., 1990: Organization of clouds and precipitation in extratropical cyclones. *Extratropical Cyclones: The Erik Palmén Memorial Volume*, 129-153.

Browning, K. A., 2004: The sting at the end of the tail: Damaging winds associated with extratropical cyclones. *Q. J. Roy. Meteor. Soc.*, 130,597, 375-399.

Buizza, R., P. L. Houtekamer, G. Pellerin, Z. Toth, Y. Zhu, and M. Wei, 2005: A comparison of the ECMWF, MSC, and NCEP global ensemble prediction systems. *Mon. Weather. Rev.*, 133(5), 1076-1097.

Buizza, R., M. Milleer, and T. N. Palmer, 1999: Stochastic representation of model uncertainties in the ECMWF ensemble prediction system. *Q. J. Roy. Meteor. Soc.*, 125(560), 2887-2908.

Carlson, T. N., 1980: Airflow Through Midlatitude Cyclones and the Comma Cloud Pattern. *Mon. Wea. Rev.*, 108, 1498–1509.

Cattiaux, J., R. Vautard, C. Cassou, P. Yiou, V. Masson-Delmotte, and F. Codron, 2010: Winter 2010 in Europe: A cold extreme in a warming climate. *Geophys. Res. Lett.* 37, L20704. doi:10.1029/2010GL044613

Celik, A. N., 2004: A statistical analysis of wind power density based on the Weibull and Rayleigh models at the southern region of Turkey. *Renew Energ,* 29 593–604.

Cheng, X., S. Xie, H. Tokinaga, and Y. Du, 2011: Interannual variability of high-wind occurrence over the North Atlantic. *J. Climate.* doi: 10.1175/2011JCLI4147.1.

Clark, M., 2011: A provisional climatology of cool-season quasi-linear convective systems in the UK. 6th European Conference on Severe Storms (ECSS 2011) 3 - 7 October 2011, Palma de Mallorca, Balearic Islands, Spain.[Available online at https://www.essl.org/ECSS/2011/programme/abstracts/88.pdf]

Clark, P. A., K. A. Browning, and C. Wang, 2005: The sting at the end of the tail: Model diagnostics of fine-scale three-dimensional structure of the cloud head. *Q. J. Roy. Meteor. Soc.*, *131*(610), 2263-2292.

Compo, G. P., J. S. Whitaker, P. D. Sardeshmukh, Matsui, N., Allan, R. J., Yin, X., B.E. Gleason, Jr., R. S. Vose, G. Rutledge, P. Bessemoulin, S. Bronnimann, M. Brunet, R. I. Crouthamel, A. N. Grant, P. Y. Groisman, P. D. Jones, M. C. Kruk, A. C. Kruger,G. J. Marshall, M. Maugeri, H. Y. Mok, Ø. Nordli, T. F. Ross, R. M. Trigo, X. L. Wang, S. D. Woodruff, and Worley, S. J., 2011 : The twentieth century reanalysis project. *Q. J. Roy. Meteor. Soc*, 137(654), 1-28.

Cornes, R. C., P. D. Jones, 2011: Am examination of storm activity in the northeast Atlantic region over the 1851-2003 period using the EMULATE gridded MSLP data series. *J. Geophys. Res*. 116, D16110, doi:10.1029/2011JD016007.

Cornes, R. C., P. D. Jones, K. R. Briffa, and T.J. Osborn, 2013: Estimates of the North Atlantic Oscillation back to 1692 using a Paris–London westerly index. *Int. J. Climatol*., 33(1), 228-248.

Cotton, W. R., and R. A. Anthes, 1989: Storm and Cloud Dynamics. International Geophysics Series, Vol. 44, Academic Press, 883pp.

Courtier, P., E. Andersson, W. Heckley, D. Vasiljevic, M. Hamrud, A. Hollingsworth, F. Rabier, M. Fisher, and J. Pailleux, 1998: The ECMWF implementation of three-dimensional variational assimilation (3D-Var) : I: Formulation. Buizza, R., M. Milleer, and T. N. Palmer, 1999: Stochastic representation of model uncertainties in the ECMWF ensemble prediction system. *Q. J. Roy. Meteor. Soc.*, 124(550), 1783-1807.

Dacre, H. F., and S. L. Gray, 2009: The Spatial Distribution and Evolution Characteristics of North Atlantic Cyclones. *Mon. Weather. Rev*. 137, 99-115.

Dacre, H. F., M. K. Hawcroft, M. A. Stringer, K. I. Hodges., 2012: An Extratropical Cyclone Atlas: A Tool for Illustrating Cyclone Structure and Evolution Characteristics. *Bull. Am. Meteorol. Soc.*, 93:10, 1497-1502.

Davies, T., M. J. P. Cullen, A. J. Malcolm, M. H. Mawson, A. Staniforth, A. A. White, and N. Wood, 2005: A new dynamical core for the Met Office's global and regional modelling of the atmosphere. *Q. J. Roy. Meteorol. Soc.*, 131(608), 1759-1782.

Davis, C., N. Atkins, D. Bartels, L. Bosart, M. Coniglio, G. Bryan, W. Cotton, D. Dowell, B. Jewett, R. Johns, D. Jorgensen, J. Knievel, K. Knupp, W. Lee, G. Mcfarquhar, J. Moore, R. Przybylinski, R. Rauber, Br. Smull, R. Trapp, S. Trier, R. Wakimoto, M.

Weisman and Ziegler, C., 2004: The Bow Echo and MCV Experiment. *Bull. Amer. Meteor. Soc*, 85, 1075-1093.

Dee, D. P., S. M. Uppala, A. J. Simmons, P. Berrisford, P. Poli, S. Kobayashi, S., U. Andrae, M. A. Balmaseda, G. Balsamo, P. Bauer, P. Bechtold, A. C. M. Beljaars, , L. van de Berg, J. Bidlot, N. Bormann, C. Delsol, R Dragani, M. Fuentes, A. J. Geer, L. Haimberger, S. B. Healy, H. Hersbach, E. V. Hólm, L. Isaksen, P. Kållberg, M. Köhler, M. Matricardi, A. P. McNally, B. M. Monge-Sanz, J. J. Morcrette, B. K. Park, C. Peubey, P. de Rosnay, C. Tavolato, C., J. N. Thépaut, and Vitart, F., 2011: The ERA-Interim reanalysis: Configuration and performance of the data assimilation system. *Q. J. Roy. Meteor. Soc*., 137(656), 553-597.

Donat, M. G., G. C. Leckebusch, S. Wild, and U. Ulbrich, 2011: Future changes in European winter storm losses and extreme wind speeds inferred from GCM and RCM multi-model simulations. *Natural Hazards and Earth System Sciences*, 11, 1351-1370.
Dotzek, N., and C. Forster, 2011: Quantitative comparison of METEOSAT thunderstorm detection and nowcasting with in situ reports in the European Severe Weather Database (ESWD), *Atmos. Res*., 100, 511-522, doi:10.1016/j.atmosres.2010.12.013.

Earl, N., S. Dorling, R. Hewston, and R. von Glasow, 2013: 1980-2010 variability in UK surface wind climate. *J. Clim*. 26: 1172–1191. DOI:10.1175/JCLI-D-12-00026.1.

Eckhardt, S., A., Stohl, H. Wernli, P. James, C. Forster, and N. Spichtinger, 2004: A 15-year climatology of warm conveyor belts. *J Climate*, 17(1), 218-237

EEA, 2012: European Environment Agency (EEA) report - Climate change, impacts and vulnerability in Europe 2012. [Available online at: http://www.eea.europa.eu/publications/climate-impacts-and-vulnerability-2012]

EQECAT, 2009) [online]. [Available online at: http://www.eqecat.com/resources/ExtraTropicalStormKlaus.pdf] ]

Fink, A. H., S. Pohle, J. G. Pinto, and P. Knippertz, 2012. Diagnosing the influence of diabatic processes on the explosive deepening of extratropical cyclones. Geophys. Res. Lett. 39(7).

Frank, H.P., and D. Majewski, 2006: Hindcasts of historic storms with the DWD models GME, LMQ and LMK using ERA-40 reanalyses. – Newsletter 109, ECMWF, Reading.

Froude, L. S. R., 2010: TIGGE: Comparison of the prediction of Northern Hemisphere extratropical cyclones by different ensemble prediction systems. *Wea. Forecasting*, 25, 819–836.

Galvin, J., and S. Willington, 2011: From Observations to Forecasts–Part 10: Conceptual models of mid-latitude weather systems and the interpretation of synoptic charts. *Weather*, 66(8), 204-213.

Gatzen, C., T. Púčik, and D, Ryva, 2011: Two cold-season derechoes in Europe. *Atmos. Res.,* 100(4), 740-748.

Gray, S. L., O. Martínez-Alvarado, L. H. Baker, and P. A. Clark, 2011: Conditional symmetric instability in sting-jet storms. *Quart. J. Roy. Meteor. Soc*, 137(659), 1482-1500.

Gronas, S., 1995: The seclusion intensification of the New Year's day storm 1992. *Tellus* 47A, 733–746.

Guy Carpenter, 2009 [online]. [Available online at: http://www.guycarp.com/portalapp/publicsite/catdocument.pdf?instratreportid=1788]

Harrison, G., L. C. Cradden, and J. P. Chick, 2008: Preliminary assessment of climate change impacts on the UK onshore wind energy resource. *Energ. Source.* 30 (14), 1286-1299.

Hawkins, E., and R. Sutton, 2009: The potential to narrow uncertainty in regional climate predictions. *Bull. Am. Meteor. Soc*. 90, 1095-1107. doi:10.1075/2009BAMS2607.1

Henry, A. J. 1922: J. Bjerknes and H. Solberq on the life cycle of cyclones and the polar front theory of atmospheric circulation. *Mon. Weather. Rev*, 50, 468.

Hess, P., and H. Brezowsky, 1952: Katalog der Grosswetterlagen Europas. Ber Dt Wetterdienstes in der US-Zone, Nr 33; 39 pp.

Hewston, R., 2008: Weather, Climate and the Insurance Sector. PhD Thesis. University of East Anglia.

Hewston, R., and S. R. Dorling, 2011: An analysis of observed maximum wind gusts in the UK. *J. Wind. Eng. Ind. Aerod*. 99, 845-856. doi:10.1016/j.jweia.2011.06.004

Hill, K. A., and G. M. Lackmann, 2009: Analysis of Idealized Tropical Cyclone Simulations Using the Weather Research and Forecasting Model: Sensitivity to Turbulence Parameterization and Grid Spacing. *Mon. Weather. Rev.* 137(2):745–765, ISSN 0027-0644. doi:10.1175/2008MWR2220.1.

Hong, S. Y., Dudhia, J., and Chen, S. H. 2004: A revised approach to ice microphysical processes for ;the bulk parameterization of clouds and precipitation. *Mon. Weather. Rev.* 132(1), 103-120.

Hong, S. Y. ,2008: Quantitative precipitation forecast experiments of heavy rainfall over Jeju Island on 14-16 September 2007 using the WRF model. *Asia-Pacific Journal Of Atmospheric Sciences*, 45(1):71–89, FEB 2009. ISSN 1976-7633.

Houtekamer, P. L., and L. Lefaivre, 1997: Using ensemble forecasts for model validation. *Mon. Weather. Rev.*, 125(10), 2416-2426.

Hurrell, J. W., Y. Kushnir, G. Ottersen, and M. Visbeck, 2003: *The North Atlantic Oscillation: Climate Significance and Environmental Impact*. Amer. Geophys. Union. 279 pp.

Ide, K., P. Countier, M. Ghil, and A. C. Lorenc, 1997: Unified notation for data assimilation: operational, sequential and variational. J. Meteorol. Soc. Japan, 75, 181–189.

Inness, P. M. and S. Dorling, 2012: Operational Weather Forecasting. Wiley-Blackwell. 89pp.

Irwin, J. S., 1979: A theoretical variation of the wind profile power-law exponent as a function of surface roughness and stability. *Atmos. Environ*. 13, 191–194.

Jacobson, M., 2005: Fundamentals of Atmospheric Modeling (2nd ed.) New York: Cambridge University Press. 828pp.

James, P. M., 2007: An objective classification method for Hess and Brezowsky Grosswetterlagen over Europe. *Theor. Appl. Climatol.* 88(1), 17-42.

Jamil, M., S. Parsa, and M. Majidi, 1995: Wind power statistics and evaluation of wind energy density. *Renew. Energ.* 6(5), 623–8.

Janjic, Z., T. Black, M. Pyle, B. Ferrier, H. Chuang, D. Jovic, R. Rozumalski, J. Michalakes, D. Gill, J. Dudhia, M. Duda, M. Demirtas, L. Nance, J. Wolff, L. Bernardet, P. McCaslin, and M. Stoelinga, 2009: User's guide for the nmm core of the weather research and forecast (wrf) modeling system version 3. WRF-NMM V3: User's Guide. 173pp.

Jenkinson, A. F., and F. P. Collison, 1977: An initial climatology of gales over the North Sea. Tech. report. *Synoptic Climatology Branch Memorandum No. 62*, Meteorological Office

Johnson, C., and R. Swinbank, 2009: Medium-range multimodel ensemble combination and calibration. *Quart. J. Roy. Meteor. Soc*., 135A, 777–794, doi:10.1002/qj.383.

Johnson, C., B. J. Hoskins, N. K. Nichols, and S. P. Ballard, 2006: A singular vector perspective of 4DVAR: The spatial structure and evolution of baroclinic weather systems. *Mon. Weather. Rev.*, 134(11), 3436-3455.

Jolliffe, I. T., and D. B. Stephenson, (eds.) 2003: Forecast Verification: A Practicioner's Guide in Atmospheric Science, Chichester, U.K.: Wiley.

Jones, P. D., M. Hulme, and K. R. Briffa, 1993: A comparison of Lamb circulation types with an objective classification scheme. *Int. J. Climatol*. 13, 655-663.

Jones, P. D., T. Jonsson, and D. Wheeler, 1997: Extension to the North Atlantic Oscillation using early instrumental pressure observations from Gibraltar and South-West Iceland. Int. J. Climatol. 17, 1433-1450.

Jones, P.D., C. Harpham, and K. R. Briffa, 2013: Lamb weather types derived from Reanalysis products. *Int. J. Climatol*. 33, 1129-1139. DOI: 10.1002/joc.3498

Jung, T., F. Vitart, L. Ferranti, and J. Morcrette, 2011: Origin and predictability of the extreme negative and NAO winter of 2009/10. Geophys. Res. Lett. 38, L07701. doi:10.1029/2011GL046786.

Jung, T., E. Klinker, and S. Uppala, 2005: Reanalysis and reforecast of three major European storms of the twentieth century using the ECMWF forecasting system. Part II: Ensemble forecasts. *Meteor. Appl*., 12, 111–122.

Justus, C. G., W. R. Hargraves, and A. Yalcin, 1976: Nationwide assessment of potential output from wind powered generators. *J. Appl. Meteorol.* 15, 673-678.

Keller, J. H., S. C. Jones, J. L. Evans, and P. A. Harr, 2011: Characteristics of the TIGGE multimodel ensemble prediction system in representing forecast variability associated with extratropical transition. *Geophys. Res. Lett.*, 38(12), L12802.

Klawa, M., U. Ulbrich, 2003: A model for the estimation of storm losses and the identification of severewinter storms in Germany. Nat. Hazards Earth Syst. Sci. 3, 725-732.

Knippertz, P., A. H. Fink, S. Pohle, J. G. Pinto, T. Trzeciak, and J. Owen, 2012: Diagnosing the Influence of Diabatic Processes on the Explosive Deepening of Extratropical Cyclones over the North Atlantic Ocean. European Storms Workshop 3rd – 5th September 2012, University of Leeds, Leeds. [Available online at http://www.cgs.leeds.ac.uk/europeanstorms/]

Kremer, E., 1998: Largest claims reinsurance premiums for the Weibull model. *Blätter der deutschen Gesellschaft für Versicherungsmathematik.* 279–284.

Kruschke, T., P. Lorenz, R. Osinski, G. C. Leckebusch, U. Ulbrich, T. Hofherr, P. Miesen, E. Bedacht, E. Faust, 2012: High resolution footprints of European winter storms derived through dynamical and statistical downscaling. European Storms Workshop 3rd – 5th September 2012, University of Leeds, Leeds.
[Available online at http://www.cgs.leeds.ac.uk/europeanstorms/]

Lockwood, M., R. G. Harrison, T. Woolings, and S. K. Solanki, 2010: Are cold winters in Europe associated with low solar activity? *Environ. Res. Lett*. 5(2). doi:10.1088/1748-9326/5/2/024001

Lockwood, M., R. G. Harrison, M. J. Owens, L. Barnard, T. Woollings, and F. Steinhilber, 2011: The solar influence on the probability of relatively cold UK winters in the future. *Environ. Res*. *Lett*. 6(3). doi:10.1088/1748-9326/6/3/034004

Malmquist, D. L., Ed., 1999: European windstorms and the North Atlantic Oscillation: Impacts, characteristics, and predictability. Vol. 1. Bermuda Biological Station for Research, Risk Prediction Initiative, No. 2, 21 pp

Martínez-Alvarado, O., F. Weidle, and S. L. Gray, 2010: Sting jets in simulations of a real cyclone by two mesoscale models. *Mon. Weather Rev.*, 138(11), 4054-4075.

Martínez-Alvarado, O., J. Chagnon, S. L. Gray, R. Plant, J. Methven, H. Joos, M. Bötcher, and H. Wernli, 2012(a): Diabatic processes and the structure of the warm conveyor belt. European Storms Workshop 3rd – 5th September 2012, University of Leeds, Leeds.
[Available online at http://www.cgs.leeds.ac.uk/europeanstorms/]

Martínez-Alvarado, O., S. L., Gray, J. L. Catto and P. A. Clark, 2012(b): Sting jets in intense winter North-Atlantic windstorms. *Environ. Res. Lett*. 7 024014

Matsueda, M., 2009: Blocking predictability in operational mediumrange ensemble forecasts. *SOLA*, 5, 113–116, doi:10.2151/sola.2009–029.

Matsueda, M., and H. Endo, 2011: Verification of medium-range MJO forecasts with TIGGE. Geophy Res Lett, 38(11), L11801.

Matthews, A. J., B. J. Hoskins, and M. Masutani, 2004. The global response to tropical heating in the Madden–Julian oscillation during the northern winter. *Q. J. Roy. Meteor. Soc*., 130(601), 1991-2011.

McCallum, E., 1990: The Burns' day storm, 25 January 1990. *Weather* 45, 166–173.

Michalakes, J., J. Dudhia, S. Chen, L. Hart, J. Klemp, J. Middlecoff, and W. Skamarock, 2001: Development of a next generation regional weather research and forecast model developments in teracomputing: Proceedings of the ninth ecmwf workshop on the use of high performance computing in meteorology. World Scientific, pages 269–276.

Miglietta, M. M., and A. Regano, 2008: An observational and numerical study of a flash-flood event over south-eastern Italy. *Nat. Hazards. Earth. Syst. Sci*, 8(6), 1417-1430.

Molteni, F., R. Buizza, T. N. Palmer, and T. Petroliagis, 1996: The ECMWF ensemble prediction system: Methodology and validation. *Q. J. Roy. Meteor. Soc*, 122(529), 73-119.

Morrison, H., J. A. Curry, and V. I. Khvorostyanov, 2005: A new double-moment microphysics parameterization for application in cloud and climate models, Part I: Description. *J. Atmos. Sci.,* 62*,* 1665–1677.

Morrison, H., G. Thompson, and V. Tatarskii, 2009: Impact of cloud microphysics on the development of trailing stratiform precipitation in a simulated squall line: Comparison of one-and two-moment schemes. *Mon. Weather Rev.*, 137(3), 991-1007.

Motta, M., R. J. Barthelmie, and P. Vølund, 2005: The influence of nonlogarithmic wind speed profiles on potential power output at Danish offshore sites. *Wind Energ*, 8, 219−236.

Mullen, S. L., and R. Buizza, 2001: Quantitative precipitation forecasts over the United States by the ECMWF ensemble prediction system. *Mon. Weather Rev.*, 129(4), 638-663.

Munich Re, 1999: Topics 2000: Natural Catastrophes – the current position. Munich Reinsurance Company, Munich.

Munich Re, 2002: Winter Storms in Europe (II) - Analysis of 1999 Losses and Loss Potentials. Munich Reinsurance Company, Munich.

Mureau, R., F. Molteni, T. N. Palmer, 1993: Ensemble prediction using dynamically-conditioned perturbations. *Q. J. Roy. Meteor. Soc.*, 119: 299–323.

Nolan, D. S., J. A. Zhang, and D. P. Stern, 2009: Evaluation of planetary boundary layer parameterizations in tropical cyclones by comparison of in situ observations and high-resolution simulations of Hurricane Isabel, 2003: Part I: Initialization, maximum winds, and the outer-core boundary layer. *Mon. Weather. Rev*., 137(11), 3651-3674.

Odell, L., P. Knippertz, S. Pickering and B. Parkes, 2012: The deepest extra-tropical cyclone ever recorded: The role of diabatic heating and of Greenland's topography European Storms Workshop 3rd – 5th September 2012, University of Leeds, Leeds. [Available online at http://www.cgs.leeds.ac.uk/europeanstorms/]

Osborn, T. J., 2011: Winter 2009/2010 temperatures and a record-breaking North Atlantic Oscillation index. *Weather.* 66, 19-21.

Oswald, J., M. Raine, A. Ashraf-Ball, 2008: Will British weather provide reliable electricity? *Energ. Policy*. 36, 3212–3225.

Pappenberger, F., J. Bartholmes, J. Thielen,H. L. Cloke, R.Buizza, and A. de Roo, 2008: New dimensions in early flood warning across the globe using grand-ensemble weather predictions. *Geophys. Res. Lett.*, 35, L10404, doi:10.1029/2008GL033837.

Park, Y., R. Buizza, and M. Leutbecher, 2008: TIGGE: Preliminary results on comparing and combining ensembles. Quart. J. Roy. Meteor. Soc., 134, 2029–2050, doi:10.1002/qj.334.

Parton, G. A., G. Vaughan, E. G. Norton, K. A. Browning, and P. A. Clark, 2009: Wind profiler observations of a sting jet. Quart. J. Roy. Meteor. Soc, 135(640), 663-680.

Parton, G. A.,A. Dore, and G. Vaughan, 2010: A climatology of midtropospheric mesoscale strong wind events as observed by the MST radar, Aberystwyth. *Meteor. Appl*., 17, 340–354,doi:10.1002/met.203.

Pattanayak, S., and U. C. Mohanty, 2008: A comparative study on performance of MM5 and WRF models in simulation of tropical cyclones over Indian seas. *Current Science*, 95(7), 923-936.

Pattanaik, D. R., and Y. V. Rama Rao, 2009: Track prediction of very severe cyclone 'Nargis' using high resolution weather research forecasting (WRF) model. *Journal of earth system science*, 118(4), 309-329.

Persing, J., and M. T. Montgomery, 2003: Hurricane superintensity. *J. Atmos. Sci.* 60(19), 2349-2371.

Petersen, E. L., N. J. Mortensen, L. Landberg, J. Hojstrup, and P. F. Helmut, 1998: Wind power meteorology, Part I: climate and turbulence. *Wind Energy.* 1, 25–45.

Pinto, J., 2012: Clustering of windstorms: dynamical background, diagnostic studies and associated impacts. European Storms Workshop 3rd – 5th September 2012, University of Leeds, Leeds.
[Available online at http://www.cgs.leeds.ac.uk/europeanstorms/]

Pryor, S. C., M. Nielsen, R. J. Barthelmie, and J. Mann, 2004: Can satellite sampling of offshore windspeeds ealistically represent windspeed distributions? Part II: quantifying uncertainties associated with sampling strategy and distribution fitting methods. *J. Appl. Meteorol.* 43, 739–750.

Pryor, S. C., and R. J. Barthelmie, 2010: Climate change impacts on wind energy: a review. Renew Sust. Energ. Rev. **14**, 430–437.

Pryor, S. C., R. J. Barthelmie, N. E. Clausen, M. Drew, I. MacKellar, and E. Kjellström, 2011: Analyses of possible changes in intense and extreme windspeeds over northern Europe under climate change scenarios. *Clim. Dynam*. doi:10.1007/s00382-010-0955-3

Richardson, D., R. Buizza, and R. Hagedorn, 2005: Final report of the 1stWorkshop on the THORPEXInteractiveGrandGlobal Ensemble, TIGGE : WMO TD-1273, WWRP-THORPEX Rep. 5, 39 pp.

Risk Management Solutions, 2009 [online]. [Available online at: http://www.rms.com/ClientResources/Catupdates/CatUpdatePublic.asp?event_id=2752]

Rodwell, M. J., D. P. Rowell, and C. K. Folland, 1999: Oceanic forcing of the wintertime North Atlantic Oscillation and European climate. *Nature*, 398, 320–323.

Sanders, F. and J. R. Gyakum, 1980: Synoptic–dynamic climatology of the 'bomb'. *Mon. Weather Rev.*, 108, 1589–1606.

Scaife, A. A., T. Spangehl, D. Fereday, U. Cubasch, U. Langematz, H. Akiyoshi, S. Bekki, P. Braesicke, N. Butchart, M. Chipperfield, A. Gettelman, S. Hardiman, M. Michou, E. Rozanov, and T. G. Shepherd, 2011: Climate Change Projections and Stratosphere-Troposphere Interaction, *Clim Dynam.* In Press doi:10.1007/s00382-011-1080-7

Schultz, D. M., D. Keyser, and L. F. Bosart, 1998: The effect of largescale flow on low-level frontal structure and evolution in midlatitude cyclones. *Mon. Wea. Rev*., 126, 1767–1791.

Schultz, D. M., and G. Vaughan, 2011: Occluded fronts and the occlusion process: A fresh look at conventional wisdom. *Bull. Am. Meteorol. Soc.* 92: 443–466 ES19–ES20.

Seaman, R., W. Bourke, Steinle, P., Hart, T., Embery, G., Naughton, M., and Rikus, L. 1995: Evolution of the Bureau of Meteorology's Global Assimilation and Prediction system. Part 1: analysis and initialisation. *Aust. Met. Mag*, *44*, 1-18.

Seguro, J. V., and T. W. Lambert, 2000: Modern estimation of the parameters of the Weibull windspeed distribution for wind energy analysis. *J. Wind. Eng. Ind. Aerod* 85(1), 75–84.

Serreze, M. C., F. Carse, R. G. Barry, and J. C. Rogers, 1997: Icelandic Low Cyclone Activity: Climatological Features, Linkages with the NAO, and Relationships with Recent Changes in the Northern Hemisphere Circulation. *J. Climate*. 10, 453-464.

Shaffrey, L. Coauthors, I. Stevens, W. A. Norton, M. J. Roberts, Pier Luigi Vidale, J. D. Harle, A. Jrrar, M. J. Woodage, M. E. Demory, J. Donners, D. B. Clark, A. Clayton, J. W. Cole, S. S. Wilson, W. M. Connolley, T. M. Davies, A. M. Iwi, T. C. Johns, J. C. King, A. L. New, J. M. Slingo, A. Slingo, L. Steenman-Clark, and G. M. Martin, 2009: UK HiGEM: The new UK high-resolution global environment model-model description and basic evaluation. *Journal of Climate*,*22*(8), 1861-1896.

Shapiro, M. A., and D. Keyser, 1990: Fronts, jet streams and the tropopause. Extratropical *Cyclones, The Erik Palmen Memorial Volume*, C. W. Newton and E. O. Holopainen, Eds., Amer. Meteor. Soc., 167–191.

Shutts, G., 2005: A kinetic energy backscatter algorithm for use in ensemble prediction systems. *Q. J. Roy. Meteor. Soc.*, 131(612), 3079-3102.

Sinden, G., 2007: Characteristics of the UK wind resource: Long-term patterns and relationship to electricity demand. *Energ. Policy.* 35, 112-127

Skamarock, W. C., and J. B. Klemp, 2008: A time-split nonhydrostatic atmospheric model for weather research and forecasting applications. *J.Comput. Phys.*, 227(7), 3465-3485.

Skamarock, W. C., J. B. Klemp, J. Dudhia, D. O. Gill, D. M. Barker, M. G. Duda, X.-Y. Huang, W. Wang, and J. G. Powers, 2008: A description of the advanced research WRF version 3. NCAR Technical Note, (NCAR/TN475+STR).

Smart, D. J., and K. A. Browning, 2009: Morphology and evolution of cold-frontal misocyclones. *Q. J. Roy. Meteorol. Soc.*, 135(639), 381-393.

Smits, A. A. K. T., A. M. G. Klein Tank, and G. P. Können, 2005: Trends in storminess over the Netherlands, 1962–2002. *International Journal of Climatology*, *25*(10), 1331-1344.

Stensrud, D. J., 2007: *Parameterization schemes: Keys to understanding NWPmodels*. Cambridge University Press.

Swiss Re, 2002: An Introduction to Reinsurance. Zurich, Swiss Reinsurance Company: 34.

Swiss Re, 2011: Natural Catastrophes and man-made disasters in 2010: a year of devastating and costly events. Sigma 40

Swiss Re, 2012: Natural Catastrophes and man-made disasters in 2011: historic losses surface from record earthquakes and floods. Sigma No 2/2012

Takle, E. S., and J. M. Brown, 1978: Note on the use of Weibull statistics to characterize wind-speed data. *J. Appl. Meteorol*. 17(4), 556–559.

Tao, W. K., J. J. Shi, S. S. Chen, S. Lang, P. L. Lin, S. Y. Hong, C. Peters-Lidard, and A. Hou, 2011: The impact of microphysical schemes on hurricane intensity and track. *Asia-Pacific Journal of Atmospheric Sciences*, 47(1), 1-16.

Times Online, 2009 [online]. [Available online at: http://www.timesonline.co.uk/tol/news/world/europe/article5580412.ece]

Toth Z, and E. Kalnay, 1993: Ensemble forecasting at NMC: the generation of perturbations. *Bull. Am. Meteorol. Soc.* 74: 2317–2330.

Toth, Z., and E. Kalnay, 1997: Ensemble forecasting at NCEP and the breeding method. *Mon. Weather. Rev.*, 125(12), 3297-3319.

Troccoli, A., K. Muller, P. Coppin, R. Davy, C. Russel, and A. L. Hirsch, 2011: Long-term wind speed trends over Australia. *J. Climate*. 25, 170-183. doi:10.1175/2011JCLI4198.1

UKMO, 2011: Met Office Surface Data Users Guide. [Available online at http://badc.nerc.ac.uk/data/ukmomidas/ukmo_guide.html#5.5].

Ulbrich, U., G. C. Leckebusch, and J. G. Pinto, 2009: Extra-tropical cyclones in the present and future climate: a review. *Theor. Appl. Climatol*. 96, 117-131.

Vautard, R., J. Cattiaux, P. Yiou, J. Thépaut, and P. Ciais, 2010: Northern Hemisphere atmospheric stilling partly attributed to an increase in surface roughness. *Nat. Geosci*. 3, 756-761. doi: 10.1038/NGE0979

Wang, X. I., F. W. Zwiers, V. R. Swail, and Y Feng, 2009: Trends and variability of storminess in the Northeast Atlantic region, 1874-2007. *Clim. Dynam.* 33, 1179-1195.

Wang, S. C., S. X. Huang, and Y. Li, 2006: Sensitive numerical simulation and analysis of rainstorm using nested WRF model. *Journal of Hydrodynamics, Ser. B*, 18(5), 578-586.

Wedi, N.P., M. Hamrud, G. Mozdzynski, G. Austad, S. Curic, and J. Bidlot, 2012: Global, non-hydrostatic, convection-permitting, medium-range forecasts: progress and challenges. ECMWF Newsletter No. 133 – Autumn 2012.

Wei, M., Z. Toth, R. Wobus, and Y. Zhu, 2008: Initial perturbations based on the ensemble transform (ET) technique in the NCEP global operational forecast system. *Tellus A*, 60(1), 62-79.

Weigel, A., M. Liniger, P. Della-Marta, D. Baggenstos, D. Bolius, and C. Appenzeller, 2008: The use of ECMWF long-range forecast products at MeteoSwiss. ECMWF Forecast Products Users Meeting 11th –13th June 2008, Reading, UK.

Weisman, M. L., 2001: Bow echoes: A tribute to TT Fujita. *Bull. Am. Meteorol. Soc.*, 82(1), 97-116.

Weisser, D., 2003: A wind energy analysis of Grenada: an estimation using the 'Weibull' density function. *Renew. Energ*. 28, 1803–12.

Wheatley, D. M., R. J. Trapp, and N. T. Atkins, 2006: Radar and damage analysis of severe bow echoes observed during BAMEX. *Mon. Weather Rev.*, 134(3), 791-806.

Wheeler, D., J. Mayes 1997: Regional Climates of the British Isles. London, Routledge, 437 pp.

Whitaker, J. S., G. P., Compo, and J. N. Thépaut, 2009: A comparison of variational and ensemble-based data assimilation systems for reanalysis of sparse observations. *Mon. Weather. Rev.*, 137(6), 1991-1999.

Wiegand, L, A. Twitchett, C. Schwierz, and P. Knippertz, 2011: Heavy precipitation at the Alpine south side and Saharan dust over central Europe: A predictability study using TIGGE. Weather and Forecasting, 26(6), 957-974.

Wilks, D. S. 1990: Maximum likelihood estimation for the gamma distribution using data containing zeros. *J. Climate.* 3, 1495–1501.

Woodroffe, A., 1988: Summary of weather pattern developments of the storm of 15/16 October 1987. *Meteorol. Mag.*, 117, 99–103.

Woollings, T., 2010: Dynamical influences on European climate; an uncertain future. *Phil. T. R. Soc. A.* 368, 3733-3756. doi:10.1098/rsta.2010.0040

Woollings, T., M. Lockwood, G. Masato, C. Bell, and L. Gray, 2010: Enhanced signature of solar variability in Eurasian winter climate. *Geophys. Res. Lett.* 37, L20805. doi:10.1029/2010GL044601

Zhang, Z., and T. N. Krishnamurti, 1999: A perturbation method for hurricane ensemble predictions. *Mon. Weather. Rev.*, 127(4), 447-469.

## List of acronyms

3D-VAR - 3-dimensional variational data assimilation

4D-VAR - 4-dimensional variational data assimilation

ARW - Advanced Research WRF

AVHRR - Advanced Very High Resolution Radiometer

BADC - British Atmospheric Data Centre

BoM - Australian Bureau of Meteorology

CCB - cold conveyor belt

CMA - Chinese Meteorological Agency

CMC - Canadian Meteorological Centre

COSMO - Consortium for Small-scale Modelling

CPTEC - Brazilian Centre for Weather Prediction and Climate Studies

CS - Convective systems

DCB - Dry conveyor belt

DMGS - Daily Maximum Gust Speed

DWD - Deutscher Wetterdienst

DSCS – Dry slot convective systems

ECMWF - European Centre for Medium-Range Weather Forecasts

eDMGS – extreme DMGS (top 1% 1980-2010 DMGS at each UKMO station)

ENSO - El Niño–Southern Oscillation

EPS - Ensemble Prediction System

ETC - extra-tropical cyclone

GenSi - Generalized multivariate statistical interpolation

GFS - Global Forecasting System

GSI - Gridded statistical interpolation

HadGEM1 - Hadley Centre Global Environmental Model version 1

HiGEM - High Resolution Global Environmental Model

HM- Hourly Mean

JMA - Japan Meteorological Agency

KMA - Korean Meteorological Administration

LAM - Limited Area Model

MCH – MeteoSchweiz

MIDAS - Met Office Integrated Data Archive System

MJO - Madden–Julian oscillation

MODIS - Moderate-resolution Imaging Spectroradiometer

NAO - North Atlantic Oscillation

NCAR - National Center for Atmospheric Research

NCEP - National Centers for Environmental Protection

NERC - Natural Environment Research Council

NMM - Non-hydrostatic Mesoscale Model

NWP - numerical weather prediction

QLCS – Quasi-linear convective systems

rCCB – returning cold conveyor belt

SJ – Sting Jet

Strong PG – Strong Pressure Gradient

THORPEX - The Observing System Research and Predictability Experiment

TIGGE - THORPEX Interactive Grand Global Ensemble

UKMO - UK Meteorological Office

UM - Unified Model

WCB - warm conveyor belt

WPS – WRF Pre-processing System

WRF - Weather Research and Forecasting

WSM3 - WRF Single-Moment 3-class